

THAYNÁ ALICE BRITO ALMEIDA

**SUSTAINABILITY STRATEGIES FOR AGRICULTURAL WATER SECURITY AND
ENVIRONMENTAL PROTECTION IN SEMI-ARID AREAS**

Recife
Pernambuco, Brazil
2024

THAYNÁ ALICE BRITO ALMEIDA

**SUSTAINABILITY STRATEGIES FOR AGRICULTURAL WATER SECURITY AND
ENVIRONMENTAL PROTECTION IN SEMI-ARID AREAS**

Thesis submitted to the Agricultural Engineering Graduate Program of the Federal Rural University of Pernambuco in partial fulfillment of the requirements for the degree of Doctor in Agricultural Engineering.

Advisor: Prof. PhD. Abelardo Antônio de Assunção Montenegro

Co-Advisors: Prof. PhD. Thieres George Freire Silva, and Prof. PhD. João Luis Mendes Pedroso de Lima

Recife
Pernambuco, Brazil

2024

Dados Internacionais de Catalogação na Publicação
Universidade Federal Rural de Pernambuco
Sistema Integrado de Bibliotecas da UFRPE

A447s Almeida, Thayná Alice Brito.

Sustainability strategies for agricultural water security and environmental protection in Semi-arid areas / Thayná Alice Brito Almeida. – Recife, 2024.

203 f.; il.

Orientador(a): Abelardo Antônio de Assunção Montenegro.

Co-orientador(a): Thieres George Freire.

Co-orientador(a): João Luis Mendes Pedroso de Lima.

Tese (Doutorado) – Universidade Federal Rural de Pernambuco, Programa de Pós-Graduação em Engenharia Agrícola, Recife, BR-PE, 2024.

Inclui referências.

1. Água - Conservação. 2. Águas residuais. 3. Águas subterrâneas. 4. Solos - Conservação 5. Termografia. I. Montenegro, Abelardo Antônio de Assunção, orient. II. Freire, Thieres George, coorient. III. Lima, João Luis Mendes Pedroso de, coorient. IV. Título

CDD 630

THAYNÁ ALICE BRITO ALMEIDA

Sustainability strategies for agricultural water security and environmental protection in Semi-arid areas

Thesis presented to the Federal Rural University of Pernambuco, as partial fulfillment of the requirements for the Graduate Program in Agricultural Engineering, to obtain the title of Doctor in Agricultural Engineering.

DEFENDED and APPROVED on July 24, 2024.

Examination Board

Abelardo Antônio de Assunção Montenegro
Federal Rural University of Pernambuco - UFRPE

João Pedroso de Lima
Coimbra University - UC

José Amilton Santos Júnior
Federal Rural University of Pernambuco - UFRPE

Daniel Green
Heriot-Watt University – HWU

Victor Hugo Rabelo Coelho
Federal University of Paraíba - UFPB

Yuri Jacques Agra Bezerra da Silva
Federal University of Piauí - UFPI

"The heavens declare the glory of God; the skies proclaim the work of his hands. Day after day they pour forth speech; night after night they reveal knowledge. They have no speech, they use no words; no sound is heard from them."

(Psalm 19:1-3)

Dedication

I dedicate my thesis to my beloved parents, Dimas Almeida and Vanda Brito, for their tireless dedication to our family and for teaching me the value of education. I also dedicate it to my nephews, Dimas Neto, Anthony, and Arthur. You are the best part of my life.

Acknowledgements

“For from him and through him and for him are all things. To him be the glory forever! Amen.” (Romans 11:36). I thank God for His grace and infinite mercy toward me. Lord, You have granted me so many privileges.

To my parents, Dimas and Vanda, all my love and gratitude. They not only supported me but lived through my busy routine, from fieldwork to conferences, online classes, late-night article revisions, and corrections. They were also my sponsors for many years. To my nephews (Netinho, Anthony, and Tutu), who recharge my energy and bring me joy every day—you allow me to experience the best life has to offer. To my godparents, for always rooting for me, and to my siblings, who make me feel special. To Raphael Lins, thank you for your patience, help in the field, and for listening to me present and talk about my work results countless times. To my lifelong friends, my sisters, Mariana and Nadijane, thank you for understanding my absence and for continuing to pray for me.

To my academic siblings at the Water and Soil Laboratory: Giselle, Moisés, Aline, Tamiris, Lizandra, Luandson, Lucas, Lion, Ítallo, Oto, Filipe Alexandre, Paulo Eduardo, and Cláudio Vinícius. A special thanks to Ailton Carvalho and Rodrigo Soares for their constant partnership and tireless help. To Soheil, Romeu, Ricardo, and Professor Isabel de Lima for welcoming me at the University of Coimbra. To the farmers of the Nossa Senhora do Rosário Settlement: Mr. Josa, Mr. Edilson, Mr. Adelmo, and Vivaldo. A special thanks to my friend Mr. Josa for kindly offering part of his land for my research, and for his joy and willingness.

To my advisor, Abelardo Montenegro, for his trust, encouragement and all the opportunities throughout these years of partnership, and for being a great professional inspiration and example of dedication. To my co-advisors: Professor Thieres Silva, for his advice, for being a great inspiration, and for his encouragement and belief in me; and Professor João Pedroso de Lima, for supervising my sandwich doctoral program, for welcoming me to the University of Coimbra, and for all the support and guidance since my undergraduate studies, with his creative ideas.

To the Federal Rural University of Pernambuco (UFRPE) and Graduate Program in Agricultural Engineering (PGEA). To the Department of Civil Engineering of the Faculty of Sciences and Technology of the University of Coimbra (FCTUC), Coimbra, Portugal. To all professors, students, and staff of these institutions, especially to the entire team at the Water and Soil Laboratory (LAS/UFRPE).

To the Pernambuco Science and Technology Support Foundation - FACEPE (IBPG-1155-5.03/20), to the National Council for Scientific and Technological Development – CNPq, and The Coordination for the Improvement of Higher Education Personnel (Capes), particularly the CAPES-PrInt program. To the MAI/DAI Academic Master's and Doctorate for Innovation Program and all individuals and institutions who directly or indirectly contributed to this research, especially the National Institute of Semiarid (INSA), Pernambuco Water and Sewage Company (COMPESA), and TPF Engineering. I also thank the Portuguese Foundation for Science and Technology (FCT), through projects ASHMOB (CENTRO-01-0145-FEDER-029351), MEDWATERICE (PRIMA/0006/2018), and through the strategic project UIDB/04292/2020 granted to MARE—Marine and Environmental Sciences Centre, University of Coimbra, Department of Civil Engineering.



Summary

List of figures.....	13
General Abstract.....	18
General Introduction	19
References.....	23
Chapter I: Water management strategies in a scarcity situation: a review about semiarid agriculture addressing climate change, soil degradation, water scarcity, and conservation practices for sustainable water management.....	26
I.1 Introduction	27
I.2 Impact of climate change on agricultural production in the semiarid region.....	28
I.3 Groundwater and the impact of climate change on future water supply in the semiarid region	30
I.4 Importance of agricultural use of domestic effluent in agricultural production and the sustainable use	31
I.5 Fires and soil degradation in semiarid environments: impact on agricultural expansion and erosion.....	34
I.6 Strategies for agriculture production with water scarcity.....	35
I.7 Sustainability and efficiency in the use of conservation practices in semiarid regions	36
I.8 Advanced vegetation monitoring methods	40
I.9 Conclusion.....	42
References.....	43
Chapter II: Evaluating ash mobilization dynamics and hydrological response of soil after wildfire under simulated rainfall: laboratory and field conditions	54
II.1 Introduction	55
II.2 Material and methods	57
II.2.1 Satellite-derived data a study area.....	57
II.2.2 Experimental field setup.....	58
II.2.2.1 Burned area and Ash distribution	60
II.2.2.3 Runoff and Soil moisture	61
II.2.2.4 Disaggregation rate, sediment concentration and soil loss	62
II.2.3 Experimental laboratory setup	62
II.2.3.2 Percentage of ash in the flume	65

II.2.4 Statistical analysis	65
II.3 Results and discussion.....	66
II.3.1 Land use and burned areas	66
II.3.2 Soil moisture, runoff and erosion rates, soil loss and time to the beginning of runoff ..	74
II.3.3 Ash transport	77
II.3.3 Effectiveness of ash layouts	81
II.4 Conclusion.....	83
References.....	84
Chapter III: Hydrogeological trends in an alluvial valley in the Brazilian semiarid: impacts of observed climate variables change and exploitation on groundwater availability and salinity	
.....	91
III.1 Introduction.....	92
III.2 Material and methods.....	95
III.2.1 Study area.....	95
III.2.1.1 Geology and Hydrogeology of the study area	98
III.2.2 Data and methods.....	99
III.2.2.1 Meteorological data	99
III.2.2.2 Groundwater level and electrical conductivity data.....	99
III.2.2.3 Water use in irrigated areas	100
III.2.3 Assessment of temporal stability of groundwater levels and salinity	100
III.2.4 Temporal trend analysis	101
III.2.5 Exploratory and statistical analyses	102
III.3. Results and discussion	102
III.3.1 Level, salinity, and climatic temporal variation.....	102
III.3.3. Temporal Stability of groundwater levels and electrical conductivities	106
III.3.4. Identification of groundwater monthly and annual trend analysis.....	109
III.3.4 Analysis of the factors affecting GW availability and quality for irrigation	120
III.4 Conclusions.....	123
References.....	124
Chapter IV: Domestic wastewater reuse in irrigation and conservation practices: short-term effects of on soil carbon, salinity and soil moisture in Brazilian semiarid region.....	
.....	131

IV.1 Introduction	132
IV.2 Materials and Methods	133
IV.2.1 Experimental Site	133
IV.2.2 Treatments and Experimental Design	136
IV.2.3 Metereological monitoring.....	138
IV.2.4 Soil moisture and conservation techniques efficiency	138
IV.2.5 Biometric and Physiological Index Analyses.....	139
IV.2.6 Soil Salinity and Soil Total Organic Matter	139
IV.2.7 Statistical Analysis	140
IV.3 Results and Discussion.....	142
IV.3.1 Rainfall and climatic conditions during Palma Cultivation	142
IV.3.2 Effects of Wastewater Irrigation and different soil cover conditions on the Soil Electrical Conductivity and Organic Matter	143
IV.3.3 Organic Carbon and Salinity Spatial Dynamics at the Experimental Area.....	148
IV.4. Conclusion.....	153
References.....	154
Chapter V: Evaluating Daily Water Stress Index (DWSI) using thermal imaging of Neem tree canopies under bare soil and mulching conditions	159
V.1 Introduction	160
V.2 Material and Methods.....	163
V.2.1 Characterization of the study area	163
V.2.2 Image Acquisition and analysis	165
V.2.3 Water stress indicator.....	167
V.2.4 Statistical and geostatistical analysis.....	167
V.3. Results and discussion.....	169
V.3.1 Changes in soil moisture and climatic conditions	169
V.3.2 Daily Water Stress Index	173
V.3.3 Relationships between thermal indices and meteorological parameters	176
V.3.4 Plant canopy status mapping	179
V.4 Conclusions	188
References.....	189

General conclusions and finals considerations	195
Knowledge Sharing.....	198
Publications and other relevant activities conducted on the doctoral research.....	201

List of figures

General Introduction

Figure 1. Graphical abstract of the studied domain, comprising ecohydrological analysis of processes taking place at the hillslopes and bottom valley of the Mimoso Rivulet Catchment.....	22
---------------------------------------------------------------------------------------------------------------------------------------------------------------------------------------------------	----

Chapter II

Figure 1. Location of study area, and experimental field layout (no scale).....	59
Figure 2. Rainfall spatial distribution of 60 mm h ⁻¹ intensity for 10% of slope.....	60
Figure 3. Spatial layouts of ash cover tested in the soil flume experiments.....	61
Figure 4. Schematic representation of the laboratory setup used in the experiments (not to scale).....	63
Figure 5. Rainfall spatial distribution of 100 mm h ⁻¹ and 60 mm h ⁻¹ intensity for 10 and 30% of slope.....	64
Figure 6. Annual time series, seasonal and annual trend, and Boxplot with mensal distribution of fire foci from 2014 to 2022.....	66
Figure 7. Spatial distribution of rainfall from 2014 to 2022 in Ipanema River Basin, Brazilian semiarid region.....	69
Figure 8. Spatial distribution land use and land cover between 2014 to 2022 in the Ipanema River Basin, Brazilian semiarid region.....	71
Figure 9. Spatial distribution of fire foci from 2014 to 2022 in Ipanema River Basin, Brazilian semiarid region.....	73
Figure 10. Runoff rates and sediment concentration in the five layouts investigated.....	74
Figure 11. Total soil loss amounts (average and standard deviation bars from all samples collected) observed during a complete experiment for the 5 layouts.....	75
Figure 12. Concentrations of sediments (NTU) for runoff surface water samples and Sediment Loss collected during simulated rain events.....	76
Figure 13. Ash transportation (g min ⁻¹) by rainfall and rainfall + inflow for the five layouts.....	77
Figure 14. Box plot mass of ash in each layout of distribution for both 10 and 30% of slope, and 60- and 100-mm h ⁻¹ rainfall simulation.....	80

Figure 15. Comparison of cover percentage among five different layouts before and after rainfall simulation considering two rain intensities (60- and 100-mm h ⁻¹) and two slopes (10 and 30%).....	81
Figure 16. Correlations among ash removed (in grams) observed by rainfall simulator under five ash layouts and two slopes.....	82

Chapter III

Figure 1. Location map of the Mimoso Alluvial Valley, Alto Ipanema Basin, Pesqueira municipality of Pernambuco, Brazil.....	96
Figure 2. Piezometer installation, using manual hammer. View of the adopted piezometers, with the open zone for slug test and groundwater regular monitoring. Kriged maps saturated hydraulic conductivity, soil types, and surface saturated hydraulic conductivity (Source: adapted from Montenegro, 1997).....	97
Figure 3. (a) Rainfall, (b) groundwater abstractions and reference evapotranspiration from 2000 to 2019 in the Mimoso Alluvial Valley, Brazil.....	103
Figure 4. Boxplots of the annual mean values of (a) groundwater level, (b) electrical conductivity, and abstraction values between 2000 and 2019 in the Mimoso Alluvial Valley.....	105
Figure 5. Relative mean difference and temporal standard deviation for (a) potentiometric levels, (b) electrical conductivity, (c) wells, (d) piezometers with high saturated hydraulic conductivity, and (e) piezometers with low saturated hydraulic conductivity in the Mimoso Alluvial Aquifer.....	107
Figure 6. Annual time series for mean temperature and rainfall from 2000 to 2019, with associated trend lines.....	112
Figure 7. Annual time series and associated trend lines of groundwater level in piezometers Pz 3.8 (A), Pz 4.8 (B), Pz 4.10 (C) from 2000 to 2019.....	113
Figure 8. Annual time series and associated trend lines of electrical conductivity in well (A), PZL (B), PZH (C) from 2000 to 2019.....	114
Figure 9. Annual time series of rainfall (A) and reference evapotranspiration (B) from 2000 to 2019, with associated trend line.....	115

Figure 10. Annual time series of the general averages of (a) groundwater level (m), (b) electrical conductivity (dS m^{-1}), and (c) abstraction ($\text{m}^3 \text{ year}^{-1}$), from 2000 to 2019, with the associated trend lines.....	117
Figure 11. Annual time series of salinity (dS m^{-1}) for the (a) PW, (b) PZH group, and (c) PZL group from 2000 to 2019, with the associated trend lines.....	119
Figure 12. Principal component analysis, plotting of scores of the first two principal components (A) and Spearman's correlation matrix (B) of the Mimoso Valley variables. Note: the correlation *, ** and *** is significant at the 0.05, 0.01 and 0.001 level, respectively.	121
Figure 13. Principal component analysis, plotting the scores of the first two principal components and loads matrix for the components.....	122

Chapter IV

Figure 1. Location map of the Alto Ipanema basin, municipality of Pesqueira-PE and study area.....	134
Figure 2. Sketch (not to scale) of the experimental plots and their respective soil cover condition.....	137
Figure 3. Temporal distribution of rainfall, Air temperature, Relative humidity and soil moisture in plots with treatments T1 to T7, from August 2023 to April 2024.....	142
Figure 4. Temporal behavior of soil total organic carbon (TOC) under different soil cover conditions (bare soil, mulch, mulch with biochar).....	144
Figure 5. Temporal behavior of soil electrical conductivity (ES) under different soil cover conditions (bare soil, mulch, mulch with biochar).....	145
Figure 6. Box plots of Electrical conductivity (dS m^{-1}) for bare soil, mulch and mulch+biochar soil cover conditions to 0-0.1 m (A) and 0.10 – 0.20 (B) soil layers.....	146
Figure 7. Semivariogram models for Total organic carbon content (A) and Electrical conductivity (B) for layers 0 – 0.10 m (0.1) and 0.10 – 0.20 m (0.2), in three different monitoring campaign (C1, C2 and C3).....	149
Figure 8. Kriging maps for the evaluated periods (C1, C2, and C3) for total organic carbon (TOC) and soil electrical conductivity (EC) in the 0-0.10 m (Layer 0.1 m) and 0.10-0.20 m (Layer 0.2 m) layers.....	151
Figure 9. Spatial distribution of NVI, NDSI and DWSI in the selected field plots in three different moments of experiment.....	152

Chapter V

Figure 1. Location of the experimental area in the Alto Ipanema basin in the state of Pernambuco, Brazil and sketches and photographs of two erosion plots and treatments in the studied area: Neem + mulch and Neem + bare soil.....	164
Figure 2. Sketch of the procedure of capturing thermograms (A); processing images and extracting representative grids and contour from sampled leaves (B).....	166
Figure 3. Daily time series of soil moisture and rainfall (A), air and soil temperature (B), accumulated soil moisture (C) and accumulated soil temperature (D) at the two plots in 2017: Neem (bare soil in black) and Neem with mulch cover (in green).....	170
Figure 4. Monthly soil moisture variation for both soil cover condition (bare in black and mulch in green), along 2017.....	171
Figure 5. Temporal distribution of wind speed, in meter per seconds, to 2017 and box plot of monthly values.....	172
Figure 6. Monthly Water Balance (CWB), monthly average plant height (PH), stem diameter (SD), leaf temperature (T_L) and DWSI under bare soil and mulch soil cover conditions.....	175
Figure 7. Plots of soil moisture (A), soil temperature (B) and DWSI (C), soil moisture and soil temperature (D), soil moisture and DWSI and soil temperature and DWSI (F), for mulch and bare soil cover condition. Dashed lines represent regression lines. Full line represents the 1:1 line.....	177
Figure 8. Principal component analysis, plotting of scores of the first two principal components, and Spearman's correlation matrix.....	178
Figure 9. Box plot of daily water stress indicator for March, May and September, of mulching treatment and bare soil, for three different leaves.....	180
Figure 10. Kriging maps for surface temperature referring to representative leaves for March, May and September, considering bare soil and mulch cover conditions.....	183
Figure 11 The canopy DWSI cumulative frequency curves for plants evaluated in the respective months (March, May and September) under bare soil and mulch conditions.....	185
Figure 12. Histograms of distribution of DWSI for the months of March, May, and September, under Mulch and Bare soil conditions, following mapping via Kriging and SGS techniques.....	187

Knowledge Sharing

Figure 1. Field monitoring with the collaboration of undergraduate students and local school students.....198

Figure 2. Presentation of scientific works in Symposium and Congresses.....199

Figure 3. Field actions in hydro-agricultural reuse demonstration units and experimental areas.....199

General Abstract

Climate change poses significant challenges to global agriculture, particularly in the semiarid. Water scarcity is a significant environmental issue in semiarid regions, requiring ecohydrological management of the available water resources. In the Brazilian semiarid, alluvial valleys are strategic for water supply and food production, even during drought periods, for local rural communities. At those areas, water availability depends not only on direct recharge at the unconfined aquifers, but also on the hydrological processes taking place at the hillslopes of the valley catchment. Crop production and climate change have increased groundwater pumping, and also have expanded cultivation to steep lands, where clearing the native vegetation is usually carried out by fire forces. Soil and water conservation practices, such as vegetative cover and vegetative barriers, can be used to reduce surface runoff and soil loss, thereby improving soil fertility and agricultural productivity, and thus increasing infiltration and base flow components. Studies on using lower-quality water for agricultural purposes identify an alternative water source for irrigation, reducing pressure on higher-quality resources, prioritizing direct human consumption, and supporting water resource management. Furthermore, managing burned areas aims to minimize environmental damage and control erosion in these regions. This doctoral Thesis addresses topics related to advanced monitoring techniques and productive coexistence with water scarcity, the adoption of conservation practices, and agricultural water reuse for smallholding farming. It aims to investigate hydrological processes, soil conservation techniques, and water and soil loss due to water erosion in experimental plots in the laboratory and representative areas of the Agreste region of Pernambuco State, Brazil. The main results of this study indicate that water scarcity and salinization are significant challenges in semiarid Brazil, affecting groundwater availability and quality. Studies in the Mimoso Catchment reveal correlations between groundwater salinity, rainfall patterns, and overexploitation effects, emphasizing the need for effective groundwater management strategies. Domestic wastewater reuse in irrigation shows potential benefits for water conservation but requires careful management to mitigate risks to soil carbon and salinity. Practices like mulching and biochar application help control salinity and improve organic carbon content, contributing to sustainable agriculture in the semiarid Brazilian context, and also reducing soil erosion and increasing soil moisture at the hillsides of the catchment. Monitoring crop water stress is crucial in semiarid regions to maintain vegetation canopy during the dry season, and infrared thermal imaging effectively assesses canopy temperature variations under different soil cover conditions, aiding precise water stress diagnosis and management, particularly at afforested areas. Geostatistical techniques enhance the mapping of Water Stress Indices, supporting accurate agricultural decisions amidst varying meteorological conditions. Additionally, research shows that concentrated burning in smaller areas reduces soil disaggregation rates and alters physical soil characteristics, with implications for managing post-fire landscapes. In conclusion, integrating sustainable practices, advanced technologies, and effective management strategies is essential for addressing the multifaceted challenges of climate change, wildfires, water scarcity, and salinization in semiarid catchments. These approaches are pivotal for promoting agricultural sustainability and resilience in semiarid regions worldwide, particularly for smallholding farming.

Keywords: water and soil conservation, wastewater, groundwater, wildfire, thermography.

General Introduction

In many parts of the world, especially in arid and semiarid regions, the limited available water resources pose a significant obstacle to the development of agricultural production (He et al., 2021). Consequently, the impact of climate change on agricultural water security has been widely discussed in recent years. Additionally, the increasing disruption of the water cycle due to extreme weather conditions is expected to further destabilize global agricultural water supply (Mathur and AchutaRao, 2020; Grusson et al., 2021). Carvalho et al. (2020) warn about the worsening drought scenarios in Northeastern Brazil, predicting a reduction in the number of rainy days in the coming decades and impacts on the future availability of water resources. Combined with soil degradation from agricultural use and deforestation, this trend is likely to increase environmental vulnerability and desertification indices in the region, exacerbating water scarcity.

The higher frequency and duration of droughts in the Northeast, coupled with rising temperatures, may intensify environmental degradation and its interplay with unsustainable land-use practices, ultimately leading to a greater risk of desertification (Silva et al., 2020; Marengo et al., 2017). Additionally, the risk of wildfires is notably high in semiarid and arid climates, amplified by hot and dry summers (Stavi, 2019). However, these fires are often caused by human activities, such as controlled burns for land clearing after rains or agricultural expansion (Marinho et al., 2021; Abreu et al., 2022), which are traditional practices in family farming to prepare the soil for seasonal crops.

Regarding the effects and worsening of illegal wildfires, a less frequently considered but potentially significant factor that controls post-fire runoff is the presence of ash on the soil surface (Woods and Balfour, 2008). Ash is formed by the combustion of vegetation and layers of litter and debris, and its potential effects on runoff and erosion have important implications for post-fire management. According to Liang et al. (2021), returning carbonized biomass ash to the soil can enhance the carbon sequestration capacity of the soil-plant ecosystem. Furthermore, wildfires alter the hydrological cycle by affecting soil structure, infiltration rates, and water retention capacity, leading to increased erosion and flooding risks. Therefore, studies focused on understanding hydrological processes, particularly in post-fire landscapes, are crucial for supporting effective management and decision-making strategies aimed at mitigating these impacts.

According to Montenegro et al. (2020), understanding various hydrological variables is crucial for the proper management of water resources. Efficient decision-support tools are

necessary to inform policy implementation and aid in managing Brazil's natural resources, such as the use of increasingly precise and rapid sensors and detection tools. One example is the application of thermography and drone mapping, which have provided reliable results in the integrated management of soil, water, and the atmospheric environment. These tools also offer spatially distributed data, making them effective for irrigation management and control (Camoglu et al., 2021). Additionally, the use of rainfall simulators in laboratory experiments with representative experimental plots (Montenegro et al., 2020) and field experiments with erosion plots considering observed rainfall hydrological profiles in the semiarid region (Lopes et al., 2020) has been widely employed to study surface runoff and soil erosion processes.

Regarding productive coexistence with water scarcity, one increasingly prominent strategy is the reuse of lower-quality water. According to Carvalho et al. (2020), agricultural reuse should be encouraged in rural and urban communities and incorporated as an essential strategy at various levels of implementation, becoming one of the necessary tools to ensure water sustainability in the semiarid region. Conservation management is also an efficient tool for optimizing water use in agriculture. This technique makes water more readily available to plants and improves the soil's microclimatic conditions, notably reducing temperature, as demonstrated by de Lima et al. (2021) in soil covered with rice straw and in maintaining soil moisture in field research conditions, as proven by Lima et al. (2020) in the production of oilseeds under rainfed conditions in the Brazilian semiarid region, and in controlling erosion processes.

In parallel, the use of biochar, a carbon-rich residue produced by the pyrolysis and gasification of biomass such as wood under anaerobic conditions (Viaene et al., 2023), offers significant benefits for soil protection and nutrient viability. Biochar is known for its low density, high porosity, pH, cation exchange capacity, surface area, and functional groups like carboxyl, hydroxyl, and phenolic groups (Hussain et al., 2020). Its effectiveness has been demonstrated in various applications, including erosion control in burned areas (Prats et al., 2021), mitigating salinity and pollutants associated with lower-quality water irrigation (Lima et al., 2021; Mclennon et al., 2020; Xie et al., 2023). These benefits highlight biochar's efficiency and feasibility as a tool for improving soil health and managing water resources.

Alluvial valleys are inseparable components of the semiarid landscapes, and their ecohydrological sustainability depends both on the protection of catchment area at the hillsides and on the water resources management at the wetter bottom (Almeida et al., 2024). Brown et al. (2005) have investigated the impact of vegetation cover changes on water yield, resulting

from changes in evapotranspiration patterns, and so in daily flows and flow duration curves, for deforested, afforested areas, among others. It is highlighted that changes catchment response is a slow process, and larger impacts are expected for low flows, which controls lateral recharge for catchment valleys. Fan et al. (2019) point out that hillslopes are key features of landscapes, and lateral flows from ridges to valleys regulate the spatial temporal distribution of water, energy and vegetation across the landscape, where valleys are wetter than the hilltops. Zhu and Zhu (2014) have highlighted the relevance of adoption of conservation practices such as grass surface and contour earth banks in hilly areas in China, where pressure for food production has been expanded to steep sloping lands. It has been identified reductions in soil losses and increases in infiltration. Lima et al. (2020) developed a paired plot investigation of the mulching impact on soil moisture at afforested hillsides in the Brazilian semiarid and demonstrated the environmental hydrological benefits on adopting such conservation practices at the hilltops of the landscape. Investigating the role of conservation practices adoption at steep areas in semiarid Brazil, Souza et al. (2023) have verified that palm barriers can be highly effective in increasing infiltration, and also soil moisture.

Starting from the hypothesis that conservation practices, including mulching, Palma vegetative barriers, and treated wastewater enhance water use efficiency, soil quality, erosion control, and organic carbon stocks, these actions are expected to promote agricultural sustainability and resilience in water-scarce environments without environmental harm. This Thesis aims to investigate hydrological processes, soil conservation techniques, cultivation conditions, and losses of water, soil, and nutrients due to water erosion in experimental laboratory plots and representative areas of the semiarid region of Pernambuco.

This Thesis addresses topics related to the spatial and temporal dynamics of alluvial groundwater reservoirs, the impacts of climate variation on water availability in a highly monitored alluvial valley, and the use of treated effluents as an alternative water source for irrigation. It also explores advanced monitoring methods. Chapter I presents a literature review exploring the challenges of agricultural production in semiarid environments, as well as possible solutions and sustainable uses of water and soil. It introduces concepts such as "Nature-based Solutions" and the use of domestic effluents for forage irrigation. Chapter II examines the increase in anthropogenic fires and their association with agricultural expansion. It also experimentally evaluates the effect of different burning layouts on mitigating adverse soil effects, such as ash transport and soil erosion on a slope within an alluvial valley. Chapter III discusses the temporal stability and trend analysis of potentiometric levels and salinity in

an intensively monitored alluvial aquifer in the semiarid region. Chapter IV addresses the spatial variability of soil organic carbon and electrical conductivity in forage cactus cultivation irrigated with treated domestic effluent on a family scale, also within the Mimoso alluvial valley, and the effect of bioretention structures in controlling salinity. Finally, Chapter V applies thermography to determine plant water stress under different soil management practices in dryland conditions at the hilltop of the Mimoso alluvial catchment.

Figure 1 presents a graphical abstract of the studied catchment and application of agricultural engineering strategies, and the connexion between the main ecohydrological processes involved.

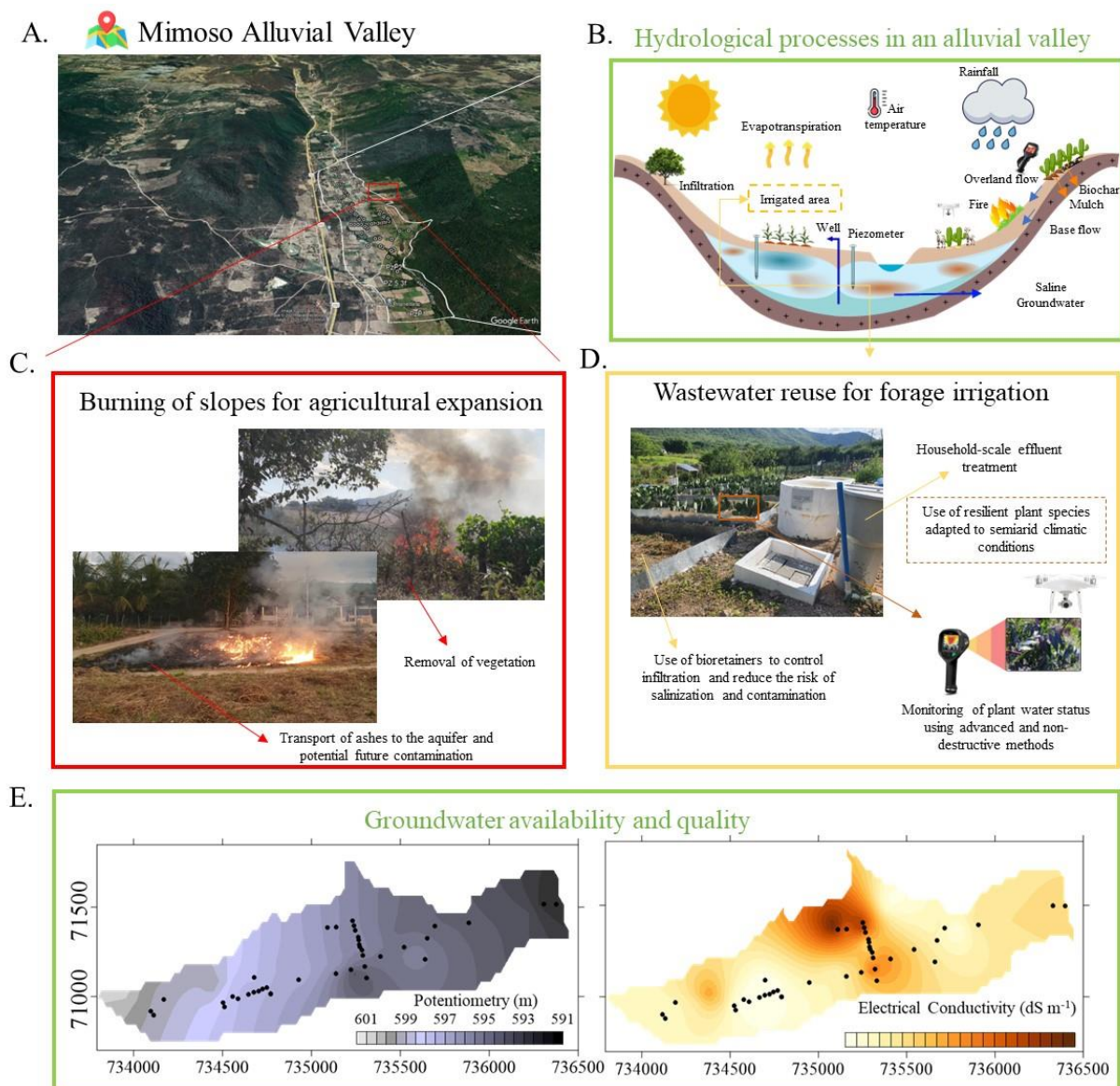


Figure 1. Graphical abstract of the study area in the Mimoso Alluvial Valley (A), featuring ecohydrological analysis of processes occurring on the hillslopes and valley bottom of the

Mimoso Rivulet Catchment (B), fire incidence in slope areas (C), the wastewater reuse system (D), and the distribution of groundwater availability and quality (E).

References

- Abreu, M. C., Lyra, G. B., de Oliveira-Júnior, J. F., Souza, A., Pobočíková, I., de Souza Fraga, M., & Abreu, R. C. R. (2022). Temporal and spatial patterns of fire activity in three biomes of Brazil. *Science of the Total Environment*, 844(June 2021). <https://doi.org/10.1016/j.scitotenv.2022.157138>
- Almeida, T. A. B., Montenegro, A. A. de A., Mackay, R., Montenegro, S. M. G. L., Coelho, V. H. R., de Carvalho, A. A., & da Silva, T. G. F. (2024). Hydrogeological trends in an alluvial valley in the Brazilian semiarid: Impacts of observed climate variables change and exploitation on groundwater availability and salinity. *Journal of Hydrology: Regional Studies*, 53. <https://doi.org/10.1016/j.ejrh.2024.101784>
- Brown, A.E.; Zhang, L.; McMahon, T.A.; Western, A.W.; Vertessy, R.A. 2005. A review of paired catchment studies for determining changes in water yield resulting from alterations in vegetation. *Journal of Hydrology*, n.310, p.28-61.
- Camoglu, G.; Demirel, K.; Kahriman, F.; Akcal, A.; Nar, H.; Boran, A.; Eroglu, I.; Genc, L. 2021. Discrimination of water stress in pepper using thermography and leaf turgor pressure probe techniques. *Agricultural Water Management*, n.254, p.1-10. DOI: 10.1016/j.agwat.2021.106942
- Carvalho, A. A.; Montenegro, A. A. A.; Tabosa, J. N.; Almeida, T. A. B.; Silva, A. G. O.; Silveira, A. V. M. 2020. Reúso hidroagrícola: uma solução para convivência com a escassez hídrica no Sertão e Agreste pernambucano. *Journal of Environmental Analysis and Progress*, v.5, n.2, p.140-150. DOI: 10.24221/jeap.5.2.2020.2841.140-150
- de Lima, J. L. M. P., da Silva, J. R. L., Montenegro, A. A. A., Silva, V. P., & Abrantes, J. R. C. B. (2020). The effect of vegetal mulching on soil surface temperature in semiarid Brazil. *Bodenkultur*, 71(4), 185–195. <https://doi.org/10.2478/boku-2020-0016>
- Fan, Y., Clark, M., Lawrence, D. M., Swenson, S., Band, L. E., Brantley, S. L., Brooks, P. D., Dietrich, W. E., Flores, A., Grant, G., Kirchner, J. W., Mackay, D. S., McDonnell, J. J., Milly, P. C. D., Sullivan, P. L., Tague, C., Ajami, H., Chaney, N., Hartmann, A., ... Yamazaki, D. (2019). Hillslope Hydrology in Global Change Research and Earth System Modeling. *Water Resources Research*, 55(2), 1737–1772. <https://doi.org/10.1029/2018WR023903>

- Grusson, Y.; Wesström, I.; Svedbeg, E.; Joel, A. Influence of climate change on water partitioning in agricultural watersheds: Examples from Sweden. *Agricultural Water Management*, n.249, p.1-18, 2021. DOI: 10.1016/j.agwat.2021.106766
- He, G., Geng, C., Zhao, Y., Wang, J., Jiang, S., Zhu, Y., Wang, Q., Wang, L., Mu, X., 2021. Food habit and climate change impacts on agricultural water security during the peak population period in China. *Agricultural Water Management* 258, 107211. <https://doi.org/10.1016/j.agwat.2021.107211>
- He, G., Geng, C., Zhao, Y., Wang, J., Jiang, S., Zhu, Y., Wang, Q., Wang, L., Mu, X., 2021. Food habit and climate change impacts on agricultural water security during the peak population period in China. *Agricultural Water Management* 258, 107211. <https://doi.org/10.1016/j.agwat.2021.107211>
- Liang, F., Feng, L., Liu, N., He, Q., Ji, L., De Vrieze, J., Yan, S., 2022. An improved carbon fixation management strategy into the crop–soil ecosystem by using biomass ash as the medium. *Environmental Technology and Innovation* 28, 102839. <https://doi.org/10.1016/j.eti.2022.102839>
- Lima, C.A.; Montenegro, A.A.A.; Lima, J.L.P.M.; Almeida, T.A.B.; Santos, J.C.N. Uso de coberturas alternativas do solo para o controle das perdas de solo em regiões semiáridas. *Engenharia Sanitária e Ambiental*, v.25, n.3, p.531-542, 2020. DOI: 10.1590/s1413-41522020193900
- Marengo, J. A.; Torres, R. R.; Alves, L. M. Seca no Nordeste do Brasil: passado, presente e futuro. *Theoretical and Applied Climatology*, n.129, v.3-4, p.1189-1200, 2017. DOI: 10.1007/s00704016-1840-8
- Marinho, A.A.R., Gois, G. de, Oliveira-Júnior, J.F. de, Correia Filho, W.L.F., Santiago, D. de B., Silva Junior, C.A. da, Teodoro, P.E., de Souza, A., Capristo-Silva, G.F., Freitas, W.K. de, Rogério, J.P., 2021. Temporal record and spatial distribution of fire foci in State of Minas Gerais, Brazil. *Journal of Environmental Management* 280. <https://doi.org/10.1016/j.jenvman.2020.111707>
- Mathur, R., AchutaRao, K., 2020. A modelling exploration of the sensitivity of the India's climate to irrigation. *Clim. Dyn.* 54, 1851–1872.
- Mclennon, E., Solomon, J.K.Q., Neupane, D., Davison, J., 2020. Biochar and nitrogen application rates effect on phosphorus removal from a mixed grass sward irrigated with reclaimed wastewater. *Science of the Total Environment* 715, 137012. <https://doi.org/10.1016/j.scitotenv.2020.137012>

- Montenegro, A.A.; Almeida, T.A.; Lima, C.A.; Abrantes, J.R.; de Lima, J.L. Evaluating Mulch Cover with Coir Dust and Cover Crop with Palma Cactus as Soil and Water Conservation Techniques for Semiarid Environments: Laboratory Soil Flume Study under Simulated Rainfall. *Hydrology*, v.7, n.61, 2020. DOI: 10.3390/hydrology7030061
- Prats, S.A., Merino, A., Gonzalez-Perez, J.A., Verheijen, F.G.A., De la Rosa, J.M., 2021. Can straw-biochar mulching mitigate erosion of wildfire-degraded soils under extreme rainfall? *Science of the Total Environment* 761, 143219. <https://doi.org/10.1016/j.scitotenv.2020.143219>
- Silva, M. V.; Pandorfi, H.; Lopes, P. M. O.; Silva, J. L. B.; Almeida, G. L. P.; Silva, D. A. O.; Santos, A.; Rodrigues, J. A. M.; Batista, P. H. D.; Jardim, M. R. F. Pilot monitoring of caatinga spatial-temporal dynamics through the action of agriculture and livestock in the brazilian semiarid. *Remote Sensing Applications: Society and Environment*, n.19, p.1-9, 2020. DOI: /10.1016/j.rsase.2020.100353
- Souza, T. E. M. S.; Souza, E. R.; Montenegro, A. A. A.; Bayabil, H. 2023. Could Forage Palm and Stone Barrier Be as Effective as Native Vegetation in Controlling Runoff and Erosion in the Brazilian Semiarid Region? *Agronomy-Basel*. v.13, p.3026.
- Stavi, I. Wildfires in grasslands and shrublands: a review of impacts on vegetation, soil, hydrology, and geomorphology.2019. *Water*, 11, p. 1042, 2019.
- Viaene, J.; Peiren, N.; Vandamme, D.; Lataf, A.; Cuypers, A.; Jozefczak, M.; Vandecasteele, B. (2023) Biochar amendment to cattle slurry reduces NH₃ emissions during storage without risk of higher NH₃ emissions after soil application of the solid fraction. *Waste Manag.*, v.167, pp. 39-45.
- Woods, S.W., Balfour, V.N., 2008. The effect of ash on runoff and erosion after a severe forest wildfire, Montana, USA. *International Journal of Wildland Fire* 17, 535–548. <https://doi.org/10.1071/WF07040>
- Xie, Y., Wang, H., Guo, Y., Wang, C., Cui, H., Xue, J., 2023. Effects of biochar-amended soils as intermediate covers on the physical, mechanical and biochemical behaviour of municipal solid wastes. *Waste Management* 171, 512–521. <https://doi.org/10.1016/j.wasman.2023.10.004>
- Zhu, T.X.; Zhu, A.X. 2014. Assessment of soil erosion and conservation on agricultural sloping lands using plot data in the semiarid hilly loess region of China. *Journal of Hydrology: Regional Studies*, n.2, p.69-83.

Chapter I: Water management strategies in a scarcity situation: a review about semiarid agriculture addressing climate change, soil degradation, water scarcity, and conservation practices for sustainable water management

Abstract: Climate change is a pressing global issue with profound impacts on agricultural productivity, food security, livelihoods, and public health, exacerbated by rising temperatures, irregular rainfall patterns, and extreme weather events. These challenges are particularly acute in semiarid regions, where they intensify water scarcity and quality issues, leading to declining groundwater levels and reduced water yield. To booster resilience in semiarid agriculture, mainly for smallholding farmers, integrating sustainable water management practices are imperative. This chapter addresses gaps in understanding principles, practices, and recent advancements aimed at enhancing resilience and adaptive capacity in semiarid agriculture amidst ongoing climate change. Implementing sustainable land management and proactive adaptation measures is crucial to mitigate these impacts. Integrated approaches, such as climate-smart agriculture, intercropping, and forage cactus cultivation, are highlighted as effective strategies to enhance productivity and resilience in dry areas. Moreover, advanced methods like drone imagery and thermography for assessing water stress in vegetation are discussed as vital tools for monitoring and optimizing agricultural practices in semiarid regions. Additionally, strategies like wastewater reuse combined with mulching show promise in controlling salinity, improving soil water content, crop yields, and water use efficiency.

Keyword: Water scarcity, alternative water sources, climate change, soil water conservation, semiarid

I.1 Introduction

The global population living in water-scarce areas has risen significantly from 2.04 to 2.36 billion between 2010 and 2020, with projections reaching 2.70 billion by 2030 (World Water, 2023; Dougaheh et al., 2023). Developing countries, heavily reliant on natural resources like water, soil, and pastures, are more vulnerable to climate change impacts than developed nations (Kalhori et al., 2023). These challenges are exacerbated by factors such as land degradation, droughts, and climate variability.

Climate, encompassing average temperature, rainfall, and humidity over specific periods, shapes environmental and socio-economic conditions (Karimi et al., 2020). Climate change and water scarcity pose significant risks to sustainable development across various domains, including environmental health, human well-being, food security, economic activities, natural resources, and infrastructure (Tillerad et al., 2023; Karimi et al., 2024). Strategies for water management, crucial in mitigating these risks, often inadvertently intersect with issues of insecurity and conflict (Leal Filho et al., 2022). Effective responses demand short, medium, and long-term adaptations within ecological and social systems (Karamidehkordi et al., 2024).

The sixth Sustainable Development Goal (SDG) prioritizes enhancing water quality, improving water-use efficiency, and reducing water degradation and scarcity globally (Mark et al., 2022). This goal aligns closely with SDG 2, focused on achieving food security and sustainable agriculture, and intersects with SDG 3 (Good health and well-being), SDG 12 (Responsible production and consumption), SDG 13 (Climate action), and SDG 15 (Life on land). Various environmental, economic, and engineering solutions have been proposed to mitigate water scarcity over the years.

Ingrao et al. (2023) emphasized the urgent need for interdisciplinary approaches to address water scarcity effectively. Public education, highlighted by Petruzzello et al. (2023), plays a pivotal role in water conservation efforts, alongside science-based policies for sustainable resource management initiatives. Scholarly attention to water sector adaptive capacity underscores the critical role of addressing water scarcity in shaping development pathways and climate adaptation (Siders, 2019).

The Brazilian Semiarid region, marked by multiple vulnerabilities in social, environmental, economic, and institutional dimensions, faces compounded challenges such as historical droughts, low water availability, and desertification exacerbated by soil degradation and human activities (Santos et al., 2023). These issues are compounded by factors like poor

governance, high poverty levels, economic stagnation, and inadequate sustainable development measures.

In semiarid regions, concerns about the long-term availability and quality of water resources are exacerbated by climate change impacts, reducing both surface water and groundwater availability (Karan et al., 2022). Rainfall variability and drought occurrences, coupled with high evapotranspiration rates, severely constrain water availability in surface reservoirs and shallow aquifers (Fontes Júnior and Montenegro, 2017). Groundwater, crucial for small-scale agriculture and domestic supply during droughts, faces over-exploitation and quality degradation due to unrestricted use (Patel et al., 2020; Houéménou et al., 2020). Sustainable strategies like wastewater reuse are increasingly advocated to enhance agricultural resilience and water sustainability in semiarid regions (Carvalho et al., 2020).

In addition to these aspects, exploring specific impacts on agricultural practices, case studies of successful water management strategies in semiarid regions, socio-economic implications, technological innovations, and their applications could provide valuable insights. This comprehensive approach would highlight effective practices for sustainable water management in semiarid areas affected by climate change and soil degradation.

1.2 Impact of climate change on agricultural production in the semiarid region

Agricultural production is mainly influenced by human-induced management interventions; however, climate plays an extremely important role (Ibrahin and Johansson, 2021). According to He et al. (2021), the climate affects the use of water in agriculture by altering key elements of crop growth, such as precipitation, evaporation and radiation, having a direct impact on the supply and demand of water for agriculture, indirectly affecting crop water productivity. Climate change, with increasing global carbon dioxide concentration and changes in temperature, precipitation and other climate parameters, plays a significant role in influencing agricultural productivity (Singh and Kumar, 2021). Conceptually, the term “climate change” refers to statistical changes in climate over a longer period due to natural variability or human activity (IPCC Climate Change Synthesis Report, 2021). This dynamic change remains a development challenge for many countries around the world, especially developing countries because of their dependence on climate conditions in rainfed agriculture (Aniah et al., 2019).

Among other effects, climate change has modified the trajectory of water within the hydrological cycle and the distribution of water across the landscape (Grusson et al., 2021).

Studies show that climate change impacts, among other components, soil water, evapotranspiration and discharge (Gul et al., 2023). These impacts are suggested to be strongly linked to changes in local precipitation and temperature patterns (Putnam and Broecker, 2017). According to Tesfaye et al. (2019), the combined effect of changing precipitation patterns and rising temperatures can negatively impact water availability and increase the occurrence of droughts. As a result, water resources may become temporarily stressed in some regions, particularly under drought conditions, and future changes in climate, land use, and water management could potentially have adverse effects on both the replenishment and exploitation of groundwater resources, exacerbating water stress. To mitigate the hydrological impacts and use water resources sustainability, it is crucial to understand the consequences of climate variability on hydrological responses.

According to Verrot and Destouni (2016), when rainwater reaches the soil surface, an initial partition occurs between surface runoff and infiltration, and any change in the frequency and intensity of rainfall can potentially influence the partition between these components. Grusson et al. (2021) emphasized that a change in the volume of infiltrated water will influence the soil moisture content and the evapotranspiration rate, consequently influencing the efficiency of water use by agricultural species.

According to Asante et al. (2021), many rural populations are sinking into poverty and deprivation in agricultural production and livestock farming because they are located in areas geographically sensitive to climate change and the spatial-temporal variability of climate parameters. This exposes them to the impacts and risks of climate change and variability. Given the current global population expansion, global agricultural water consumption may increase from the current 2,700 billion m³ to 3,200 billion m³ by 2050. By then, about 6 billion people, or 67% of the global population, will face water scarcity due to the extreme water extraction needed for agricultural production (UN, 2015).

In this regard, in the United Nations 2030 Agenda for Sustainable Development, member states agreed to take urgent action to combat climate change and develop national adaptation plans and other adaptation planning processes (UN, 2019). However, Ibrahim and Johansson (2021) highlight that it is not just climate change that is impacting the agricultural sector, noting that inadequate agricultural practices also constitute environmental risks and pose serious threats to the global climate.

1.3 Groundwater and the impact of climate change on future water supply in the semiarid region

In many parts of the world, groundwater is often considered the only source of perennial water available, especially in arid and semiarid regions, where it plays an important role in supplying families and cities during the dry season (Coelho et al., 2017). Despite the advantages in using water from alluvial valleys in the semiarid region, this resource is limited and has experienced qualitative and quantitative degradation in recent decades caused by anthropogenic (overexploitation and pollution) and natural (type of climate and global warming) restrictions (Bahir et al, 2020). In the semiarid region, specifically, the semiarid climate that extends across large portions of this area causes extreme water deficits due to low rainfall and high evapotranspiration (Montenegro and Ragab, 2010). These deficits can sometimes cause low water infiltration, which threatens aquifers (Coelho et al, 2017).

In addition to the observed increase in groundwater usage and rainfall, changes in surface conditions that affect runoff and infiltration processes are crucial (Peña-Arancibia et al., 2020). A comprehensive understanding of the hydro-saline dynamics of groundwater is essential to protect groundwater resources under conditions of climate change and increasing anthropogenic pressures. However, understanding the spatial and temporal patterns of groundwater geochemistry on a regional scale over a long period is challenging due to the lack of data and effective statistical approaches to characterize complex natural processes and anthropogenic activities (Yang et al., 2020).

Despite the advantages presented, the use of water from alluvial valleys in the semiarid region is susceptible to salt accumulation processes in both the unsaturated and saturated zones. This is due to the edaphoclimatic conditions of the region, which include high evaporation rates, poor spatial and temporal distribution of rainfall, and the presence of shallow soils, which favour the occurrence of intermittent rivers and streams (Montenegro and Montenegro, 2006). Therefore, water sources in these areas alternate according to the time of year between temporary rivers and shallow wells. In some rural communities in the northeastern semiarid region, groundwater from alluvial valleys represents the main water source.

A comprehensive understanding of the hydrossaline dynamics of groundwater is essential for protecting groundwater resources under conditions of climate change and increasing anthropogenic pressures (Zang et al., 2022). Assessing the quantity and quality of water has significant implications for the potential of groundwater as a resource and can indicate where negative impacts can be mitigated, as well as provide an assessment framework

for water conservation programs (Slama and Sebei, 2020). Reddy et al. (2019) highlight that groundwater quality varies in space and time (seasonal periods), influenced by aquifer depth and rock type in the area. Mohsine et al. (2023) also support the interference of spatial and temporal variables on water quality, emphasizing the importance of monitoring its variation. With this information, it is possible to define usage patterns and avoid problems arising from the improper management of irrigation water.

In turn, water quality is influenced by factors of natural and anthropogenic origin, where their constituents can act individually or jointly to deteriorate water. The main natural source influencing groundwater quality is the mineral composition of the rock formation (Khalid, 2019). Other natural processes include rock and soil weathering, atmospheric processes involving evapotranspiration, leaching of organic matter and nutrients present in the vadose zone, as well as precipitation events, mineral dissolution, natural recharge, and water-rock interaction (Abdel-Satar et al., 2017).

Among the anthropogenic factors that can affect water quality, changes in land use and land cover, as well as improper disposal of urban effluents, are notable (Kawo and Karuppanan, 2018). Another practice that can lead to contamination of these waters is agriculture, due to the extensive use of chemicals (Eltarabily et al., 2018). The residues of pesticides, insecticides, and fertilizers in large quantities alter the chemical characteristics of the water.

Therefore, monitoring water salinity is extremely important from both agricultural and environmental perspectives, as crops struggle to absorb and extract water under high soil salinity. From an analytical standpoint, addressing spatial and temporal variability can be efficient in describing and analyzing the true hydrochemical status of groundwater (Huang et al., 2018). Additionally, understanding the spatial and temporal patterns of groundwater geochemistry on a regional scale over an extended period is challenging due to the lack of data and effective statistical approaches to characterize complex natural processes and anthropogenic activities (Yang et al., 2020).

1.4 Importance of agricultural use of domestic effluent in agricultural production and the sustainable use

Agriculture is the main water consumer (~80-90%), while global water demand has tripled along with the substantial decline in freshwater resources since 1950, with a water collapse predicted by 2050 (UN-Water, 2018). The feasibility of new strategies to address the

demand for drinking water in areas affected by water scarcity has been widely studied. These strategies can use social technologies as an instrument, understood as a solution developed and/or applied in interaction with the local population, with a low cost, simple handling and replication capacity (Sousa et al., 2017).

Unconventional water (saline water, treated wastewater and grey water) has been used successfully in irrigated agriculture (cereals, oilseeds, date palm, perennial forage grasses, vegetables, forestry and aquaculture), suggesting that, if treated properly, this water can help rehabilitate marginal and degraded lands to meet demands (Hussain et al., 2018). For these reasons, unconventional water resources have been used as an alternative option to partially meet water demands with positive environmental effects on the hydrological cycle, water reserves, green cover and climate in the region (Hussain et al., 2019).

Another important aspect to be considered in productive coexistence with water scarcity is hydro-agricultural reuse, especially in semiarid regions, where the water supply is insufficient to meet demand and this limits agricultural practices, leaving the population vulnerable. In general, arid and semiarid regions are characterized by a lack of rainfall, high temperatures, strong sunlight and high evapotranspiration rates, which contribute to an unfavourable water balance (ANA, 2017). Locations with these characteristics present unstable hydrography in relation to water flow. In Brazilian semiarid regions, the water supply for human consumption in the municipality depends on surface springs, which mostly have intermittent flow regime (Maragon et al., 2020).

According to Magwaza et al. (2020), the association of sanitation and agriculture forms a closed cycle, where nutrients from treated sewage, essential for plant growth, are recovered and water is reused. Furthermore, political and ecological factors must be considered in the management of water resources, as highlighted by Silva et al. (2019). The use of wastewater for irrigation is a promising alternative to improve food production in semiarid areas. Furthermore, the use of treated effluents in irrigated agriculture has been considered an essential alternative for the efficient use of water, in addition to ensuring the sustainability of environmental systems, as it minimizes the volume of effluents discharged into water bodies (Carvalho et al., 2020).

Looking for technological alternatives to solve this problem, researchers from INSA's Water Resources Center developed the SARA technology (Environmental Sanitation and Water Reuse), which promotes the collection and treatment of household sewage, to produce an alternative source of water and nutrients in family farming (Mayer et al., 2019; Santos et al.,

2018). the following requirements need to be considered: i) ease of installation, operation and maintenance, ii) stability and operational efficiency, iii) compact dimensions and iv) affordable cost were considered. The single-family raw sewage collection and treatment system consists of a grease trap, an equalization tank, a UASB reactor and two polishing ponds operating in a sequential batch regime. The lagoons aim to decay bacteria from the coliform group, minimize water loss through evaporation and maintain nutrients. In this system, the objective is to reduce the organic load, achieve sanitary safety of the water produced and preserve nutrients, especially $\text{NH}_4\text{-N}$ and P, fundamental for the nutrition of selected crops. Initial results demonstrated an average BOD removal efficiency of 74% and was effective in removing pathogens and absence of helminth eggs, meeting the sanitary recommendations of the World Health Organization (WHO) for proper use. In general, the reuse system increased the availability of water on the property by $40 \text{ m}^3 \text{ year}^{-1}$, reducing expenses with mineral fertilization and water purchase.

Although wastewater irrigation has proven to be a valuable resource in agriculture, its use can result in excessive accumulation of nutrients in the soil, which is harmful to the environment (McLennon et al., 2020). In this way, Biochar is defined as the residue from subjecting organic matter (agricultural, industrial or domestic) to high temperatures under anaerobic conditions, also known as pyrolysis (Lehmann and Joseph, 2009). Some of the known transformative agronomic benefits of biochar include (i) increasing soil water holding capacity, reducing nutrient leaching with a simultaneous increase in nutrient availability, positive effects on cation exchange capacity and stimulation of soil microbial activity. Therefore, applying biochar to soil improves soil quality by retaining a greater proportion of the nutrients that flow through the soil and thus limiting nutrient loading in aquatic systems.

The use of waste or residual biomass for biochar production has received substantial attention due to its potential for carbon sequestration, waste management and environmental remediation of pollutants (Teshnizi et al., 2023). A fundamental characteristic of biochar is its sorption capacity resulting from its large surface area, negative surface charge and physical characteristics of the porous structure (Lima et al., 2021). Due to these properties, the combined effects are increased nutrient retention and use efficiency, as well as reduced leaching. The use of biochar in agriculture has become increasingly popular in recent decades; the main objective is to improve soil properties and structure and contribute to the sequestration of C by the soil.

Kaetzl et al. (2019) showed that biochar filters perform better than sand filters in removing faecal bacteria in wastewater due to larger surface areas and adsorption capacity,

demonstrated by lower contamination of plant water irrigation effluents. Obedece et al. (2022) highlighted the environmental importance of biochar in rural areas of developing countries in immobilizing aquatic contaminants for water reuse. The authors noted the immense potential of fruit peel waste to produce high-performance biochar as an alternative green carbonaceous material that can be applied to adsorb unwanted organic and inorganic constituents from wastewater as well as improve waste management.

1.5 Fires and soil degradation in semiarid environments: impact on agricultural expansion and erosion

Semiarid regions present a higher risk of fire, where hot and dry summers increase the frequency and occurrence of forest fires for a long period of the year, often motivated by anthropic management (Stavi, 2019). According to Lucas-Borja et al. (2022), adequate monitoring and management of semiarid landscapes affected by forest fires is necessary to reduce their effects on the hydrological response of the soil in the rainy season. Fires can have a significant impact on soil degradation in semiarid environments, particularly in areas undergoing agricultural expansion. Agricultural expansion is a major driver of deforestation and woodland degradation in dry areas. Clearing of native vegetation for cropland or pasture, combined with unsustainable management practices, accelerates soil erosion and desertification processes (Peplau et al, 2023).

According to Acheampong et al. (2019), the expansion of cultivated lands is often cited as the greatest cause of deforestation in dry tropical areas, with the rate of deforestation being around 8.5 to 10 times the rate of planting. This pressure on land use can lead to the degradation of woodlands, particularly in areas where the vegetation is fragile and prone to self-accelerating degradation processes. Soil properties and processes are often negatively affected in fire events, either directly by heating or indirectly through fires and destruction of plant diversity (Girona-García et al., 2019).

Ebel et al. (2022) evaluated the interference of land cover in the restoration of natural systems and in the hydraulic properties of the soil after fires. The authors highlight that in addition to the risks to human lives and the built environment, post-fire changes in runoff generation can impact water resources through harmful effects on water quality. In this aspect, Thomas et al. (2021), analyzing the effects of fires on sediment production in various fire scenarios, found that, in general, the catchment sediment load increased with the burned areas.

Wildfires can turn positive forest services into disadvantages, increasing surface runoff and soil erosion and damaging slopes and aquatic life in downstream rivers (Thomas et al., 2021).

1.6 Strategies for agriculture production with water scarcity

The adverse effects caused by human overuse of natural resources and inadequate land use management are accelerating land degradation and, in extreme cases, leading to desertification. This process is exacerbated by the impact of climate change on the natural cycles of Earth's systems, such as the water, carbon, and nitrogen cycles (Keesstra et al., 2018). In response, the United Nations has defined 17 Sustainable Development Goals, many of which aim to establish sustainable use of natural resources, ecosystem restoration, biodiversity conservation, carbon sequestration, and sustainable water resource management. A common solution to these challenges can be found in ecosystem rehabilitation, requiring new holistic approaches that are more time and cost-effective, addressing multiple issues efficiently (Keesstra et al., 2016). These actions to protect, sustainably manage, and restore natural or modified ecosystems address societal challenges in an adaptive and effective manner, simultaneously providing benefits to human well-being and biodiversity, and are known as "Nature-Based Solutions" (Hrabanski and Le Coq, 2022).

Recent studies suggest several adaptive measures to ensure the sustainability of agricultural systems, including the application of mulch from plant residues, crop rotation, use of resistant cultivars, soil conservation methodologies, water use efficiency measures, organic farming, reduction in the use of chemical fertilizers, herbicides, and pesticides, nutrient management, soil compaction control, and precision agriculture (NordGen, 2019; Costantini et al., 2020;).

Most of these adaptive measures are integrated and derived from the scope of Climate-Smart Agriculture (CSA), which serves as a guiding approach for transforming and reorienting agricultural systems. CSA effectively supports development and ensures food security in a changing climate. It aims to achieve three main objectives: sustainably increasing agricultural productivity and incomes; adapting and building resilience to climate change; and reducing and/or removing greenhouse gas emissions whenever possible (FAO, 2020).

Two methods that are especially relevant for adapting to climate change are Conservation Agriculture and the increasingly emerging Regenerative Agriculture. The term Conservation Agriculture refers to the combination of three pillars: minimal soil disturbance, permanent soil cover, and rotation and intensification of cover crops (FAO, 2019).

Regenerative Agriculture involves practices such as organic farming, composting, and mulching, with a primary focus on restoring the health of degraded soils by increasing soil organic matter (Rhodes, 2017).

At the national level, Brazil has been actively working on mitigating and adapting to climate change through the establishment of a Low Carbon Emission Economy in Agriculture. One of the sectoral plans developed in accordance with Article 3 of Decree 7,390/2010 aims to organize the planning of actions to adopt sustainable production technologies selected to meet the country's commitments to reduce greenhouse gas (GHG) emissions in the agricultural sector. This plan is known as the ABC Plan (Low Carbon Emission). The plan aims to improve the efficiency in the use of natural resources and increase the resilience of production systems and rural communities, enabling the adaptation of the agricultural sector to climate change. To achieve this, the plan encourages the adoption of Sustainable Production Systems that ensure the reduction of GHG emissions while simultaneously increasing producers' income, especially through the expansion of sustainable technologies such as the adoption of conservation practices (Brazil, 2012).

A conservationist approach suggested by Paye et al. (2022) to sustain agricultural production is the integration of cover crops into forage production systems. The authors hypothesized that, in addition to providing soil cover, this integration can deliver various ecosystem services, such as improving soil organic matter storage, nutrient cycling, water retention, and weed suppression. The application of surface mulch is an effective technique for conserving and optimizing the agricultural use of water and soil, especially in arid and semiarid areas (Montenegro et al., 2020). Mulch forms a physical insulating layer on the soil surface, which slows down and prevents the exchange of water and energy between the soil and the atmosphere (Liao et al., 2021). The effectiveness of mulch in controlling soil evaporation and increasing infiltration has been documented in several studies that will be detailed in the next section. Besides water conservation benefits, studies have shown that surface mulch also helps regulate soil temperature variations (Li et al., 2021), alters soil microbiology (Blaise et al., 2021), improves soil physical properties and fertility (Ramadhan, 2021), and affects crop growth, physiology, and ultimately yields and water use efficiency (Kaur et al., 2021).

1.7 Sustainability and efficiency in the use of conservation practices in semiarid regions

The climatic conditions in semiarid agroecological zones place significant demands on agricultural soil and water management. These areas are characterized by high daily

temperatures, strong winds, and low humidity, which limit soil moisture availability essential for crop growth (Aluku et al., 2021). Irrigation has been recommended as a technique to manage water availability for crops. However, if irrigation is insufficient during critical growth stages, it can drastically reduce productivity. Therefore, both excessive and inadequate water supply can severely impact crop growth.

Kaur et al. (2021) emphasized that enhancing water productivity is an imperative practice aimed at using the least amount of water possible to achieve higher yields. Agronomic interventions, such as mulching, prove to be a practical solution in maintaining optimal soil moisture and temperature regimes, promoting higher crop yields (Sekhon et al., 2020; Kaur et al., 2021). Furthermore, these techniques help prevent runoff, potentially increasing crop productivity, human and animal food security, income levels, and living standards (Aluku et al., 2021).

For these regions, Montenegro et al. (2020) found in their studies involving low-cost conservation practices the potential of mulching and barrier formation with Forage Cactus as effective treatments in reducing runoff and soil loss, while increasing soil moisture content. Therefore, these techniques are promising soil and water conservation methods for semiarid environments. Furthermore, the cultivation of Forage Cactus along with sorghum has been widely promoted in the semiarid region due to its nutritional contribution and low production cost (Jardim et al., 2021). The yield, quality, competition, and economic benefit of the intercropping of Forage Cactus and millet were evaluated by Souza et al. (2019) under covered and uncovered soil conditions, where the intercropping resulted in good economic returns. However, competitive ability parameters demonstrated that Forage Cactus exerted strong dominance over the millet crop, reducing efficiency and affecting certain phases of the cycle.

Conservation tillage practices have been widely promoted to stimulate the formation and preservation of stable water aggregates, leading to improved soil water availability. They are also advocated for their potential to promote the accumulation of organic matter in the soil surface layer and nutrient availability, thus increasing biomass and microbial activity (Zhang et al., 2022). Santos et al. (2008), evaluating the performance of water conservation techniques in bean cultivation, such as contour planting with stone rows, level planting, mulching with bean straw, bare soil, and soil with native vegetation cover (caatinga) in plots in the semiarid region of Pernambuco, found that losses of organic carbon were significantly higher under non-conservation soil management conditions.

Investigating at both spatial and temporal scales, Montenegro et al. (2019) assessed the distribution of soil moisture near the surface and evaluated the impact of soil conservation techniques on reducing surface runoff. They utilized small-scale experimental plots under natural rainfall conditions located in the Alto Ipanema River Basin, Brazil, with different soil cover conditions (bare soil, natural vegetation cover, mulch, Forage Cactus). Their findings indicated that both Forage Cactus rows and soil covers yielded promising hydrological results.

Lima et al. (2020) examined the importance of mulching and perennial unconventional oilseed species in controlling soil erosion in erosion plots under natural rainfall conditions. They found that soil cover led to higher soil moisture retention and lower values of surface runoff and soil loss. The development of oilseed structure reduced the direct impact of raindrops on the soil, resulting in reduced soil loss compared to bare soil.

At the scale of experimental watersheds, Silva Júnior et al. (2011), Melo and Montenegro (2015), and Lopes et al. (2019) conducted extensive compilations of soil profile moisture measurements for different vegetation cover conditions to support management plans and enable more adequate calibration and validation of numerical models at different scales. Among the main findings of the latter study, it is worth highlighting the analysis of temporal stability of spatially distributed measurements, capable of optimizing sampling grids.

Ebel et al. (2022) assessed the interference of soil cover on the reestablishment of natural systems and soil hydraulic properties after wildfires. The authors emphasized that besides risks to human lives and the built environment, post-fire changes in runoff generation can impact water resources through detrimental effects on water quality. In this regard, Thomas et al. (2021), analyzing the effects of fires on sediment production in various fire scenarios, found that sediment yield generally increased with burned areas. Forest fires can turn positive forest services into disadvantages, increasing surface runoff and soil erosion and damaging slopes and aquatic life downstream (Thomas et al., 2021).

Vieira et al. (2018) propose that mitigation measures can be applied to help reduce the negative effects of post-fire water erosion, both on-site and off-site. Among the existing techniques, the application of surface mulch on burned soil is considered effective in reducing post-fire soil erosion. The authors explain that this is mainly because mulch provides surface coverage to the soil before vegetation regeneration, thereby minimizing raindrop detachment while enhancing soil stabilization. In this regard, Prats et al. (2018) conducted rainfall simulations in the laboratory to investigate the influence of post-fire soil cover layers and erosion flow concentration under five soil surface conditions (bare soil, with a protective layer

of charcoal, ash, stones, and a combination of treatments), simulating field conditions under three rainfall intensities.

Regarding the application of wastewater via irrigation, Carvalho et al. (2021) investigated the combined performance of irrigation with treated sewage and mulching on forage sorghum and soil attributes in Northeast Brazil. They found that mulching led to a 24% increase in productivity compared to areas where conservation practices were not implemented, potentially controlling salinity while contributing to greater organic matter incorporation. The authors highlighted that irrigation with treated sewage had no negative agronomic impacts on the soil, as typical rainfall events in the Brazilian semiarid region allowed effective leaching of salt in shallow sandy soils. Almeida et al. (2021), evaluating the impact of wastewater use and sewage sludge application as soil cover on soil attributes in an irrigated corn plantation in the northeastern Brazilian semiarid region, observed that the presence of sludge reduced salt content and promoted an increase in soil organic matter content, thereby reducing the risk of salinization.

In addition to optimizing water use, soil conservation practices are being utilized to reduce runoff and soil losses, prevent soil degradation, and improve the fertility and productivity of agricultural soils. This subject has been addressed based on detailed hydrometeorological measurements, monitoring campaigns, and modeling activities in well-instrumented experimental rural basins, such as those belonging to the Hydrological Network of the Brazilian Semiarid Region (REHISA) (Santos et al., 2010; Montenegro et al., 2019; Lopes et al., 2019). Such field studies under natural rainfall provide an excellent opportunity to enhance understanding of the real impact of different agricultural conservation practices on water security and soil protection. However, collecting representative data on surface runoff and soil loss under natural conditions in semiarid environments is highly challenging, as the number of rainfall runoff events is typically very limited (Montenegro et al., 2020). Moreover, field studies, especially those under natural rainfall conditions, are typically time-consuming and resource-intensive, as they often require many years to yield representative results.

Rainfall simulators have been applied in both laboratory-based and field studies, offering the advantage of allowing controlled and reproducible rainfall events of varying intensity and duration (Iserloh et al., 2021). Abrantes et al. (2018) used a rainfall simulator to assess the conditions for accurate measurement of shallow flow velocities, as this information is crucial for understanding and modeling sediment and pollutant transport dynamics by overland flow. The authors compared traditional and well-established techniques of dye and

salt tracer with the newer thermal marker technique in estimating shallow flow velocities, as well as evaluating and estimating Reynolds and Froude numbers, flow velocity and slope, and soil roughness. The thermal tracer allowed efficient measurement of average flow velocities in space.

Liu et al. (2019) evaluated the effects of four different rainfall intensities and soil slopes on runoff production and their impacts on soil conservation. The authors estimated the effects on soil microtopography under conservation management compared to conventional tillage, as well as on surface runoff and soil loss under different rainfall intensities and slopes. Using rainfall simulation, they could quantify the effects of changes in rill geometry on erosion and soil conservation under various rainfall events and develop management strategies for areas under similar conditions.

Montenegro et al. (2020) investigated the performance of mulching with coconut husk powder (*Cocos nucifera* L.) and vegetative barrier with cactus palm at different angles (*Opuntia ficus indica* Mill.) as soil and water conservation techniques in a laboratory soil plot under simulated rainfall. The simulations included uniform patterns of both advanced and delayed rainfall, generating runoff hydrographs and soil loss monitored at the downstream end of the trough. The results indicate that mulching with coconut husk powder and the cover crop of cactus palm were effective in reducing runoff and soil loss while increasing soil moisture content, making them suitable soil and water conservation techniques for semiarid environments.

Parhizkar et al. (2021) analyzed the efficiency of rice straw cover on hydrological variables of loamy clay soil under high-intensity and low-frequency simulated rainfall events, in three slope length conditions. In their investigation, the authors concluded that rice straw was efficiently used as an organic soil conditioner, reducing soil erosion and surface runoff, and consequently decreasing the risk of soil degradation. They encourage further research, however, to analyze the scaling up of the hydrological effects from plot mulching to the slope scale.

1.8 Advanced vegetation monitoring methods

Water stress in crops severely disrupts crop growth and reduces yields (Jiang et al., 2020). The need to optimize water use, especially in arid and semiarid regions where water supply is scarce, has prompted researchers to develop new monitoring technologies. Drought

status is typically described by soil moisture and water stress indices, but plant water status is regulated by both soil moisture and atmospheric evaporation demand (Liu et al., 2022). Thus, relying solely on soil moisture to assess drought impacts on plants can be misleading (Wilson et al., 2020).

Among the numerous technologies used in agriculture, drones, infrared thermography, robots, hyperspectral and fluorescence imaging, and wireless sensor networks, plant-based methods are crucial for assessing plant health (Parihar et al., 2021). Authors such as Brunini and Turco (2016) suggested that canopy temperature is a parameter useful for detecting biotic and abiotic plant stress symptoms, acting as a good indicator of water stress and directly influencing plant metabolism. Canopy temperature reflects the thermal state of the crop and is closely related to stomatal conductance and crop water use efficiency (Huo et al., 2019). According to Gutiérrez et al. (2018), plants lose significant amounts of water through their stomatal pores while absorbing CO₂ for photosynthesis. When water availability decreases, stomata close to conserve water, reducing evaporative cooling and increasing leaf temperature. Thus, thermal imaging can be employed to measure leaf temperature responses to water stress conditions and infer impacts on transpiration and stomatal behavior.

Infrared thermography detects and maps the spatial temperature profile of an object/body using its emitted infrared radiation (Parihar et al., 2021). Infrared thermography is suitable due to its non-destructive nature, providing a thermal profile of an object/body quickly and enabling post-examination of the image. For canopy temperature monitoring, Valím et al. (2019) calculated vine water stress indices from thermal images of canopies, emphasizing the importance of non-destructive monitoring using proximity thermal sensors for vegetative parameters monitoring. Liu et al. (2020) also highlighted the use of thermography as an effective and non-destructive method to study canopy characteristics. These methods enable a more comprehensive understanding of vegetation dynamics by considering temperature variations in addition to spectral characteristics. Integrating thermography into monitoring protocols can enhance the accuracy and depth of information gathered, allowing for a more holistic assessment of vegetation health and responses to environmental changes. By combining thermal data with existing monitoring techniques, researchers can gain valuable insights into ecosystem functioning and resilience, contributing to more effective natural resource management strategies.

Leaf surface temperatures under wet and dry reference conditions are also commonly used to normalize temperature measurements to current environmental conditions and

subsequently calculate a crop water stress index, aiding in irrigation scheduling for various crops (Gutiérrez et al., 2018; Poirier-Pocovi et al., 2021). Moreover, thermal imaging provides temperature measurements across the entire canopy, offering potential for rapid spatiotemporal measurements and assessment of water status throughout the plant (Gutiérrez et al., 2018). According to Camoglu et al. (2021), another critical aspect is that temperatures obtained with infrared thermometers are at leaf level and at the point of measurement only, providing no information about the entire area, whereas thermal cameras can determine the temperature of all items in the image individually. This provides valuable data on spatial temperature distribution, enabling separation of the desired item's temperature from images.

Sun et al. (2019) used a multispectral system to accurately retrieve leaf chlorophyll and moisture content, finding that chlorophyll fluorescence effectively reflects photosynthesis and crop water under water stress. Ihuoma and Madramootoo (2017) emphasized that the Normalized Difference Vegetation Index (NDVI) can be applied to detect water stress in plants. In recent years, several salinity indicators have been developed to detect soil salt-affected areas from satellite imagery. In particular, Multispectral Instrument (MSI) imagery has already proven to be a promising tool for assessing soil salinity and, ultimately, for producing electrical conductivity (EC) maps. Gerardo and de Lima (2022) explored the assessment of soil salinity in irrigated rice fields using two types of multispectral-based indices: vegetation indices (such as Normalized Difference Vegetation Index, Green Normalized Difference Vegetation Index, Generalized Difference Vegetation Index, and Soil Adjusted Vegetation Index) and salinity indicators based on visible and near-infrared bands (Normalized Difference Salinity Index) and shortwave infrared bands (Salinity Index ASTER). Their study focuses on the Lower Mondego Valley in Central Portugal during the period 2017–2018. The authors emphasized that these salinity indices are effective for mapping soil salinity and serve as valuable tools for assessing salinity issues in rice cultivation areas.

1.9 Conclusion

Semiarid agriculture faces daunting challenges exacerbated by climate change, soil degradation, and water scarcity. Conservation practices such as conservation agriculture, water harvesting, and efficient irrigation play a pivotal role in sustainable water management and enhancing agricultural productivity. These strategies bolster farmers' resilience against climate variability and ensure long-term sustainability in semiarid regions. Prioritizing climate-resilient water management practices is crucial to secure dependable water access, reduce wastage, and

enhance efficiency, thereby supporting smallholder farmers and fostering long-term food security.

Additionally, the implementation of conservation practices, advanced monitoring methods, reduction of wildfires, and post-burn management strategies that enable ash reuse are essential. These measures contribute significantly to mitigating environmental impact, improving soil fertility, and optimizing resource utilization in semiarid agricultural landscapes.

References

- Abdel-Satar, A. M.; Al-Khabbas, M.H.; Alahmad, W.R.; Yousef, W.M.; Alsomadi, R.H.; Iqbal, T. Quality assessment of groundwater and agricultural soil in Hail region, Saudi Arabia. *Egyptian Journal of Aquatic Research*, v.43, n.1, p.55–64, 2017.
- Abrantes, J.R.C.B., Prats, S.A., Keizer, J.J., Lima, J.L.M.P. De, 2018. Soil & Tillage Research Effectiveness of the application of rice straw mulching strips in reducing runoff and soil loss: Laboratory soil flume experiments under simulated rainfall 180, 238–249. <https://doi.org/10.1016/j.still.2018.03.015>
- Acheampong, E. O., Macgregor, C. J., Sloan, S., & Sayer, J. (2019). Deforestation is driven by agricultural expansion in Ghana's forest reserves. *Scientific African*, 5. <https://doi.org/10.1016/j.sciaf.2019.e00146>
- Almeida, T. A. B.; Montenegro, A. A. A.; Carvalho, A. A.; Tabosa, J.N. 2021. Variabilidade espacial do solo e da cultura em milho irrigado com efluente doméstico. *DYNA*, v. 88, n. 219, p.111-117. DOI: 10.15446/dyna.v88n219.92874.
- ANA, Conjuntura dos Recursos Hídricos no Brasil Agência Nacional de Águas , Brasília, Brasil, 2017. DOI: 10.7868 / s0016675817100046
- Aniah, P., Kaunza-Nu-Dem, M.K., Ayembilla, J.A., 2019. Smallholder farmers' livelihood adaptation to climate variability and ecological changes in the savanna agro ecological zone of Ghana. *Heliyon* 5, e01492. DOI: 10.1016/j.heliyon.2019.e01492
- Asante, F.; Guodaar, L.; Arimiyaw, S. 2021. Climate change and variability awareness and livelihood adaptive strategies among smallholder farmers in semiarid northern Ghana. *Environmental Development*, n.39, p.1-14. DOI: 10.1016/j.envdev.2021.100629
- Bahir, M.; Ouhamdouch, S.; Ouazar, D.; El Moçayd, N. Climate change effect on groundwater characteristics within semiarid zones from western Morocco, v.11, p.1-14, 2020.

- Blaise, D.; Velmourougane, K.; Santosh, S.; Manikandan, A. 2021. Intercrop mulch affects soil biology and microbial diversity in rainfed transgenic Bt cotton hybrids. *Science of the Total Environment*, n. 794, p.1-10.
- Brazil. 2012. Ministério da Agricultura, Pecuária e Abastecimento. Plano setorial de mitigação e de adaptação às mudanças climáticas para a consolidação de uma economia de baixa emissão de carbono na agricultura: plano ABC (Agricultura de Baixa Emissão de Carbono) / Ministério da Agricultura, Pecuária e Abastecimento, Ministério do Desenvolvimento Agrário, coordenação da Casa Civil da Presidência da República. Brasília: MAPA/ACS, 173 p.
- Brunini, R.G. e Turco, J. E. P. 2016. Water stress indices for the sugarcane crop on different irrigated surfaces. *Revista Brasileira de Engenharia Agrícola e Ambiental*, v.20, n.10, p.925-929, DOI: 10.1590/1807-1929/agriambi.v20n10p925-929
- Camoglu, G.; Demirel, K.; Kahriman, F.; Akcal, A.; Nar, H.; Boran, A.; Eroglu, I.; Genc, L. 2021. Discrimination of water stress in pepper using thermography and leaf turgor pressure probe techniques. *Agricultural Water Management*, n.254, p.1-10. DOI: 10.1016/j.agwat.2021.106942
- Carvalho, A. A.; Montenegro, A.A.A.; de Lima, J.L.M.P.; Silva, T.G.F.; Pedrosa, E.M.R., Almeida, T.A.B. 2021. Coupling Water Resources and Agricultural Practices for Sorghum in a Semiarid Environment. *Water*, n.13, v.16, p.1-25. DOI: 10.3390/w13162288
- Carvalho, A. A.; Montenegro, A. A. A.; Tabosa, J. N.; Almeida, T. A. B.; Silva, A. G. O.; Silveira, A. V. M. 2020. Reúso hidroagrícola: uma solução para convivência com a escassez hídrica no Sertão e Agreste pernambucano. *Journal of Environmental Analysis and Progress*, v.5, n.2, p.140-150. DOI: 10.24221/jeap.5.2.2020.2841.140-150
- Coelho, V. H. R.; Montenegro, S. M. G. L.; Almeida, C. N.; Silva, B. B.; Oliveira, L. M. M.; Gusmao, A. C. V.; Freitas, E. S.; Montenegro, A. A. A. Alluvial groundwater recharge estimation in semiarid environment using remotely sensed data. *Journal of Hydrology*, v. 548, p.1-15, 2017.
- Costantini, E.A.C.; Antichi, D.; Almagro, M.; Hedlund, K.; Sarno, G.; Virto, I. 2020. Local adaptation strategies to increase or maintain soil organic carbon content under arable farming in Europe: inspirational ideas for setting operational groups within the European innovation partnership. *Journal of Rural Studies*, n.79, p. 102-115.

- Ebel, B. A.; Moody, J. A.; Martins, B. A. Post-fire temporal trends in soil-physical and -hydraulic properties and simulated runoff generation: Insights from different burn severities in the 2013 Black Forest Fire, CO, USA. *Science of the Total Environment*, n.802, p.1-14, 2022. DOI: 10.1016/j.scitotenv.2021.149847
- Eltarabily et al., 2018).
- Eltarabily, M. G.; Negm, A.M.; Yoshimura, C.; Abdel-Abdel-Fattah, S.; Saavedra, O.C. Quality Assessment of Southeast Nile Delta Groundwater for Irrigation. *Water Resources*, v. 45, n. 6, p.975–991, 2018.
- FAO. Climate-smart agriculture. Food and agriculture organization of the united Nations. 2020. Disponível em: <http://www.fao.org/climate-smart-agriculture/en/>
- FAO. Three principles of conservation agriculture. 2019. Food and agriculture organization of the United Nations. Disponível em: <http://www.fao.org/emergencies/fao-in-action/stories/stories-detail/en/c/216752/>
- Gerardo, R. De Lima, I.P. Sentinel-2 Satellite Imagery-Based Assessment of Soil Salinity in Irrigated Rice Fields in Portugal. *Agriculture*, [S. l.], v. 12, n. 9, p. 1490, 2022. DOI: 10.3390/agriculture12091490.
- Girona-García, A.; Ortiz-Perpiñá ,O.; Badía-Villas, D. Dinâmica dos estoques de carbono do solo após queima prescrita para restauração de pastagens em matagais dos Pirineus Centrais (NE-Espanha). *J. Ambiente. Gerenciar*, n.233, p.695–705, 2019.
- Grusson, Y.; Wesström, I.; Svedbeg, E.; Joel, A. Influence of climate change on water partitioning in agricultural watersheds: Examples from Sweden. *Agricultural Water Management*, n.249, p.1-18, 2021. DOI: 1 0.1016/j.agwat.2021.106766
- Gul, N., Salam, H. A., & Ashraf, M. (2023). Potential Impacts of Climate Change Using Long-Term Historical Climate Data on Evapotranspiration (ET) and Groundwater Contribution to Wheat and Cotton Crop. *International Journal of Environment and Climate Change*, 13(7), 142–159. <https://doi.org/10.9734/ijecc/2023/v13i71861>
- He, G., Geng, C., Zhao, Y., Wang, J., Jiang, S., Zhu, Y., Wang, Q., Wang, L., Mu, X., 2021. Food habit and climate change impacts on agricultural water security during the peak population period in China. *Agricultural Water Management* 258, 107211. <https://doi.org/10.1016/j.agwat.2021.107211>
- Hrabanski, M.; Le Cop, J. F. Climatisation of agricultural issues in the international agenda through three competing epistemic communities: Climate-smart agriculture,

- agroecology, and nature-based solutions. *Environmental Science and Policy*, n.129, p.311-320, 2022. DOI: 10.1016/j.envsci.2021.10.022
- Huo, Z.L. Li, Z. Xing. 2019. Temperature/emissivity separation using hyperspectral thermal infrared imagery and its potential for detecting the water content of plants. *Int. J. Remote Sens.*, 40, 1672-1692.
- Hussain, M. I.; Muscolo, A.; Farooq, M.; Ahmad, W. Sustainable use and management of non-conventional water resources for rehabilitation of marginal lands in arid and semiarid environments. *Agricultural Water Management*, n.221, p.462-476, 2019. DOI: 10.1016/j.agwat.2019.04.014
- Hussain, R.; Ghosh, K.K.; Ravi, K. (2021). Impact of biochar produced from hardwood of mesquite on the hydraulic and physical properties of compacted soils for potential application in engineered structures. *Geoderma*, v.385, p.1-13.
- Ihuoma, S.O., Madramootoo, C.A., 2017. Recent advances in crop water stress detection. *Comput. Electron. Agric.* 141, 267–275. <https://doi.org/10.1016/j.compag.2017.07.026>.
- IPCC - The Intergovernmental Panel on Climate Change, 2021. Special report on climate change and land.
- Iserloh, T.; Isidoro, J. M. G. P.; de Lima, J. L. M. P.; Marzen, M.; de Lima, M. I. P.; Green, D.; Seeger, M.; Ries, J.B. Rumo à harmonização na simulação de chuva, EGU General Assembly 2021, online, 19–30 de abril de 2021, EGU21-5667, DOI: 10.5194/egusphere-egu21-5667, 2021.
- Jiang, T., Dou, Z., Liu, J., Gao, Y., Malone, R.W., Chen, S., Feng, H., Yu, Q., Xue, G., He, J., 2020. Simulating the influences of soil water stress on leaf expansion and senescence of winter wheat. *Agric. For. Meteorol.* 291, 108061 <https://doi.org/10.1016/j.agrformet.2020.108061>.
- Kaetzl, K.; Lubken, M.; Uzun, G.; Gehring, T.; Nettmann, D.; Stenchly, K.; Wichern, M. 2019. On-farm wastewater treatment using biochar from local agroresidues reduces pathogens from irrigation water for safer food production in developing countries. *Science of The Total Environment*, v.682, p.601-610. DOI: 10.1016/j.scitotenv.2019.05.142
- Kaur, L.; Kaur, A.; Brar, A. S. Water use efficiency of green gram (*Vigna radiata* L.) impacted by paddy straw mulch and irrigation regimes in north-western India. *Agricultural Water Management*, n.258, p. 1-8, 2021. DOI: /10.1016/j.agwat.2021.107184

- Kawo, N. S.; Karuppannan, S. Groundwater quality assessment using water quality index and GIS technique in Modjo River Basin, central Ethiopia. *Journal of African Earth Sciences*, v. 147, p. 300–311, 2018.
- Keesstra, S.; Nunes, J.; Novara, A.; Finger, D.; Avelar, D.; Kalantari, Z.; Cerdà, A. The superior effect of nature-based solutions in land management for enhancing ecosystem services. *Science of the Total Environment*, p.997-1009, 2018. DOI: 10.1016/j.scitotenv.2017.08.077
- Keesstra, S.D., Bouma, J., Wallinga, J., Tittonell, P., Smith, P., Cerdà, A., Montanarella, L., Quinton, J.N., Pachepsky, Y., van der Putten, W.H., Bardgett, R.D., Moolenaar, S., Mol, G., Jansen, B., Fresco, L.O., 2016. The significance of soils and soil science towards realization of the United Nations Sustainable Development Goals. *Soil*, n.2, p.111–128. DOI: 10.5194/soil-2-111-2016.
- Khalid, S. An assessment of groundwater quality for irrigation and drinking purposes around brick kilns in three districts of Balochistan province, Pakistan, through water quality index and multivariate statistical approaches. *Journal of Geochemical Exploration*, v. 197, p. 14–26, 2019.
- Leal Filho, W., Totin, E., Franke, J. A., Andrew, S. M., Abubakar, I. R., Azadi, H., Nunn, P. D., Ouweneel, B., Williams, P. A., & Simpson, N. P. (2022). Understanding responses to climate-related water scarcity in Africa. In *Science of the Total Environment* (Vol. 806). Elsevier B.V. <https://doi.org/10.1016/j.scitotenv.2021.150420>
- Khalid, S. An assessment of groundwater quality for irrigation and drinking purposes around brick kilns in three districts of Balochistan province, Pakistan, through water quality index and multivariate statistical approaches. *Journal of Geochemical Exploration*, v. 197, p. 14–26, 2019.
- Leal Filho, W., Totin, E., Franke, J. A., Andrew, S. M., Abubakar, I. R., Azadi, H., Nunn, P. D., Ouweneel, B., Williams, P. A., & Simpson, N. P. (2022). Understanding responses to climate-related water scarcity in Africa. In *Science of the Total Environment* (Vol. 806). Elsevier B.V. <https://doi.org/10.1016/j.scitotenv.2021.150420>
- Liao, Y.; Cao, H.; Liu, X.; Li, H.; Hu, Q.; Xue, W. By increasing infiltration and reducing evaporation, mulching can improve the soil water environment and apple yield of orchards in semiarid areas. *Agricultural Water Management*, n. 253, p.1-12, 2021. DOI: 10.1016/j.agwat.2021.106936

- Lima, C.A.; Montenegro, A.A.A.; Lima, J.L.P.M.; Almeida, T.A.B.; Santos, J.C.N. Uso de coberturas alternativas do solo para o controle das perdas de solo em regiões semiáridas. *Engenharia Sanitária e Ambiental*, v.25, n.3, p.531-542, 2020. DOI: 10.1590/s1413-41522020193900
- Lima, J.R. de S., De Goes, M. da C.C., Hammecker, C., Antonino, A.C.D., De Medeiros, É.V., De Sá Barretto Sampaio, E.V., De Barros Silva Leite, M.C., Da Silva, V.P., De Souza, E.S., Souza, R., 2021. Effects of poultry manure and biochar on acrisol soil properties and yield of common bean. a short-term field experiment. *Agriculture (Switzerland)* 11, 1–11. <https://doi.org/10.3390/agriculture11040290>
- Liu, Y.; Xin, Y.; Xie, Y.; Wang, W. Effects of slope and rainfall intensity on runoff and soil erosion from furrow diking under simulated rainfall. *Catena*, n.177, p.92-100, 2019. DOI: 10.1016/j.catena.2019.02.004
- Liu, L., Gao, X., Ren, C., Cheng, X., Zhou, Y., Huang, H., Zhang, J., & Ba, Y. (2022). Applicability of the crop water stress index based on canopy–air temperature differences for monitoring water status in a cork oak plantation, northern China. *Agricultural and Forest Meteorology*, 327. <https://doi.org/10.1016/j.agrformet.2022.109226>
- Liu, M., Guan, H., Ma, X., Yu, S., & Liu, G. (2020). Recognition method of thermal infrared images of plant canopies based on the characteristic registration of heterogeneous images. *Computers and Electronics in Agriculture*, 177. <https://doi.org/10.1016/j.compag.2020.105678>
- Lopes, I.; Montenegro, A.A.A.; Lima, J.L.M.P. Performance of Conservation Techniques for Semiarid Environments: Field Observations with Caatinga, Mulch, and Cactus Forage Palma. *Water*, n.11, p.1-15, 2019. DOI:10.3390/w11040792
- Lucas-Borja, M.E; Plaza-Álvarez, P.A.; Uddin, S.M.M.; Parhizkar, M.; Zema, D.A. Short-term hydrological response of soil after wildfire in a semiarid landscape covered by *Macrochloa tenacissima* (L.) Kunth. *Journal of Arid Environments*, v.198, 2022.
- Magwaza, S. T.; Magwaza, L.S.; Odindo, A.O.; Mditshwa, A. Hydroponic technology as decentralised system for domestic wastewater treatment and vegetable production in urban agriculture: A review. *Science of the Total Environment*. n.698, 2020. DOI: 10.1016 / j.scitotenv.2019.134154
- Maragon, B. B.; Silva, T. A.; Calijuri, M. L.; Alves, S. C.; Santos, V. J.; Oliveira, A. P. S. Reuse of treated municipal wastewater in productive activities in Brazil's semiarid regions.

- Journal of Water Process Engineering, v.37, p.1-9, 2020. DOI: 10.1016/j.jwpe.2020.101483
- Mayer, M. C.; Medeiros, S. S., Batista, M.D.; Barbosa, R. A.; Lambais, G. R.; Santos, S. L.; Haandel, A. V. Tratamento de esgoto na zona rural visando ao reúso agrícola no semiárido brasileiro. Revista DAE, v.69, n.229, pp. 104-114 | Ed. Esp. Mar. 2021. <https://doi.org/10.36659/dae.2021.023>
- McLennon, E., Solomon, J.K.Q., Neupane, D., Davison, J., 2020. Biochar and nitrogen application rates effect on phosphorus removal from a mixed grass sward irrigated with reclaimed wastewater. Science of the Total Environment 715, 137012. <https://doi.org/10.1016/j.scitotenv.2020.137012>
- Melo, R.O., Montenegro, A.A.A. Dinâmica temporal da umidade do solo em uma bacia hidrográfica no semiárido Pernambucano. Revista Brasileira de Recursos Hídricos, n.20, v.2, p.430-441, 2015.
- Mohsine, I., Kacimi, I., Abraham, S., Valles, V., Barbiero, L., Dassonville, F., Bahaj, T., Kassou, N., Touiouine, A., Jabrane, M., Touzani, M., el Mahrad, B., & Bouramtane, T. (2023). Exploring Multiscale Variability in Groundwater Quality: A Comparative Analysis of Spatial and Temporal Patterns via Clustering. Water (Switzerland), 15(8). <https://doi.org/10.3390/w15081603>
- Montenegro, A. A. A.; Montenegro, S. M. G. L. Variabilidade espacial de classes de textura, salinidade e condutividade hidráulica de solos em planície aluvial. Revista Brasileira de Engenharia Agrícola, v.10, p.30-37, 2006.
- Montenegro, A. A. A.; Ragab, R. Hydrological response of a Brazilian semiarid catchment to different land use and climate change scenarios: modeling study. Hydrological Processes, v.24, p.2705-2723, 2010.
- Montenegro, A. A. A.; Lopes, I.; Carvalho, A. A.; Lima, J. L. M. P.; Souza, T. E. M. S.; Araújo, H. L.; Lins, F. A. C.; Almeida, T. A. B.; Montenegro, H. C. L. A. Spatio Temporal Soil Moisture Dynamics and Runoff under Different Soil Cover Conditions in a Semiarid Representative Basin in Brazil. Advances in Geosciences, v.48, n.19, p.19–30, 2019. DOI: 10.5194/adgeo-48-19-2019
- Montenegro, A.A.; Almeida, T.A.; Lima, C.A.; Abrantes, J.R.; de Lima, J.L. Evaluating Mulch Cover with Coir Dust and Cover Crop with Palma Cactus as Soil and Water Conservation Techniques for Semiarid Environments: Laboratory Soil Flume Study

- under Simulated Rainfall. *Hydrology*, v.7, n.61, 2020. DOI: 10.3390/hydrology7030061
- NordGen, Nordic Agriculture and Climate Change: Mitigation and Adaptation Recommendations from Leading Researchers and Private Companies within the Nordic Plant Breeding. The Nordic Genetic Resource Centre. NordGen Publication Series (2019)
- Parhizkar, M.; Shabanpour, M.; Lucas-Borja, M. E.; Zema, D. A.; Li, S.; Tanaka, N.; Cerdà, A. Effects of length and application rate of rice straw mulch on surface runoff and soil loss under laboratory simulated rainfall. *International Journal of Sediment Research*, n.36, p.468-478, 2021. DOI: 10.1016/j.ijsrc.2020.12.002
- Parihar, G.; Saha, S.; Giri, L. I. Application of infrared thermography for irrigation scheduling of horticulture plants. *Smart Agricultural Technology*, n.1, p.1-16, 2021. DOI: 10.1016/j.atech.2021.100021
- Paye, W. S.; Ghimire, R.; Acharya, P.; Nilahyane, A.; Mesbah, A. O.; Marsalis, M. A. Cover crop water use and corn silage production in -semiarid irrigated conditions. *Agricultural Water Management*, n.260, p.1-10, 2022. DOI: 10.1016/j.agwat.2021.107275
- Penã-Arancibia, J.L.; Mainuddin, M.; Ahmad, M.D.; Hodgson, G.; Murad, K.F.I.; Ticehurst, C.; Maniruzzaman, M.; Mahboob, M.G.; Kirby, J.M. Groundwater use and rapid irrigation expansion in a changing climate: Hydrological drivers in one of the world's food bowls. *Journal of Hydrology*, v.581, p.1-16, 2020. <https://doi.org/10.1016/j.jhydrol.2019.124300>
- Peplau, T., Poeplau, C., Gregorich, E., & Schroeder, J. (2023). Deforestation for agriculture leads to soil warming and enhanced litter decomposition in subarctic soils. *Biogeosciences*, 20(5), 1063–1074. <https://doi.org/10.5194/bg-20-1063-2023>
- Poirier-Pocovi, M.; Volder, A.; Bailey, B. N. Modeling of reference temperatures for calculating crop water stress indices from infrared thermography. *Agricultural Water Management*, n.233, p.1-13, 2020. DOI: /10.1016/j.agwat.2020.106070
- Prats, S.A., Abrantes, J.R.C. de B., Coelho, C. de O.A., Keizer, J.J., de Lima, J.L.M.P., 2018. Comparing topsoil charcoal, ash, and stone cover effects on the postfire hydrologic and erosive response under laboratory conditions. *Land Degradation and Development* 29, 2102–2111. <https://doi.org/10.1002/ldr.2884>
- Putnam, A.E. e Broecker, W.S. Human-induced changes in the distribution of rainfall. *Science Advances*, n.3, e1600871, 2017. DOI: 10.1126/sciadv.1600871

- Ramadhan, M. N. Yield and yield components of maize and soil physical properties as affected by tillage practices and organic mulching. *Saudi Journal of Biological Sciences*, n.28, p.7152-7159, 2021. DOI: /10.1016/j.sjbs.2021.08.005
- Reddy, B. M.; Sunitha, V. Prasad, M.; Reddy, Y.S.; Reddy, M.R. Groundwater for Sustainable Development Evaluation of groundwater suitability for domestic and agricultural utility in semiarid region of Anantapur, Andhra Pradesh State, South India. *Groundwater for Sustainable Development*, v. 9, p. 100262, 2019.
- Rhodes, C. J. The imperative for regenerative agriculture. *Science Progress*, n.100, v.1, p.80-129, 2017. DOI: 0.3184/003685017X14876775256165
- Santos, T. E. M.; Montenegro, A. A. A.; Silva Júnior, V. P.; Montenegro, S. M. G. L. Erosão hídrica e perda de carbono orgânico em diferentes tipos de cobertura do solo no semiárido, em condições de chuva simulada. *Revista Brasileira de Recursos Hídricos*, v.13, p.29-34, 2008. DOI: 10.21168/rbrh.v13n2.p113-125
- Santos, T.E.M.; Silva, D.D.; Montenegro, A.A.A. Temporal variability of soil water content under different surface conditions in the semiarid region of Pernambuco State. *Revista Brasileira de Ciência do Solo*, n.34, v.5, p.1733-1741, 2010.
- Santos, T.E.M.; Montenegro, A. A. A.; Silva Júnior, V. P.; Montenegro, S. M. G. L. Erosão hídrica e perda de carbono orgânico em diferentes tipos de cobertura do solo no semiárido, em condições de chuva simulada. *Revista Brasileira de Recursos Hídricos*, n.13, p.29-39, 2008.
- Sekhon, K. S.; Kaur, A.; Thaman, S.; Sidhu, A. S.; Garg, N.; Choudhary, O. P.; Buttar, G. S.; Chawla, N. Irrigation water quality and mulching effects on tuber yield and soil properties in potato (*Solanum tuberosum* L.) under semiarid conditions of Indian Punjab. *Field Crops Research*, n.247, 2020.
- Silva, L. P. B. e Hussein, H. Produção de escala na hidropolítica regional: uma análise da bacia do rio La Plata e do sistema aquífero Guarani na América do Sul. *Geoforum*, n.99, p.42–53, 2019.
- Silva Junior, V.P.; Montenegro, A.A.A.; Silva, T.P.N.; Guerra, S.M.S.; Santos, E.S. Produção de água e sedimentos em bacia representativa do semiárido pernambucano. *Revista Brasileira de Engenharia Agrícola e Ambiental*, n.15, v.10, p.1073-1081, 2011.
- Singh, R. K.; Kumar, M. Assessing vulnerability of agriculture system to climate change in the SAARC region. *Environmental Challenges*, p.1-25, 2021. DOI: 10.1016/j.envc.2021.100398

- Slama, T.; Sebei, A. Spatial and temporal analysis of shallow groundwater quality using GIS, Grombalia aquifer, Northern Tunisia. *Journal of African Earth Sciences*, n. 170, p.1-17, 2020.
- Sousa, A. B.; Costa, C. T. F.; Firmino, P. R. A.; Batista, V. S. Tecnologias sociais de convivência com o Semiárido na região do Cariri cearense. Brasília: *Cadernos de Ciência and Tecnologia*, v.34, n.2, p.197-220, 2017.
- Stavi, I. Wildfires in grasslands and shrublands: a review of impacts on vegetation, soil, hydrology, and geomorphology.2019. *Water*, 11, p. 1042, 2019.
- Sun, J., Shi, S., Yang, J., Gong, W., Qiu, F., Wang, L., Du, L., Chen, B., 2019. Wavelength selection of the multispectral lidar system for estimating leaf chlorophyll and water contents through the PROSPECT model. *Agric. For. Meteorol.* 266–267, 43–52. DOI: 10.1016/j.agrformet.2018.11.035.
- Tesfaye, S.; Taye, G.; Birhane, E. Observed and model simulated twenty-first century hydro-climatic change of Northern Ethiopia. *Journal of Hydrology*, v.22, 2019.
- Teshnizi, F.A.; Ghobaninia, M.; Abbasi, F.; Hallett, P.D.; Sepehrnia, N. 2023. Biochar and flow interruption control spatio-temporal dynamics of fecal coliform retention under subsurface drip irrigation. *Journal of contaminant Hydrology*, v.253. DOI: 10.1016/j.jconhyd.2022.104128
- Thomas, G.; Rosalie, V.; Olivier, C.; Girolamo, A. M.; Lo Porto, A. Modelling Forest fire and firebreak scenarios in a Mediterranean mountainous catchment: Impacts on sediment loads. *Journal of Environmental Management*, n.289, p.1-10, 2021. DOI: /10.1016/j.jenvman.2021.112497
- UN-Water, The United Nations World Water Development Report 2018: Nature-based Solutions for Water. Unesco, Paris (2018)
- Valín, M. I., Araújo-Paredes, C. A., Rodrigues, A. S., Alonso, J., & Mendes, S. (2019). Utilização de técnicas de termografia para a avaliação do estado hídrico da vitis vinífera cv Loureiro. 899–905. https://doi.org/10.26754/c_agroing.2019.com.3442
- Verrot, L. e Destouni, G. Worldwide soil moisture changes driven by future hydro-climatic change scenarios. *Hydrology and Earth System Sciences Discussions*, 2016. DOI: 10.5194/hess-2016-165
- Vieira, D. C. S., Serpa, D., Nunes, J. P. C., Prats, S. A., Neves, R., & Keizer, J. J. (2018). Predicting the effectiveness of different mulching techniques in reducing post-fire

- runoff and erosion at plot scale with the RUSLE, MMF and PESERA models. *Environmental Research*, 165, 365–378. <https://doi.org/10.1016/j.envres.2018.04.029>
- Wilson, T.G., Kustas, W.P., Alfieri, J.G., Anderson, M.C., Gao, F., Prueger, J.H., McKee, L. G., Alsina, M.M., Sanchez, L.A., Alstad, K.P., 2020. Relationships between soil water content evapotranspiration, and irrigation measurements in a California drip irrigated Pinot noir vineyard. *Agric. Water Manag.* 237, 106186.
- Yang, J.; Ye, M.; Tang, Z.; Jiao, T.; Song, X.; Pei, Y.; Liu, H. Using cluster analysis for understanding spatial and temporal patterns and controlling factors of groundwater geochemistry in a regional aquifer. *Journal of Hydrology*, n.583, p.1-15, 2020. DOI: 10.1016/j.jhydrol.2020.124594
- Zhang, X., Wu, X., Zhao, R., Mu, W., & Wu, C. (2022). Identifying the facts and driving factors of deceleration of groundwater table decline in Beijing during 1999 – 2018. 607(January).
- Zhang, H., Shi, Y., Dong, Y., Lapen, D.R., Liu, J., Chen, W., 2022. Subsoiling and conversion to conservation tillage enriched nitrogen cycling bacterial communities in sandy soils under long-term maize monoculture. *Soil and Tillage Research* 215, 105197. <https://doi.org/10.1016/j.still.2021.105197>

Chapter II: Evaluating ash mobilization dynamics and hydrological response of soil in a semi-arid environment after wildfire under simulated rainfall: laboratory and field conditions

Abstract: Wildfires typically transform vegetation and litter into a heterogeneous layer of ash covering the soil surface that can substantially modify the postfire hydrological and erosive response of the soil. However, determining the role of the ash layer in the erosion process is challenging, as it can be difficult to distinguish it from eroded sediments. Laboratory and field experiments addressed knowledge gaps by investigating ash mobilization and the impacts of burning layouts under simulated rainfall. Five different spatial layouts of vegetation distribution and ash cover were tested: T1 - uniform application; T2 – a circular area at the center of the flume; T3 - three distributed fractions arranged in a circular pattern; T4 – a along the flume line; T5 – a continuous stripe along the contour lines. These layouts were observed in the field over monitoring periods, reflecting common burn patterns used by local farmers when clearing the area. In order to support the evaluations, a preliminary survey using satellite images was conducted to analyze the incidence of fire foci between 2014 and 2022 and its relationship with land use and cover, terrain slope, and annual rainfall totals. Field assessments of soil hydraulic characteristics with a 10% slope and 60 mm/h rainfall, measured surface runoff and erosion. Laboratory tests were conducted on 10% and 30% slopes, with 0.5 L/s inflow and rainfall intensities of 60 and 100 mm/h, considering a waterproof and representative soil surface. Based on the satellite images, an increase in fire foci was detected over the years, showing a strong correlation with the expansion of agricultural areas, supporting the hypothesis that fire is used for land clearing and opening new agricultural areas. Additionally, a higher incidence of fire foci was observed in flat and moderately sloped areas, as well as in years with higher rainfall records. The results concerning erosion and ash transport demonstrated that concentrated burning in smaller areas reduced soil disaggregation rates, causing less alteration in soil physical characteristics. In laboratory experiments, it was observed that the smaller the area of ash concentration, the less ash mass was transported by surface runoff and highlight the rainfall intensity as a significantly factor for transport of ash, compared to the slope factor. Overall, the mean efficiency of layouts was ranked as: $L3 > L2 > L4 > L5 > L1$, with an average reduction of 30% in L3 compared with L1. These results can help reduce environmental damage from extensive burning, while extension efforts raise awareness in the agricultural community to eventually eliminate the use of fire.

Keywords: semiarid, wildfire, runoff, ash, rainfall simulator

II.1 Introduction

Land degradation represents a global environmental challenge, leading to the deterioration of the physical, chemical, and biological features of the soil, thereby potentially impeding food security, compromising ecosystem services, affecting livelihoods, and diminishing the overall quality of life (Kumar et al., 2022). In Brazil, the Northeast, particularly the semi-arid region, experiences high rates of soil degradation due to the substantial influence of climatic conditions on land degradation processes (Silva et al., 2020; Refatti et al., 2023; Oliveira et al., 2022). To exacerbate matters, the synergistic impact of rainfall variability and intensive land use renders this region highly susceptible to climate change in the upcoming century (IPCC Climate Change Synthesis Report, 2021).

The Brazil semiarid region spanning a total area of 1.13 million km², accommodating 27.8 million inhabitants across 1262 municipalities, is acknowledged as one of the most densely populated semiarid regions globally (MI/SUDENE, 2022). It also harbors a vast and diverse ecosystem, encompassing 1500 plant, 178 mammalian, 591 avian, 177 reptilian, 79 amphibian, 241 fish, and 221 bee species (MMA, 2007). These species thrive in the dry deciduous forest biome known as Caatinga.

The risk of fire is significantly heightened in semiarid and arid climates, where the combination of hot and dry summers amplifies the frequency and prevalence of wildfires throughout the year (Stavi, 2019). Nevertheless, fire source is often anthropogenic, including prescribed burns applied for post-rainfall burn-off or the execution of pile burns, both concurrently serving the purpose of creating new agricultural spaces (Marinho et al., 2021; Abreu et al., 2022). These prescribed burnings represent traditional techniques predominantly employed in family farming to prepare the soil for planting seasonal crops. In this context, they are authorized by the Federal Government (Oliveira-Júnior et al., 2017). Nevertheless, they entail diverse economic, ecological, landscape, and social losses, particularly in the protected nature reserves within the country (Freitas et al., 2020). Natural or anthropogenic wildfires exert notable impacts on soil and water, instigating diverse hydrological and geomorphological alterations in the landscape over both short and long periods (Lucas-Borja et al., 2022). Moreover, these fires can compromise the beneficial services provided by the forests leading to heightened runoff, soil erosion, and impairment to slopes and aquatic life in downstream rivers (Thomas et al., 2021). The combustion of vegetation and alterations in soil characteristics can also catalyse soil degradation (Zema, 2021).

Soil hydrology following a fire is a physical process influenced by several environmental drivers (e.g., vegetation dynamics, soil changes, water and sediment flows) (Lucas-Borja et al., 2023). An occasionally overlooked yet potentially pivotal factor governing post-fire runoff is the presence of ash on the soil surface (Woods and Balfour, 2008). Ash results from the combustion of vegetation, litter, and duff layers. The potential occurrence of ash on the topsoil, its influence on runoff and its consequential impact on erosion carry significant implications for post-fire management. According to Liang et al. (2021), reintegrating the carbonized biomass ash into the soil has the potential to enhance the carbon fixation capacity of the crop–soil ecosystem, thereby contributing to achieve the '4% Soils for Food Security and Climate' goal launched at COP21. Prats et al. (2021) investigated the application of diverse post-fire soil erosion mitigation solutions, encompassing various covers and treatment combinations under the influence of controlled rainfall. The potential effects of mobilizing the ashes, along with the methods available for retaining ashes at the fire site, are still being investigated. Moreover, the contribution of the ash to the overall erosion process remains uncertain and unknown, primarily due to the challenging nature of separating the ash and char fraction from other components such as litter, soil, and eroded sediments.

Wildfire-induced runoff and erosion pose substantial challenges for burned areas on a global scale, yet its mitigation garner limited public and scientific attention. To address this issue, Carmona et al. (2023) investigated short-term changes (1-year post-wildfire) in soil properties and individual ecosystem functions in a Mediterranean forest. Their findings indicate that, aside from pH, forest fires did not significantly modify soil properties. Conversely, decomposition of organic matter and nutrient cycling exhibited significant increases in unburned soils compared to burnt sites. In efforts to remedy these deficits, Liang et al. (2022) explored the impact of utilizing ashes as fertilizer on tomato crops in Ezhou, China. The results indicate that this practice serves as a viable and potentially effective strategy for enhancing soil carbon sequestration and plant production.

This study aims to fill existing knowledge gaps by investigating the erosion of burned areas in field and laboratory settings. The specific objectives are: i) compare the soil hydrological response in areas affected by fire under different burning conditions (e.g. fire time, layout of plant material deposition); ii) comprehending the physical process of ash mobilization resulting from rainfall-runoff and assessing its impact on various ash spatial layouts and iii) examining how variations in rainfall intensity and slope influence the ash mobilization. The

results of this investigation may give planners insight on suitable practices towards mitigation of contamination and erosion risks in fire-affected areas of the semiarid environment.

II.2 Material and methods

II.2.1 Satellite-derived data study area

An initial investigation into the relationship between fire outbreaks, land use and its changes, terrain slope, and average annual rainfall was conducted to identify significant parameters for further analysis. Data from the Climate Hazards Group InfraRed Precipitation with Station (CHIRPS) spanning 2014 to 2022 (https://developers.google.com/earth-engine/datasets/catalog/UCSB-CHG_CHIRPS_DAILY, accessed on 10 September 2023) was utilized, covering the area between latitudes 08°18'S - 9°12'S and longitudes 36°0'W - 38°0'W. CHIRPS data is highly accurate and serves as an excellent alternative in regions of Brazil where more precise data, such as from rain gauges, may be lacking (Souza et al., 2023). Elevation and slope data were derived from the Shuttle Radar Topography Mission (SRTM) digital elevation model (DEM) with a 30 m resolution (Farr and Kobrick, 2000).

Geospatial data from the MapBiomias Brazil project (2022), which includes land use and land cover information derived from the Landsat series between 2014 and 2022, were used to generate thematic maps of the Ipanema River Basin (IRB) in Brazil's Northeast region, commonly known as the Drought Polygon. The IRB is part of the São Francisco River Basin, playing a crucial role in providing hydropower for nearby urban centers (Coelho et al., 2017). A cost-effective, open-access methodology was employed to produce annual thematic maps, incorporating up to 105 layers of land use and land cover information. The accuracy of these maps was validated by calculating overall hit rates, as well as commission and omission error rates for each land use class. This validation process encompassed categories such as natural and non-natural forest formations, agriculture, non-vegetated areas, and water bodies (MapBiomias Brazil Project, 2022).

Data on fire occurrences were obtained from CPTEC/INPE through the BDQueimadas platform (CPTEC/INPE, 2023). Currently, CPTEC/INPE utilizes various environmental polar orbit and geostationary satellites to monitor 'fire foci' across South America. In this study, long-term time series data on fire foci in the Ipanema River Basin (IRB), spanning the period from 2014 to 2022, were analyzed. The fire occurrence data were extracted in annual format using an algorithm. The data obtained from BDQueimadas termed “fire foci” is defined based on pixels exhibiting elevated temperatures. These pixels are characterized by having the lowest

values of grey level in the images of the infrared thermal region band 3 (3.7 μm) of the AVHRR. Identification criteria include a minimum area of 1 km^2 (Souza and Stosic, 2005). The detection may indicate various phenomena, encompassing a burn, a small part of a fire, or other source of high temperature. Additionally, it may flag the reflection of light on exposed granites (Nunes et al., 2015; Caúla et al., 2016).

II.2.2 Experimental field setup

The study was conducted in the state of Pernambuco, Brazil (Fig. 1). This semiarid tropical region receives approximately 430 mm year^{-1} of summer rainfall, with potential evapotranspiration above 1800 mm year^{-1} (Lins et al., 2024). The site used for this study (Fig. 1, Table 1), a slope (with an area of 0.7 ha) located on a small rural property in the Mimoso Alluvial Valley, has a Regolitic Neossol soil, derived from sedimentary rock formations such as sandstones and claystones. The soil is characterized by a vegetation cover that includes both bare soil and predominantly natural and/or spontaneous vegetation. The non-bare areas are primarily covered by small and medium-sized shallow caatinga, with no trees or shrubs present. The physical and chemical characteristics of the soil are summarized in Table 1.

Table 1. Physical and chemical properties of the layer (0–20 cm) of soil in the study sites.

Layout	Bd	Pd	S	Clay	Silt	EC	TOC
	g cm^{-3}		g Kg^{-1}			dS m^{-1}	g Kg^{-1}
L1	1.23	2.49	640.9	206	153.1	0.23	43.4
L2	1.22	2.47	603.6	196	200.4	0.69	37.8
L3	1.24	2.42	650.8	186	163.2	0.64	42.0
L4	1.27	2.48	685.8	186	128.2	0.91	42.9
L5	1.27	2.31	662.4	176	161.6	0.48	39.9

where: Bd: bulk density; Pd: particle density; S: total sand; TOC: total organic carbon; EC: electrical conductivity of saturation extract.

Two experimental plots (replicates) with 1.5×0.5 m were installed at study site (Fig. 2). Undisturbed and disturbed soil samples were collected from each plot at each study site. In the lower section of each plot, gutters were installed to collect samples of water and sediment immediately after runoff began. The plots had an average slope of 10 and 10.25 % and they were spaced 0.20 m apart.

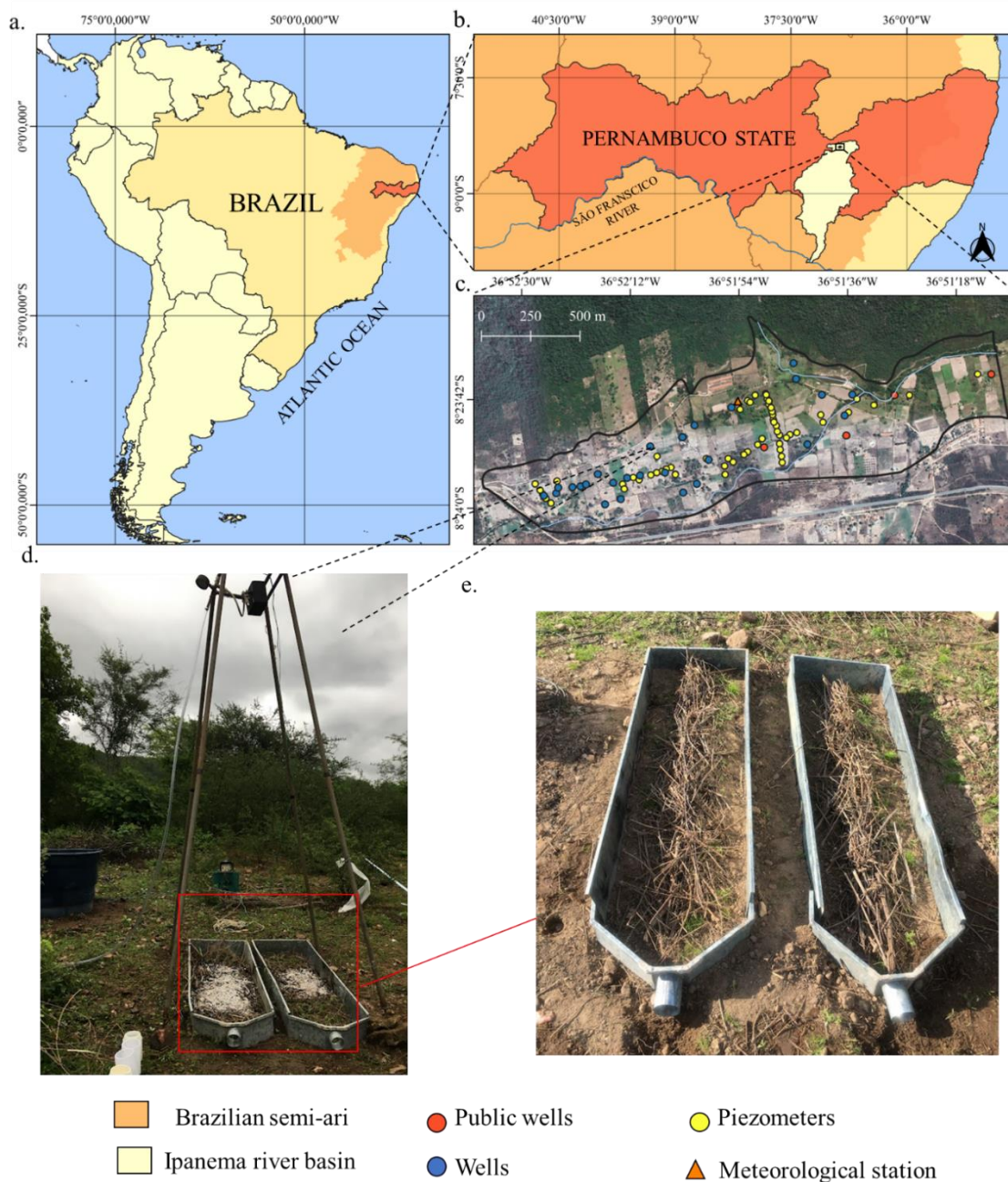


Figure 1. Location of study area, and experimental field layout (no scale).

To simulate rainfall, a rainfall simulator with a Veejet 80-100" sprinkler nozzle from the Spraying Systems Company, and an electronic system to perform oscillating movements was placed 2.78 m above ground level and supported in a rectangular frame with removable steel tubes forming four legs. The precipitation lasted for 30 minutes working with a pressure of 50 kPa. The rainfall exhibited consistent intensities (Fig.3) ranging between 42- and 86-mm h⁻¹, with mean varying of 58.4 to 62.8 mm h⁻¹ over 3 successive measurements. This variation was

primarily attributed to wind interference in the field. The uniformity of rainfall distribution was determined by calculating the Christiansen Uniformity Coefficient (Montebeller et al., 2001) with values above $83 \% \pm 0.4\%$.

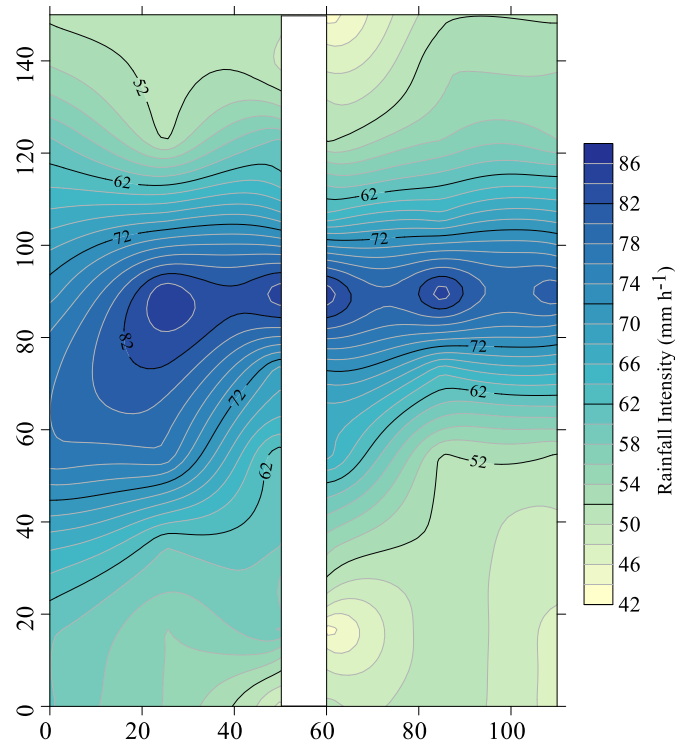


Figure 2. Rainfall spatial distribution of 60 mm h^{-1} intensity for 10% of slope.

II.2.2.1 Burned area and Ash distribution

Five spatial layouts of ash cover were used, as depicted in Figure 2. The five ash cover layouts (L1 to L5) were subject to testing under a simulated rain intensity, and 10% of slope. The five application layouts corresponded to distinct ash cover distributions, each verified as real burning scenarios conducted by rural farmers as a method for managing agricultural areas during droughts, or between rain events. Layout 1 (L1): uniformly distributed over the surface of the flume; Layout 2 (L2): material concentrated in a circular shape in the center of the flume, simulating a scenario where the farmer gathers all the vegetation cover in a single circular area; Layout 3 (L3): three ash fractions arranged in a circular pattern to simulate the separation of waste in different parts of the area; Layout 4 (L4): continuous patch of ashes along the longitudinal midsection of the flume and Layout 5 (L5): continuous patch of ashes along the transversal midsection of the flume.

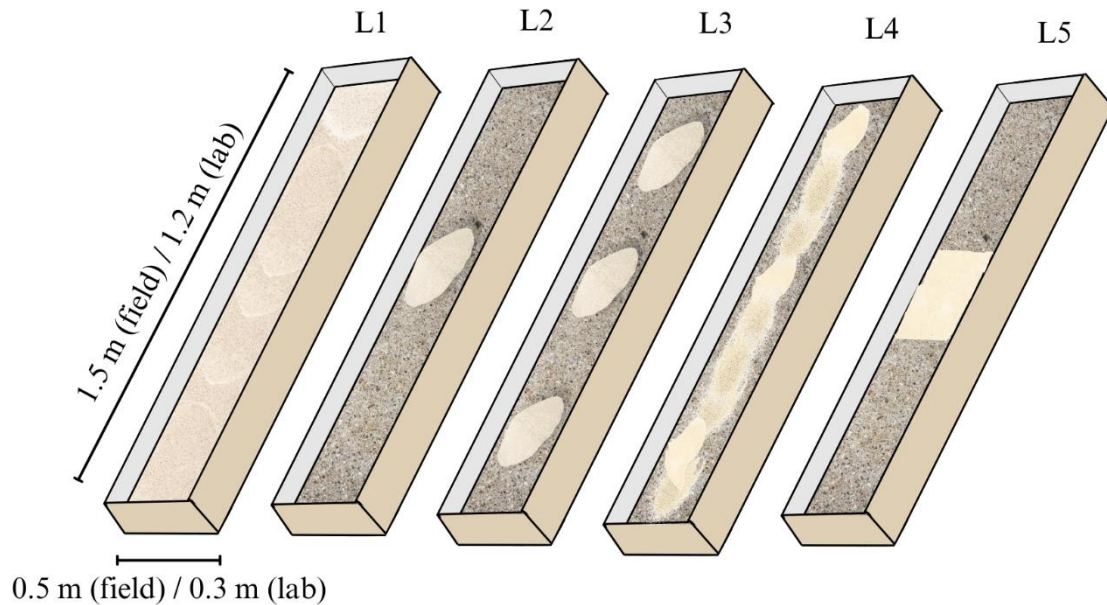


Figure 3. Spatial layouts of ash cover tested in the soil flume experiments.

The predominant plant species identified in the area were *Mimosa quadrivalvis* L., *Sida cordifolia* L., and *Mesosphaerum suaveolens* (L.) Kuntze. The average moisture content of the plant material, before burning, was $35.5 \pm 0.8\%$. The mean mass of plant material per plot ranged from 1.080 ± 0.4 Kg. Air temperature varied from 28 to 31 °C and air relative humidity was 76% at the moment of the burning. The fire durations for the different layouts were as follows: L1 - 13 minutes; L2 - 6.2 minutes; L3 - 8 minutes; L4 - 11.2 minutes; and L5 - 5.3 minutes.

Ash samples were collected from the five different layouts evaluated after the fire was extinguished, in locations with visually larger ash deposits. Similar volumes of ash were collected at each point and the samples were placed in plastic bags and taken to the laboratory. The five samples from each point were mixed into a single homogeneous composite sample, then sieved through a 2-mm mesh sieve. Regarding color, the sample was classified as black ash (23%) and white ash (77%). The pH in water was 7.4 ± 0.1 .

II.2.2.3 Runoff and Soil moisture

To estimate surface runoff, water was collected in cups, at 1-min intervals for a duration of 30 sec at each interval, from gutters installed at the bottom of each plot. Soil moisture was determined by the difference between simulated rainfall and runoff.

II.2.2.4 Detachment ratio, sediment concentration and soil loss

Soil Detachment ratio were determined taking into account the mass of disaggregated dry soil (Kg) in each container during water collection (30 sec), according to Bezerra & Cantalice (2006). To quantify the sediment concentration, the collected runoff water was stored in 1-L containers and transported to the laboratory. Portable turbidity was determined in the collected runoff samples to quantify the effect of ash and sediment concentration in each entire samples volume collected. After decanting the solid material, the supernatant was suctioned off and the sediments were transferred to cans and dried in a forced circulation oven for 48 h at a constant temperature of 105 °C. After drying, the material was weighed to quantify the amount of dry sediment in the runoff volume.

II.2.3 Experimental laboratory setup

Laboratory experiments were conducted utilizing a soil flume and a rainfall simulator in laboratory conditions (Figure 4). This study encompassed a total of forty scenarios, encompassing: (i) five distinct ash layouts (see Figure 2); (ii) two precipitation intensities (60 mm h⁻¹ and 100 mm h⁻¹); (iii) inflow (0.5 L s⁻¹, starting close to the surface runoff); (iv) two slopes (10 and 30%). All experimental conditions were repeated three times for each scenario. The schematic representation of the laboratory setup is illustrated in Figure 3, where ash transport via rainfall and surface runoff was examined employing various spatial layouts of ash cover. The setup consists of a rectangular soil flume, impervious flume, measuring 1.2 m in length by 0.3 m in width, an upstream water inflow system, and a rainfall simulator.

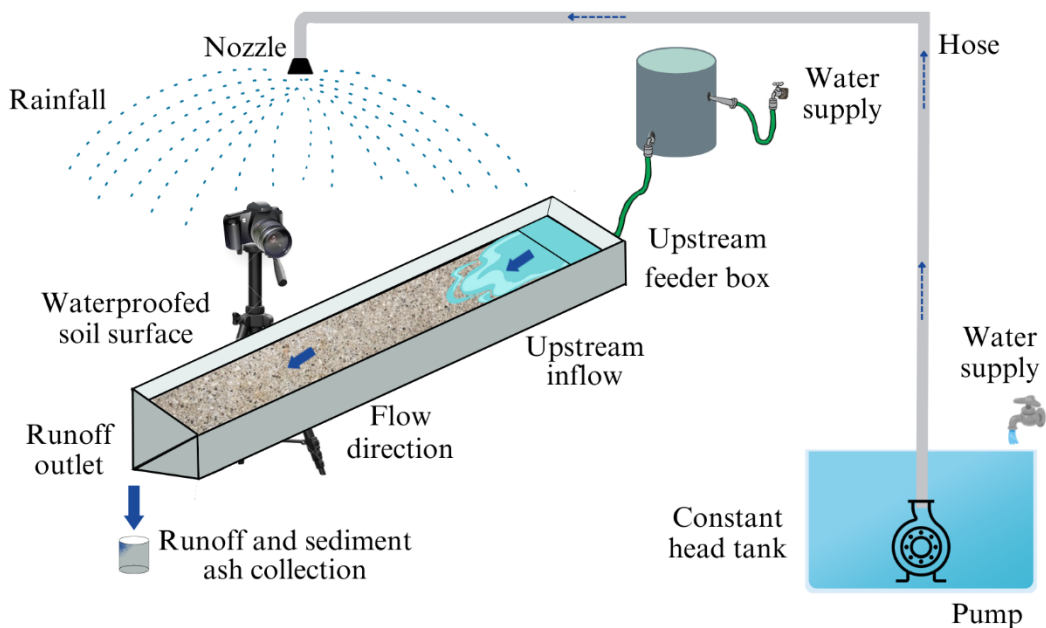


Figure 4. Schematic representation of the laboratory setup used in the experiments (not to scale).

The soil flume was filled with pre-screened and air-dried substrate described by Abrantes et al. (2018), sealed with a surfactant to exclusively facilitate the mobilization of ash particles, preventing infiltration, and inhibiting the mobilization of soil particles. Between each test, the soil flume underwent a cleaning process, complete drying, and waterproofing, if necessary, thus ensuring consistent initial conditions throughout the tests. The surface's hydraulic characteristics, such as friction and texture, were intentionally maintained to ensure an accurate simulation of the soil's hydraulic properties, including roughness. All ash samples underwent sieving to remove particles larger than 10 mm, weighed, and applied in accordance with the designated ash layout distribution (refer to Figure 3). The total quantity per layout of ash used was 0.45 kg. This amount was determined based on post-burned area site sampling in the field experiment.

Water was introduced in the flume through two independent systems: run-on and rainfall. The run-on was conveyed through a system installed upstream of the flume (Fig. 1) where the incoming flow was stabilized and evenly divided through the section. The water inflow system, positioned upstream of the soil flume, was employed to replicate upslope flow (e.g., runoff), akin to the methodologies utilized in experiments by Prats et al. (2018) and Abrantes et al. (2018). This system comprised a feeder box and a constant head tank with a

flow control valve, to allow uniform application of water flow into the flume's surface (upstream inflows in Fig. 1). The volume of water and consequent applied discharge was adjusted to the conditions of the test (slope) to be 0.5 L min^{-1} for each run.

The utilized rainfall simulator featured a downward oriented full-cone nozzle, specifically the 3/8-HH-22 FullJet from Spraying Systems Co, positioned 2.25 m above the geometric center of the soil flume surface, with a spray angle varying not linearly between 82 and 90 degrees based on pressure. A submerged pump (76.2 mmSQ Grundfos Holding A/S.), installed in a constant head reservoir and a pressure reducing valve that allowed a steady operating pressure of 140 Kpa to 60 mm h^{-1} and 180 Kpa to 100 mm h^{-1} at the nozzle. Both rainfall intensities were characterized by a uniformity coefficient of $92.8 \pm 0.6\%$ (Christiansen et al., 1942). Measurements were conducted using 30 rain gauges distributed uniformly across the surface of the flume (Fig. 5).

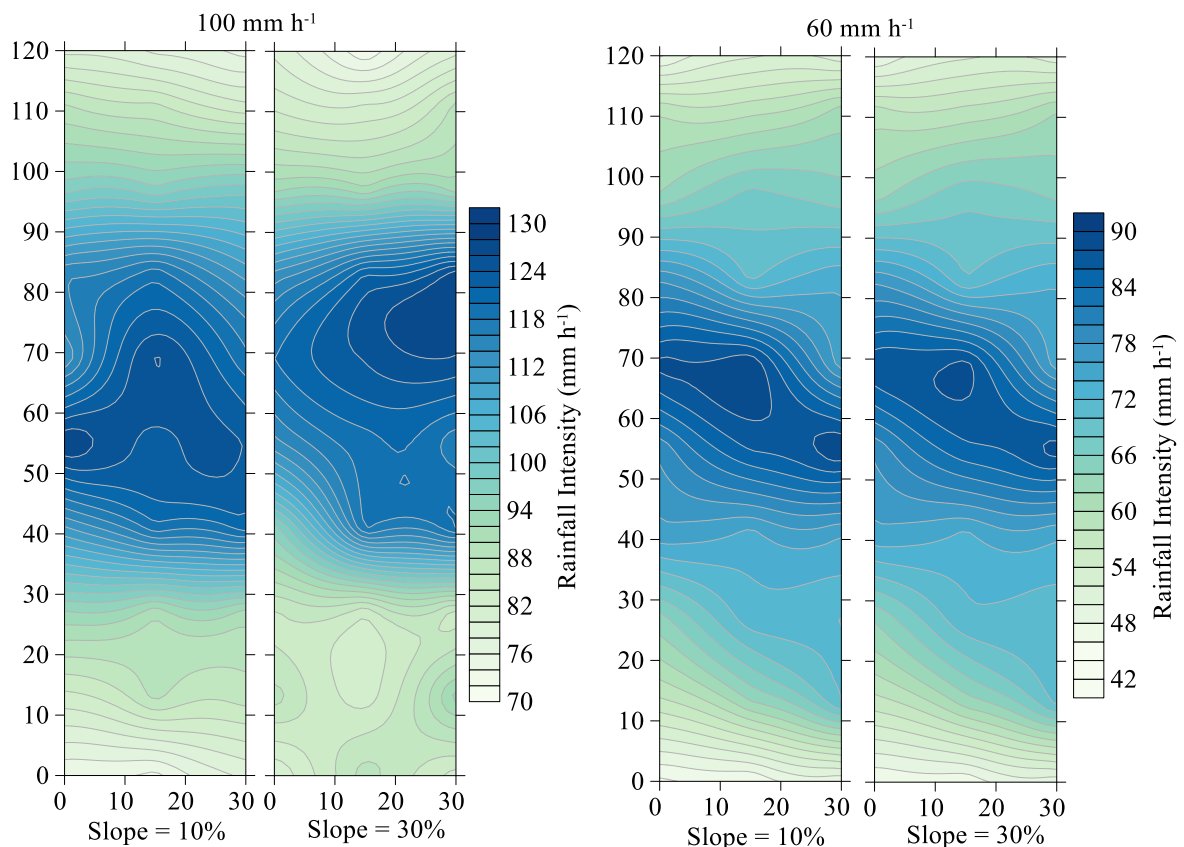


Figure 5. Rainfall spatial distribution of 100 mm h^{-1} and 60 mm h^{-1} intensity for 10 and 30% of slope.

The choice of the two precipitation intensities used was informed by the research by Santos & Montenegro (2012), which involved the evaluation of 29 years of rainfall data for the Brazilian region. The study characterized the rainfall pattern into advanced, intermediate, and delayed patterns and examined the frequency of rainfall intensity. The advanced pattern, predominant in the semiarid region, 50 % of the rainfall intensity values exceeded 38 mm h⁻¹, reaching values of up to 300 mm h⁻¹, corresponding to a depth of 10 mm in 2 min. Additionally it was determined that approximately 30 % of the rainfall intensities within the advanced pattern exceed 60 mm h⁻¹. The selection of a rainfall intensity of 100 mm h⁻¹ aimed to simulate a future scenario attributed to global climate change (Lins et al., 2023).

The runoff was collected at 30-seconds intervals throughout a total test duration of 10 minutes. Collected samples were dried in a temperature oven at 105 °C, enabling precise weighting of ash mobilization.

II.2.3.2 Percentage of ash in the flume

Images of the flume were captured using a portable camera placed 1.0 m above the ground surface in the middle of the soil flume (Fig. 3). Photographs were taken for each treatment condition. The Python language and OpenCV database were used to process the images using a processing algorithm, with the PyCharm software interface. To extract the percentages of ash coverage, the image was binarized and then the ratio between white pixels (referring to ash) and the total number of pixels was calculated.

II.2.4 Statistical analysis

The temporal record of fire foci was evaluated by the Mann-Kendall test (Mann, 1945; Kendall, 1975) and Sen's slope method (Sen, 1968) to verify if there is a significant trend and estimate the trend magnitude. The STL method employs robust locally weighted regression for smoothing (Cleveland et al., 1988), utilizing the LOESS (i.e., locally weighted scatterplot smoothing) algorithm as a component (Cleveland and Devlin, 1988). To identify the year when a sudden shift in the mean of the time series occurred, the Pettitt test (Pettitt, 1979) was employed.

Ash mass mobilized by the run-on was assessed for normal distribution and underwent classic statistical analysis. Analysis of variance (ANOVA) was employed to identify treatment main effects and interactions, and differences between treatments were evaluated using Tukey's

test ($p \leq 0.05$). Data analyses were conducted using the R Statistical Software Program (R Core Team, 2020). Boxplot graphs were generated to provide insights into the dataset.

II.3 Results and discussion

II.3.1 Land use and burned areas

Results from the remote sensing survey of fire incidences in the upper Ipanema Basin reveal a discernible pattern of wildfire variability in the Caatinga biome, with the most significant occurrences observed between August and October. Figure 6 illustrates this variability, highlighting a statistically significant upward trend ($z > \alpha$) in reported forest fire outbreaks, as confirmed by the Mann-Kendall (MK) test. Additionally, the Sen's slope estimator indicated an increase in fire foci at a rate of 1.19 per year.

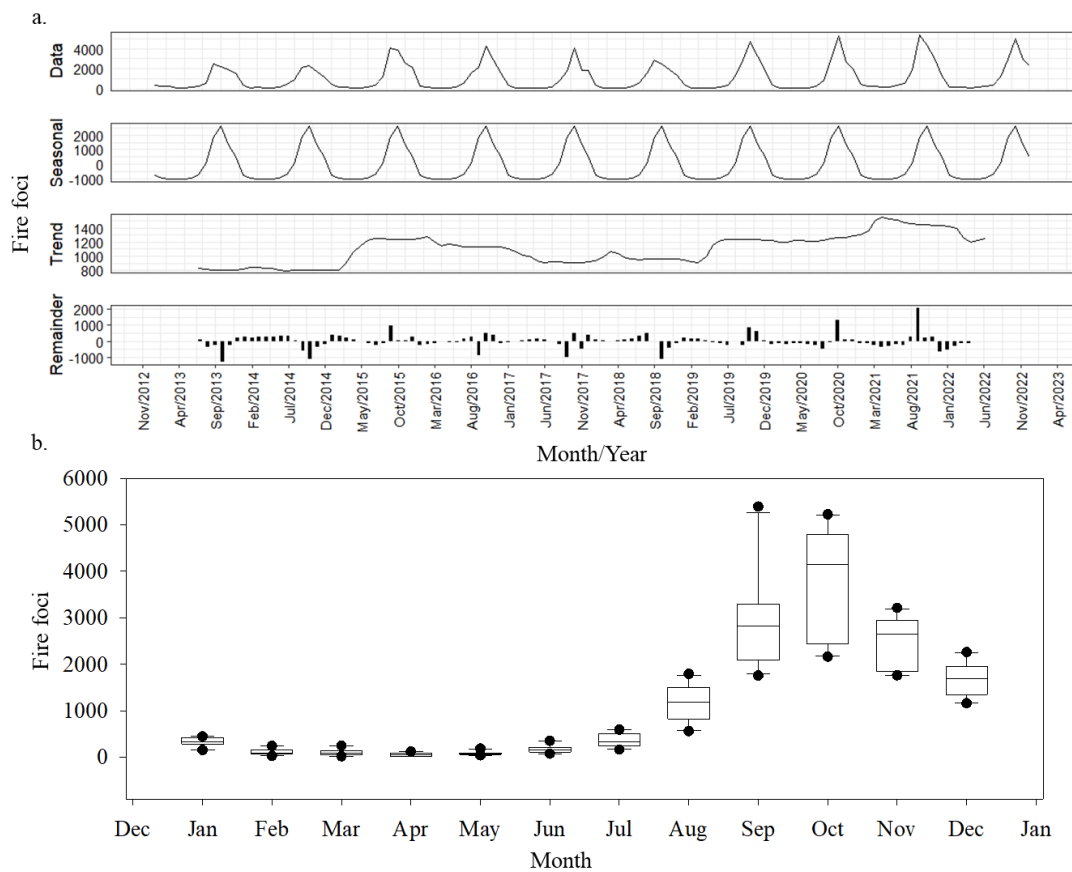


Figure 6. Annual time series, seasonal and annual trend, and Boxplot with mensal distribution of fire foci from 2014 to 2022.

The application of the STL filter revealed seasonality in the data, with a notable surge in fire outbreaks during the dry season and a decline in the rainy season. The significant

occurrences of wildfire between August and October, with strong effect of seasonality, corroborates with findings by Abreu et al. (2021), who underscore that the highest probability of wildfire events in Brazil tends to occur from August to September. This pattern aligns with the findings of Caúla et al. (2015), who, in their assessment of wildfire incidents in Brazil, highlighted a correlation with the transitional phase between dry and rainy periods. During these months, vegetation becomes more susceptible to fires due to reduced humidity and lack of rainfall (Marinho et al., 2021). Additionally, this period may coincide with the onset of rains, leading to readily available combustible material, creating a complex dynamic of disaggregation and transport.

The Pettitt test identified a significant change in the fire hotspot time series in 2018 and 2019 (Fig. 5), coinciding with a notable increase in fires. The irregularity in the rainfall regime in the Brazilian semiarid has been associated with the Intertropical Convergence Zone (ITCZ), which can result in extreme climatic events, such as droughts or heavy rainfall (Tinoco et al., 2018). Figure 6 illustrates the distribution of rainfall between 2014 and 2022.

Detecting trends in time series is essential for the effective management of natural resources. Nonparametric statistical tests, such as Pettitt test (Marinho et al., 2021), have proven valuable in this context. The Pettitt test highlighted a significant change in the fire hotspot time series in 2018 and 2019 (Fig. 5), coinciding with a notable increase in fires. Lima et al. (2020) employing the Pettitt test, observed a significant increase ($p \leq 0.05$) in fire hotspots across most Indigenous Lands in the state of Mato Grosso. This increase was associated with the presence of moderate *El Niño* and *La Niña*, contributing to the annual rise in fire hotspots.

Post-fire weather conditions, encompassing factors such as precipitation and wind, exert a significant influence on the soils affected by forest fires, impacting the distribution of ash and contributing to soil degradation (Elakiya et al., 2023). A holistic understanding of both natural disturbances (wind and rain) and human activities (post-fire logging) is imperative for unravelling the processes influencing soil degradation (Pereira et al., 2018). Precipitation plays a crucial role in affecting humidity levels and vegetation patterns, thereby influencing the speed of fire propagation (Eskandari et al., 2021). Ghorbanzadeh et al. (2019) established a direct correlation between temperature increases and forest fires. Elevated temperatures contribute to higher evapotranspiration rates, heightening the susceptibility of forests to wildfires.

The standardization and variability of rainfall in the Northeast Brazilian Semiarid (NEB) are influenced by factors such as land use, vegetation, altitude, and terrain conditions. In tandem with the impacts of climate change, which have altered rainfall patterns, these factors

collectively contribute to the emergence and persistence of reduced precipitation indices in these semiarid regions, as highlighted by Carvalho et al. (2020). This spatiotemporal variability, in conjunction with the low annual precipitation totals, results in the frequent occurrence of rainless days and consequently giving rise to drought events. The observed limited rainfall in the NEB Semiarid poses a significant threat to the Caatinga ecosystem, as emphasized by da Silva et al. (2020).

The study area experiences an average annual rainfall of approximately 700 mm, primarily concentrated from March to May, exhibiting significant variations between years (Montenegro and Montenegro, 2006). According to Köppen's classification, the IRB is subjected to a very hot semiarid climate, featuring average temperatures exceeding 23 °C, and an annual average of the crop reference evapotranspiration (ET₀) exceeding 1800 mm (Coelho et al., 2017). This climatic pattern results in a water deficit in the region for a significant proportion of the year.

The irregularity in the rainfall regime in the Brazilian semiarid has been linked with the Intertropical Convergence Zone (ITCZ), that can lead to extreme climatic events, such as drought or severe rainfall (Tinôco et al., 2018). Figure 7 presents the rainfall distribution between 2014 and 2022.

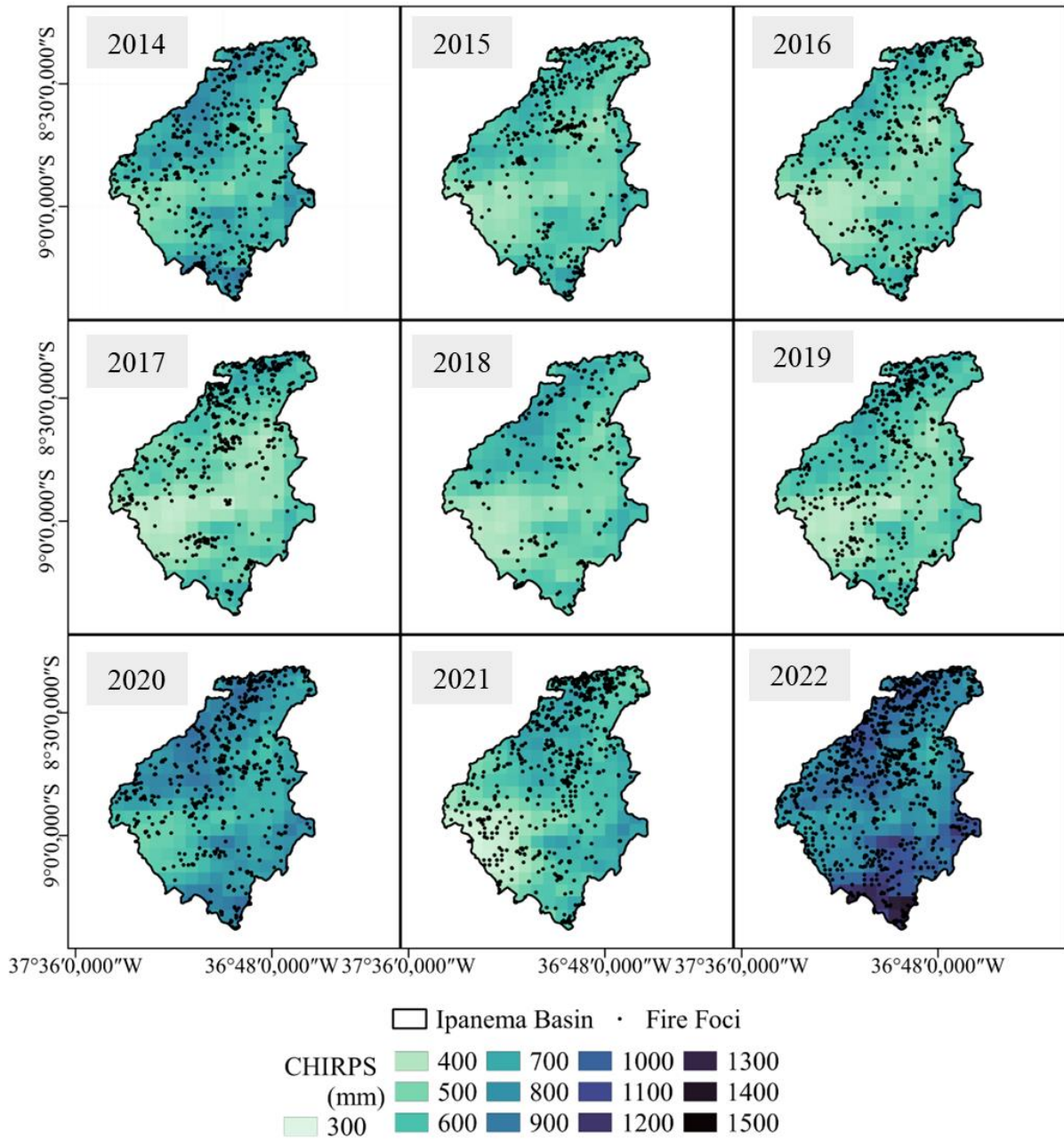


Figure 7. Spatial distribution of rainfall and fire foci from 2014 to 2022 in Ipanema River Basin, Brazilian semiarid region.

In the Ipanema Basin, the maps highlight predominant rainfall patterns between 400 and 900 mm (depicted in light blue pixels) and between 1000 and 1500 mm (represented by dark blue pixels). The average, minimum and maximum precipitation values for the years 2014 to 2022 can be observed in Table 1.

Table 1. Precipitation values for the years 2014 to 2022

Year	Average Precipitation (mm)	Maximum Precipitation (mm)	Minimum Precipitation (mm)
2014	654.2	922.7	416.9
2015	557.8	767.2	371.9
2016	540.7	778.6	353.4
2017	518.3	720.2	345.5
2018	558.1	774.7	352.3
2019	540.6	727.8	349.1
2020	741.4	990.6	471.2
2021	585.5	857.8	289.8
2022	903.1	1399.8	641.9

Based on exploratory and descriptive statistics, the study period (2014 to 2022) witnessed a total of 4718 fire foci in the IRB. Descriptive analytics unveiled an annual mean and standard deviation of 590 ± 159 fire foci, with a median of 620 fire outbreaks distributed across the Ipanema River Basin. The maximum and minimum values, respectively, were recorded in 2020 (813 fire foci per year) and 2017 (301 fire foci per year).

A positive correlation with an R^2 value of 0.8 was observed between wildfire incidents and precipitation. It is essential to emphasize that the formation of a gradient of fire incidents is likely associated with changes in land use and spatial occupation, particularly related to agriculture (as illustrated in Figure 8).

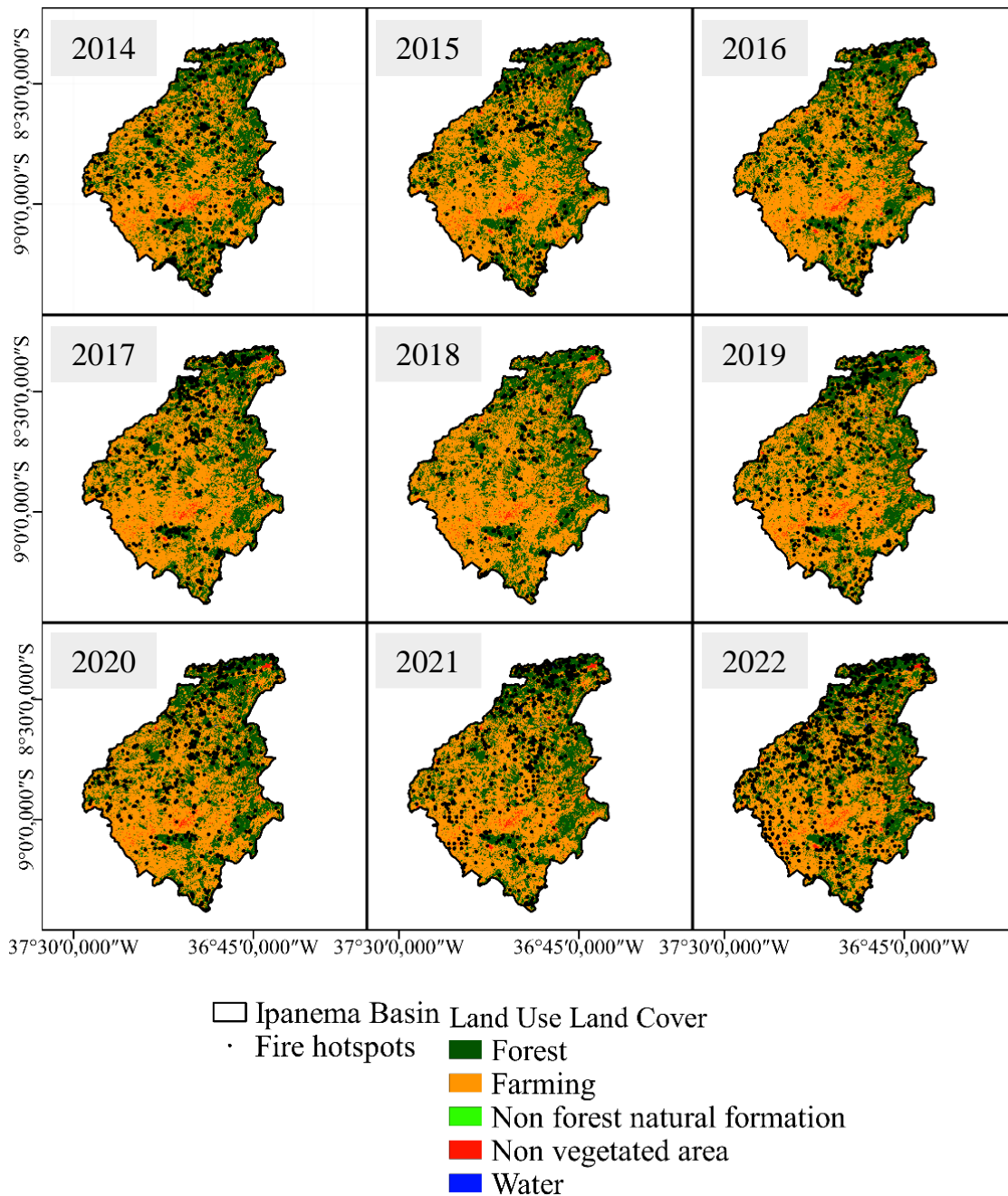


Figure 8. Spatial distribution land use and land cover and fire foci between 2014 to 2022 in the Ipanema River Basin, Brazilian semiarid region.

For the observed period, there was a reduction (9.33%) in forest cover followed by an increase (11%) in areas designated for farming and non-vegetated areas. The burning and its processes can induce various damages to the different components of the biome, such as: (I) loss of native plant species; (II) exposure to destruction and weakening of the soil organic layer; changes in the physical properties of the soil (porosity and water permeability); (III) occurrence

of landslides and erosion and (IV) mortality of animals, destruction of nests, and modification of habitat (animals migrate in search of food and shelter); among others (Roth et al., 2023; Vieira et al., 2023; Mitchell, 2023; Schmidt et al., 2023; Krüge et al., 2023).

It is noteworthy that among the key factors leading to substantial losses in ecosystem services in the Northeast Brazilian (NEB) region are imbalances resulting from deforestation, wildfires, improper irrigation water use, intensive agricultural practices, and inadequate land management. These unsuitable land use practices lead to the depletion of vegetation, water, and soil, subsequently contributing to local microclimate alterations and the exacerbation of desertification processes, which in turn reduce the socio-economic conditions of the affected regions (Barbosa et al., 2019).

Tran et al. (2023) identified a total of 13 factors influencing wildfire occurrence, including slope, aspect, plan curvature, profile curvature, topographic wetness index, valley depth, wind speed, normalized difference vegetation index, rainfall, temperature, distance to roads, and distance to rivers. The authors emphasized that distance to roads, temperature, and slope were the most critical factors for identifying areas prone to wildfires. In the Ipanema River Basin (IRB), the spatial distribution of fire foci showed significant variability, particularly in the sloped regions of the basin, which are predominantly covered by Caatinga vegetation, as illustrated in Fig. 9.

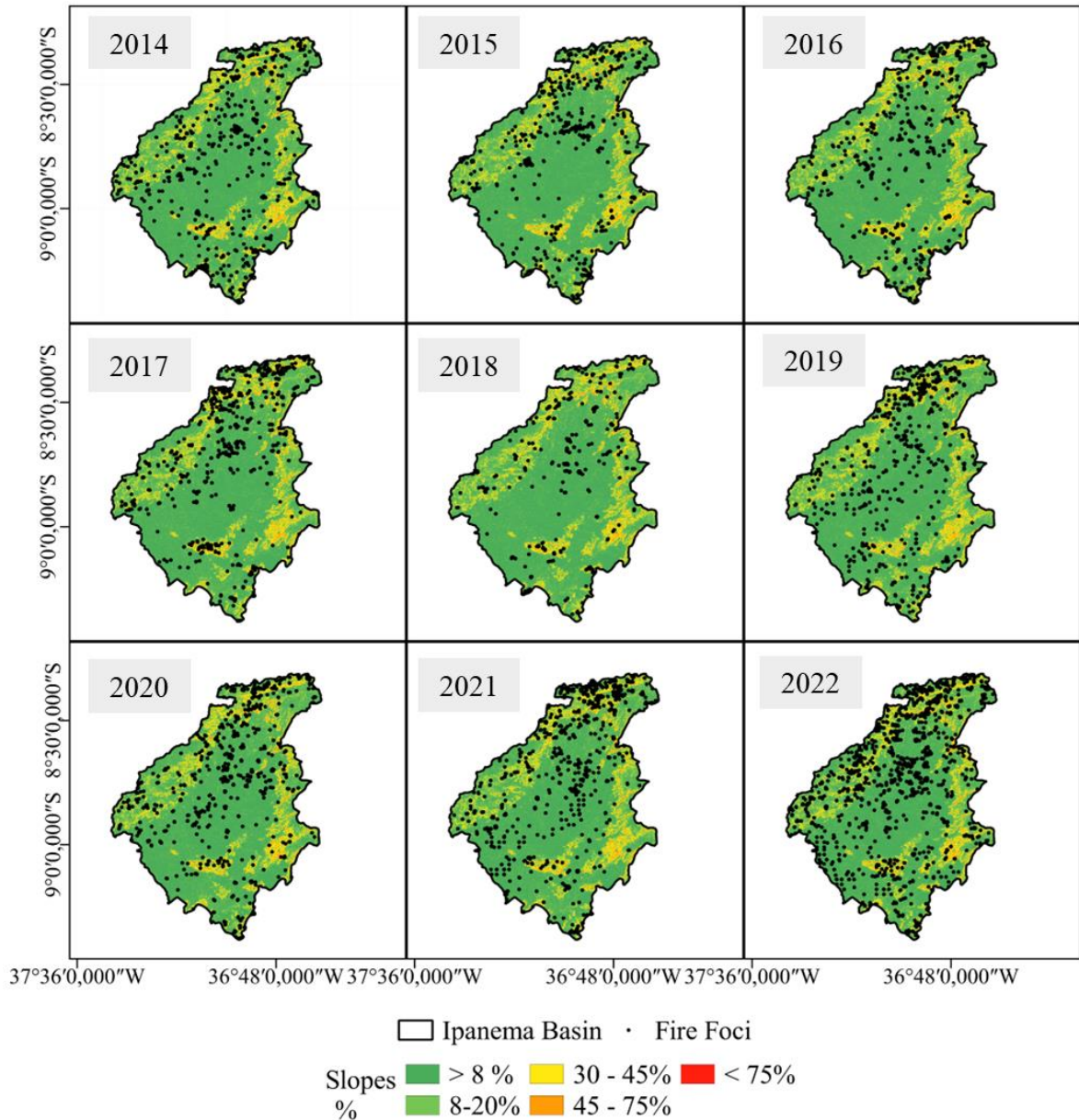


Figure 9. Spatial distribution of slope class and fire foci from 2014 to 2022 in Ipanema River Basin, Brazilian semiarid region.

The distribution of fire foci reveals a predominant concentration across low-elevation and gentle-slope terrains (8 to 20%), with a substantial concentration occurring in areas characterized by strong undulations (20 to 40%). This pattern aligns with the conclusions drawn in studies by Abreu et al. (2021) and da Silva et al. (2020), emphasizing the significant influence of agriculture and livestock as the primary contributors to degradation within the Caatinga biome.

II.3.2 Soil moisture, runoff and erosion rates, soil loss and time to the beginning of runoff

The hydrographs generated by the rainfall simulations experiments are illustrated in Figures 10. These hydrographs depict the time variability of the runoff rates and sediment concentration under a constant rainfall intensity on soil with different layouts of burned area (layouts 1 to 5) and 10% of slope.

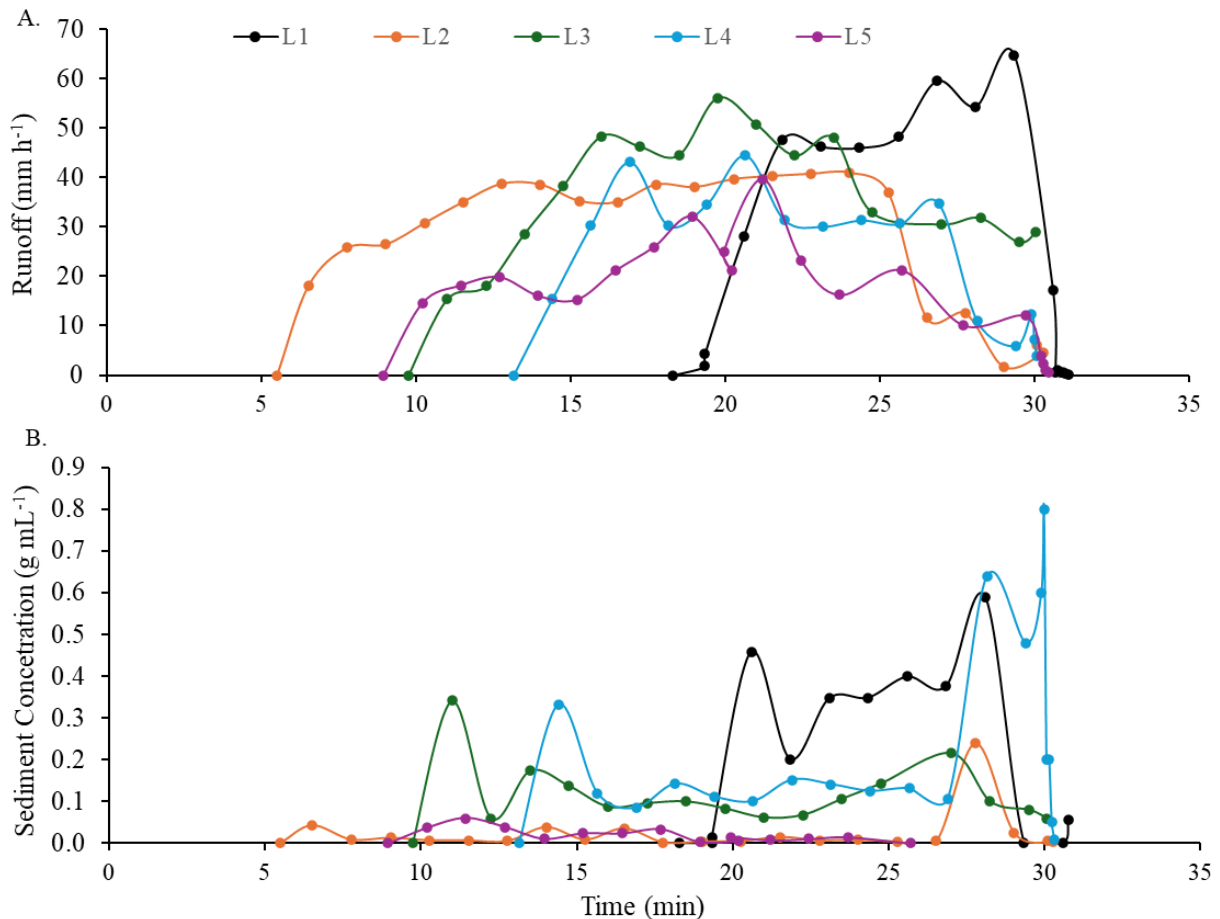


Figure 10. Runoff rates and sediment concentration in the five layouts investigated.

The layout of burned area significantly affected the soil moisture, runoff, erosion rate and instantaneous soil loss, as can be seen in Figure 11 and Table 3.

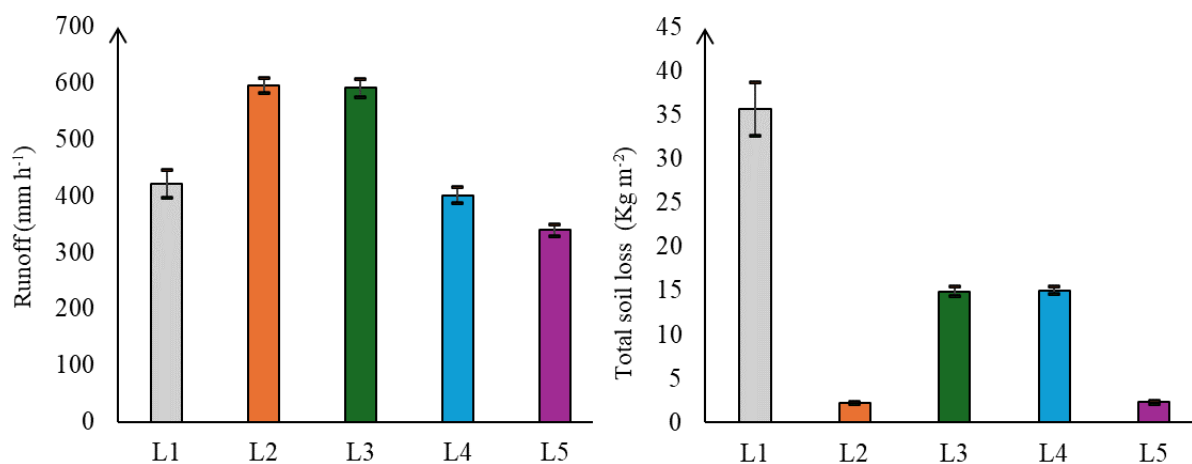


Figure 11. Total soil loss amounts (average and standard deviation bars from all samples collected) observed during a complete experiment for the 5 layouts.

The soil moisture in L1 at 30 minutes was $0.1922 \text{ cm}^3 \text{ cm}^{-3}$, which represented a 51.8% increase compared to the initial value. Additionally, it was 68.7%, 82.7%, 95.4%, and 63.5% higher than the moisture levels in L2, L3, L4, and L5, respectively.

Table 3. Soil moisture and runoff rates, beginning of runoff, disaggregation rate and total of soil loss in five different layouts with rainfall intensity of 60 mm h^{-1} .

Layout	Soil Moisture		Runoff (mm h^{-1})	Beginning of runoff (min)	Detachment Ratio ($\text{kg m}^{-2} \text{ s}^{-1}$)	Total soil loss (g)
	Before	After				
L1	0.0996	0.1922	421.10	19.36	4.28	301.30
L2	0.0953	0.1321	595.30	6.52	0.27	34.60
L3	0.1173	0.1587	591.30	9.75	1.78	26.37
L4	0.1115	0.1831	400.90	13.15	1.80	173.57
L5	0.1130	0.1221	339.20	8.94	0.27	172.23

The highest erosion was observed in the soils uniformly burned (L1) ($4.28 \pm 3.019 \text{ kg ha}^{-1}$, value averaged by slope), and the lowest in L2 and L5 ($2.24 \pm 0.535 \text{ kg ha}^{-1}$). As for runoff, the highest and lowest soil losses, were observed in L3 ($7.68 \pm 4.88 \text{ mm h}^{-1}$) and L4 ($5.07 \pm 2.554 \text{ mm h}^{-1}$), respectively.

Figure 12 presents the turbidity and sediment loss for all five different layouts. The suspended sediment concentration was evaluated using a turbidimeter for each collected runoff sample. After drying in an oven, the total soil loss per collection was determined. In general, a higher concentration of suspended solids in runoff samples was observed in L1 and L3, corresponding to the treatments of uniform burning over the area and fractional burning in three portions. The total sediment losses in L1 were 54% to 60% higher than in the other layouts.

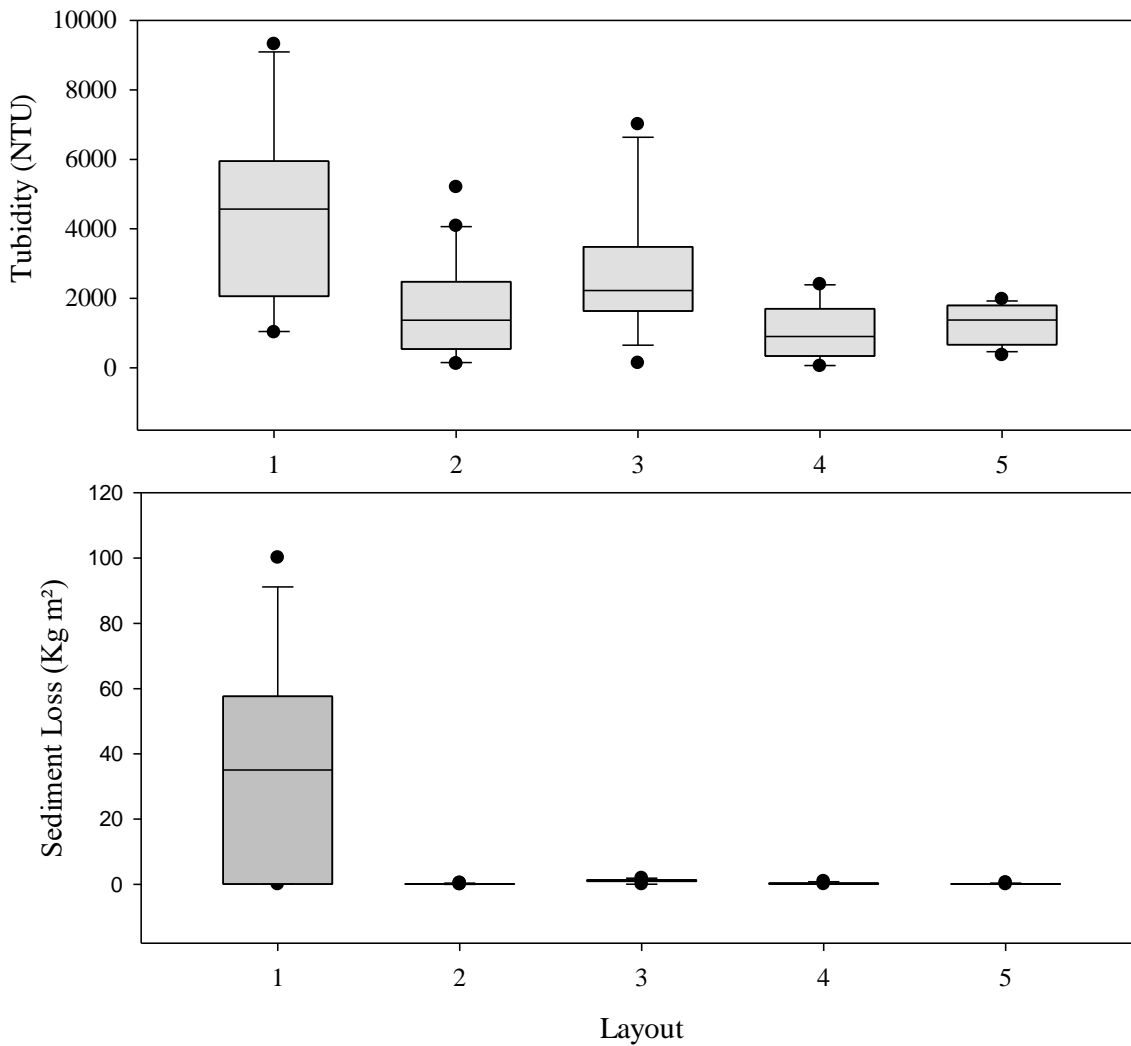


Figure 12. Concentrations of sediments (NTU) for runoff surface water samples and Sediment Loss collected during simulated rain events.

II.3.3 Ash transport

This section of the study explores the impact of different ash layouts on its mobility. The Figure 13 present the temporal variations in average of ash transported by runoff considering different distributions of ash.

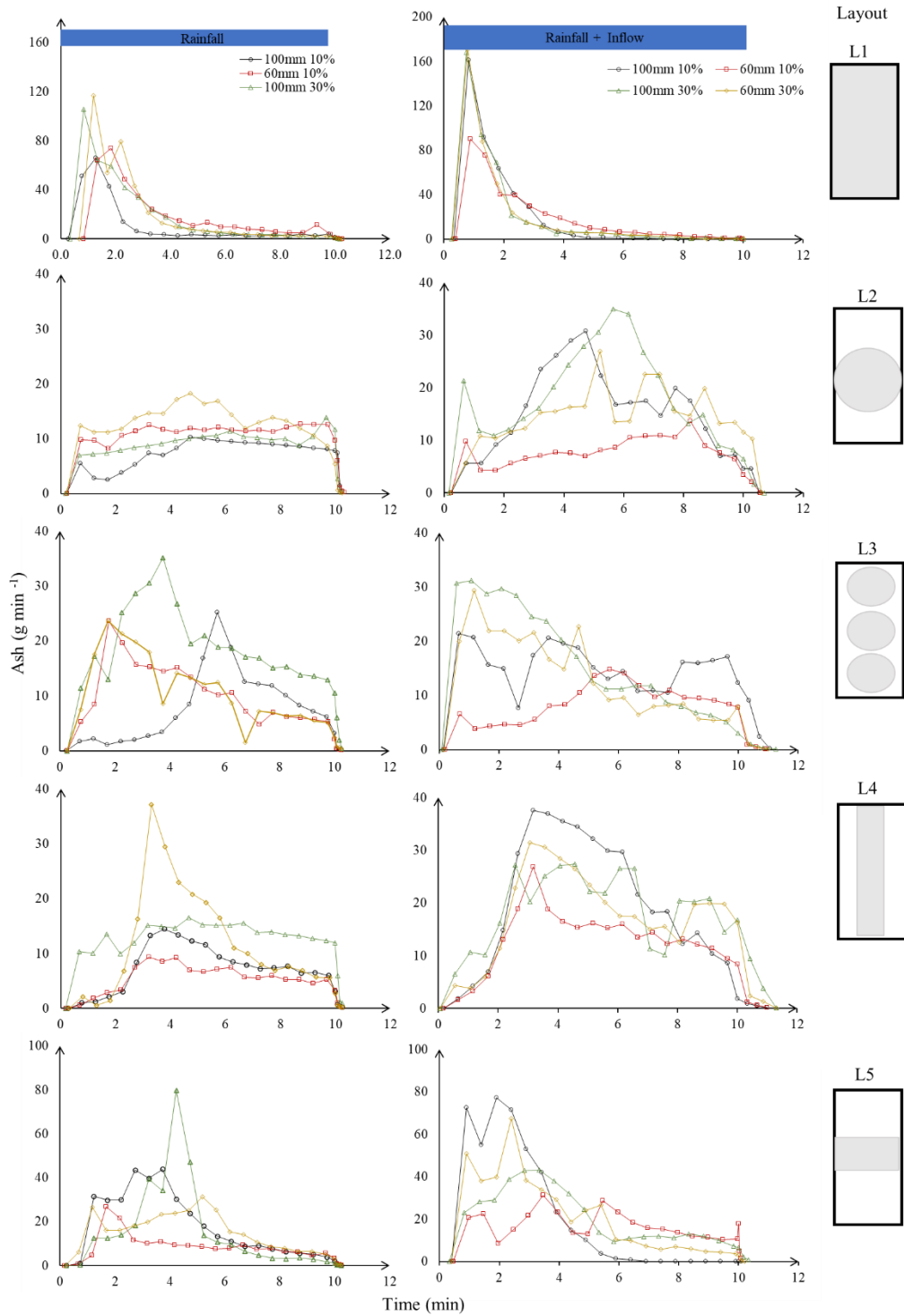


Figure 13. Ash transportation (g min^{-1}) by rainfall and rainfall + inflow for the five layouts.

Regarding to the Layout 1(uniform distribution), all applied ash content was removed by rain and rain + inflow in the first 5 minutes of the experiment. Throughout the experiment, ash particles tended to group in the downstream section of the flume, immediately upstream of the collector gutter. As particles accumulated, they initiated a downhill movement that induced significant particle mobilization during the initial minutes. This phenomenon bears resemblance to findings by Abrantes et al. (2018), which noted that diminished surface runoff could be attributed, in part, to the protective role played by the cover against the direct impact of raindrops. This protection promotes the dispersion of the kinetic energy of the raindrops, thereby mitigating the detachment of the aggregates. In this study, the higher density of the ash cover, resulting from the reduced distribution area, had an attenuating effect on soil disaggregation.

For Layouts 2 (T2) and 3 (T3), the mobilization unfolded at a more gradual pace, allowing some particles to linger at the downstream section of the flume by the end of the test. Despite the rain disaggregation of the ash cover on the surface, the limited contact of the flow with the ashes retained the particles in their original position.

The values of total ash transported in the experiments are summarized in Table 4. Regarding to start time of runoff, the Layout 1, with uniform ash distribution, runoff started significantly later compared to the others layout, under rainfall conditions of 60 mm h⁻¹ and 100 mm h⁻¹ as well as both sloping surfaces and when rainfall and rainfall + inflow were combined.

Table 4. Total amount of ash transported for all runs considering two intensities of rainfall and two slopes.

Layout	100 mm 10%		60 mm 10%		100 mm 30%		60 mm 30%		
	Start time (s)	Total (g)							
T1	R	16	369.2	50	225.7	20	400.5	41	383.8
	R+I	20	417.2	23	383.3	15	420.8	17	404.5
T2	R	13	196.2	14	160.0	10	234.0	13	262.3
	R+I	14	320.0	13	161.5	9	378.0	12	312.4
T3	R	13	202.7	16	160.8	15	378.4	15	212.6
	R+I	9	299.7	12	170.9	5	302.2	10	257.5

T4	R	16	151.3	12	113.5	10	267.5	18	236.5
	R+I	10	362.7	10	349.3	4	391.5	4	263.4
T5	R	14	363.4	10	180.7	14	319.5	11	304.2
	R+I	24	353.2	28	333.1	20	397.1	24	378.2

On average, Layouts 2 and 3 achieved a reduction in ash transport of 19% and 30%, respectively, compared to Layout 1, which exhibited the highest ash transport across all cases. Layouts 4 and 5, on the other hand, demonstrated smaller reductions in runoff, with decreases of 11% and 10%, respectively. Layouts 2, 3, and 4 showed significant differences in ash content transport from Layout 1 for 100- and 60-mm h⁻¹ intensities and on 10 and 30% slopes. For Layouts 4 and 5, the only significant difference was seen for 60 mm h⁻¹ intensity and 10% slope, considering only the rainfall.

Figure 14 shows the total ash transported along the events, in the respective treatments, for the simulated rain, rain + inflow and slope conditions.

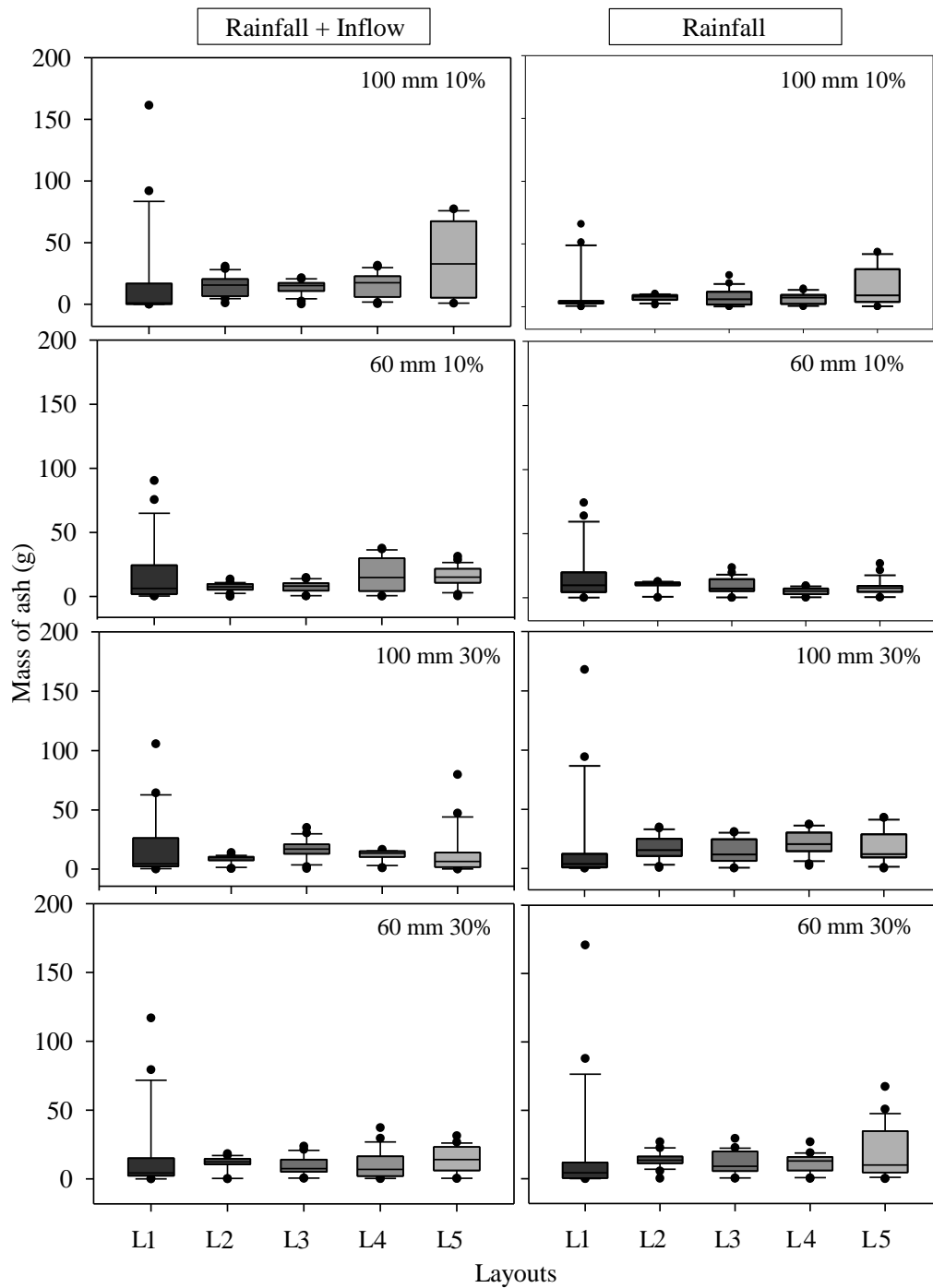


Figure 14. Box plot mass of ash in each layout of distribution for both 10 and 30% of slope, and 60- and 100-mm h^{-1} rainfall simulation.

It is observed that the presence of the upslope inflow provided an increase in the amount of ash transported. Considering all the evaluated layouts, the precipitation of 100 mm h^{-1} produced an average carried of 31.24 and 26.41 g min^{-1} for 30 and 10% slope, respectively;

while the precipitation of 60 mm h^{-1} presented mean values of 27.98 and 16.8 g min^{-1} for 30 and 10% slope, respectively. Wag et al. (2020) had similar findings, where they examined the effects of upslope inflow and rainfall on slope erosion, as well as distinguishing their individual effects on sediment production. The authors observed that upslope inflow increased sediment production five-fold, which is in line with the current study - larger amounts of ash are being transported with increasing inflow. These results emphasize the need to account for run-on in field simulations in order to accurately reflect real-life situations. Another relevant aspect raised by Wang et al. (2020) was the effect of precipitation intensity on sediment production. The authors observed that the contributions of synergistic effects increased with increasing rainfall intensity. This increase can be observed for both slopes evaluated in this paper.

II.3.3 Effectiveness of ash layouts

This laboratory study shows that distributing ashes in smaller bands (e.g., sections of areas) with higher coverage density reduced the mobility of the ashes via surface runoff. Figure 15 presents the coverage percentages at the start and end of the simulations.

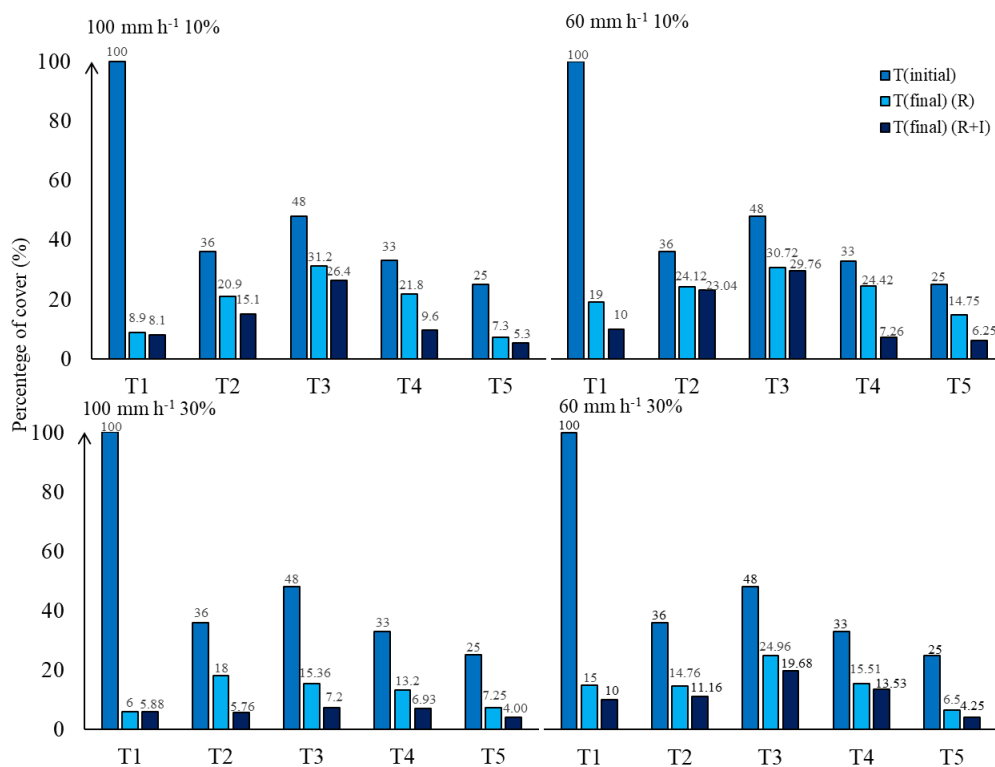


Figure 15. Comparison of cover percentage among five different layouts before and after rainfall simulation considering two rain intensities (60 - and 100-mm h^{-1}) and two slopes (10 and 30%).

The percentage coverage variation between treatments increased, especially for Layout 1 which showed the highest standard deviation and a decrease of 80 to 87% when compared before and after the tests. Distribution T2 and T3 showed higher percentage values of coverage after the simulation, corroborating with the efficiency previously shown, where the treatments were efficient in reducing the mobility of ashes through runoff.

The geometries of distribution 4 and 5 were efficient when compared to distribution T1, however, they suffered heavily from the influence of inflow and kinetic energy of the rain. In general, considering varying rainfall intensities and slopes, the 30% slope and heavier rainfall conditions were associated with a higher transport of ash (Fig. 16).

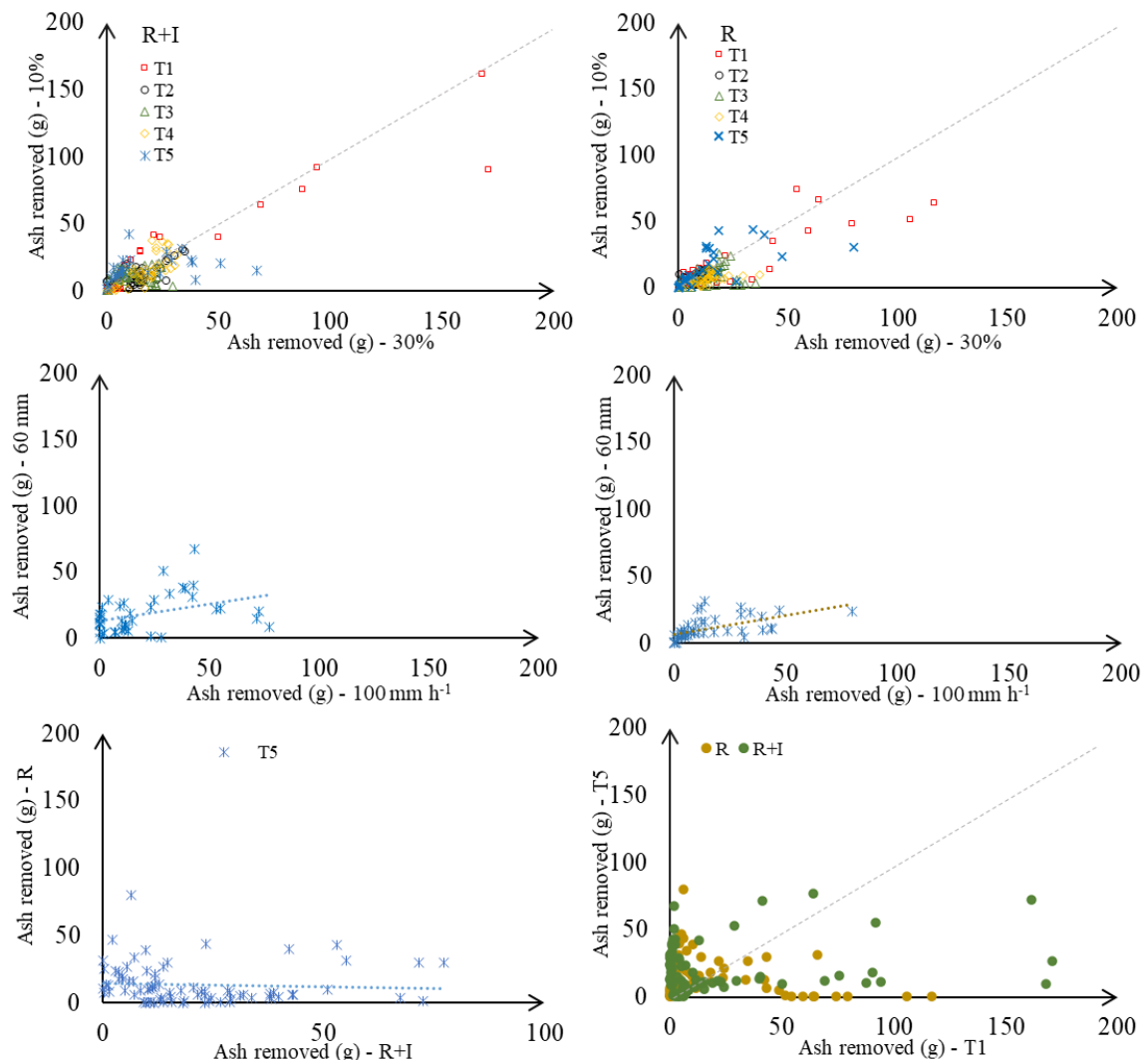


Figure 16. Correlations among ash removed (in grams) observed by rainfall simulator under five ash layouts and two slopes.

The results show that the highest coefficients of correlation ($r^2 > 0.9$) were observed for Layout 1, specifically between 30% of slope and 10% in the context of simulated rainfall. However, when factoring in both rainfall and upslope inflow, the corresponding r^2 decreased to 0.7. The remaining layouts exhibited lower coefficients, with Layouts T4, T2, T5, and T2 showing r^2 values of 0.6, 0.4, 0.2, and 0.1, respectively. Similarly, in the scenario of rainfall + inflow, Layouts T2, T4, T5, and T3 demonstrated coefficients of correlation of 0.6, 0.5, 0.4, and 0.1, respectively. It can be concluded that, overall, Layouts 3 showed lower sensitivity to changes in slope and the presence or absence of inflow.

In terms of the correlations between the two assessed rainfall intensities, Layout 1 exhibited a correlation coefficient of 0.92, followed by T2 with an r^2 of 0.43, and T4 with an r^2 of 0.42. The remaining layouts displayed coefficients lower than 0.3. Taking into account the presence of inflow, T1 continued to exhibit a high correlation coefficient of 0.92, while the other layouts showed coefficients below 0.20.

The relationship between rainfall combined with inflow and rainfall alone was significant for ash disposal Layouts 1 (T1) and 4 (T4). However, for the remaining layouts, the r^2 values remained below 0.3.

II.4 Conclusion

The main conclusions regarding the soil flume field and laboratory experiments carried out in this study, considering simulated uniform rainfall events with the addition of an upslope inflow, under five different ash layouts of distribution, are:

The decreased area of ash exposed to rain meant that the coverage density increased, which in turn reduced the rain's erosive impact on ash particles and decreased the erosion rate.

The circular distributions, single and divided into 3 fractions, reduced the mass of ash transported by runoff by 30% when compared to the uniform distribution. This result could be useful and a viable alternative for the preservation of in locus ash, providing a nutritional contribution in burned areas.

The alignment of ash parallel to the direction of the flow was more effective in minimizing the movement of ash through the flow than when the alignment was perpendicular.

These conclusions seem to clearly justify follow-up tests in field conditions, both in less steep and intensively managed agricultural areas with high erosion risk, and in recently burned areas. Future work should take into account the whole soil structure, allowing for the evaluation

of other efficient practices not only in reducing the mobility of ash but also in soil conservation and the context of agricultural soil fertility and crop productivity.

References

- Abrantes, J.R.C.B., Prats, S.A., Keizer, J.J., Lima, J.L.M.P. De, 2018. Soil & Tillage Research E ff ectiveness of the application of rice straw mulching strips in reducing runoff and soil loss: Laboratory soil flume experiments under simulated rainfall 180, 238–249. <https://doi.org/10.1016/j.still.2018.03.015>
- Abreu, M. C., Lyra, G. B., de Oliveira-Júnior, J. F., Souza, A., Pobočíková, I., de Souza Fraga, M., & Abreu, R. C. R. (2022). Temporal and spatial patterns of fire activity in three biomes of Brazil. *Science of the Total Environment*, 844(June 2021). <https://doi.org/10.1016/j.scitotenv.2022.157138>
- Abreu, R.C.R., Durigan, G., Melo, A.C.G., Pilon, N.A.L., Hoffmann, W.A., 2021. Facilitation by isolated trees triggers woody encroachment and a biome shift at the savanna–forest transition. *J. Appl. Ecol.* 58 (11), 2650–2660. <https://doi.org/10.1111/1365-2664.13994>.
- Barbosa, H.A., Lakshmi Kumar, T.V., Paredes, F., Elliott, S., Ayuga, J.G., 2019. Assessment of Caatinga response to drought using Meteosat-SEVIRI normalized difference vegetation index (2008–2016). *ISPRS J. Photogramm. Remote Sens.* 148, 235–252. <https://doi.org/10.1016/j.isprsjprs.2018.12.014>.
- Bezerra, S.A., Cantalice, J.R.B., 2006. Interrill erosion under different conditions of soil cover of sugarcane. *Braz. J. Soil Sci.* 30, 565–573. <https://doi.org/10.1590/S0100-06832006000300016>.
- Carmona-Yáñez, M.D., Francos, M., Miralles, I., Soria, R., Ahangarkolae, S.S., Vafaie, E., Zema, D.A., Lucas-Borja, M.E., 2023. Short-term impacts of wildfire and post-fire mulching on ecosystem multifunctionality in a semiarid pine forest. *Forest Ecology and Management* 541. <https://doi.org/10.1016/j.foreco.2023.121000>
- Carvalho, A. A., Abelardo, A. A., da Silva, H. P., Lopes, I., de Moraes, J. E. F., & da Silva, T. G. F. (2020). Trends of rainfall and temperature in Northeast Brazil. *Revista Brasileira de Engenharia Agrícola e Ambiental*, 24(1), 15–23. <https://doi.org/10.1590/1807-1929/agriambi.v24n1p15-23>
- Caúla, R.H., Oliveira-Júnior, J.F., Lyra, G.B., Delgado, R.C., Heilbron, P.F.L., 2015. Overview of fire foci causes and locations in Brazil based on meteorological satellite data from

- 1998 to 2011. *Environ. Earth Sci.* 74, 1497–1508. <https://doi.org/10.1007/s12665-015-4142-z>
- Caúla, R.H.; Oliveira-Júnior, J.F.; Lyra, G.B.; Delgado, R.C.; Heilbron Filho, P.F.L. Overview of fire foci causes and locations in Brazil based on meteorological satellite data from 1998 to 2011. *Environ. Earth Sci.* 2015, 74, 1497–1508.
- Christiansen, J.E., 1942. *Irrigation by Sprinkling*, California Agricultural Experiment Station Bulletin 670. University of California, Berkeley, CA, USA 128 pp.
- Cleveland, W.S., Devlin, S.J., 1988. Locally Weighted Regression: An Approach to Regression Analysis by Local Fitting. *J. Am. Stat. Assoc.*, 83(403), 596-610.
- Cleveland, W.S., Devlin, S.J., Grosse, E., 1988. Regression by local fitting. *Methods Prop. Comput. Algorithms J. Econom.* 37, 87–114.
- Coelho, V.H. R., Montenegro, S., Almeida, C. N., Silva, B. B., Oliveira, L. M., Cláudia, A., Gusmão, V., Freitas, E. S., & Montenegro, A. A. A. (2017). Alluvial groundwater recharge estimation in semiarid environment using remotely sensed data. *Journal of Hydrology*, 548, 1–15. <https://doi.org/10.1016/j.jhydrol.2017.02.054>
- Silva, J. L. B. da, Moura, G. B. de A., Silva, M. V. da, Lopes, P. M. O., Guedes, R. V. de S., Silva, Ê. F. de F. e., Ortiz, P. F. S., & Rodrigues, J. A. de M. (2020). Changes in the water resources, soil use and spatial dynamics of Caatinga vegetation cover over semiarid region of the Brazilian Northeast. *Remote Sensing Applications: Society and Environment*, 20. <https://doi.org/10.1016/j.rsase.2020.100372>
- da Silva, B. F., dos Santos Rodrigues, R. Z., Heiskanen, J., Abera, T. A., Gasparetto, S. C., Biase, A. G., Ballester, M. V. R., de Moura, Y. M., de Stefano Piedade, S. M., de Oliveira Silva, A. K., & de Camargo, P. B. (2023). Evaluating the temporal patterns of land use and precipitation under desertification in the semiarid region of Brazil. *Ecological Informatics*, 77. <https://doi.org/10.1016/j.ecoinf.2023.102192>
- Elakiya N., Keerthana G., and Safiya S. 2023. “Effects of Forest Fire on Soil Properties”. *International Journal of Plant & Soil Science* 35 (20):8-17. <https://doi.org/10.9734/ijpss/2023/v35i203780>.
- Eskandari, S., H. R. Pourghasemi, and J. P. Tiefenbacher. 2021. Fire-susceptibility mapping in the natural areas of Iran using new and ensemble data-mining models. *Environmental Science and Pollution Research* 28(34): 47395–47406. Springer Science and Business <https://doi.org/10.1007/s11356-021-13881-y>

- Farr, T. G., & Kobrick, M. (2000). Shuttle Radar Topography Mission Produces a Wealth of Data. *Eos Transactions American Geophysical Union*, 81, 583-585. <https://doi.org/10.1029/EO081i048p00583>
- Freitas, W.K., Gois, G., Pereira Junior, E.R., Oliveira Júnior, J.F., Magalhães, L.M.S., Brasil, F.C., Sobral, B.S., 2020. Influence of fire foci on forest cover in the Atlantic Forest in Rio de Janeiro, Brazil. *Ecol. Indic.* 115, 106340. <https://doi.org/10.1016/j.ecolind.2020.106340>.
- Ghorbanzadeh, O., T. Blaschke, K. Gholamnia, and J. Aryal. 2019. Forest fire susceptibility and risk mapping using social/infrastructural vulnerability and environmental variables. *Fire* 2(3): 1–27. MDPI AG. <https://doi.org/10.3390/fire2030050>.
- IPCC - The Intergovernmental Panel on Climate Change, 2021. Special report on climate change and land.
- Kendall, M.G., 1975. Rank Correlation Methods. 4th edition. Charles Griffin, London.
- Kruger, B. R., Hausner, M. B., Chellman, N., Weaver, M., Samburova, V., & Khlystov, A. (2023). Dissolved black carbon as a potential driver of surface water heating dynamics in wildfire-impacted regions: A case study from Pyramid Lake, NV, USA. *Science of the Total Environment*, 888(December 2022), 164141. <https://doi.org/10.1016/j.scitotenv.2023.164141>
- Kumar, B.P., Babu, K.R., Anusha, B.N., Rajasekhar, M., 2022. Geo-environmental monitoring and assessment of land degradation and desertification in the semiarid regions using Landsat 8 OLI/TIRS, LST and NDVI approach. *Environmental Challenges* 8, 100578. <https://doi.org/10.1016/j.envc.2022.100578>
- Liang X. M., Chen Q., Rana M. S., Dong Z. H., Liu X. D., Hu C. X., et al. (2021). Effects of soil amendments on soil fertility and fruit yield through alterations in soil carbon fractions. *J. Soil Sediment* 21 2628–2638. [10.1007/s11368-021-02932-z](https://doi.org/10.1007/s11368-021-02932-z)
- Liang, F., Feng, L., Liu, N., He, Q., Ji, L., de Vrieze, J., & Yan, S. (2022). An improved carbon fixation management strategy into the crop–soil ecosystem by using biomass ash as the medium. *Environmental Technology and Innovation*, 28, 102839. <https://doi.org/10.1016/j.eti.2022.102839>
- Lins, C. M. T., de Souza, E.R., Souza, T.E.M.S., Paulino, M.K.S.S., Monteiro, D.R., Souza Júnior, V.S., Dourado, P.R.M., Rego Junior, F.E.A, da Silva, Y.J.A., Schaffer, B., 2023. Influence of vegetation cover and rainfall intensity on soil attributes in an area

- undergoing desertification in Brazil. *Catena* 221. <https://doi.org/10.1016/j.catena.2022.106751>
- Lucas-Borja et al., 2023.
- Lucas-Borja, M.E; Plaza-Álvarez, P.A.; Uddin, S.M.M.; Parhizkar, M.; Zema, D.A. Short-term hydrological response of soil after wildfire in a semiarid landscape covered by *Macrochloa tenacissima* (L.) Kunth. *Journal of Arid Environments*, v.198, 2022.
- Mann, H.B., 1945. Nonparametric tests against trend. *Econometrica*, 13, 245–259. doi:10.2307/1907187
- MapBiomas Brazil Project – Collection [6.0 and 7.0] of the Annual Series of Land Use and Land Cover Maps of Brazil, 2022. http://mapbiomas.org/colecoes-mapbiomas-1?ca_ma_set_language=pt-BR.
- Marinho, A.A.R., Gois, G. de, Oliveira-Júnior, J.F. de, Correia Filho, W.L.F., Santiago, D. de B., Silva Junior, C.A. da, Teodoro, P.E., de Souza, A., Capristo-Silva, G.F., Freitas, W.K. de, Rogério, J.P., 2021. Temporal record and spatial distribution of fire foci in State of Minas Gerais, Brazil. *Journal of Environmental Management* 280. <https://doi.org/10.1016/j.jenvman.2020.111707>
- Mitchell, J., 2023. EasyChair Preprint Analysis of Utility Wildfire Risk Assessments and Mitigations in California. *Fire Safety Journal* 140, 103879. <https://doi.org/10.1016/j.firesaf.2023.103879>
- MI/SUDENE. Ministério da Integração Nacional/Superintendência do Desenvolvimento do Nordeste. Nova delimitação da região semiárida do Brasil/Resolução nº 115, de 23 de novembro de 2017.
- MMA, 2007. Atlas of Areas Susceptible to Desertification in Brazil [in Portuguese]. <https://unesdoc.unesco.org/ark:/48223/pf0000159542>.
- Montebeller, C.A., Carvalho, D.F., Sobrinho, T.A., Nunes, A.C.S., Rubio, E., 2001. Avaliação hidráulica de um simulador de chuvas pendular. *Braz. J. Agric. Environ. Eng.* 1, 1–5.
- Mukhopadhyay, S
- Montenegro, A.A.A., Montenegro, S.M.G.L., 2006. Variabilidade espacial de classes de textura, salinidade e condutividade hidráulica de solos em planície aluvial. *Rev. Bras. Eng. Agrícola e Ambient.* 10, 30–37. <https://doi.org/10.1590/s1415-43662006000100005>
- Nunes MTO, Sousa GM, Tomzhinski GW, Oliveira-Júnior JF, Fernandes MC. 2015. Variáveis Condicionantes na Susceptibilidade de Queimadas e Incêndios no Parque Nacional do

- Itatiaia. Anuário do Instituto de Geociências (UFRJ. Impresso) 38: 54–62. DOI:10.11137/2015_1_54_62.
- Oliveira, M.L., Santos, C.A., Oliveira, G., Silva, M.T., Silva, B.B., Cunha, J.E.B.L., et al., 2022. Remote sensing-based assessment of land degradation and drought impacts over terrestrial ecosystems in Northeastern Brazil. *Sci. Total Environ.* 835, 155490 <https://doi.org/10.1016/j.scitotenv.2022.155490>.
- Oliveira, P.T., Santos e Silva, C.M., Lima, K.C., 2017. Climatology and trend analysis of extreme precipitation in subregions of Northeast Brazil. *Theor. Appl. Climatol.* 130, 77–90. <https://doi.org/10.1007/s00704-016-1865-z>.
- Pereira, P., Francos, M., Brevik, E.C., Ubeda, X., Bogunovic, I. (2018) Post fire management. *Current Opinion in Environmental Science and Health* (In press), p.1-21, n.2.
- Pettitt, A. N., 1979. A Non-Parametric Approach to the Change-Point Problem. *J R Stat Soc Series C (Applied Statistics)*, 28 (2), pp. 126-135. <https://doi.org/10.2307/2346729>
- Prats, S.A., Abrantes, J.R.C. de B., Coelho, C. de O.A., Keizer, J.J., de Lima, J.L.M.P., 2018. Comparing topsoil charcoal, ash, and stone cover effects on the postfire hydrologic and erosive response under laboratory conditions. *Land Degradation and Development* 29, 2102–2111. <https://doi.org/10.1002/ldr.2884>
- Prats, S.A., Merino, A., Gonzalez-Perez, J.A., Verheijen, F.G.A., De la Rosa, J.M., 2021. Can straw-biochar mulching mitigate erosion of wildfire-degraded soils under extreme rainfall? *Science of the Total Environment* 761, 143219. <https://doi.org/10.1016/j.scitotenv.2020.143219>
- R Core Team, 2020. *Language and Environment for Statistical Computing*. R Foundation for Statistical Computing, Vienna, Austria. URL <https://www.R-project.org/>
- Refati, D.C., Silva, J.L.B. da, Macedo, R.S., Lima, R. da C.C., Silva, M.V. da, Pandorfi, H., Silva, P.C., Oliveira-Júnior, J.F. de, 2023. Influence of drought and anthropogenic pressures on land use and land cover change in the Brazilian semiarid region. *Journal of South American Earth Sciences* 126. <https://doi.org/10.1016/j.jsames.2023.104362>
- Roth, H.K., McKenna, A.M., Simpson, M.J., Chen, H., Srikanthan, N., Feghel, T.S., Nelson, A.R., Rhoades, C.C., Wilkins, M.J., Borch, T., 2023. Effects of burn severity on organic nitrogen and carbon chemistry in high-elevation forest soils. *Soil & Environmental Health* 1, 100023. <https://doi.org/10.1016/j.seh.2023.100023>
- Santos, T.E.M. dos, Montenegro, A.A.A., 2012. Erosividade e padrões hidrológicos de precipitação no Agreste Central pernambucano Erosivity and rainfall hydrological

- patterns in the Pernambuco Agreste Central. *Revista Brasileira de Engenharia Agrícola e Ambiental* 871–880.
- Schmidt, A., Ellsworth, L. M., Tilt, J. H., & Gough, M. (2023). Application of deep convolutional networks for improved risk assessments of post-wildfire drinking water contamination. *Machine Learning with Applications*, 11(December 2022), 100454. <https://doi.org/10.1016/j.mlwa.2023.100454>
- Sen, P.K. 1968. Estimates of the regression coefficient based on Kendall's tau. *J Am. Stat. Assoc.* 63(324), 1379–1389.
- Sousa, L. B., Montenegro, A. A., da Silva, M. V., Almeida, T. A. B., de Carvalho, A. A., da Silva, T. G. F., & de Lima, J. L. M. P. (2023). Spatiotemporal Analysis of Rainfall and Droughts in a Semiarid Basin of Brazil: Land Use and Land Cover Dynamics. *Remote Sensing*, 15(10). <https://doi.org/10.3390/rs15102550>
- Souza, M.C.S., Stosic, B. 2005. Technical Efficiency of the Brazilian Municipalities: Correcting Nonparametric Frontier Measurements for Outliers. *Journal of Productivity Analysis*, n.24, p.157–18.
- Stavi, I. Wildfires in grasslands and shrublands: a review of impacts on vegetation, soil, hydrology, and geomorphology.2019. *Water*, 11, p. 1042, 2019.
- Thomas, G.; Rosalie, V.; Olivier, C.; Girolamo, A.M.; Lo Porto, A. Modelling Forest fire and firebreak scenarios in a Mediterranean mountainous catchment: Impacts on sediment loads. *Journal of Environmental Management*, n.289, p.11-0, 2021.
- Tinôco, I.C.M., Bezerra, B.G., Lucio, P.S., Barbosa, L.M., 2018. Characterization of rainfall patterns in the semiarid Brazil. *Anu. Inst. Geocienc.* 41, 397–409. https://doi.org/10.11137/2018_2_397_409.
- Tran, T. T. K., Bateni, S. M., Rezaie, F., Panahi, M., Jun, C., Trauernicht, C., & Neale, C. M. U. (2023). Enhancing predictive ability of optimized group method of data handling (GMDH) method for wildfire susceptibility mapping. *Agricultural and Forest Meteorology*, 339. <https://doi.org/10.1016/j.agrformet.2023.109587>
- Vieira, D. C. S.; Serpa, D.; Nunes, J. P. C.; Prats, S. A.; Neves, R.; Keizer, J. J. Predicting the effectiveness of different mulching techniques in reducing post-fire runoff and erosion at plot scale with the RUSLE, MMF and PESERA models. *Environmental Research*, n.165, p.365-378, 2018. DOI: 10.1016/j.envres.2018.04.029
- Wang, L., Zheng, F., Zhang, X.J., Wilson, G. V., Qin, C., He, C., Liu, G., Zhang, J., 2020. Discrimination of soil losses between ridge and furrow in longitudinal ridge-tillage

under simulated upslope inflow and rainfall. *Soil and Tillage Research* 198, 104541.
<https://doi.org/10.1016/j.still.2019.104541>

Woods, S.W., Balfour, V.N., 2008. The effect of ash on runoff and erosion after a severe forest wildfire, Montana, USA. *International Journal of Wildland Fire* 17, 535–548.
<https://doi.org/10.1071/WF07040>

Zema, D.A., Plaza-Alvarez, P.A., Xu, X., Carra, B.G., Lucas-Borja, M.E., 2021a. Influence of forest stand age on soil water repellency and hydraulic conductivity in the Mediterranean environment. *Sci. Total Environ.* 753, 142006.

Chapter III: Hydrogeological trends in an alluvial valley in the Brazilian semiarid: impacts of observed climate variables change and exploitation on groundwater availability and salinity

Abstract: Water scarcity significantly impacts the development of semiarid regions. In Brazil, groundwater from alluvial valleys of temporary rivers is a crucial water source in the semiarid zone. However, processes of salt accumulation and frequent aquifer overexploitation for communal irrigation, exacerbated by climate change, threaten future groundwater availability. Salinization also poses a significant challenge. This chapter assesses the influence of climate variability and exploitation on groundwater accessibility, quantity, and quality. Spatiotemporal data analysis from monthly field campaigns conducted from 2000 to 2019 in the Mimoso Rivulet Basin, Pernambuco State, Brazil, was performed. Results show that salinity variability is linked to the salt balance, particularly in areas with low hydraulic permeability and groundwater irrigation. Groundwater salinity correlates strongly with rainfall and groundwater levels. Evapotranspiration rise, coupled with declining rainfall and groundwater levels, exacerbates groundwater scarcity and overexploitation. Groundwater salinity exhibits a decreasing trend in pumping wells but no significant trend in piezometers. Groundwater pumping emerges as a management alternative to control salinity, crucial for mitigating long-term water shortages in this severely water-scarce region.

Keywords: Temporal stability, groundwater dynamics, Mann Kendall, Sen's Slope

III.1 Introduction

Dry periods are part of the natural cycle of a semiarid environment, usually influencing the availability of water resources for different purposes. The Brazilian semiarid region is characterized by an irregular rainfall regime and high potential evapotranspiration rates (Montenegro and Ragab, 2010). Based on historical data and future trends, Marengo and Bernasconi (2015) highlighted the high risk of aridification in the Brazilian semiarid lands based on regional climate projections (i.e., prediction of rainfall reductions, temperature increases, and water deficits for longer periods). In this context, Carvalho et al. (2020) predicted a reduction in the number of rainy days, with impacts on future water resources availability. This increase in aridity, along with land degradation by agricultural use and deforestation, tends to increase environmental vulnerability and desertification rates in the semiarid region of Brazil, aggravating scenarios of water scarcity (Silva et al., 2022).

Although Brazil holds more than 12% of the global renewable freshwater, its population frequently faces water scarcity, particularly in the Northeast region, which presents less than 4% of the national water resources but supports about 35% of the national population (Rodrigues et al., 2015). Field hydrological studies in the Northeast region are still very limited due to the large area of the country and the high costs involved in continuous field monitoring campaigns, despite several efforts from Brazilian agencies to provide funds to support these investigations (Melo et al., 2020). For groundwater, the ground-based monitoring network is particularly sparse and restricted to a few widely distributed wells (Melo et al., 2020). The national monitoring network consists of about 375 wells across of all Brazil, complemented by a small number of observation wells monitored in only 21 active experimental basins.

Some studies carried out in other semiarid regions worldwide identified a progressive reduction of groundwater availability and depletion (e.g., Famiglietti, 2014; Cuthbert et al., 2019; Hu et al, 2019; Bahir et al., 2020), which, if occurring in the Brazilian semiarid, can limit even more the access to water in the region. For instance, Bahir et al. (2020) observed a significant decline in the piezometric levels of a regional aquifer located in a semiarid region in Morocco for 43 years due to the adverse effects of climate change, followed by a spatial-temporal deterioration of the groundwater quality during the monitored period.

Considering the geological characteristics of the Brazilian semiarid region (i.e., a crystalline domain, comprising impermeable and fissured igneous and metamorphic Precambrian rocks, with shallow soils), alluvial aquifers are essential for agricultural and domestic water supply, given the scarce availability of surface water. Nevertheless, these

aquifers usually present limited water volumes as a result of their geomorphological characteristics, the shallow soils at the hillslope boundaries, and the dimensions of the geological formations (Andrade et al., 2014; Fontes Júnior et al., 2017; Montenegro and Ragab, 2010). Such features generally reduce the groundwater recharge of alluvial aquifers in the area, raising concerns about water availability, particularly during prolonged droughts (Coelho et al., 2017). Mackay et al. (2005) identified potential links between hillslope runoff, groundwater use, subsurface controls, and the annual and longer-term variations in water availability and water quality in alluvial valleys of Brazilian semiarid, being groundwater salinity strongly correlated to the geology, soil texture, irrigation leaching, water table depths, and surface water salinity of the mainstream tributaries. Mott MacDonalds (2006) developed a comprehensive study of the potential of alluvial valleys for water security in the semiarid region of Pernambuco State Semiarid, Brazil, including the Mimoso Valley investigated in this paper, where the Knowledge and Research Programme (KaR) project proposed relevant guidelines towards sustainable management alternatives for small alluvial valleys in the studied region, such as adoption of a participatory approach for controlling over pumping during drought periods, and strategies for reducing applied irrigation water depths, which could increase groundwater salt contents.

In addition to the climatic impact, the anthropogenic pressures (e.g., increasing the aquifer pumping rates and salt leaching from irrigated areas) also might lead to the qualitative and quantitative depletion of the alluvial groundwater, causing an excessive lowering of piezometric levels (Ribeiro et al., 2015), along with salt accumulation hazards (Schoups et al., 2005; Montenegro et al., 2010). Besides that, deforestation has been highlighted as a main cause of climatic variability in Brazil (Mu and Jones, 2022). Thus, there is a growing need to develop regular monitoring programs for a sustainable use of the alluvial groundwater resources in parallel with studies for identifying the recharge dynamics and potential mitigation measures (Burte et al., 2009; Coelho et al., 2017; Zhang et al., 2022). Alluvial valleys present strong seasonal variation in terms of stored water volume and salinity due to anthropogenic, hydrological, and climatic conditions (Burte et al., 2005; Andrade et al., 2012; Panzand et al., 2018). Hence, long-term groundwater quantity and quality monitoring are essential for the development of sustainable management strategies (Kumar and Sangeetha, 2020), providing bases for alluvial aquifer sustainability (Abdullahi et al., 2015; Gibrila et al., 2018; Silva Filho et al., 2020).

The Mimoso Stream Basin, located in the semiarid region of Pernambuco State, is one of the 21 active experimental basins identified by Melo et al. (2020) with long-term studies and groundwater monitoring in Brazil. During recent decades, some studies in this basin advanced toward understanding the spatial and temporal distribution of groundwater (e.g., Montenegro, 1997; Monteiro et al., 2014; Fontes Júnior e Montenegro, 2017), groundwater quality (e.g., Andrade et al., 2012), the spatial distribution of groundwater recharge (e.g., Montenegro et al., 2010; Coelho et al., 2017), and the use of groundwater for agricultural production and water consumption (e.g., Mackay et al., 2005; Mott MacDonalds, 2006; Montenegro et al., 2010; Souza et al., 2011; Santos et al., 2018). The investigations were conducted in the alluvial valley of the Mimoso Stream Basin based on field hydrological monitoring at plot scale employing a dense piezometric network installed in 1995, aiming at spatiotemporal analysis of groundwater quality and quantity. All studies highlighted the potential of the alluvial areas in semiarid Brazil for small-scale irrigated agriculture but also pointed out the risks of groundwater depletion and salinization of both the groundwater and irrigated soils.

Despite a large number of studies on groundwater sustainability of small alluvial aquifers, investigations coupling long-term time series analysis of climate and hydrological variables at representative locations, using land use assessment of irrigated valleys, are still scarce, particularly in the Brazilian semiarid. The number of studies on groundwater availability in alluvial aquifers located in irrigated communities is also low, particularly taking into account the floodplain heterogeneity of hydraulic properties and their influence on the spatiotemporal distribution of salinity. The Brazilian semiarid region has been subjected to significant land use and land cover changes (Silva et al., 2022) and long drought periods (Brito et al., 2021). For instance, the drought that occurred between 2011 and 2016 was considered highly severe, affecting almost all of the northeast region of Brazil, with significant impacts on water security, population, and economic activities (Brito et al., 2018). Further studies assessing the dynamics of climate-groundwater interactions are still needed, particularly addressing the climate interaction with groundwater levels and salinity.

Hence, the main aim of this study is to assess and explain the impact of climate and anthropogenic changes on groundwater quantity (levels) and quality (salinity) in an active experimental alluvial valley located in the semiarid region of Brazil, and their implications for sustainable groundwater use. The specific aims are: (i) to identify stable representative locations for groundwater levels and salinity in a highly heterogeneous field, aiming to investigate stable representative monitoring locations across a dense network, according to the

aquifer hydraulic properties; and (ii) to carry out a long-term trend analysis of stable point time-series for both groundwater level and salinity, relating them to the agricultural use (e.g., temporal exploitation patterns), heterogeneities (e.g., saturated soil hydraulic conductivity, soil physical attributes, silt and sandy percentage, and geochemical parameters), and climatic dynamics in the region. A novel framework is developed and presented, coupling temporal stability analysis (and its dependence on aquifer hydraulic properties), long-term trend assessments, and multivariate statistical tests to provide insights on the joint impact of rainfall regime, evapotranspiration dynamics, groundwater levels, pumping rates, and hydraulic spatial variability on the groundwater salinity distribution.

III.2 Material and methods

III.2.1 Study area

The study was conducted in the Mimoso Stream Basin, located within the Alto Ipanema Basin (AIB), in the Pernambuco State, Brazil. The Mimoso Alluvial Valley (MAV) is part of the springs of the Ipanema River, a tributary of the São Francisco River Basin - one of the biggest river basins in Brazil, covering 7.5% of the country and contributing to the development of six states (Alagoas, Bahia, Goiás, Minas Gerais, Pernambuco, and Sergipe).

The MAV has a shallow unconfined aquifer with an average thickness of around 10 m, about 3 km in length, and 300 m in width, with a natural slope of approximately 0.3% (West-East) (Montenegro et al., 2003). The sides of the valley are characterized by shallow soils over crystalline basement fractured rocks. Groundwater resources are found in the fissured and weathered areas of the granites and, more significantly, in the alluvial deposits along the river (Dane, 2005). Rock weathering processes are usually associated with soil salt concentrations. In irrigated areas with shallow water tables, capillary flows tend also to increase soil salinity (Montenegro, 1997). The drainage network of AIB is composed of the Mimoso, Ipaneminha, and Jatobá streams. The Mimoso, although intermittent, is the main surface watercourse of the basin (Montenegro & Montenegro, 2006).

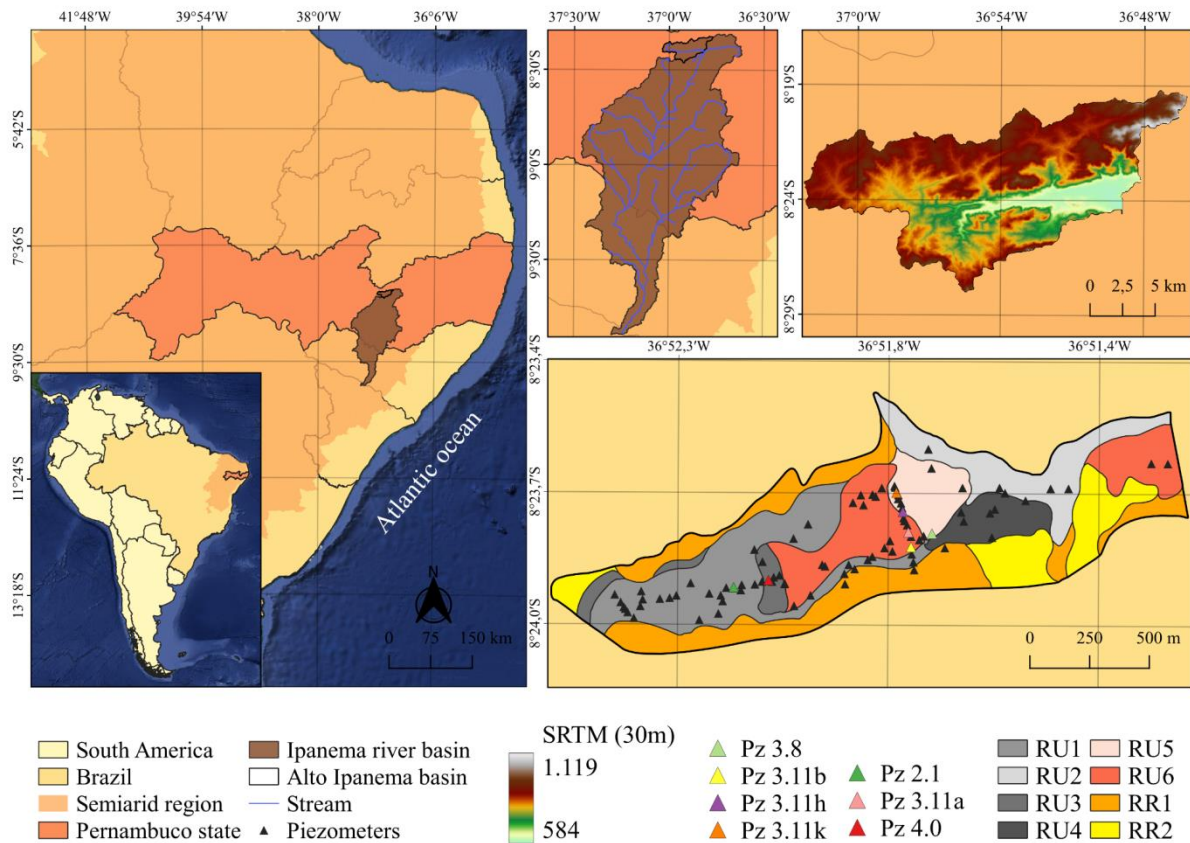


Figure 1. Location map of the Mimoso Alluvial Valley, Alto Ipanema Basin, Pesqueira municipality of Pernambuco, Brazil.

The pedological classification of the alluvial valley, according to Correa and Ribeiro (2001), is distributed as: RR1 – Regolithic Neosol + Litholic Neosol; RR2 Regolithic Neosol; RU1 Regolithic Neosol Tb (Eutric medium sand); RU2 Fluvic Neosol Tb (Eutric medium); RU3 Fluvic Neosol (Sodium medium); RU4 Fluvic Neosol (Sodium medium sand); RU5 Fluvic Neosol (Sodium saline); RU5 Fluvic Neosol (Saline sodium).

The study area has a network of pumping wells and georeferenced piezometers. Each piezometer is about 6 m deep and has a diameter of 75 mm (Montenegro, 1997). During piezometers installation, slug tests and infiltration experiments were carried out at each location, in order to characterize both saturated hydraulic conductivity and basic infiltration rate, respectively (Kelly, 1995; Montenegro, 1997). In addition, undisturbed soil sampling was performed for texture and electrical conductivity characterization in laboratory, at Federal Rural University of Pernambuco State, Brazil. Soil samples were also analyzed in laboratory at Newcastle University, to assess dispersity characteristics for salt transport (Montenegro, 1997, Montenegro and Montenegro, 2002). Direct measurements have included spatial

mapping of farm units, well locations and capacities, formations and soils, geophysical measurements of aquifer depth and groundwater flows (Last, 2004), borehole investigations of lithology and hydraulic property measurements, as well as infiltration capacities and recharge characteristics observed in Figure 2 adapted from Montenegro (1997).

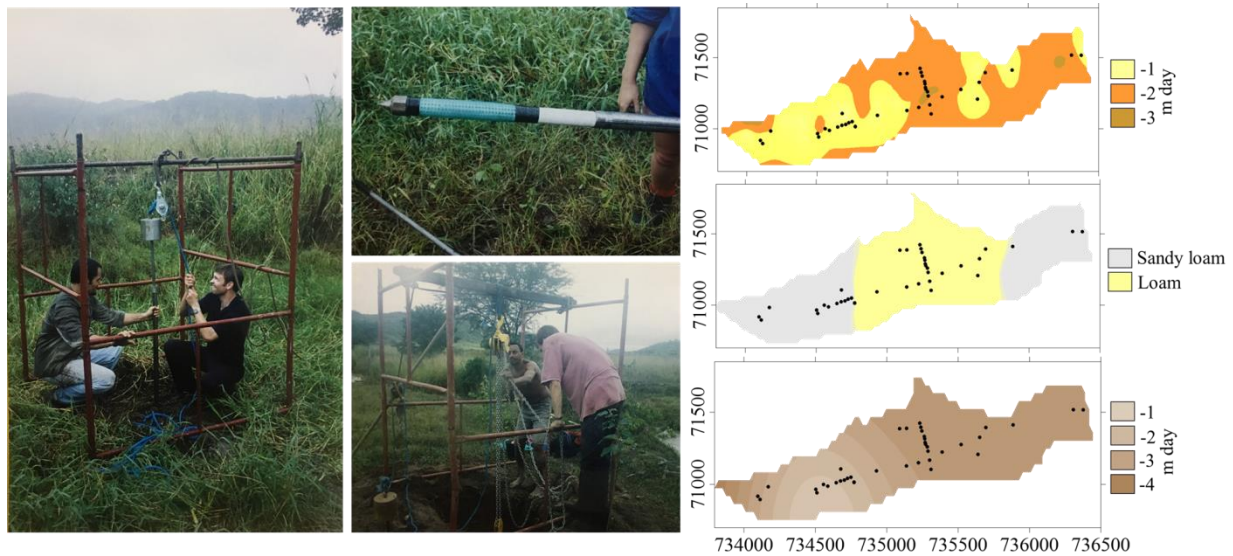


Figure 2. Piezometer installation, using manual hammer. View of the adopted piezometers, with the open zone for slug test and groundwater regular monitoring. Kriged maps saturated hydraulic conductivity, soil types, and surface saturated hydraulic conductivity (Source: adapted from Montenegro, 1997)

Slug test analysis was carried out adopting the Bouwer and Rice (1976) methodology. Saturated hydraulic conductivity varied from -4.53 to -0.66 m day⁻¹, with mean and median values of -2.14 and -2.11 m day⁻¹ respectively and showing a log-Normal behavior. Spatial variability of both saturated hydraulic conductivity and basic infiltration are presented in Figure 2. A classification into three classes had been adopted in order to group the monitoring points in regions showing similar geological and hydrogeological properties, considering criteria adopted by Montenegro (1997). Such regions are supposed to present the same pathways of groundwater flow and salt transport.

It is worth to mention that this research evolved from a scientific and academic effort supported by the United Kingdom Department for International Development (DfID) which was undertaken in Northeast Brazil. The project's overall aim was to demonstrate methods that

would build the capacity of local communities in semiarid areas to achieve the sustainable use of groundwater resources for agricultural production.

The climate in the study area is classified as BSh (extremely hot and semiarid) according to the Köppen classification, with an average annual rainfall of 630 mm, an average temperature of 23°C, and a potential evapotranspiration of approximately 2000 mm per year, registered from 2000 to 2015 (Fontes Júnior and Montenegro, 2017). The valley sides are quite steep, with slopes of around 10-30%. Saturated zone monitoring at the alluvial valley through piezometers (Montenegro et al., 2003) reveals that the average depth of the water table fluctuates between 2.0 and 4.0 m during the rainy and dry periods, respectively.

During the installation of 50 piezometers in 1995, slug tests (according to Bouwer and Rice, 1976) and infiltration tests were carried out to characterize, respectively, the aquifer saturated hydraulic conductivity (varied from 0.1 to 125 m day⁻¹, with an arithmetic mean value of 23.4 m day⁻¹, and geometric mean of 4.8 m day⁻¹) (Montenegro, 1997) and the basic soil infiltration rate (varied from 0.1 to 93 m day⁻¹, with arithmetic mean of 7.1 m day⁻¹) (Montenegro and Montenegro, 2006). The 5 m deep piezometers were installed along transects in 1995 (and complemented with an additional set of 30 piezometers in 2005), adopting a regular separation distance of approximately 30 m, to allow geostatistical investigations of spatial variability structure of the hydraulic properties.

III.2.1.1 Geology and Hydrogeology of the study area

Groundwater resources are limited to fissured and weathered zones of the granitoids and, more importantly to the Mimoso Alluvial Valley, a narrow river alluvial deposit. The alluvial deposits are fine to medium heterogeneous sands, containing some fine material (silt and clay) (Montenegro, 1997). The soils in the crystalline regions are generally shallow with low infiltration rates and limited storage potentials. According to Kelly (1995), the sandy material contains coarse grains of quartz and pink feldspar fragments. The size of the quartz fragments ranges from 2-10 mm. The coarse sands present as much as 30% of the soil material. Biotite, muscovite and gneiss are dominant. In contrast, on the northern boundary, granite, syenite, and gabbro are present, representing a granite complex, which may be associated with the quartz fragments in the alluvial fans (C I S A G R O, 1991).

Soil sampling analyses were conducted in the laboratories of the Federal Rural University of Pernambuco State (UFRPE) and Newcastle University to characterize texture, electrical conductivity, and dispersive qualities for salt transport (Montenegro, 1997;

Montenegro et al, 2002). Based on the geological and hydrogeological properties of the MAV, two classes of monitoring wells and piezometers were defined (low hydraulic conductivity, with $K_{sat} \leq 0.8 \text{ m day}^{-1}$, and high hydraulic conductivity, with $K_{sat} > 0.8 \text{ m day}^{-1}$), following the criteria established by Montenegro (1997). These regions were assumed to have similar pathways of groundwater flow and salt transport.

III.2.2 Data and methods

III.2.2.1 Meteorological data

The meteorological data was recorded from 2000 to 2019 by a complete automatic agrometeorological station (Campbell Scientific) installed in the MAV, which provides air temperature, relative air humidity, global solar radiation, atmospheric pressure, wind speed and direction, and rainfall records. Minimum and maximum air temperature and relative humidity were used to calculate the reference evapotranspiration (ET_0) using the FAO-56 Penman-Monteith equation (Allen, 1998).

III.2.2.2 Groundwater level and electrical conductivity data

For this study, 241 months of groundwater level and electrical conductivity data was collected between January 2000 and December 2019 from 54 piezometers and 33 wells. The piezometers, around 6 m in depth and with a 75 mm diameter, present screens and gravel filters. The wells, on the other hand, vary in size, comprising community wells with larger diameters and equipped with multilevel radial collectors aimed at increasing groundwater exploitation, and individual wells for supplying individual irrigation plots. Water level measurements were taken manually each month using a water level meter, while electrical conductivity was measured in water samples taken from the same piezometers and wells during the level campaigns.

Due to textural and hydrogeological variations in groundwater systems in the MAV, investigations regarding electrical conductivity were carried out considering the grouping proposed by Mackay and Montenegro (1996), Montenegro (1997), and Montenegro et al. (2003), where the authors divided the aquifer into two regions: piezometers with high hydraulic conductivity saturated (PZH) and piezometers with low saturated hydraulic conductivity (PZL). Additionally, wells (PW) were considered separately, depending on the extraction dynamics, which allows for greater groundwater circulation compared to aquifer regions near the piezometers.

III.2.2.3 Water use in irrigated areas

The most important economic activity in the Mimoso Alluvial Valley is agriculture, with wells being drilled mainly for irrigating vegetables, maize, and pasture. Farmers use a variety of irrigation techniques, such as normal sprinklers, micro sprinklers, drip irrigation, and xique-xique irrigation (which is a local “homemade” system that typically consists of drip lines with small orifices). Additionally, irrigation is conducted using 3-15 CV centrifugal pumps. The average water extraction in the wells of the MAV is approximately 45 m³ day⁻¹, reaching around 300 m³ day⁻¹ in some communal wells (Monteiro et al., 2014). According to Dane (2005), based on detailed field monitoring, the total abstraction in the valley for irrigation was nearly 129.000 m³ year⁻¹ in 2004.

To estimate water exploitation for irrigation in the alluvial valley, the actual consumption was taken into account for each farm and its respective farmers based on the water requirements of the irrigated crops and the ET₀ calculated using FAO-56 Penman-Monteith equation (Doorenbos et al., 1997; Allen et al., 1998). The data obtained from the field monitoring, supplemented by interviews with farmers concerning the crops grown in the MAV over the years and the irrigation management adopted in the farms, enabled the building of a database with the required parameters to estimate the daily and monthly groundwater abstractions at the monitoring wells. The vegetation dynamic in the MAV, considering the irrigated areas, was obtained from the MapBiomass network, which reconstructed annual land use and land cover information for Brazil based on Landsat data (MapBiomass Brazil, 2023).

III.2.3 Assessment of temporal stability of groundwater levels and salinity

To find representative piezometers of the average aquifer dynamics, the temporal stability of groundwater levels and electrical conductivities (EC) over the studied period were considered following the methodology proposed by Vachaud et al. (1985). This methodology is based on the calculation of the relative difference of each location record to the mean value, allowing the analysis of deviations between the values observed individually in space and the average among them:

$$\delta_{ij} = \frac{(X_{ij} - \bar{X}_j)}{\bar{X}_j} \quad (1)$$

where δ_{ij} is the relative difference between the determination interval for location i at time j ; X_{ij} the piezometric level or electrical conductivity at location i and time j ; and X_j the average value of the level or electrical conductivity for all positions N , at time j . The mean of the relative difference for each location i is defined by Equation 2:

$$\bar{\delta}_i = \frac{1}{m} \sum_{j=1}^m \delta_{ij} \quad (2)$$

where m represents the number of months studied.

The Standard Deviation of the Relative Difference was calculated as:

$$\sigma_i = \sqrt{\frac{1}{m-1} \sum_{j=1}^m (\delta_{ij} - \bar{\delta}_i)^2} \quad (3)$$

The chosen piezometer locations must yield precise and indicative measurements of both groundwater level and salinity, with a mean relative difference close to zero and a low standard deviation. Following the identification of these representative points, the R-squared values were calculated between the point values and the average of the entire dataset to validate the results and, thus, to assess the representativeness of the stable locations.

III.2.4 Temporal trend analysis

To analyze, detect, and estimate the trends in groundwater level, electrical conductivity, and climatic series, the seasonal non-parametric Mann-Kendall test (Mann, 1945; Kendall, 1975) and the Sen's slope method (Sen, 1968) were applied considering representative locations and average of data series. The Mann-Kendall test assumes that the data are serially independent. However, hydrometeorological, hydrological, and climatologic time series may have autocorrelation, particularly in aquifers, which might cause errors for the trend test, increasing the significance of data (Yue et al., 2002). Thus, to eliminate the influence of autocorrelation, the seasonal and trend decomposition using the LOESS (STL) method was adopted. The STL method is a time-series decomposition approach that uses a robust locally weighted regression as a smoothing method (Cleveland et al., 1988) and a locally weighted regression algorithm (Cleveland and Devlin, 1988). The STL method defines the original data Y_t at time $T_{(t)}$ and decomposes it into the trend _{t} , seasonal _{t} , and residual _{t} components, as follows in Equation 4:

$$Y_t = Trend_t + Seasonal_t + Residual_t \quad (4)$$

The trend component is considered a relatively stable variable, representing low-frequency data trends. In contrast, the seasonal component is a periodic and steady data disturbance item, with high-frequency changes mainly induced by seasonal modifications. The remaining variables are residuals caused by irregular random disturbances (Cheng et al., 2021). The Pettitt test (Pettitt, 1979) was used to identify the year at which there was a sudden shift in the mean of the time series.

III.2.5 Exploratory and statistical analyses

To find explanatory variables for the groundwater level and the salinity, Spearman's correlation coefficient was used to analyze the correlation between electrical conductivity, groundwater level, rainfall, and groundwater abstraction over the 20 years.

In order to allow a long-term temporal procedure, statistical analysis was carried out on the raw data for water levels and electrical conductivities. If the time series lengths were shorter than 20 years either for water levels or electrical conductivity, or alternatively the number of faults was greater than 3 consecutive months, the monitoring point was disregarded, and not included in the analysis.

Principal Component Multivariate Analysis (PCA) was employed in the Comprehensive R Archive Network [CRAN] package of R programming language, using the FactoMineR package, to identify the most influential variables (rainfall or groundwater abstraction) associated with groundwater salinity and level dynamics. The Standard Precipitation Index (SPI) (McKee et al., 1993) was used to classify the variability of monthly rainfall, which might influence the groundwater recharge and interfere on irrigation dynamics.

III.3 Results and discussion

III.3.1 Level, salinity, and climatic temporal variation

After statistical analysis of the available dataset, 35 piezometers and 33 pumping wells were selected for the spatiotemporal analysis. Among the selected piezometers, 14 were located

at zones with high saturated hydraulic conductivity (PZH), and 13 were at zones with low conductivity (PZL).

Figure 3 shows the groundwater abstraction and reference evapotranspiration estimates along with the observed rainfall data from 2000 to 2019 in the MAV. The groundwater individual abstractions at the set of public and private wells were significantly variable over the years, presenting an average of $12,354 \text{ m}^3 \text{ month}^{-1}$, reaching a maximum value of $24,352 \text{ m}^3 \text{ month}^{-1}$ in October 2012. The variations in the groundwater abstractions are associated with the rainfall regime and plant requirements, which, consequently, are dependent on temperature, evapotranspiration, and plant phenological phases.

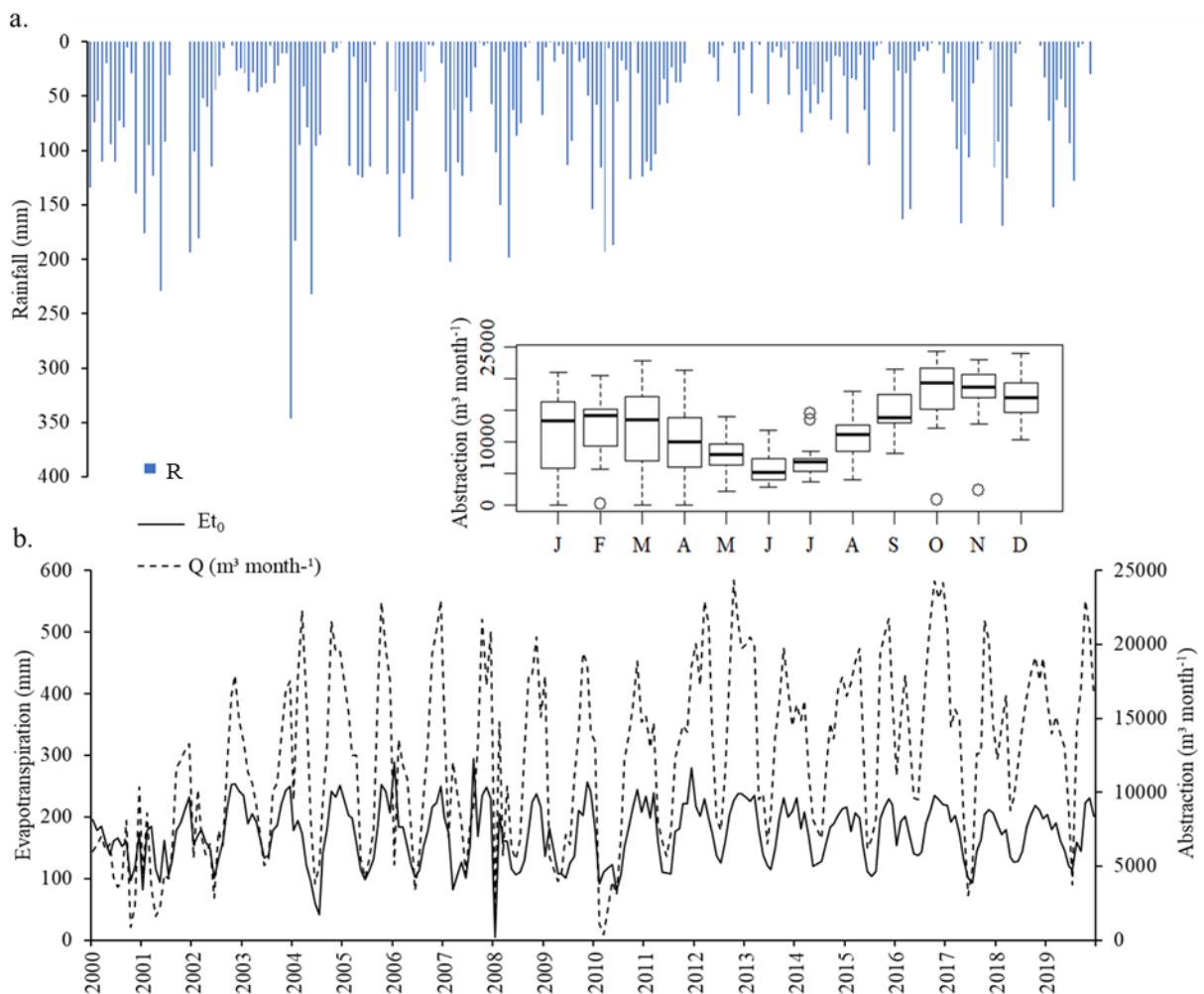


Figure 3. (a) Rainfall, (b) groundwater abstractions and reference evapotranspiration from 2000 to 2019 in the Mimoso Alluvial Valley, Brazil.

It is possible to observe in Figure 3 an increase in groundwater abstractions during the dry season in the region (August to March), because of the intensification of crops throughout the year, including vegetables, peppers, pasture, and fruit crops. Low abstractions were observed during the rainy season since the soil moisture in the MAV is usually very high, restricting vegetable development and agricultural activities. According to Penã-Arancibia et al. (2020), the increase in irrigated areas was attributed to the availability of alluvial groundwater in the region, which allows farmers to diversify the production and harvest more than one crop per year. From an economic perspective, such an increase is very important for the region; however, it is necessary to adopt adequate water and soil management for optimizing the alluvial groundwater use for irrigation and maintaining water security for the future. Studies worldwide indicate that frequent drawdown patterns of groundwater level fluctuations are related to excessive abstraction (e.g., Dangar et al., 2021, Mojid et al., 2021, Nigatu et al., 2022, Pragay et al., 2023).

Although, disregarding the anthropic influence, if groundwater level fluctuation depends mainly on seasonal recharge from rainfall, it is expected to show a fluctuation pattern that directly simulates the trend of rising or falling water level. This may imply the presence or absence of total monthly recharge according to rainfall distribution and lateral flow from the alongside hillslopes. Figure 4 shows the boxplots containing the mean annual values of groundwater levels and electrical conductivity for all analyzed wells and piezometers between 2000 and 2019. Abstractions in wells are also presented.

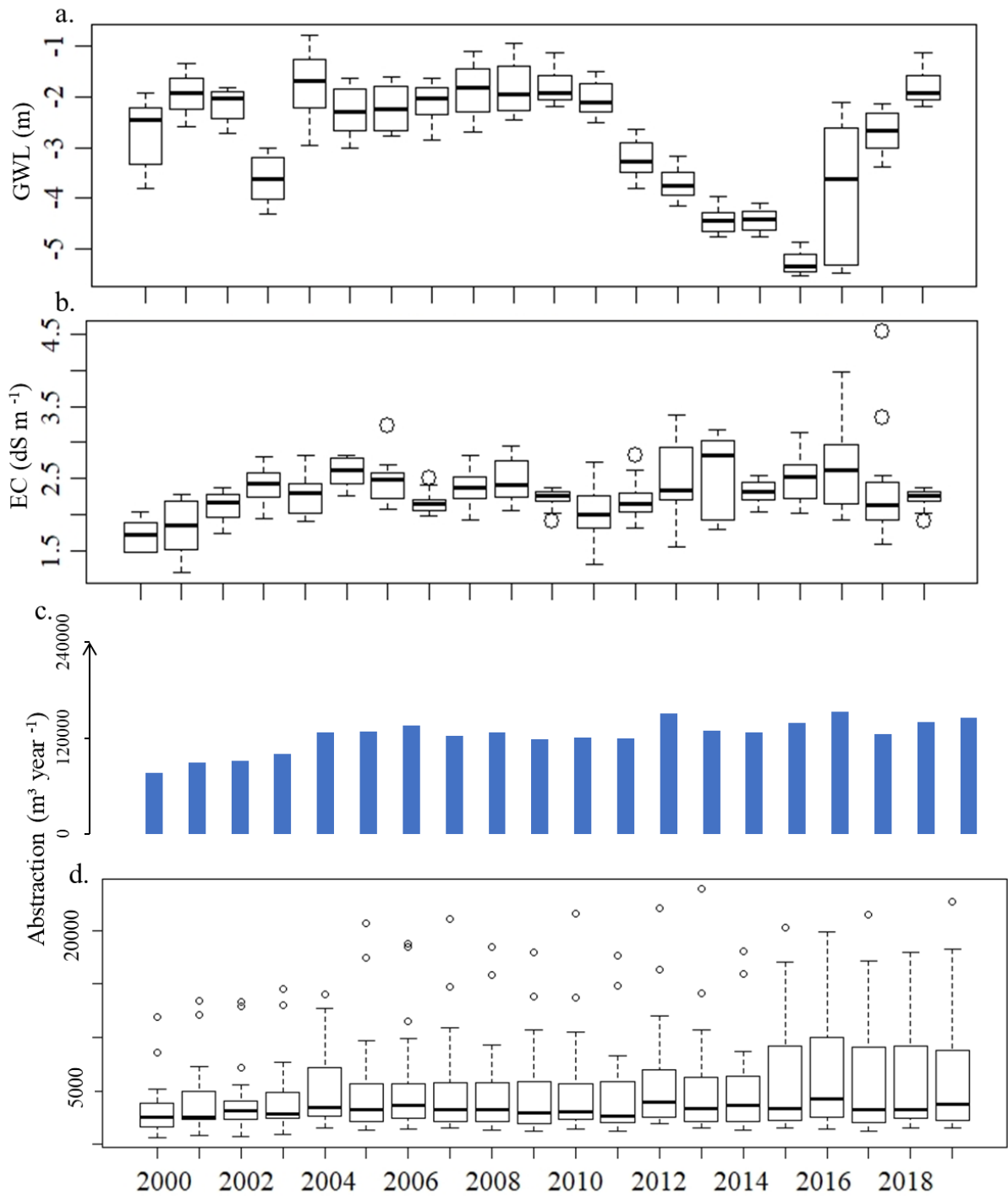


Figure 4. Boxplots of the annual mean values of (a) groundwater level, (b) electrical conductivity, and abstraction values between 2000 and 2019 in the Mimoso Alluvial Valley.

Overall, no outlier measurements are apparent for the water table levels (Figure 4a), with higher mean level (-1.74 m) during the time-series observed in 2004 caused by an above-average accumulated annual rainfall of 1183 mm (Figure 4a). The lower mean levels (from -

3.22 to -5.28 m) were observed from 2012 to 2016 due to the below average annual rainfall volumes (218, 413, 482, 405, and 498 mm, respectively). Contrastingly, Figure 4b displays outliers for electrical conductivity (measurements shown as an open circle) for six years of analysis. These outliers were also observed by Andrade et al. (2012) when studying the spatial dependence of electrical conductivity in the MAV. These results suggest that there are periods of significant salinity rise, most notably near the border of the valley, around the hillslopes.

The response of the alluvial aquifer level to rainfall events is much more pronounced than the electrical conductivity (EC) response. According to Fontes Júnior et al. (2012), the water table dynamics in the MAV are primarily determined by the rainfall distribution, whereas the temporal variability of EC and its correlation to the rainfall regime are less obvious due to the salt transport dynamics in the saturated zone of the aquifer which are caused by other factors such as geological impediments and local heterogeneities. Montenegro et al. (2003) analyzed a short-term spatiotemporal dynamic of the electrical conductivity variability in the MAV and highlighted the hydraulic conductivity and the soil texture as determining factors in the local saline dynamics. The variability of groundwater abstraction variability and the distribution of irrigation plots distribution can also interfere the variability and magnitude of salt contents in groundwater (Monteiro et al., 2014), making imperative the need to seasonally assess the variability of parameters related to water quality, as pointed out by Kisi and Ay (2014).

III.3.3. Temporal Stability of groundwater levels and electrical conductivities

Figure 4 shows the stable piezometers and wells regarding the mean and standard deviation values of groundwater levels and electrical conductivities, and low and high saturated hydraulic conductivity, where positive relative differences indicate overestimations of the mean values, whereas negative relative differences correspond to underestimation of the mean. The points closest to the mean represent the most stable wells and piezometers in terms of groundwater level and electrical conductivity variations during the 20-year monitoring period. The representative piezometers identified for the groundwater levels were Pz 3.8, Pz 4.8, and Pz 4.10, which presented, respectively, mean relative differences of -0.05, -0.04, and -0.03 in absolute values, and standard deviations of 17.3, 11.1, 14.6% (Figure 5a). For electrical conductivity, representative piezometers were not identified (Figure 5b).

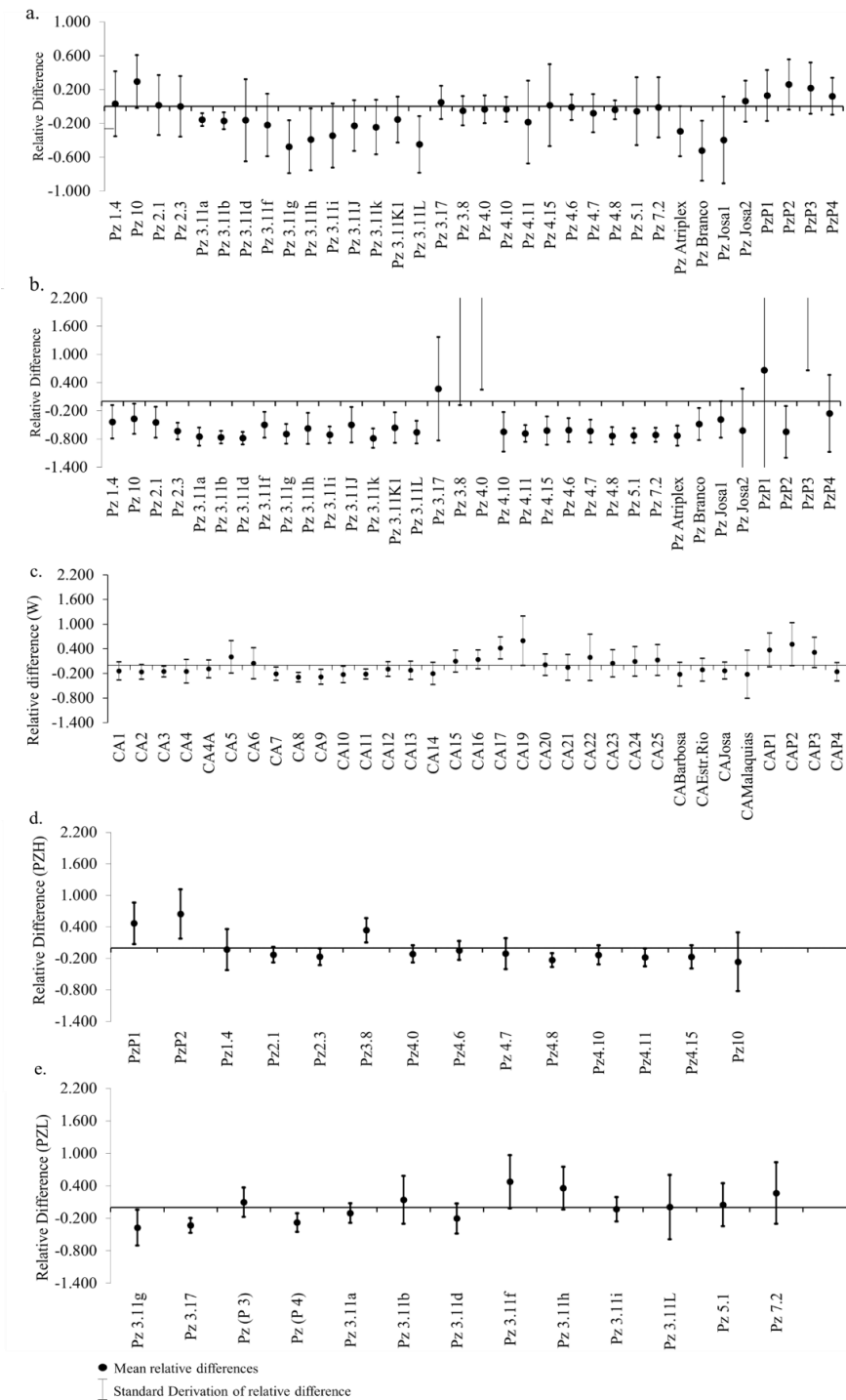


Figure 5. Relative mean difference and temporal standard deviation for (a) potentiometric levels, (b) electrical conductivity, (c) wells, (d) piezometers with high saturated hydraulic conductivity, and (e) piezometers with low saturated hydraulic conductivity in the Mimoso Alluvial Aquifer.

It is possible to identify that the groundwater level stability is associated with the location of the piezometers, along the longitudinal axis of the alluvial valley (i.e., along the river bed) (Fontes Júnior et al., 2012). Although readings of GWL at some piezometers do not correspond exactly to the mean value, the differences between the values of Pz 3.8, Pz 4.8, and Pz 4.10 were minimal, with high R^2 values, ranging from 0.95 (Pz 4.8) to 0.89 (Pz 3.8) indicating that these piezometers could be adopted as a reference to provide mean representative values of the general behavior of groundwater level in the MAV. Regarding EC, coefficients of determination varied between 0.0433 and 0.2722, demonstrating the non-stability of the piezometers for EC, which can be explained by the low amplitude of the average electrical conductivity variation. In addition, the limited circulation of groundwater and the local heterogeneities marked by the high degree of variability in the local chemical characteristics of the soil (Andrade et al., 2012) contribute to the concentration of salts at isolated points of the alluvial valley, particularly in areas subject to waterlogging and with low infiltration capacity (see also infiltration map in Figure 2), as well as shallow groundwater levels.

For aquifers with good circulation, the groundwater would be mixed by advection, attenuating the local variability and allowing the identification of mean representative behavior. However, in calculating the mean electrical conductivity, the non-stationarity of salinity, influenced by local characteristics (e.g., geology, soil, and distribution of irrigated plots), promotes an erroneous smoothing in the spatial variability; hence, these points identified as stable do not properly represent the saline dynamics of aquifer as a whole.

To investigate the above-mentioned hypothesis for the mean electrical conductivity values, the observation points were grouped into three different classes, according to the mean hydraulic conductivity obtained from the slug tests and geostatistical analysis, for clustering the MAV into wells (PW), piezometers with high saturated hydraulic conductivity (PZH), and piezometers with low saturated hydraulic conductivity (PZL).

A total of 33 wells were considered in the stability analysis of electrical conductivity, which showed an average value of 0.81 dS m², with an average standard deviation of 0.35 and a variance of 0.12. The group PZH is composed of 14 piezometers located in a recharge sandy region with stable behavior of salinity and high hydraulic conductivity (Montenegro et al., 2003), presenting average electrical conductivity of 0.73 dS m² and standard deviation and variance of 0.12 and 0.01, respectively. The group PZL is in regions with presence of loam soils, which are, overall, associated with the presence of high content of dissolved salts in the

saturated zone. The group is composed by 13 piezometers and shows a mean electrical conductivity of 1.11 dS m², a standard variation of 0.24, and a variance of 0.05. According to Montenegro et al. (2004), loam soils generally exhibit higher electrical conductivities due to the lower infiltration rates (and washout degrees) and/or the predominance of upward capillary flows that tend to concentrate salts in the unsaturated profile.

The consistency of groups identified by the cross analysis of hydraulic properties with the representative monitoring areas identified by time stability analysis mutually proved the method validity in identifying the area that could represent spatial average of the salinity over time. The well CA 3 (well number 3) presented a mean relative difference of -0.14 and a standard deviation of 13%. Regarding the PZH group, the piezometer Pz 4.0 with a mean electrical conductivity of 0.70 dS m² and a relative difference and standard variation, respectively, of -0.12 and 16.5%. For the PZL group, the piezometer highlighted as presenting the better performance was the Pz 3.11a, with a mean electrical conductivity of 0.97 dS m² and a relative difference and standard variation of -0.11 and 17.2%, respectively.

III.3.4. Identification of groundwater monthly and annual trend analysis

Table 1 presents the monthly trend analysis by the seasonal MK test and the magnitude of the Sen's slope test for the groundwater level and electrical conductivity time-series. The data analyzed presented decreasing trends of groundwater level and electrical conductivity. Ribeiro et al. (2015) also observed decreasing trends of groundwater levels and electrical conductivity in the Elqui River, Chile, which was considered alarming since an increase in water demand was expected in the region, probably over-pressuring the groundwater resources in the future.

The highest slope values were found for Pz 3.8 from May to July, with a maximum of 0.09 meters per month in May. Penã-Arancibia (2020) has attributed similar declines to seasonal drawdowns, associated with the aquifer recharge-discharge cycles in northwest Bangladesh. The lower extreme values of the groundwater table in the MAV are a result of the dry periods in the semiarid region, as the aquifers tend to drain to the watercourse during this time and are recharged during the rainy season. In addition, the rainfall deficit increases the tendency of drawdown (Sishodia et al. 2016), as shown in Table 1 for August and September, where evaluated piezometers presented a downward trend in the monthly average groundwater levels.

Regarding electrical conductivity, the well group showed seasonal stability, with no trend across the year (except for January), with a mean decrease of 0.016 dS per month associated with an increase in the pumping rates and an absence of rainfall. On the other hand, the PZH and PZL showed a similar monthly downward trend of electrical conductivity even for periods without rainfall, influenced by groundwater extraction (by pumping for irrigation).

Table 1. Trend analysis indicated by arrows and slopes of (a) groundwater levels (m month⁻¹), (b) electrical conductivity, (c) rainfall (mm month⁻¹), maximum, minimum and average temperature (°C month⁻¹), reference evapotranspiration (mm month⁻¹), and (d) abstractions (m³ month⁻¹).

	Jan	Feb	Mar	Apr	May	Jun	Jul	Aug	Sep	Oct	Nov	Dec
A. Groundwater level												
Pz 3.8	↔	↓	↓	↓	↓	↓	↓	↓	↓	↓	↓	↓
	-0.052	-0.072	-0.073	-0.094	-0.099	-0.013	-0.085	-0.083	-0.070	-0.062	-0.057	-0.055
Pz 4.8	↔	↓	↓	↓	↔	↔	↔	↔	↔	↔	↔	↔
	-0.010	-0.047	-0.076	-0.092	-0.087	-0.056	-0.081	-0.101	-0.063	-0.055	-0.040	-0.044
Pz 4.10	↔	↔	↔	↔	↔	↔	↔	↓	↓	↔	↔	↓
	-0.040	-0.058	-0.074	-0.072	-0.059	-0.080	-0.089	-0.014	-0.089	-0.076	-0.076	-0.083
C. Electrical conductivity												
Well	↓	↔	↔	↔	↔	↔	↔	↔	↔	↔	↔	↔
	-0.016	0.006	-0.007	-0.005	-0.003	-0.003	-0.006	-0.001	0.006	-0.01	-0.007	-0.009
PZH	↓	↓	↓	↓	↓	↓	↓	↓	↔	↓	↓	↔
	-0.010	-0.010	-0.009	-0.009	-0.013	-0.010	-0.011	-0.006	-0.005	-0.007	-0.009	-0.006
PZL	↓	↓	↓	↓	↓	↓	↓	↓	↔	↓	↔	↓
	-0.027	-0.029	-0.028	-0.021	-0.023	-0.019	-0.018	-0.015	-0.016	-0.014	-0.012	-0.016
D. Rainfall, temperature and reference evapotranspiration												
R	↔	↔	↔	↔	↔	↔	↔	↓	↓	↑	↔	↓
	0.038	-0.019	0.045	-0.093	0.037	-0.033	-0.060	-0.082	-0.076	0.069	-0.043	-0.038
Tmin	↑	↑	↑	↑	↔	↔	↔	↑	↑	↑	↑	↑
	0.086	0.050	0.078	0.088	0.071	0.017	0.027	0.051	0.068	0.095	0.073	0.078
Tmax	↑	↔	↑	↑	↔	↑	↑	↑	↑	↑	↑	↑
	0.086	0.133	0.071	0.124	0.121	0.047	0.155	0.083	0.128	0.133	0.717	0.083
Tm	↑	↑	↑	↑	↔	↑	↑	↑	↑	↑	↑	↑
	0.008	0.098	0.061	0.975	0.107	0.024	0.106	0.079	0.114	0.101	0.072	0.076
ET₀	↑	↔	↔	↔	↑	↔	↔	↔	↑	↑	↑	↑
	0.770	1.343	0.116	1.038	0.0975	1.231	0.629	0.165	0.941	1.161	0.1406	0.727
D. Abstraction												
Q	↑	↔	↑	↔	↑	↑	↔	↑	↑	↑	↑	↔
	375.1	597.1	313.9	521.4	419.8	341.4	259.7	227.4	467.48	366.9	420.6	288.5

↑= upward trend; ↓= decreasing trend; ↔ = no trend.

The decreasing trends linked to the months considered dry (August to March) also showed a strong relationship with the water abstraction for irrigation, considering that the crop water demand increases. The point Pz 4.10 showed a decreasing trend for the months of August, September and December, with a maximum of 0.089 m month⁻¹ in September.

As for rainfall, the months of August, September and December presented a decreasing slope, while the month of October presented a rise for rainfall of $0.6 \text{ mm. month}^{-1}$. The reduction in rainfall is critical, since it is the regulating component for water security in semiarid regions (Montenegro et al., 2003). Linked to rainfall, evapotranspiration is also another critical component of the hydrological cycle, influencing local water availability (Paulino et al., 2019), and directed affected by climate change and temperature increases.

In the present study, evapotranspiration presented increasing seasonal trends for the months of January, May, September, October, November, and December, with a maximum of $1.16 \text{ mm month}^{-1}$ in September, followed by $1.23 \text{ mm month}^{-1}$ in May. Groundwater pumping for irrigation reflects the evapotranspiration dynamics, also showing increasing trends in January, March, May, June, and from August to November; the later period corresponding to the region's dry period, where agricultural cultivation is usually intensified, resulting in a higher number of pumping hours. In such period, the maximum slope of $467 \text{ m}^3 \text{ month}^{-1}$ was identified in September, coinciding with the maximum slope of evapotranspiration and slope of rainfall.

The minimum, maximum and mean temperatures showed increasing trends in most of the months evaluated, with maximum values of ascent of $0.095^\circ\text{C month}^{-1}$ (October); $0.717^\circ\text{C month}^{-1}$ (November) and $0.975^\circ\text{C month}^{-1}$ (April), respectively. The increase in evapotranspiration rates is accompanied by an increase in temperature, as seen in Figure 6, where significant upward trends were identified in the temperature series.

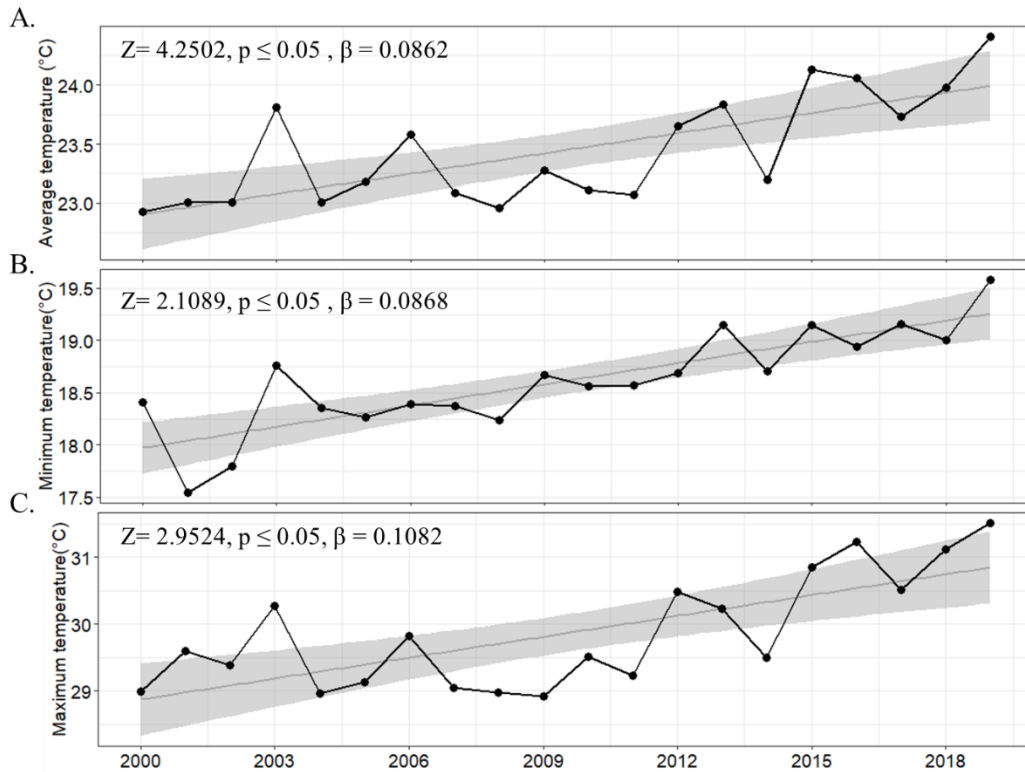


Figure 6. Annual time series for mean temperature and rainfall from 2000 to 2019, with associated trend lines.

The minimum, maximum, and mean temperatures exhibited slopes of 0.086, 0.108, and 0.086, respectively. Carvalho et al. (2020) found similar trends in the temperature pattern across the entire Brazilian Northeast region, which were attributed largely to climate change and the associated excessive emissions of greenhouse gases. Montenegro and Ragab (2010) had previously predicted a temperature increase for the Mimoso Region and highlighted that this rise in temperature can have impacts on the availability of water resources, resulting from decreased water recharge.

Figure 7 presents the annual time series for groundwater level and electrical conductivity, for the points evaluated in the period from 2000 to 2019.

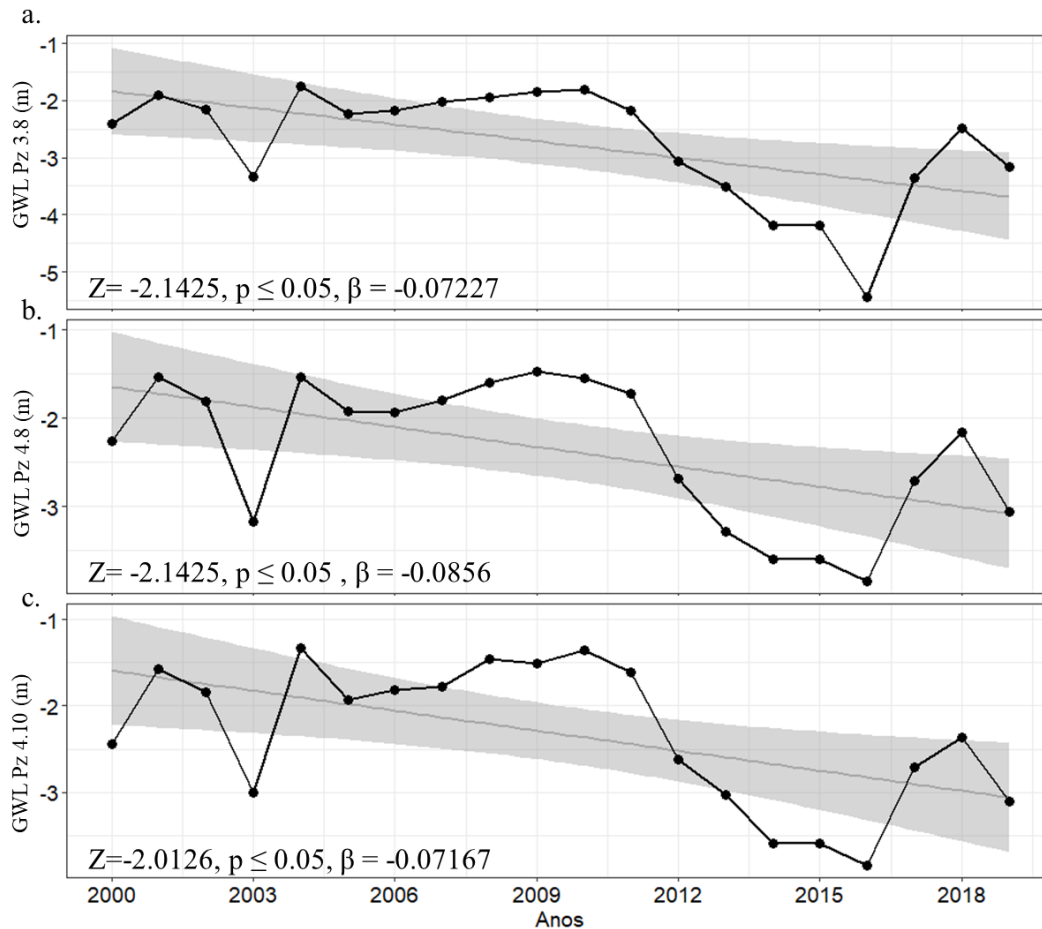


Figure 7. Annual time series and associated trend lines of groundwater level in piezometers Pz 3.8 (A), Pz 4.8 (B), Pz 4.10 (C) from 2000 to 2019.

It is verified that the groundwater level is decreasing significantly at the evaluated piezometers, with annual decreases ranging from 0.07 m to 0.08 m per year. The average trend is $-0.073 \text{ m year}^{-1}$ (Figure 6). All declines are statistically significant at the 90% significance level, and present values close to each other and to the mean, which indicates an effectiveness of the mean representation for the points, highlighting that stability is sensitive to the presence of trend.

The Figure 8 presents the mean electrical conductivity for the stable points (one well and two piezometers). It is observed that the Mimoso aquifer is not subject to salt accumulation when considering PW and the PZH groups, presenting a better hydraulic conductivity which determines the migration velocity of salts and hence the residence time and attenuation potential. High conductivity values will be associated with low salinity risk and a better water

circulation. However, an increase can be observed in PZL group with Sen's Slope of $0.026 \text{ dS year}^{-1}$.

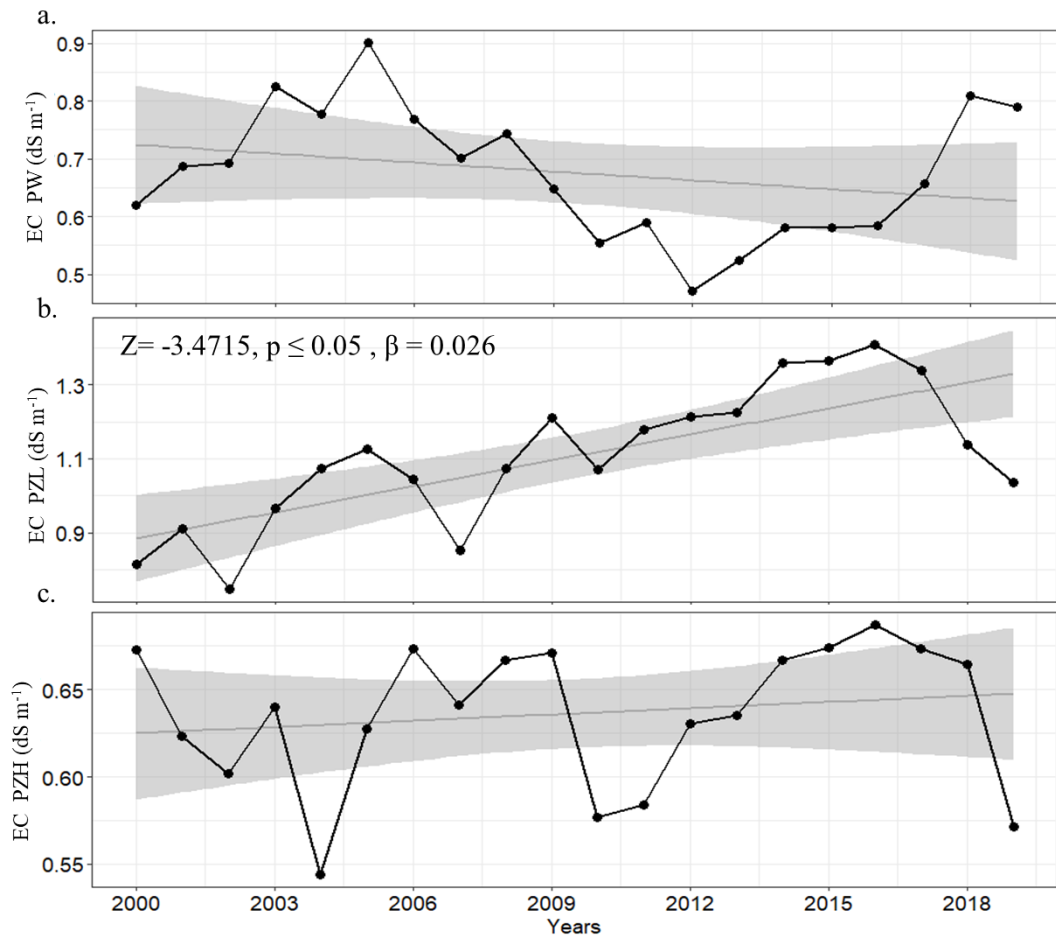


Figure 8. Annual time series and associated trend lines of electrical conductivity in well (A), PZL (B), PZH (C) from 2000 to 2019.

Figure 9 displays the yearly time series of rainfall (A) and evapotranspiration (B) from January 2000 to December 2019, depicting the trends, the residual components obtained through STL decomposition, and the linear regression trends. It can be verified that the seasonal values display a stable pattern over time, with distinct cycles of dry and wet periods. Both rainfall and evapotranspiration exhibit a seasonality of 12 months.

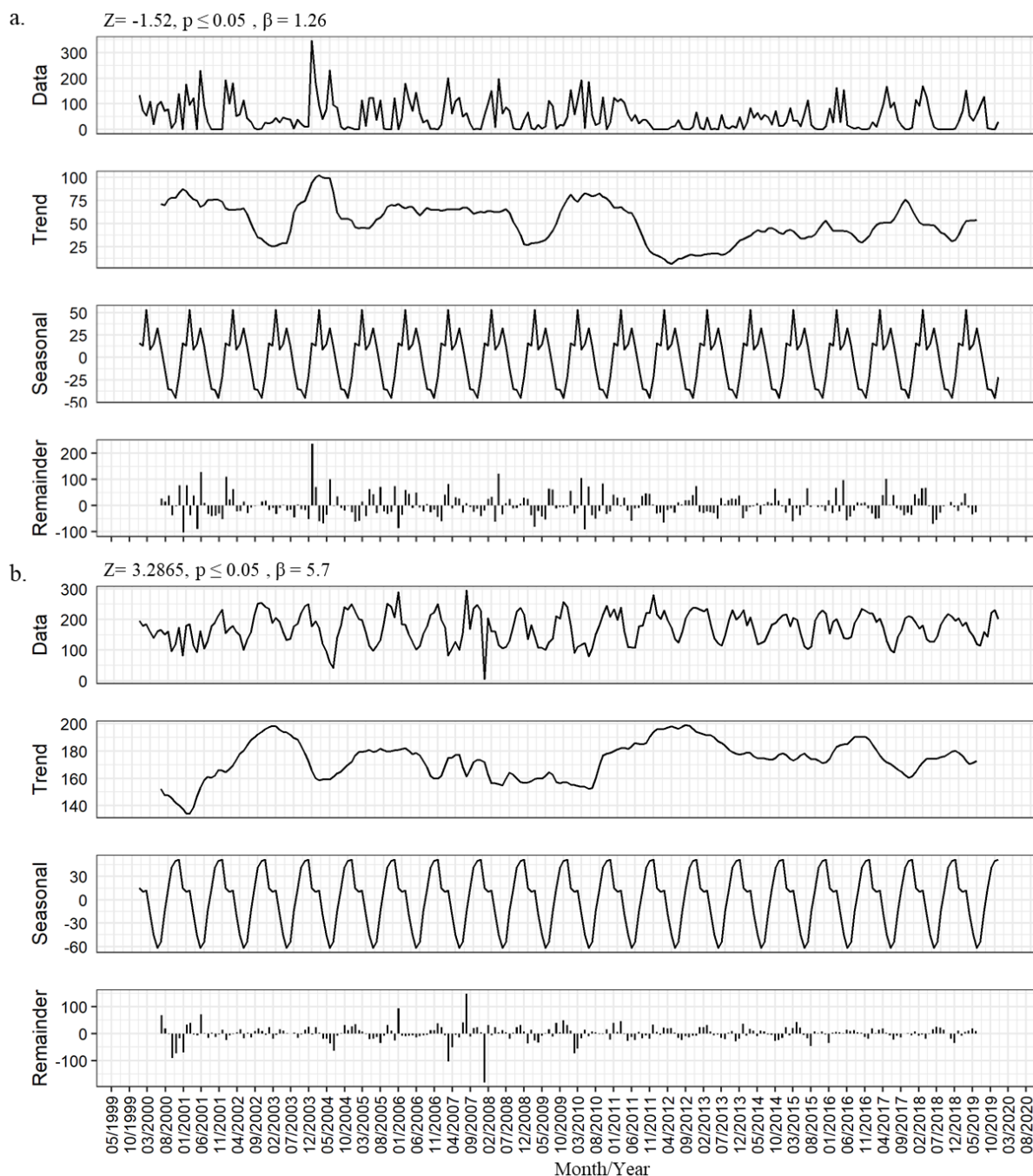


Figure 9. Annual time series of rainfall (A) and reference evapotranspiration (B) from 2000 to 2019, with associated trend line

Over the analyzed period, rainfall showed a decreasing trend ($Z = -1.52, p < 0.05$), with an average annual decline of $1.26 \text{ mm year}^{-1}$, without a standard trend variation between the years until 2011, according to Pettit test. In addition, a trend analysis in relation to the total number of rainy days, number of days with rainfall greater than 5, 10, 15 and 20 mm showed

that the total number of days and the number of days with rainfall greater than 5 mm present a reduction trend of 1.87 and 1 rainy day per year, respectively, which represents 28% and 13% of the number of rainy days over 5 mm per year. The findings obtained are in agreement with Carvalho et al. (2020), who studied the long-term trend of rainfall, the number of rainy days, and the temperature in Northeast Brazil and found a decrease in rainfall and the number of rainy days in the semiarid region. This behavior could lead to lower resilience during future extreme events and longer periods of drought, which could trigger significant social, economic, and environmental consequences (Del-Toro-Guerrero and Kretzschmar, 2020; Vazifekkhah and Kaya, 2019).

The reference evapotranspiration showed an increase of 5.7 mm year^{-1} , which corroborates to the study developed by Paulino et al. (2019), where the authors detected increasing trends at $4.74 \text{ mm year}^{-1}$ at ET_0 in Ceará State, Brazil. Peña-Arancibia et al. (2020) warn that the increase in ET_0 should intensify the exploitation of aquifers, as groundwater use is strongly related to evapotranspiration and rainfall. Therefore, the demand for irrigation is expected to increase significantly in the coming decades, due to higher ET_0 rates and plant water requirement.

Figure 10 illustrates the average annual behavior for groundwater level, electrical conductivity, and groundwater abstraction. Furthermore, these variables exhibited a regular and consistent seasonal pattern.

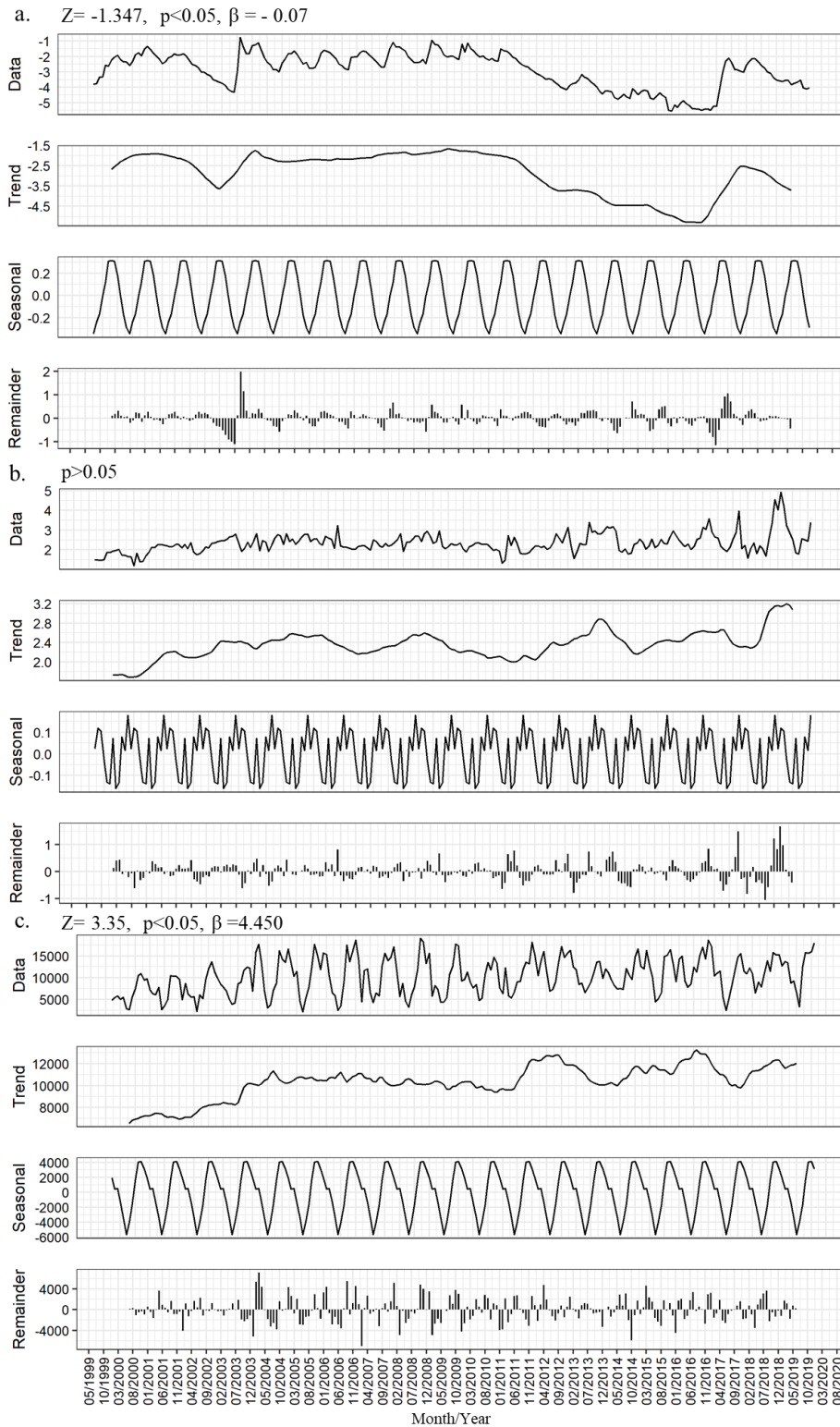


Figure 10. Annual time series of the general averages of (a) groundwater level (m), (b) electrical conductivity (dS m^{-1}), and (c) abstraction ($\text{m}^3 \text{ year}^{-1}$), from 2000 to 2019, with the associated trend lines.

Groundwater extractions have increased by 4,450 m³ per year ($Z= 3.35$, $p<0.05$). As agricultural production is an important factor in this region and the aquifer levels are decreasing, this extraction could lead to a collapse of the aquifer storage in the future. Furthermore, groundwater levels are decreasing by 0.07 m per year, mainly due to rainfall decrease and evapotranspiration increase. It means that recharge it is expected to reduce and, as evapotranspiration increases, the demand for groundwater also increases for irrigation. Hence, the consequence is that there is positive feedback that will eventually lead to irrigation having to be reduced to meet the reducing water availability and higher crop demand. Hu et al. (2019) and Bibi et al. (2019) also have identified that reductions in groundwater levels were largely due to the effects of climate change, in their studied areas.

The electrical conductivity of the aquifer showed little variation from year to year, with seasonal cycles. According to the STL plot and the remainders line, there was no discernible long-term trend, although there was a slight increase from 2000 to 2005. The Mann–Kendall tests demonstrated that there was no significant Z -value, confirming that the salinity of the Mimoso Aquifer is highly variable in both space and time. This variability is the result of a variety of factors, including geological conditions and the presence of discharge areas caused by capillary rise, making it challenging to discern any trends in the yearly average.

Thus, an investigation with regional trends determined with the Regional-Kendall test can be observed in Figure 11 grouped by 3 different regions considering hydrological similarities.

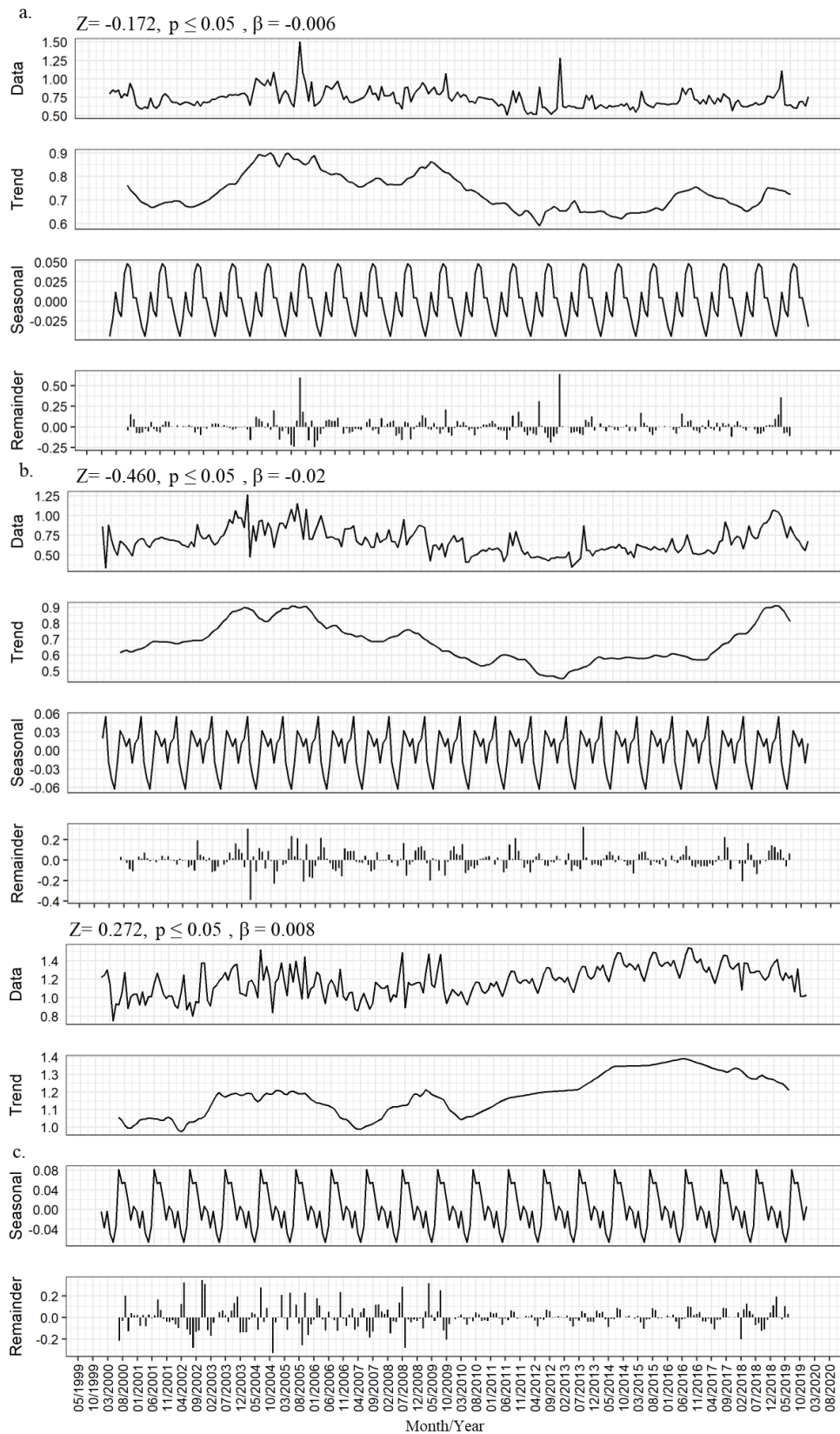


Figure 11. Annual time series of salinity (dS m^{-1}) for the (a) PW, (b) PZH group, and (c) PZL group from 2000 to 2019, with the associated trend lines.

The data derived from the STL show for PW a decrease trend in the EC, being the trend over the first 10 years since 2009, while the last three years were variable, with shift for increase. The Mann–Kendall tests confirmed the potential reduction in the EC, showing a significant Z-value ($p < 0.001$) of -0.006 dS m^{-1} . This potential reduction can be explained by pumping water, which increases water circulation. This better circulation also extends to the sandy areas where a salinity growth pattern is not observed in the PZH. However, the PZL region in Mimoso aquifer showed an increasing trend, confirmed by the MK tests, with a potential increase of 0.008 dS m^{-1} . According to the Pettit test, the growth trend is observed from September 2014, coincident with the beginning of a long dry period. There are weak and non-delimited interannual seasonal patterns (when compared to the GWL), due to the anthropic influence of pumping.

Comparing the seasonal time series from Figure 12a and c a strong correlation between groundwater level and abstraction is observed. Thus, groundwater pumping significantly impacts groundwater levels. For salinity, the seasonal patterns are more complex. However, some similarity can be identified between the seasonal series for rainfall and salinity for piezometers located at zones of high electrical conductivity. Nevertheless, it seems to occur an additional hydrological component, which could account for salt leaching at irrigated fields.

III.3.4 Analysis of the factors affecting GW availability and quality for irrigation

To validate the results obtained in the previous analyses and to illustrate the seasonal effects on the behavior of groundwater levels and water salinity, Principal Component Analysis (PCA) was applied to the original matrix of piezometric level and electrical conductivity, with abstraction and rainfall as supplementary variables. Figure 12 presents the biplot of the PCA for the groundwater level and electrical conductivity and their relations with rainfall and abstraction for the rainy, dry and normal periods (A) and a Spearman's correlation matrix (B).

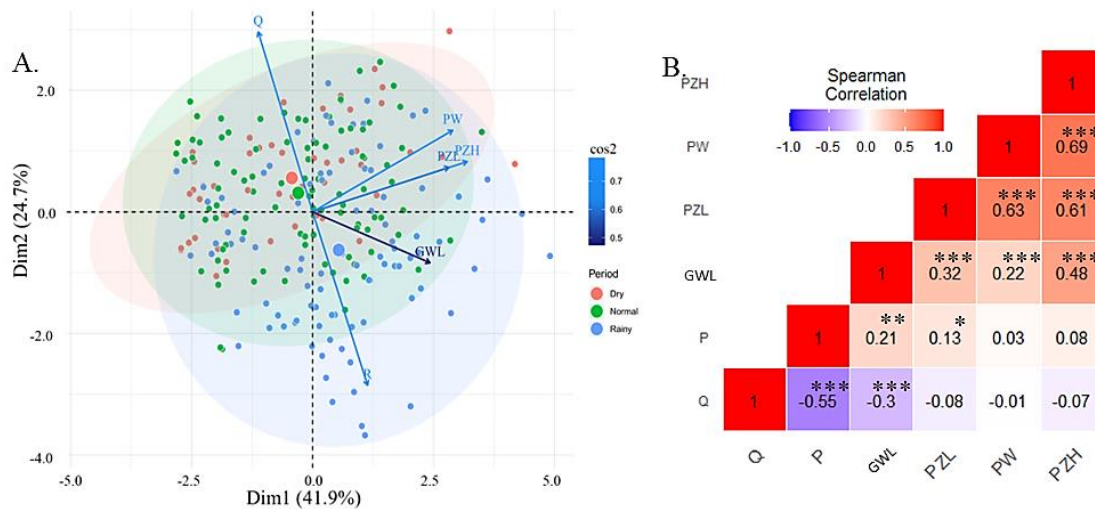


Figure 12. Principal component analysis, plotting of scores of the first two principal components (A) and Spearman's correlation matrix (B) of the Mimoso Valley variables. Note: the correlation *, ** and *** is significant at the 0.05, 0.01 and 0.001 level, respectively.

Main components Dim1 and Dim2 explain 66.6% of the total variance, with emphasis on Dim1, which by itself explains 41.9% of the total data variance. For this component, the variables related to salinity (electrical conductivity in PW, PZH, and PZL) were positively grouped and presented loads of 0.60, 0.73 and 0.57, respectively, denoting a strong positive correlation, inversely influenced by rainfall and groundwater level, as expected (A). Besides that, the dry period is strongly influenced by the abstraction (Q), considering the demand of irrigated areas. In the correlation matrix, PZH x PZL (0.61), PZH x PW (0.69) and PW x PZL (0.63) showed strong correlations ($p < 0.001$) (B). In the present study, the PCA score plot in relation to the dry, normal and rainy period highlighted crucial information about rainfall characteristics in water extraction and electrical conductivity, noting that for the alluvial valley, with vector Q strongly associated with centroids of the dry and normal period, while P and GDL are closer to the rainy season. From the Spearman Correlation Table, it can be verified that salinity for PZH and PZL is strongly related to groundwater levels.

The PCA results can serve as a basis for a more in-depth approach to elucidate the effects of water regime, inter-year climatic factors on agronomic management behavior in semiarid conditions (Saab et al., 2019). This PCA result was also observed by Carvalho et al. (2021), in an irrigated area, observing that high cumulative rainfall influences strongly groundwater salinity distribution. In addition, Carvalho et al. (2020) highlight that there is a

tendency to increase the length of dry interval, in days, for the Brazilian semiarid region, thus, the intensification of groundwater uses during such intervals.

In addition, a complementary PCA analysis was applied to long term piezometric groundwater levels, with rainfall, evapotranspiration, pumping rates and cropped areas as supplementary variables. Total agricultural areas at the basin were also included. Biplot of the PCA is presented in Figure 13.

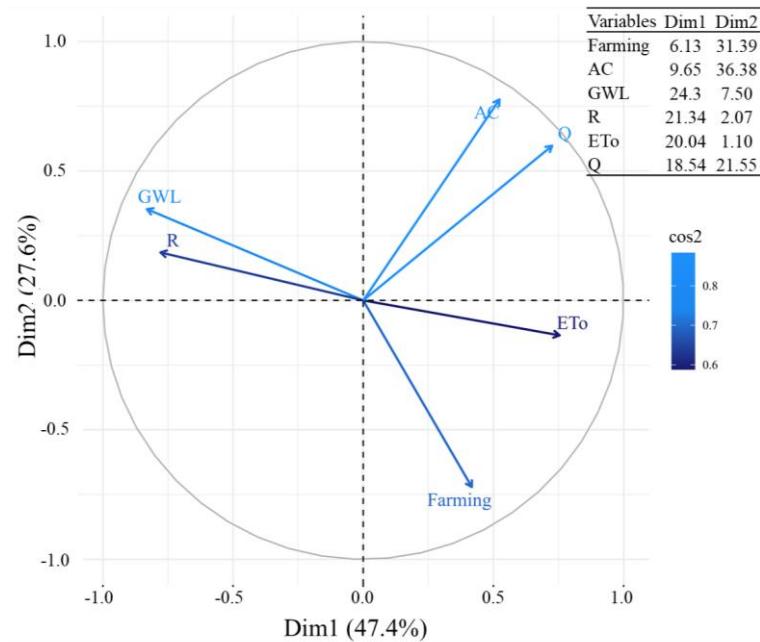


Figure 13. Principal component analysis, plotting the scores of the first two principal components and loads matrix for the components.

Main components Dim 1 and Dim 2 explain 75% of the total variance and Dim1 alone explains 47.4% of the total variance. For this component, rainfall was positively grouped with groundwater levels, presenting a load equal to 21.34. Evapotranspiration (ET0), total cropped area (AC) and discharge from wells (Q) were negatively grouped, presenting a strong correlation with groundwater levels. Evapotranspiration showed the strongest impact on groundwater levels among them, which could be explained by the additional transpiration components from deep roots of arboreal species at the valley (such as the “Algaroba”, *Prosopis juliflora*), and capillary rise from shallow groundwater areas, particularly at lower elevation regions, along the dry rivulet beds in the valley, and fallow lands which operate as evaporative sink zones (or dry drainage areas, as discussed by Konukcu et al., 2006).

III.4 Conclusions

The occurrence of temporal stability for the potentiometric level in the Mimoso Rivulet Alluvial Valley was verified, allowing the identification of piezometers that adequately represent the mean behavior over time. However, there was no global temporal stability for electrical conductivity. Decreasing seasonal trends in the water table during the dry period were identified, and these trends are related to the natural discharge of the aquifer, as well as the high extractions of groundwater for irrigation in this region.

Trends of rising temperatures, increased evapotranspiration, and decreased annual rainfall were identified, indicating a potential increase in the future use of groundwater resources. There was an increase in the amount of groundwater abstracted from the wells due to a rise in the evapotranspiration rate and the intensification of farming activities in the irrigated areas, which, combined with the decreasing amount of water in the aquifer, is a warning sign of a possible constraint to or restriction to future irrigation.

Although relevant insights on the dynamics of climate and anthropogenic-groundwater interactions have been produced in this paper, further studies assessing the role of the unsaturated zone on such processes are still necessary. The main limitations of the present research include the lack of a deeper analysis of secondary salinization, particularly in regions with shallow water tables. In addition, this research neglected the vegetation cover influence on the groundwater dynamics, which can be investigated in future studies.

The time stability analysis method together with trend analysis allowed a robust sustainability investigation for the aquifer in terms of quantity and quality (salinity), which can be adopted in other regions to build an effective groundwater management system. The application of the filter to remove autocorrelation proved to be essential for a more precise trend analysis assessment, where it was possible to identify a yearly pattern of variation in electrical conductivity after categorizing piezometers based on their hydraulic conductivity ranges. Thus, temporal stable piezometers for zones of high and low hydraulic conductivities could be identified.

Zones of low hydraulic conductivity presented a trend for increasing salinity, while areas with hydraulic conductivity and sandy soils tended a decrease in groundwater salinity due to hydrological components such as recharge and groundwater circulation. Regardless of the location of the pumping well at the Mimoso Aquifer, pumping proved to be effective in controlling groundwater salinity. The findings of this study can be employed in the current and further management and planning of groundwater in semiarid regions.

References

- Abdullahi, M.G.; Toriman, M.E; Gasim, M.B.; Garba, I., 2015. Trends Analysis of Groundwater: Using Non-Parametric Methods in Terengganu Malaysia. *J. Earth Sci. Clim. Change*, 6, 1-15. <https://doi.org/10.4172/2157-7617.1000251>
- Allen, R.G., Pereira, L.S., Raes, D., Smith, M., 1998. Crop evapotranspiration – guidelines for computing crop water requirements. In: first ed.; FAO Irrigation and Drainage Paper 56: Rome, Italy, pp. 1–297.
- Andrade, T. S.; Montenegro, S. M. G. L.; Montenegro, A. A. A.; Rodrigues, D. F. B., 2014. Estimation of alluvial recharge in the semiarid. *Rev. Eng. Agric.*, 34(2), 211-221. <http://dx.doi.org/10.1590/S0100-69162014000200003>
- Bahir, M., Ouhamdouch, S., Ouazar, D., El, N., 2020. Groundwater for Sustainable Development Climate change effect on groundwater characteristics within semiarid zones from western Morocco. *Groundw. Sustain. Dev.* 11, 100380. <https://doi.org/10.1016/j.gsd.2020.100380>
- Bibi, S., Wang, L., 2019. Response of Groundwater Storage and Recharge in the Qaidam Basin (Tibetan Plateau) to Climate Variations From 2002 to 2016 *J. Geophys. Res. Atmos.* 1–17. <https://doi.org/10.1029/2019JD030411>
- Bouwer, H. and Rice, R. C., 1976. A slug test for determining hydraulic conductivity of unconfined aquifers with completely or partially penetrating wells. *Water Resour. Res.*, 12, 423-428.
- Brito, C.S.; Silva, R.M.; Santos, C.A.G.; Brasil Neto, R.M.; Coelho, V.H.R., 2021. Monitoring meteorological drought in a semiarid region using two long-term satellite-estimated rainfall datasets: A case study of the Piranhas River basin, northeastern Brazil. *Atmos. Res.*, 250. <https://doi.org/10.1016/j.atmosres.2020.105380>
- Burte, J., Coudrain, A., Frischkorn, H., Chaffaut, I., Burte, J., Coudrain, A., Frischkorn, H., Chaffaut, I., Kosuth, P., 2009. Impacts anthropiques sur les termes du bilan hydrologique d'un aquifère alluvial dans le Nordeste semiaride, Brésil / Human impacts on components of hydrological balance in an alluvial aquifer in the semiarid Northeast, Brazil. *Hydrol Sci J.*, 50(1), 95-110. <https://doi.org/10.1623/hysj.50.1.95.56337>
- Carvalho, A.A., Abelardo, A.A., da Silva, H.P., Lopes, I., de Morais, J.E.F., da Silva, T.G.F., 2020. Trends of rainfall and temperature in Northeast Brazil. *Rev. Bras. Eng. Agric. e Ambient.* 24, 15–23. <https://doi.org/10.1590/1807-1929/agriambi.v24n1p15-23>

- Carvalho, A.A.d.; Montenegro, A.A.d.A.; de Lima, J.L.M.P.; Silva, T.G.F.d.; Pedrosa, E.M.R.; Almeida, T.A.B. Coupling Water Resources and Agricultural Practices for Sorghum in a Semiarid Environment. *Water* 2021, 13, 2288. <https://doi.org/10.3390/w13162288>
- Cheng, B., Zhang, Y., Xia, R., Wang, L., Zhang, N., Zhang, X., 2021. Spatiotemporal analysis and prediction of water quality in the Han River by an integrated nonparametric diagnosis approach. *J. Clean. Prod.* 328, 129583. <https://doi.org/10.1016/j.jclepro.2021.129583>
- C I S A G R O (Companhia Integrada de Serviços Agropecuários). 1991. *Projeto de Irrigação da fazenda Nossa Senhora do Rosario-Pesqueira-PE. Pernambuco, Brazil.* (in portuguese).
- Cleveland, W. S., Devlin, S. J., and Grosse, E., 1988. "Regression by Local Fitting: Methods, Properties, and Computational Algorithms," *J. Econom.*, 37, 87-114.
- Cleveland, W.S., Devlin, S.J., 1988. Locally Weighted Regression: An Approach to Regression Analysis by Local Fitting. *J. Am. Stat. Assoc.*, 83(403), 596-610.
- Coelho, V.H.R.; Montenegro, S.M.G.L.; Almeida, C.N.; Silva, B.B.; Oliveira, L.M.M.; Gusmão, A.C.V.; Freitas, E.S.; Montenegro, A.A.A., 2017. Alluvial groundwater recharge estimation in semiarid environment using remotely sensed data. *J. Hydrol.* 548, 1–15. <https://doi.org/10.1016/j.jhydrol.2017.02.054>
- Corrêa, M. M; Ribeiro, M. R. 2001. Levantamento detalhado de solos da Fazenda Nossa Senhora do Rosário (Pesqueira-PE). Recife, UFRPE/UFPE/CNPq/BNB. 35p. Relatório Técnico
- Cuthbert, M.O., Taylor, R.G., Favreau, G., Todd, M.C., Shamsudduha, M., Villholth, K.G., MacDonald, A.M., Scanlon, B.R., Kotchoni, D.O.V., Vouillamoz, J.M., Lawson, F.M.A., Adjomayi, P.A., Kashaigili, J., Seddon, D., Sorensen, J.P.R., Ebrahim, G.Y., Owor, M., Nyenje, P.M., Nazoumou, Y., Goni, I., Ousmane, B.I., Sibanda, T., Ascott, M.J., Macdonald, D.M.J., Agyekum, W., Koussoubé, Y., Wanke, H., Kim, H., Wada, Y., Lo, M.H., Oki, T., Kukuric, N., 2019. Observed controls on resilience of groundwater to climate variability in sub-Saharan Africa. *Nature* 572, 230–234. <https://doi.org/10.1038/s41586-019-1441-7>
- Dane, K. 2005. Sustainable management of groundwater resources in Rosario-Mimoso Valley, Northeast Brazil. University of Newcastle, Thesis in Hydrogeology, 120p.
- Dangar, S., Asoka, A., Mishra, V., 2021. Causes and implications of groundwater depletion in India: A review. *J. Hydrol.* 596, 126103. <https://doi.org/10.1016/j.jhydrol.2021.126103>

- Del-Toro-Guerrero, F.J., Kretzschmar, T., 2020. Studies Precipitation-temperature variability and drought episodes in northwest Baja California, México. *J. Hydrol. Reg. Stud.* 27, 100653. <https://doi.org/10.1016/j.ejrh.2019.100653>
- Doorenbos, J., Pruitt, W. O., Aboukhaled, A., 1997. Crop water requirements. Land and Water Development Division. FAO, Rome. W. O. Pruitt. FAO Consultant.
- Famiglietti, J.S., 2014. The global groundwater crisis. *Nat. Publ. Gr.* 4, 945–948. <https://doi.org/10.1038/nclimate2425>
- Fontes Júnior, R.V. de P., Montenegro, A.A.A., Montenegro, S.M.G.L., Santos, T.E.M. dos, 2012. Estabilidade temporal da potenciometria e da salinidade em vale aluvial no semiárido de Pernambuco. *Rev. Bras. Eng. Agrícola e Ambient.* 16, 1188–1197. <https://doi.org/10.1590/s1415-43662012001100007>
- Fontes Júnior, R.V.P.; Montenegro, A.A.A. 2017. Temporal dependence of potentiometric levels and groundwater salinity in alluvial aquifer upon rainfall and evapotranspiration. *Rev. Bras. Recur. Hidr.*, 22(54). <http://dx.doi.org/10.1590/2318-0331.0217170059>
- Gibrilla, A., Anornu, G., Adomako, D., 2018. Groundwater for Sustainable Development Trend analysis and ARIMA modelling of recent groundwater levels in the White Volta River basin of Ghana. *Groundw. Sustain. Dev.* 6, 150–163. <https://doi.org/10.1016/j.gsd.2017.12.006>
- Hosseini, P., Bailey, R.T., 2022. Investigating the controlling factors on salinity in soil, groundwater, and river water in a semiarid agricultural watershed using SWAT-Salt. *Science of the Total Environment* 810. <https://doi.org/10.1016/j.scitotenv.2021.152293>
- Hu, K.X., Awange, J.L., Kuhn, M., Saleem, A., 2019. Spatio-temporal groundwater variations associated with climatic and anthropogenic impacts in South-West Western Australia. *Sci. Total Environ* 696. <https://doi.org/10.1016/j.scitotenv.2019.133599>
- Kelly, C. 1995. An investigation of the hydraulic conductivity of a shallow unconfined alluvial aquifer in Pernambuco state, North- east Brazil. MSc Dissertation. Department of Civil Engineering, Newcastle University. UK. 77p.
- Kendall M. G. 1975. Rank Correlation Methods. Griffin, London.
- Kisi, O., Ay, M., 2014. Comparison of Mann – Kendall and innovative trend method for water quality parameters of the Kizilirmak River, Turkey. *J. Hydrol.* 513, 362–375. <https://doi.org/10.1016/j.jhydrol.2014.03.005>

- Konukcu, F., Gowing, J.W., Rose, D.A., 2006. Dry drainage: A sustainable solution to waterlogging and salinity problems in irrigation areas? *Agric. Water Manag.* 83, 1–12. <https://doi.org/10.1016/j.agwat.2005.09.003>
- Lima, A. de O., Lima-Filho, F.P., Dias, N. da S., Chipana-Rivera, R., Ferreira Neto, M., Souza, A. de M., Rego, P.R.D.A., Fernandes, C.D.S., 2019. Variation of the water table and salinity in alluvial aquifers of underground dams in the semiarid region of Rio Grande do Norte, Brazil. *Bioscience Journal* 35, 477–484. <https://doi.org/10.14393/BJ-v35n2a2019-41819>
- Mackay, R., Montenegro, A.A., Montenegro, S.M.G., Wonderen, J.V., 2005. Alluvial aquifer indicators for small scale irrigation in Northeast Brazil, IAHS publication, <https://assets.publishing.service.gov.uk/media/57a08c33e5274a27b2001049/IAHSpap.pdf>
- Mackay, R., Montenegro, A.A.A., 1996. Salinity control for sustainable small-scale agriculture. Final Report to the Overseas Development Administration (ODA), UK, University of Newcastle Upon Tyne. 30p.
- Mann, H.B., 1945. Nonparametric tests against trend. *Econometrica* 13, 245–259. doi:10.2307/1907187
- MapBiomass Brazil, 2022. Plataforma de mapas e dados [online]. Available at: <http://plataforma.mapbiomas.org/map>. (Accessed 3 April 2023).
- Marengo, J.A., Bernasconi, M., 2015. Regional differences in aridity / drought conditions over Northeast Brazil: present state and future projections regional differences in aridity / drought conditions over Northeast Brazil: present state and future projections. *Climatic Change* 129, 103–115. <https://doi.org/10.1007/s10584-014-1310-1>
- McKee, T. B., N. J. Doesken, and J. Kleist, 1993: The relationship of drought frequency and duration of time scales. Eighth Conference on Applied Climatology, American Meteorological Society, Jan17-23, 1993, Anaheim CA, pp.179-186.
- Melo, D.C.D., Anache, J.A.A., Almeida, C.N., Jaqueline, V., Filho, G.M.R., Rosalem, L.M.P., Pelinson, N.S., Ferreira, G.L.R.A., Schwaback, D., Calixto, K.G., João, P.G., Duarte-carvajalino, J.C., Jhunior, H.C.S., Nóbrega, J.D., Morita, A.K.M., Leite, C.M.C., Guedes, A.C.E., R, V.H., Schwaback, D., Calixto, K.G., Siqueira, J.P.G., Duarte-carvajalino, J.C., Jhunior, H.C.S., Nóbrega, J.D., Morita, A.K.M., Leite, C.M.C., Guedes, A.C.E., 2020. The big picture of field hydrology studies in Brazil. *Hydrol. Sci. J.* 65, 1262–1280. <https://doi.org/10.1080/02626667.2020.1747618>

- Mojid, M.A., Mainuddin, M., Faisal, K., Murad, I., Mac, J., 2021. Water usage trends under intensive groundwater-irrigated agricultural development in a changing climate – Evidence from Bangladesh. *Agric. Water Manag.* 251, 1-18. <https://doi.org/10.1016/j.agwat.2021.106873>
- Monteiro, A., Montenegro, A., Montenegro, S., 2014. Modelagem de Fluxo e Análise do Potencial Hídrico de Aquífero Aluvial no Semiárido de Pernambuco. *Rev. Bras. Recur. Hídricos* 19, 151–163. <https://doi.org/10.21168/rbrh.v19n3.p151-163>
- Montenegro, A. A. A. Stochastic Hydrogeological modelling of aquifer salinization from small scale agriculture in Northeast Brazil. University of Newcastle, 1997. 272p. PhD Thesis
- Montenegro, A. A. A.; Mackay, R.; Montenegro, S.M.G.L., 2002. Coupled unsaturated saturated modelling of salinization risk in na alluvial irrigated área of North- East Brazil. *Acta Universitatis Carolinae Geologica*, 46(2/3), 593- 594.
- Montenegro, A. A. A.; Ragab, R., 2010. Hydrological response of a Brazilian semiarid catchment to different land use and climate change scenarios: modeling study. *Hydrol. Process.* 24, 2705-2723.
- Montenegro, A.A.A., Montenegro, S.M.G.L., 2006. Variabilidade espacial de classes de textura, salinidade e condutividade hidráulica de solos em planície aluvial. *Rev. Bras. Eng. Agrícola e Ambient.* 10, 30–37. <https://doi.org/10.1590/s1415-43662006000100005>
- Montenegro, S. M. G. L.; Montenegro, A. A. A.; Mackay, R.; Oliveira, A. S. C., 2003. Dinâmica hidro-salina em aquífero aluvial utilizado para agricultura irrigada familiar em região semiárida. *Rev. Bras. Recur. Hidr.*, 8, 85-92.
- Montenegro, S.M.G.L.; Montenegro, A.A.A.; Ragab, R., 2010. Improving agricultural water management in the semiarid region of Brazil: experimental and modelling study. *Irrigation Science*, 28(4), 301-316. <http://dx.doi.org/10.1007/s00271-009-0191-y>
- Mott MacDonalds. Project R8333- Sustainable Use of Groundwater in the Semi-ariird Ribbon Valleys of Northeast Brazil, Final Technical Report, Cambridge, 96p., 2006. <https://assets.publishing.service.gov.uk/media/57a08c41ed915d622c00121b/R8333-FTR.pdf>
- Mu, Y.; Jones, C. 2022. An observational analysis of precipitation and deforestation age in the Brazilian Legal Amazon; *Atmospheric Research*, 271. <https://doi.org/10.1016/j.atmosres.2022.106122>

- Nigatu, Z.M.; Fan, D.; You, W.; Melesse, A.M.; Lun, P.; Yang, X.; Wan, X.; Jiang, Z., 2022. Crop production response to soil moisture and groundwater depletion in the Nile Basin based on multi-source data. *Sci. Total Environ.* 825. <https://doi.org/10.1016/j.scitotenv.2022.154007>
- Paulino, C.E.N.; Studart, T.M.C.; Campos, J.N.B.; Petana, C.J.; Lun, R.M.; Alves, J.M.B., 2019. Trends in Crop Reference Evapotranspiration and Climatological Variables Across Ceará State – Brazil. *Rev. bras. meteorol.*, 34 (1), 79- 88. <https://doi.org/10.1590/0102-7786334017>
- Peña-Arancibia, J.L., Mainuddin, M., Ahmad, M.D., Ibn, K.F., Ticehurst, C., Maniruzzaman, M., Mahboob, M.G., Kirby, J.M., 2020. Groundwater use and rapid irrigation expansion in a changing climate: Hydrological drivers in one of the world’s food bowls. *J. Hydrol.* 581. <https://doi.org/10.1016/j.jhydrol.2019.124300>
- Pettitt, A. N., 1979. A Non-Parametric Approach to the Change-Point Problem. *J R Stat Soc Series C (Applied Statistics)*, 28 (2), pp. 126-135. <https://doi.org/10.2307/2346729>
- Prayag, A.G.; Zhou, V.; Stigter, T.; Verzijl, A., 2023. Assessing the impact of groundwater abstractions on aquifer depletion in the Cauvery Delta, India. *Agric. Water Manag.* 279, 1-18. <https://doi.org/10.1016/j.agwat.2023.108191>
- Ribeiro, L., Kretschmer, N., Nascimento, J., Buxo, A., Rötting, T., Soto, G., Oyarzún, J., Maturana, H., Oyarzún, R., Kretschmer, N., Nascimento, J., Buxo, A., Rötting, T., Soto, G., 2015. Evaluating piezometric trends using the Mann- Kendall test on the alluvial aquifers of the Elqui River basin, Chile Evaluating piezometric trends using the Mann-Kendall test on the alluvial aquifers of the Elqui River basin, Chile. *Hydrol Sci J.* 6667. <https://doi.org/10.1080/02626667.2014.945936>
- Rodrigues, D.B.B., Gupta, H. V., Serrat-Capdevilla, A., Oliveira, P.T.S., Mendiondo, E.M., Maddock, T., and Mahmoud, M., 2015. Contrasting American and Brazilian Systems for Water Allocation and Transfers. *J. Water Resour.* 141 (7), 1–11. [https://doi.org/10.1061/\(ASCE\)WR.1943-5452.0000483](https://doi.org/10.1061/(ASCE)WR.1943-5452.0000483)
- Santos, E.S. ; Silva, E.F.F. ; Montenegro, A.A.A.; Souza, E.S. ; Souza, R.M.S.; Silva, R.I.J., 2018. Produtividade do pimentão sob diferentes lâminas de irrigação e doses de potássio em região semiárida. *Irriga*, 23, 518-534. <https://doi.org/10.15809/IRRIGA.2018V23N3P518-534>
- Schoups, G., Lee Addams, C., and Gorelick, S. M., 2005. Multi-objective calibration of a surface water-groundwater flow model in an irrigated agricultural region: Yaqui Valley,

- Sonora, Mexico, *Hydrol. Earth Syst. Sci.*, 9, 549–568. <https://doi.org/10.5194/hess-9-549-2005>
- Sen, P.K. 1968. Estimates of the regression coefficient based on Kendall's tau. *J Am. Stat. Assoc.* 63(324), 1379–1389.
- Silva Filho, E.L., Caetano, T.O., Ferreira, T.S.G., Cirilo, J.A., Vasconcelos, R.S., de Albuquerque, T.B.V. 2020. Avaliação do Potencial de Aproveitamento de Aluviões para a Construção de Barragens Subterrâneas no Semiárido Pernambucano, *Rev. Bras. Geogr. Fis.* 13, 5, 2402-2416.
- Sishodia, R.P., Shukla, S., Graham, W.D., Wani, S.P., Garg, K.K., 2016. *Journal of Hydrology: Regional Studies* Bi-decadal groundwater level trends in a semiarid south indian region: Declines, causes and management. *Biochem. Pharmacol.* 8, 43–58. <https://doi.org/10.1016/j.ejrh.2016.09.005>
- Souza, E.R.; Montenegro, A.A.A.; Montenegro, S.M.G.; Matos, J.A., 2011. Temporal stability of soil moisture in irrigated carrot crops in Northeast Brazil. *Agric. Water Manag.* 99, 26–32. <https://doi.org/10.1016/j.agwat.2011.08.002>
- Vachaud, G.; Silans, A. P.; Balabanis, P.; Vauclin, M., 1985. Temporal stability of spatially measured soil water probability density function. *Soil Sci. Soc. Am. J.*, 49, 822- 827. <https://doi.org/10.2136/sssaj1985.03615995004900040006x>
- Vazifekkhah, S., Kahya, E., 2019. Hydrological and agricultural droughts assessment in a semiarid basin: Inspecting the teleconnections of climate indices on a catchment scale. *Agric. Water Manag.* 217, 413–425. <https://doi.org/10.1016/j.agwat.2019.02.034>
- Yue, S., Pilon, P., Phinney, B., Cavadias, G., 2002. The influence of autocorrelation on the ability to detect trend in hydrological series. *Hydrol. Process.* 16, 1807–1829. <https://doi.org/10.1002/hyp.1095>
- Zhang, X., Wu, X., Zhao, R., Mu, W., Wu, C., 2022. Identifying the facts and driving factors of deceleration of groundwater table decline in Beijing during 1999 – 2018. *J. Hydrol.*,607. <https://doi.org/10.1016/j.jhydrol.2022.127475>

Chapter IV: Domestic wastewater reuse in irrigation and conservation practices: short-term effects of on soil carbon, salinity and soil moisture in Brazilian semiarid region

Abstract: Domestic wastewater reuse in irrigation can have positive effects on water conservation and nutrient recycling, but also poses risks to soil carbon and salinity if not managed properly. Conservation practices that balance these factors are essential for sustainable agricultural practices in the Brazilian semiarid region. For this purpose, the carbon and electrical conductivity in the soil of the semiarid region of Brazil were compared for three different cover condition: bare soil, mulch, and association between mulch and biochar. The hypothesis considered in this research was that the application of treated effluents in agriculture, besides being an alternative that can mitigate the problem of water scarcity of the semiarid region, and the soil cover condition is also capable of influencing spatial distribution of electrical conductivity (EC) and total of organic carbon (TOC). An irrigated cultivation of forage palm was evaluated for 111 days at three different times. The palm is irrigated with treated domestic effluent from the effluent single-family treatment system. Geostatistical models were applied to map the EC and TOC along the experimental area. Three indexes obtained from aerial multispectral camera images were evaluated: NDVI (Normalized Difference Vegetation Index), NDSI (Normalized Difference Salinity Index), and DWSI 4 (Disease–Water Stress Index 4). Results show that mulch promoted a control salinity and contributed to the higher incorporation of organic matter, while biochar increase significantly the organic carbon content. Regarding to the images process, salinity and vegetation indices as valuable tools to monitor and identifier management areas. Multispectral indices, NDVI and NDSI, enabled precise identification of areas with high variability, facilitating the accurate delineation of exposed soil and vegetation zones.

Keywords: wastewater reuse, semiarid, biochar, mulch

IV.1 Introduction

Agriculture is proven to contribute to human health and prosperity: 60% of the food consumed globally is in fact produced from crop cultivation (Zhou et al., 2023). In spite of this, agriculture is responsible for major environmental impacts that include resource consumption and global warming (Ingrao et al., 2023). The global population is projected to grow from 8 billion in 2022 to 10 billion in 2050, according to the latest report released by the United Nations' information center (UN, 2020). Such increase will lead to rise the demand for food in the following decades, which is expected to put more pressure on water, land and other inputs for food production, whilst climate change is likely to pose increasing challenges to agricultural production (Ingrao et al., 2023).

Furthermore, freshwater resources continue to decline due to climate change, groundwater pollution, and salinization (Kalboussi et al., 2022; Almeida et al., 2024). Climate change, a major global concern, alters rainfall patterns and increases the frequency and severity of extreme climate events, such as prolonged droughts and floods (Harris et al., 2020; Carvalho et al., 2020). These events negatively impact water availability and quality, reducing ecosystems' capacity to supply adequate water for human needs, including agriculture and food production (Ingrao et al., 2023).

In this context, designing and managing sustainable supply chains that preserve freshwater resources has become a major challenge on both corporate and policy agendas (Crovella et al., 2024). The sixth Sustainable Development Goal (SDG 6) targets improvements in water quality, increases in water-use efficiency, and reductions in water degradation and scarcity globally. Using treated wastewater for agriculture offers several theoretical advantages, such as reducing the consumption of high-quality water (e.g., from rivers, lakes, wells) for irrigation, decreasing the amount of agricultural inputs required through the use of organic matter, phosphorus, and nitrogen from wastewater, and mitigating the risk of eutrophication by reducing the discharge of wastewater directly into water bodies (Odone et al., 2024; Crovella et al., 2024; Lebu et al., 2024). These advantages are especially salient in semiarid climates, where the lack of water for irrigation makes usable wastewater an extremely valuable agricultural resource (Carvalho et al., 2021). Furthermore, the nutrients present in wastewater can significantly improve soil fertility and reduce the impact of wastewater release into rivers with low discharge or intermittent conditions. Therefore, using effluents in agriculture can be a solution for water scarcity and a means to mitigate CO₂ concentration in the atmosphere due to the organic material load present.

The National Semi-arid Institute (INSA) recommends irrigating forage palm (*Opuntia stricta*) with wastewater to ensure food security in livestock activities in the region (Araújo et al., 2019). The reuse of domestic effluents as an alternative water source in agriculture has been recommended in many studies to increase water availability in arid and semi-arid regions, address water scarcity (Corrêa et al., 2021) and reduce the use of mineral fertilizers due to the presence of organic material (Mabrouk et al., 2023). With proper management, some carbon can be retained in the soil profile or used for biomass formation, characterizing the mechanism of carbon sequestration from the atmosphere to the Earth's crust.

However, to develop systematically sustainable management practices and proposals, it is essential to understand the impacts (positive or negative) on soils and their stocks of carbon (C), nitrogen (N), and other nutrients caused by incorporating new resources and technologies, such as the treatment and reuse of domestic effluent in agriculture. Reusing wastewater can also have negative impacts, such as soil salinization and contamination of agricultural products with microbial pathogens, heavy metals, and other hazardous organic compounds (Mishra et al., 2023). One major problem associated with wastewater irrigation is the increase in soil exchangeable sodium (Na), as Na is present in high concentrations in wastewater. However, some agricultural practices can increase crop production in saline and sodic soils while minimizing negative environmental side effects.

Given this scenario, this research is based on the assumption that adopting new techniques in agricultural systems, such as the agricultural reuse of wastewater, can influence the soil's capacity to accumulate carbon and other nutrients. This chapter aims to assess the stocks of carbon and soil electrical conductivity in response to these practices, providing insights into their short-term effects on soil health and sustainability in this critical region.

IV.2 Materials and Methods

IV.2.1 Experimental Site

The study was carried out in an experimental agricultural area located in the Nossa Senhora do Rosário Settlement, within the Mimoso representative basin, in the municipality of Pesqueira-PE. The Mimoso basin is part of the Alto Ipanema basin, situated in the semi-arid region of the State of Pernambuco (Figure 1), and it serves as a tributary to the São Francisco River in its middle-lower section. The climate of the region is classified as BSh (hot semi-arid) according to the Köppen classification. The average annual reference potential

evapotranspiration is 2,000 mm, and the average annual temperature is 23°C. The region receives an average annual precipitation of 686 mm (Lima et al., 2020).

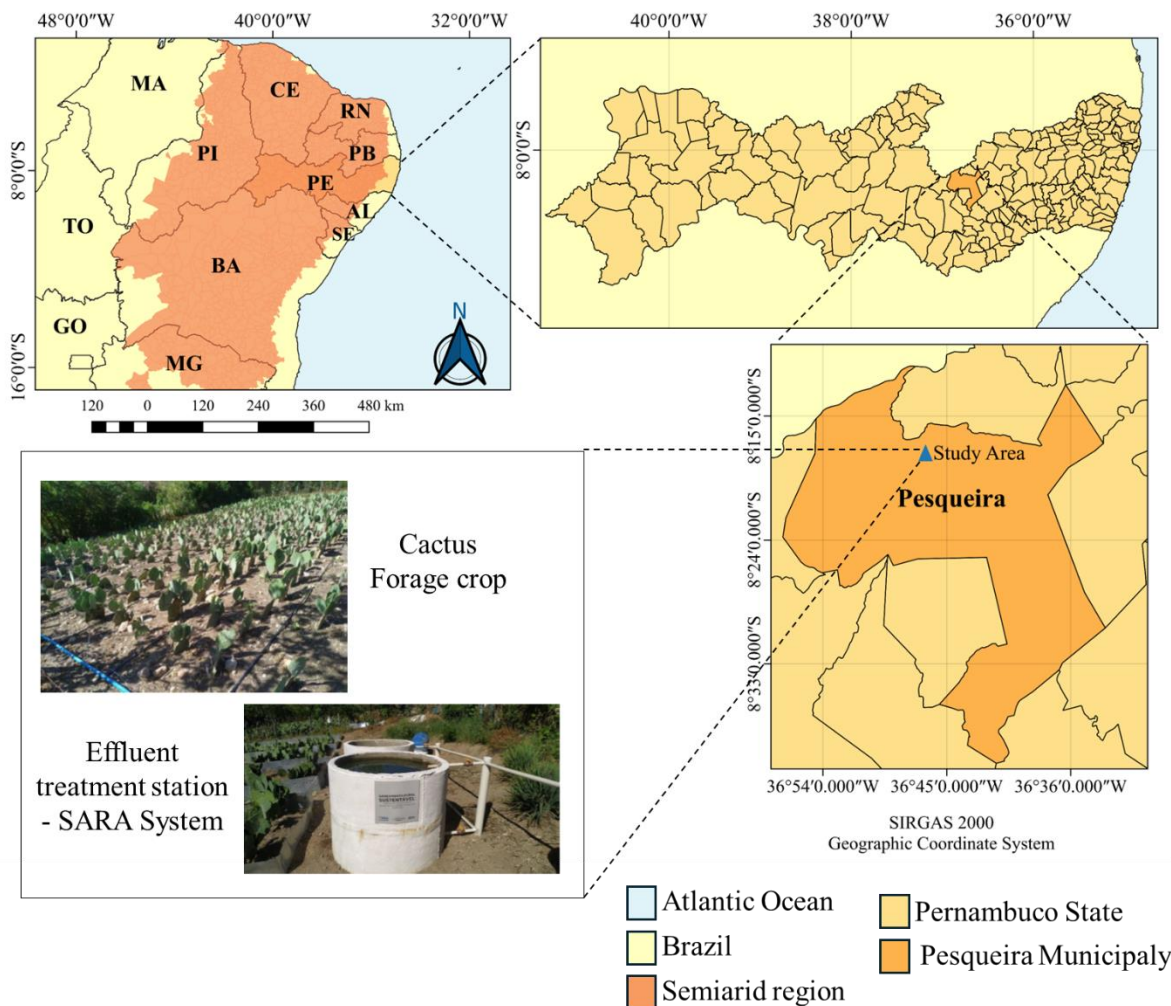


Figure 1. Location map of the Alto Ipanema basin, municipality of Pesqueira-PE and study area.

The soil in the study area is classified as Regolithic Neosol according to the Brazilian Soil Classification System (EMBRAPA, 2013). This soil type is generally shallow, with a depth of approximately 0.85 meters, and has a sandy loam texture. It is derived from Phanerozoic sedimentary deposits that form extensive aquifers and perennial rivers in the basin. In the municipality of Pesqueira, however, water resources are limited to fissured and weathered zones of granitoids and, more significantly, to narrow alluvial deposits in the Rosario-Mimoso valley. These alluvial deposits consist of fine to medium heterogeneous sands with some fine material (silt and clay) (Montenegro, 1997). The crystalline regions are characterized by

shallow soils with low infiltration rates and storage potentials, leading to ephemeral rivers and streams that flow only during the rainy season and remain dry in the summer (Mott MacDonald, 2004). The physical and chemical characteristics of the soil (extract of the saturated paste) are shown in Table 1.

Table 1. Physical and chemical characteristics of the soil (analyzed using a composite soil sample) in the experimental area, Pesqueira (Pernambuco state).

Depth	Sand	Silt	Clay	Bd	Pd	pH	EC	OC
m	%			g cm ⁻³			dS m ⁻¹	
0-0.10	74.8	8.2	17	1.34	2.56	6.3	1.2	13.27
0.10-0.20	68.4	13.3	18.3	1.42	2.42	5.7	1.4	3.93

Sd: bulk density; Pd: particle density; Pt: total porosity; pH: hydrogen potential in water; OC: organic carbon.

The effluent used for irrigation in the experiment was obtained through the SARA (Environmental Sanitation and Water Reuse) system (Mayer et al., 2021). The reuse system includes a reservoir with a total capacity of 2,650 liters for storing treated effluent, a 0.50 hp motor pump, and a localized drip irrigation system. The Effluent treatment station (ETS) treats approximately 6 m³ day⁻¹ of domestic effluent. The performance of the treatment system was evaluated based on its efficiency in removing organic matter and pathogenic organisms, as well as its ability to maintain nutrient levels (Table 2). The SARA treatment system was implemented in May 2022, with irrigation starting only in September 2022.

Table 2. Physical-chemical and microbiological parameters of domestic effluent were analyzed before treatment (in the equalization tank) and after treatment (in the reservoir following the polishing pond).

Parameters	Result		Resolution
	March 30 th , 2023	November 17 th , 2023	CONAMA 430 Art. 21 VMP
<i>a. Domestic effluent</i>			
DBO5	2,700.00mg/L	3,298.00mg/L	Max. 120 mg/L
Total Coliforms	>160000 NMP/100 mL	28000 NMP/100 mL	-
Escherichia coli	>160000 NMP/100 mL	<1.8 NMP/100 mL	-
<i>b. Domestic effluent treated</i>			
DBO5	200.0 mg/L	167,00 mg/L	Max. 120 mg/L
Total Coliforms	>160000 NMP/100 mL	26500 NMP/100 mL	-
Escherichia coli	>160000 NMP/100 mL	<6.5 NMP/100 mL	-

IV.2.2 Treatments and Experimental Design

The adopted experimental design was in randomized blocks (RBD), with three replications for each soil cover condition. Each subplot had a size of 12 m² (3 X 4 m) from the total of 108 m² (12 x 9). Each plot had 3 planting lines 1 m apart.

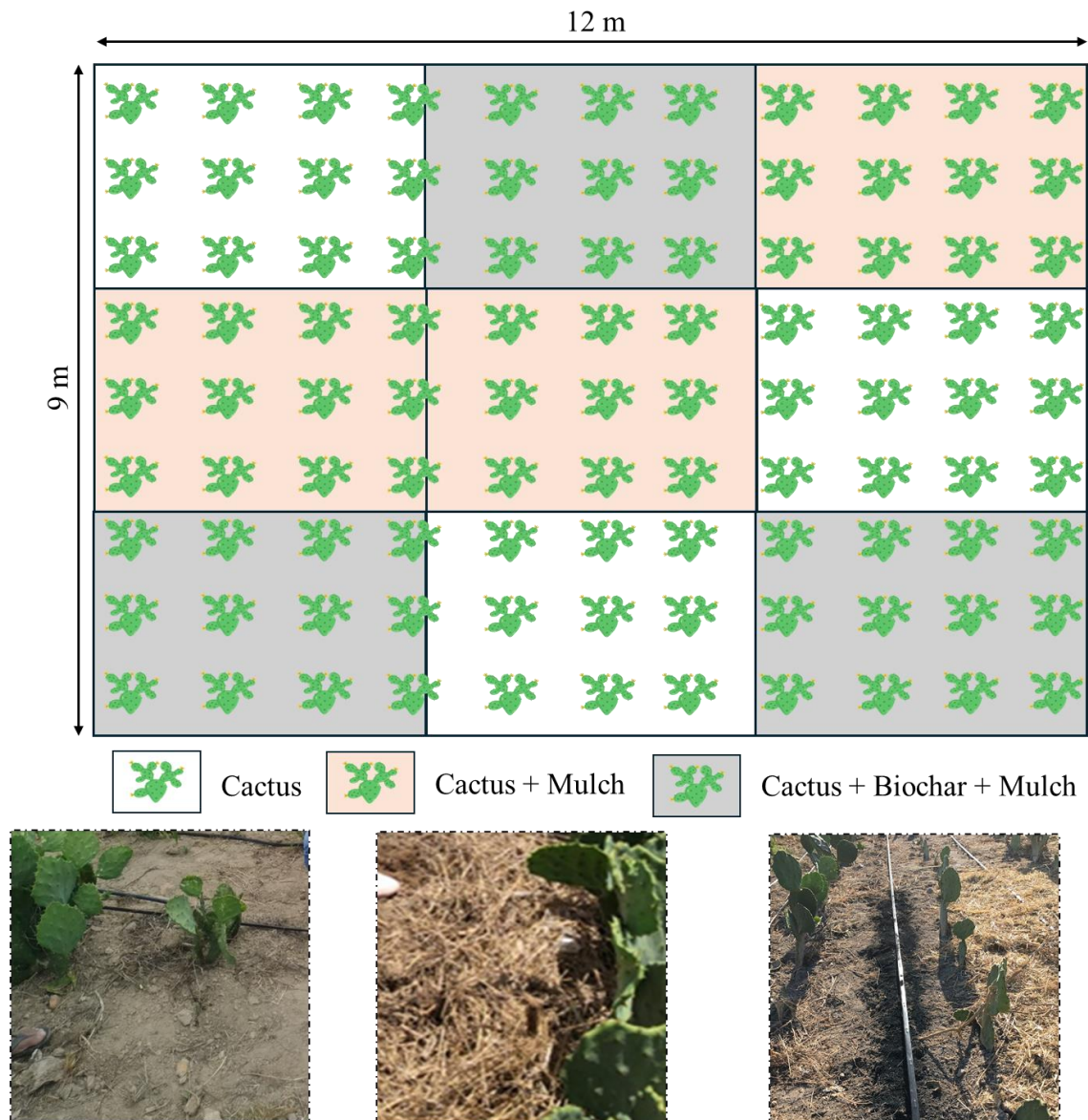


Figure 2. Sketch (not to scale) of the experimental plots and their respective soil cover condition.

In the experimental plot, forage cactus (*Opuntia stricta* (Haw) Haw.) was planted with a spacing of 1 meter between rows and 0.20 meters between plants. The forage cactus was transplanted in May 2022, and monitoring campaigns took place at three different times: C1 on November 17, 2023 (coinciding with the implementation of treatments); C2 on February 6, 2024; and C3 on April 29, 2024. Additionally, mulch was reapplied on January 12 and March 6, 2023. Three ground cover conditions were considered: i) plot without cover (bare soil); ii) plot with mulch (grass silage applied at a nominal rate of 8 t ha⁻¹); and iii) plot with mulch + biochar (grass silage applied at a nominal rate of 8 t ha⁻¹, overlain with biochar from cashew

wood pyrolysis applied at a rate of 12.5 t ha⁻¹). Biochar was generated using cashew wood (*Anacardium occidentale*) wastes through the pyrolysis process (530 °C for 10–12 h under oxygen-limited conditions). The properties of biochar are shown in Table 3.

Table 3. Chemical properties of biochar from cashew wood (*Anacardium occidentale*).

pH	P	K	Ca	Mg	Na	C	OM
1.25			g Kg ⁻¹			dag Kg ⁻¹	
7.12	0.4	8.4	1.9	2	0.9	404	87.3

OM= organic matter

A low-cost drip system was used with 1.6 mm holes at intervals of 0.2 m. The water application efficiency was 90%, according to Christiansen's Uniformity Coefficient (CUC). Irrigation depths were estimated from the water budget between rainfall and crop evapotranspiration treatment and applied every 2 days, depending on rainfall events.

IV.2.3 Metereological monitoring

To estimate the irrigation depth, reference evapotranspiration (ET_o) was calculated using the Penman–Monteith method (Allen et al., 1998). This calculation utilized data from a comprehensive automatic agrometeorological station by Campbell Scientific located in the study area, which provided measurements of temperature, relative humidity, global solar radiation, atmospheric pressure, and wind speed and direction. A Campbell Scientific TB4L automatic tipping bucket rain gauge, installed near the plots, with a resolution of 0.254 mm, will be programmed to record data at 5-minute intervals.

IV.2.4 Soil moisture and conservation techniques efficiency

Near the study area, 7 erosion plots, each 24 m² (2 × 12 m), were installed, oriented with the longer dimension downslope. The plots were bordered by 0.40 m tall metal sheets driven 0.15 m into the ground. They were placed on a longitudinal slope of 12%. Each plot received one of the following treatments: T1 – Bare soil; T2 – Forage cactus at the bottom of the plot (50% of the total length); T3 – Forage cactus at the bottom of the plot (50% of the total length) + mulch; T4 – Forage cactus throughout the plot; T5 – Forage cactus throughout the plot + mulch; T6 – mulch covering 50% of the soil surface; T7 – mulch covering all the plot soil surface. In all the experimental layouts the Forage cactus (*Opuntia stricta* (Haw) Haw.)

was planted at $1 \times 1 \text{ m}^2$ spacing between rows, and the mulch covering the soil surface at a density of 8 t ha^{-1} .

Campbell Scientific CS616 moisture probes recorded detailed soil moisture monitoring to assess the impact of natural rainfall and varying soil surface conditions on moisture dynamics. Installed horizontally at a depth of 0.2 m in each experimental plot, these sensors were connected to a Campbell Scientific CR1000 datalogger, recording data every hour.

IV.2.5 Biometric and Physiological Index Analyses

Multispectral images were acquired using a DJI Phantom 4 Multispectral with a spatial resolution of 0.5 m. The drone is equipped with an RGB camera and a set of multispectral cameras covering Blue, Green, Red, Red Edge, and Near Infrared bands, all at 2 MP with global shutter on a stabilized 3-axis gimbal (Lourenço et al., 2023).

The spectral indices NDVI (Normalized Difference Vegetation Index), NDSI (Normalized Difference Salinity Index), and DWSI 4 (Disease–Water Stress Index 4) were calculated to compare the effectiveness or deficiency of different management practices, computed using the equations provided in Table 4.

Table 4. Spectral indices and their respective equations.

Index	Equation	Index range	References
Normalized Difference Vegetation Index	$NDVI = \frac{(NIR - R)}{(NIR + R)}$	[-1, +1]	Rouse et al. 1974
Normalized Difference Salinity Index	$NDSI = \frac{(R - NIR)}{(R + NIR)}$	[-1, +1]	Khan et al. 2005
Disease–Water Stress Index 4	$DWSI\ 4 = \frac{(G)}{(R)}$	No range. Values closer to 0 indicate low stress; bigger than 1, high stress	Apan et al. 2010

where: NIR – near-infrared; R – red band; G – green band; B – blue band.

IV.2.6 Soil Salinity and Soil Total Organic Matter

For the soil electrical conductivity (EC), determined according to Teixeira et al. (2017) the usual saturation-extract method for evaluating soil salinity at the experimental plots at three different moments. To assess the soil carbon and organic matter dynamics, the methodology

proposed by Yeomans e Bremner (1988) was adopted, which is based on the determination of $K_2Cr_2O_7$ by titration with ammoniacal ferrous sulfate (0.4 mol L^{-1}) for estimating concentrations of total organic carbon (TOC).

The characterization of the soil's chemical attributes, during the three evaluated periods and under different cover conditions, was carried out according to the methodology described by Teixeira et al. (2017). The following parameters were determined: levels of exchangeable P, K^+ , and Na^+ , obtained through the Mehlich-1 extracting solution ($0.05 \text{ mol L}^{-1} HCl + 0.0125 \text{ mol L}^{-1} H_2SO_4$) and measured by colorimetry and flame photometry, respectively; levels of exchangeable Ca^{2+} and Mg^{2+} , obtained through the $1 \text{ mol L}^{-1} KCl$ extracting solution and measured by atomic absorption spectrometry. The level of exchangeable aluminum (Al^{3+}) was obtained by extraction with a $1 \text{ mol L}^{-1} KCl$ solution and volumetric determination using a $0.025N NaOH$ diluted solution, while potential acidity ($H+Al$) was obtained through extraction using calcium acetate buffered at pH 7.0 and titrated with $0.05N NaOH$. Based on the soil's exchangeable elements, the cation exchange capacity (CEC), the sum of exchangeable bases (SB), and the percentage of base saturation (V%) were calculated according to the methodology proposed by Teixeira et al. (2017).

IV.2.7 Statistical Analysis

The data were analyzed according to classical statistics to assess their behavior regarding measures of central tendency and variability, using a spreadsheet software. The distribution of the data was evaluated against the Normal distribution using the Kolmogorov-Smirnov test at a significance level of 0.05. Based on the coefficient of variation (CV) values, variability was classified following Warrick & Nielsen (1998) as low ($CV \leq 12\%$), moderate ($12 < CV \leq 60\%$), and high variability ($CV > 60\%$).

Outliers were filtered using the criteria of Hoaglin et al. (1992), which identifies outliers as data points below the lower limit (Li) or above the upper limit (Ls), respectively, estimated by the equations below:

$$Li = Qi - 1,5AP \quad (1)$$

$$Ls = Qs + 1,5AP \quad (2)$$

where: L_i = lower limit; L_s = upper limit; Q_i = lower quartile; Q_s = upper quartile; AP = range between the 1st and 3rd quartiles.

The Kolmogorov-Smirnov (KS) test will be employed, which uses a test statistic based on the maximum difference between empirical and theoretical cumulative probability functions. The null hypothesis (H_0) assumes that the data follows a normal distribution, while the alternative hypothesis (H_1) posits that the data does not follow a normal distribution. The magnitude of the difference is probabilistically established according to the probability law of this statistic, which is tabulated (Landim, 2003).

All block data were combined into a single grid for geostatistical analysis using the open-source software GEOEAS. The spatial dependence of comfort indices will be analyzed through the classical semivariogram constructed from semivariance estimates, as given by Equation 3 (Journel, 1989).

$$\hat{\gamma}(h) = \frac{1}{2N(h)} \sum_{i=1}^n [Z(X_i + h) - Z(X_i)]^2 \quad (3)$$

Where: $\hat{\gamma}(h)$ = estimated semivariance of the experimental data; $Z(x_i + h)$ e $Z(x_i)$ = observed values of the regionalized variable; and $N(h)$ = number of pairs of measured values separated by distance h .

Using the experimental semivariogram, the data were fitted to theoretical models including exponential, Gaussian, and spherical. Mathematical fitting allowed the definition of the following parameters: nugget effect (C_0), spatial dependence range (A), and sill ($C_0 + C_1$). The model that best fit the experimental values was chosen using the Leave-one-out cross-validation (Webster and Oliver, 2007), where each measured value is interpolated using kriging, and then the measured values are replaced by estimated values. Subsequently, the distribution of standardized errors is calculated, which should have a mean close to zero and a standard deviation of approximately one. The spatial dependency index (DSD) was calculated according to Cambardella et al. (1994) as the ratio between the nugget effect and the sill of the theoretical semivariograms. This criterion categorizes strong dependence when the ratio is less than 25%, moderate dependence between 25% and 75%, and weak dependence when the ratio

exceeds 75%. Following semivariogram validation, universal kriging was performed to generate spatial distribution maps using Surfer for Windows version 15.0 (SURFER, 2002).

IV.3 Results and Discussion

IV.3.1 Rainfall and climatic conditions during Palma Cultivation

Figure 3 presents the daily average soil moisture measurements in the 0–0.2 m layer of experimental plots located in Regolithic Neosol, from July 1, 2023, to April 30, 2024, totaling 273 measurements per treatment, with no failures recorded during this period. The figure also includes records of rainfall, relative humidity, and air temperature. During the rainy season in 2023 and 2024, a pronounced response is observed in the plots with mulch coverage (covering 50% of the area - T6 and the entire area - T7), showing high moisture peaks. These plots also exhibit a positive lag in recession, indicating a slower drying pattern compared to other treatments, particularly in 2023.

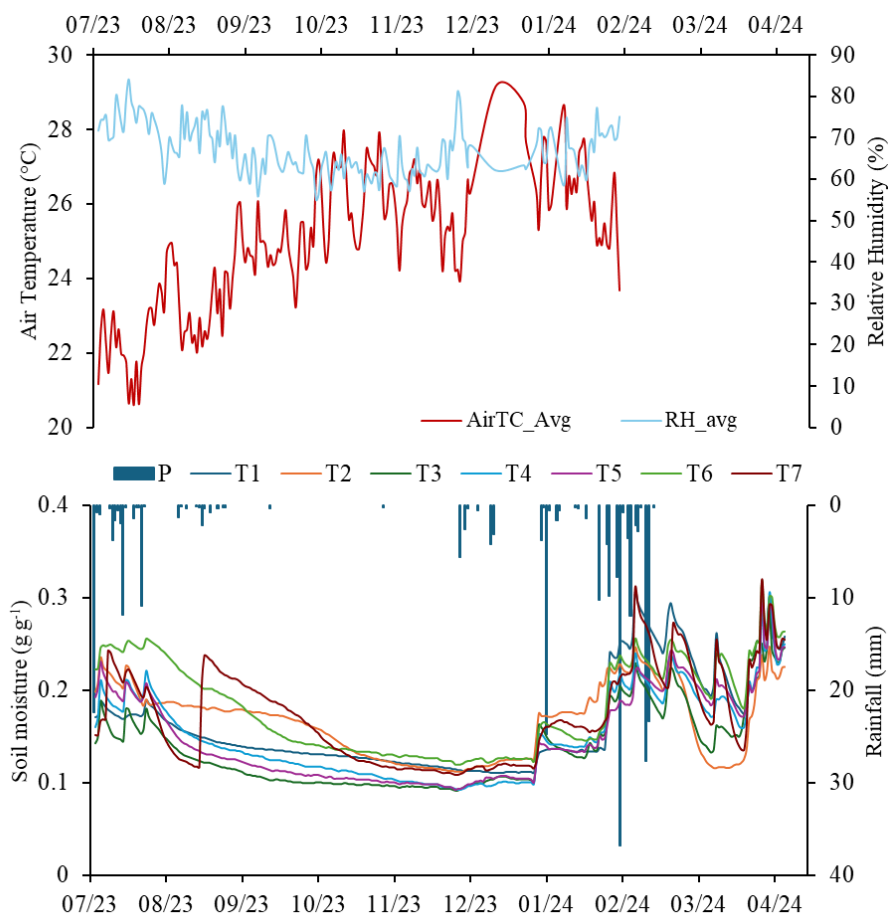


Figure 3. Temporal distribution of rainfall, Air temperature, Relative humidity and soil moisture in plots with treatments T1 to T7, from August 2023 to April 2024.

The faster wetting response in T6, which has 50% of the area covered by mulch, can be explained by the retention and barrier effect provided by the mulch and the location of the moisture sensor (in the center of the plot and 0.20 m from the beginning of the covered zone). However, this efficiency decreases over time due to the greater displacement of the mulch. Similar responses were found by Abrantes et al. (2018) in laboratory experiments evaluating the effectiveness of strip mulch. The authors concluded that strip mulch can be an effective approach to substantially reduce costs or maximize the treated area, though it does not prevent runoff generation and associated transport processes in slope areas where no mulch is applied.

Regarding the other treatments, the adoption of vegetative strips proved promising in maintaining moisture levels, showing efficiency compared to bare soil, particularly for T4 and T5 (combined with mulch) during the recession period of rains in 2024. Montenegro et al. (2020) and Montenegro et al. (2019) highlight the increase in soil water storage and the reduction of erosion rates in soils cultivated with vegetative strips. Additionally, the results underscore the efficiency of combining vegetative strips with mulch.

IV.3.2 Effects of Wastewater Irrigation and different soil cover conditions on the Soil Electrical Conductivity and Organic Matter

Figure 4 presents the organic carbon concentrations at the beginning of the experiment (C1), 81 days after implementation (C2), and 111 days after implementation (C3), according to the soil mulch conditions (bare soil, mulch, and a combination of mulch and biochar). The average total organic carbon (TOC) values at the start of the evaluation period (initial conditions) were similar across all randomly distributed blocks. The initial average TOC values ranged from 15.33 to 18.74, with high standard deviations, especially for the 0-0.10 m layer.

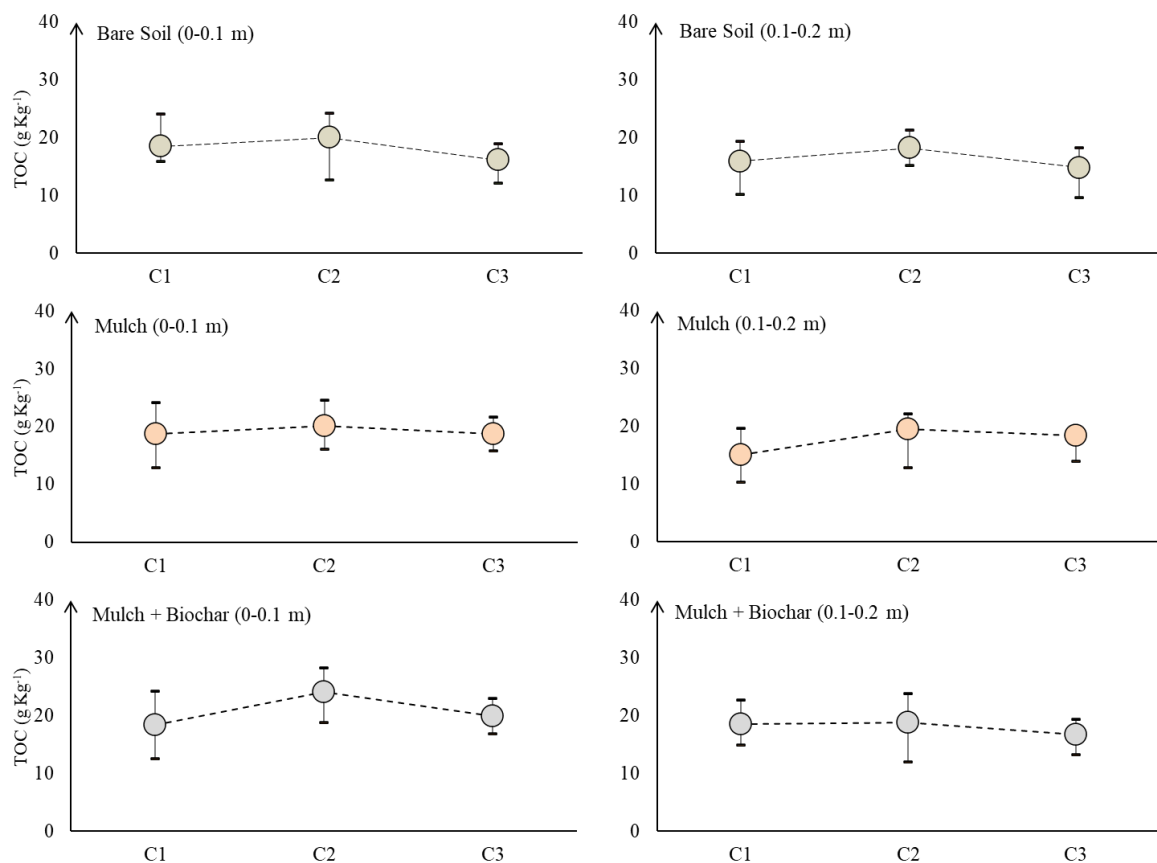


Figure 4. Temporal behavior of soil total organic carbon (TOC) under different soil cover conditions (bare soil, mulch, mulch with biochar).

An increase in TOC was observed over the first 81 days, with significant differences among the soil cover conditions.

The highest values were observed in the treatments with Mulch+Biochar and Mulch alone, showing increases of 30% and 7%, respectively, compared to the area without mulch application. Similar gains in total organic carbon (TOC) content were also observed by Kun et al. (2022), who evaluated the effects of irrigation with reclaimed water and mulch on soil organic matter content. They found that mulch promoted a greater influx of organic debris into the soil-water-plant system compared to bare soil. During the C3 period, after an accumulated precipitation of 81 mm, total carbon content decreased in all treatments due to soil loss. However, the Mulch+Biochar treatment still maintained the soil in better condition than its initial state.

Regarding to 0.1-0.2 m layer, TOC levels varied little in mulch cover condition being the most notable. Du et al. (2022) evaluated the effects of different wastewater irrigation treatments on soil properties and plant productivity in the North China Plain and observed that

conservation treatments might delay the increase of organic matter in the deep soil by retaining some of the content present in the effluent. However, the authors emphasized that this material should be reincorporated into the soil with the help of radiation and microbial activity.

The soil electrical conductivity (EC) at the beginning of the evaluation period showed high variability, with average magnitudes ranging from 0.5 to 1 dS m⁻¹ and 0.8 to 1.5 dS m⁻¹ for the 0-0.10 m and 0.10-0.20 m layers, respectively. By the end of the second evaluation, there were increases in soil EC, with averages ranging from 1.3 to 1.8 dS m⁻¹ and up to 2.8 dS m⁻¹. However, the percentage increase between treatments was lower for the mulch (9%) and mulch+biochar (12%) conditions compared to bare soil (36%), as the mulch formed a physical barrier on the soil surface, reducing energy exchange between the soil and the atmosphere. Similar results were observed by Deng et al. (2021), where the research highlights that biochar influences CW (constructed wetlands) performance by affecting physicochemical, hydraulic conditions, and biological behavior, showcasing the potential for improved wastewater treatment efficiency.

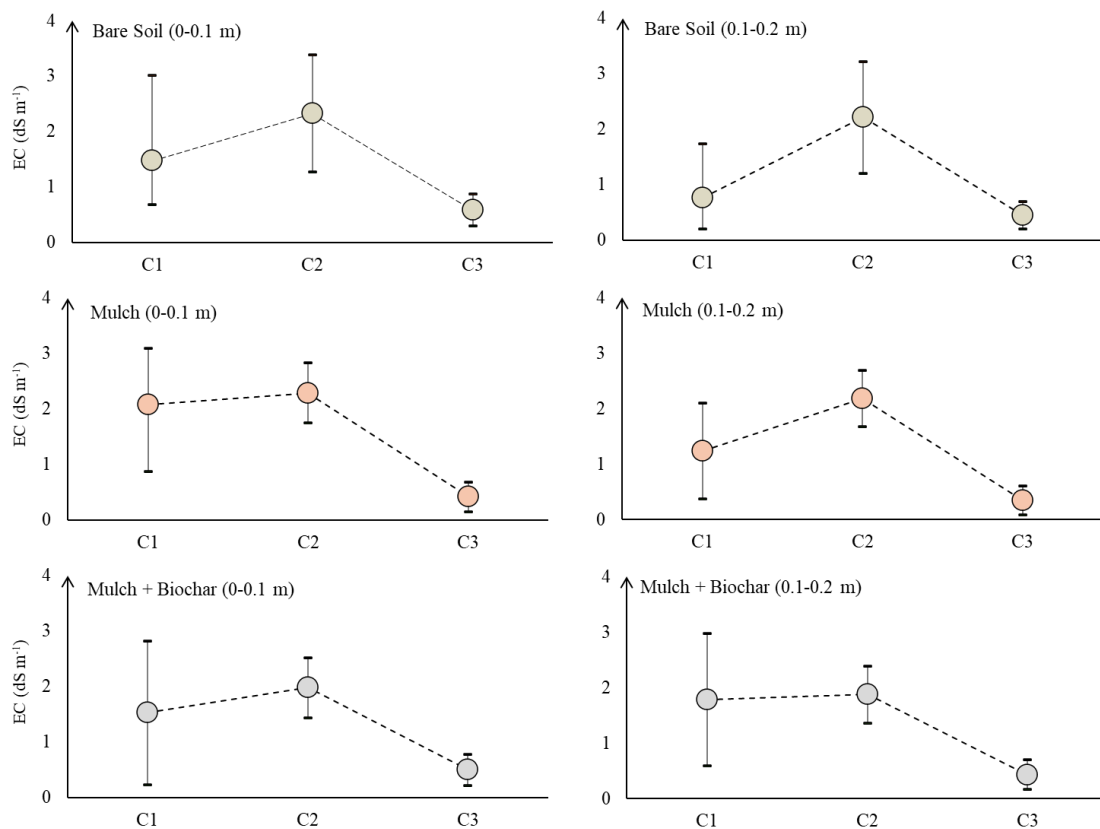


Figure 5. Temporal behavior of soil electrical conductivity (ES) under different soil cover conditions (bare soil, mulch, mulch with biochar).

Figure 6 shows that the presence of mulch and mulch+biochar reduced the range of salinity variation. The average distribution of EC did not vary significantly between bare soil and soil with only mulch. However, there was a considerable decrease in amplitude, with attenuation of extreme values. Similar results were observed by Kun et al. (2023) when evaluating the effect of mulch on soil quality in an agroforestry system irrigated with reclaimed water. The authors concluded that the possible mechanisms for restricting salt accumulation through the use of mulch under saline water irrigation included (a) inhibiting the upward movement of salts due to soil water evaporation and (b) promoting salt leaching by improving soil properties.

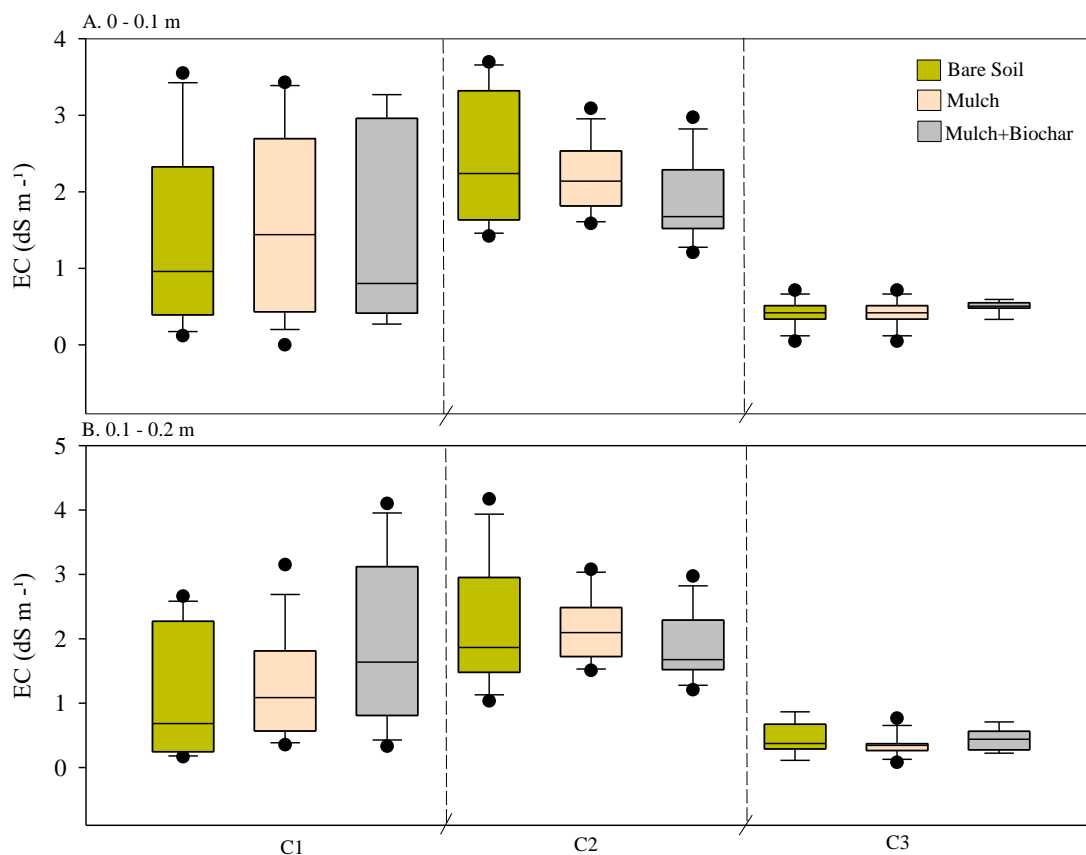


Figure 6. Box plots of Electrical conductivity (dS m^{-1}) for bare soil, mulch and mulch+biochar soil cover conditions to 0-0.1 m (A) and 0.10 – 0.20 (B) soil layers.

The main soil chemical variables did not show significant differences between treatments (Table 5). The pattern of the irrigation effect on CEC and total SB was similar for all cover conditions, with the dominant cation being Ca followed by Mg, constituting about 80% of the total CEC. In C2, a reduction in Ca content was observed for the Mulch (7%) and Mulch+Biochar (28%) conditions. The soil pH in the different studied conditions ranged from

slightly acidic to mildly alkaline, within the optimal range for the development of various crops (Qiu, 2021). Between treatments and C1 and C2, pH average increase of 11% in C3, due to a sequence of rainfall events that leached the soil. Regarding Na content, the addition of biochar to the soil surface promoted a reduction of 42% and 21% in sodium content in the 0-0.10 m and 0.10-0.20 m layers, respectively, while mulch reduced sodium content by 62% and 31% in the respective layers. Although phosphorus mobility is typically low (Baumann et al., 2020), there was a 70% increase in soil phosphorus levels observed in the 0.10-0.20 m layer under the mulch condition.

Table 5. Average values of soil chemical attributes under bare soil (BS), mulch (M), and mulch with biochar (M+B) conditions at cover condition implementation (C1), 81 days after (C2), and at the final evaluation at 111 days (C3) in the 0-0.10 m and 0.10-0.20 m layers.

Parameters		P	pH	Ca	Mg	Na	K	Al	H	SB	CEC	V	
CC	Layer	mg dm ³	(H ₂ O)	cmol _c dm ³									%
C1	BS	0.1	34	5.7	3.5	1.7	0.51	0.69	0.05	2.75	6.4	9.3	70
	BS	0.2	32	5.8	3.7	1.4	0.37	0.6	0.05	2.59	6.1	8.7	70
	M	0.1	45	5.8	3.8	1.6	0.6	0.7	0.05	2.83	6.7	9.4	69
	M	0.2	38	5.7	4	1.3	0.42	0.76	0.05	2.42	6.5	8.9	72
	M+B	0.1	43	6	5.2	1.3	0.6	0.8	0	2.39	7.9	10.3	77
	M+B	0.2	39	6	4.4	1.65	0.5	0.65	0	1.98	7.2	9.2	78
C2	BS	0.1	34	5.7	3.9	1	0.56	0.8	0.05	2.5	6.3	8.8	71
	BS	0.2	32	5.8	3.8	1.2	0.39	0.6	0.05	2.3	5.9	8.7	70
	M	0.1	45	6	3.59	1.41	0.37	0.9	0	2.06	6.3	8.6	76
	M	0.2	38	5.7	4.2	1.25	0.32	0.8	0.05	2.42	6.6	8.3	73
	M+B	0.1	40	5.6	3.7	1.2	0.42	0.7	0.05	1.93	6.2	8.4	77
	M+B	0.2	39	6	4.4	1.63	0.41	0.62	0	1.95	7.2	8.2	78
C3	BS	0.1	43	6.6	4	1.9	0.27	0.7	0	1.48	6.9	8.4	82
	BS	0.2	36	6.3	3.75	1.75	0.28	0.67	0	1.73	6.5	8.2	79
	M	0.1	38	6.8	3.5	1.65	0.28	0.73	0	1.4	6.2	7.6	81
	M	0.2	142	7.1	5.15	0.85	0.27	0.7	0	0.82	7.0	7.8	89
	M+B	0.1	34	6	3.75	1	0.23	0.62	0	2.64	5.6	8.2	68
	M+B	0.2	25	6.1	3.85	0.8	0.24	0.66	0	2.72	5.6	8.3	67

IV.3.3 Organic Carbon and Salinity Spatial Dynamics at the Experimental Area

For the spatial distribution assessment of salinity and organic carbon variables, data were considered within a single grid with a regular 2×1 m distribution. Statistical values are presented in Table 6. According to the coefficient of variation (CV) for TOC and EC across all evaluated periods, variability was classified as high ($CV > 60\%$), following the criteria of Warrick and Nielsen (1980). The data did not adhere to a normal distribution, as indicated by the Kolmogorov-Smirnov test at a significance level of 5%. However, after removing extreme values according to the criteria of Hoagli et al. (1983) the data were normalized. The high variability, also evidenced by the elevated standard deviation values, can be explained by the different treatments applied across the experimental plots. The specific dynamics of each type of cover in the interception and aggregation processes of EC and TOC in the soil contribute to this variability.

Table 6. Descriptive statistics of general of Total organic carbon content and Electrical conductivity for layers 0 – 0.10 m and 0.10 – 0.20 m, in three different monitoring campaign.

Layer	TOC			TOC			EC			EC		
	0 - 0.10 m			0.10 - 0.20 m			0 - 0.10 m			0.10 - 0.20 m		
	C1	C2	C3	C1	C2	C3	C1	C2	C3	C1	C2	C3
Mean	17.87	15.77	16.88	21.24	18.55	18.2	1.72	2.19	0.5	1.13	2.08	0.4
Median	16.64	14.68	16.6	20.72	17.27	18.21	0.96	2.02	0.48	0.76	1.92	0.37
Min	5.098	6.52	11.98	6.723	7.67	11.6	0.12	1.09	0.05	0	1.03	0.08
Max	49.93	26.04	22.25	54.48	30.63	24.43	5.24	4.39	1.33	4.1	4.17	0.86
Variance	44.37	23.08	8.285	49.95	31.94	12.41	2.15	0.53	0.04	1.19	0.48	0.04
SD	6.661	4.804	2.878	7.067	5.652	3.522	1.47	0.73	0.21	1.09	0.69	0.19
CV	2.498	3.056	5.768	2.932	3.056	5.169	0.66	2.78	2.3	0.7	2.78	1.94
p-Value (KS)	0.02	0.09	0.02	0.10	0.02	0.13	0.09	0.07	0.15	0.12	0.09	0.16

Well-defined experimental semivariograms with high spatial dependence were generated based on autocorrelation among filtered values, without extremes, of total organic carbon and electrical conductivity for periods C1, C2, and C3, as shown in Figure 7. Semivariogram parameters and validation results are presented in Table 5. Semivariances increase with higher carbon and salinity values, thus the threshold ($C_0 + C_1$) is directly related

to the amount of carbon and salt present in the soil of the study area, as also depicted in Table 5.

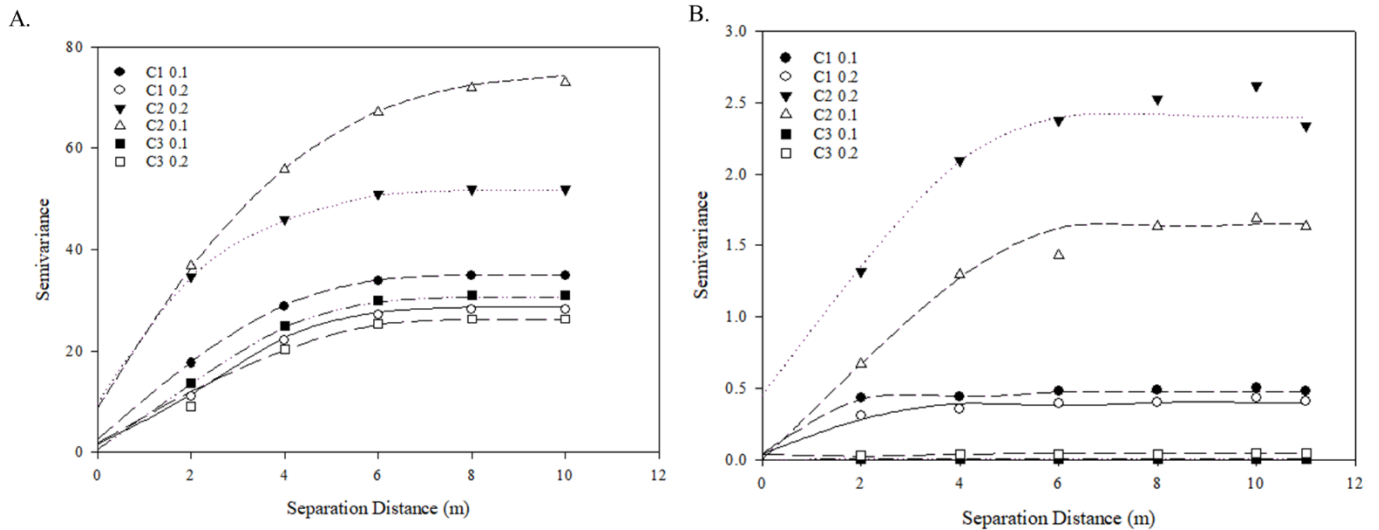


Figure 7. Semivariogram models for Total organic carbon content (A) and Electrical conductivity (B) for layers 0 – 0.10 m (0.1) and 0.10 – 0.20 m (0.2), in three different monitoring campaign (C1, C2 and C3).

The semivariogram models that best fit the data were the spherical model for EC and the exponential model for TOC (Table 7). Spatial dependency and adherence to the exponential model for total organic carbon (TOC) content were observed in various studies. In the study by Saha et al. (2021), the exponential model was found to be suitable for semivariogram fitting with TOC content and spectral reflectance data. Additionally, the study by Chen et al. (2019) compared different digital soil mapping techniques for soil organic carbon (SOC) mapping, where the exponential model was utilized in some methods, such as artificial neural networks kriging and geostatistics.

The nugget-to-sill ratio for salinity was 8.5 and 10 (C1), 18.8 and 24.5 (C2), and 18.9 and 23.8 (C3), indicating strong spatial dependence for all analysed periods, according to the classification by Cambardella et al. (1994). Total organic carbon content also showed strong spatial dependence with nugget-to-sill ratios of 5.6 and 7.2 (C1), 11.7 and 18.7 (C2), and 1.7 and 7.2 (C3).

Table 7. Semivariogram parameters and models for annual Total organic carbon content and Electrical conductivity; statistics of Leave-one-out cross-validation.

	Layer	Model	Nugget (C0)	Sill (C0 + C1)	Range (A, m)	R ²	DSD (%)	Cross- Validation	
								M	SD
A. C1									
EC (dS m ⁻¹)	0 - 0.10 m	Spherical	0.04	0.47	5.9	0.89	8.5	0.02	1.01
EC (dS m ⁻¹)	0.10 - 0.20 m	Spherical	0.04	0.4	6.3	0.86	10.0	0.01	1.10
TOC (g Kg ⁻¹)	0 - 0.10 m	Exponential	2.52	35.07	3.77	0.85	7.2	0.12	1.11
TOC (g Kg ⁻¹)	0.10 - 0.20 m	Exponential	1.61	28.65	3.76	0.97	5.6	0.10	1.09
B. C2									
EC (dS m ⁻¹)	0 - 0.10 m	Spherical	0.45	2.4	5.6	0.83	18.8	0.08	1.08
EC (dS m ⁻¹)	0.10 - 0.20 m	Spherical	0.4	1.63	4.5	0.86	24.5	0.08	1.12
TOC (g Kg ⁻¹)	0 - 0.10 m	Exponential	9.7	51.9	1.29	0.82	18.7	0.12	1.01
TOC (g Kg ⁻¹)	0.10 - 0.20 m	Exponential	8.7	74.36	8.73	0.96	11.7	0.01	1.04
C. C3									
EC (dS m ⁻¹)	0 - 0.10 m	Spherical	0.01	0.053	6.8	0.89	18.9	0.09	1.04
EC (dS m ⁻¹)	0.10 - 0.20 m	Spherical	0.01	0.042	4.8	0.93	23.8	0.11	1.06
TOC (g Kg ⁻¹)	0 - 0.10 m	Exponential	0.58	30.1	4.31	0.94	1.9	0.14	1.03
TOC (g Kg ⁻¹)	0.10 - 0.20 m	Exponential	1.88	26.21	5.25	0.98	7.2	0.07	1.08

The coefficients of determination (R²) for the adjusted models were moderate to high, with a minimum of 0.82 and a maximum of 0.98 for TOC, and from 0.83 to 0.93 for EC. Additionally, the semivariogram models were validated using the Leave-one-out cross-validation. The adjusted models were used to produce contour maps of Total Organic Carbon and Electrical Conductivity for the three evaluated scenarios using universal kriging techniques (Figure 8).

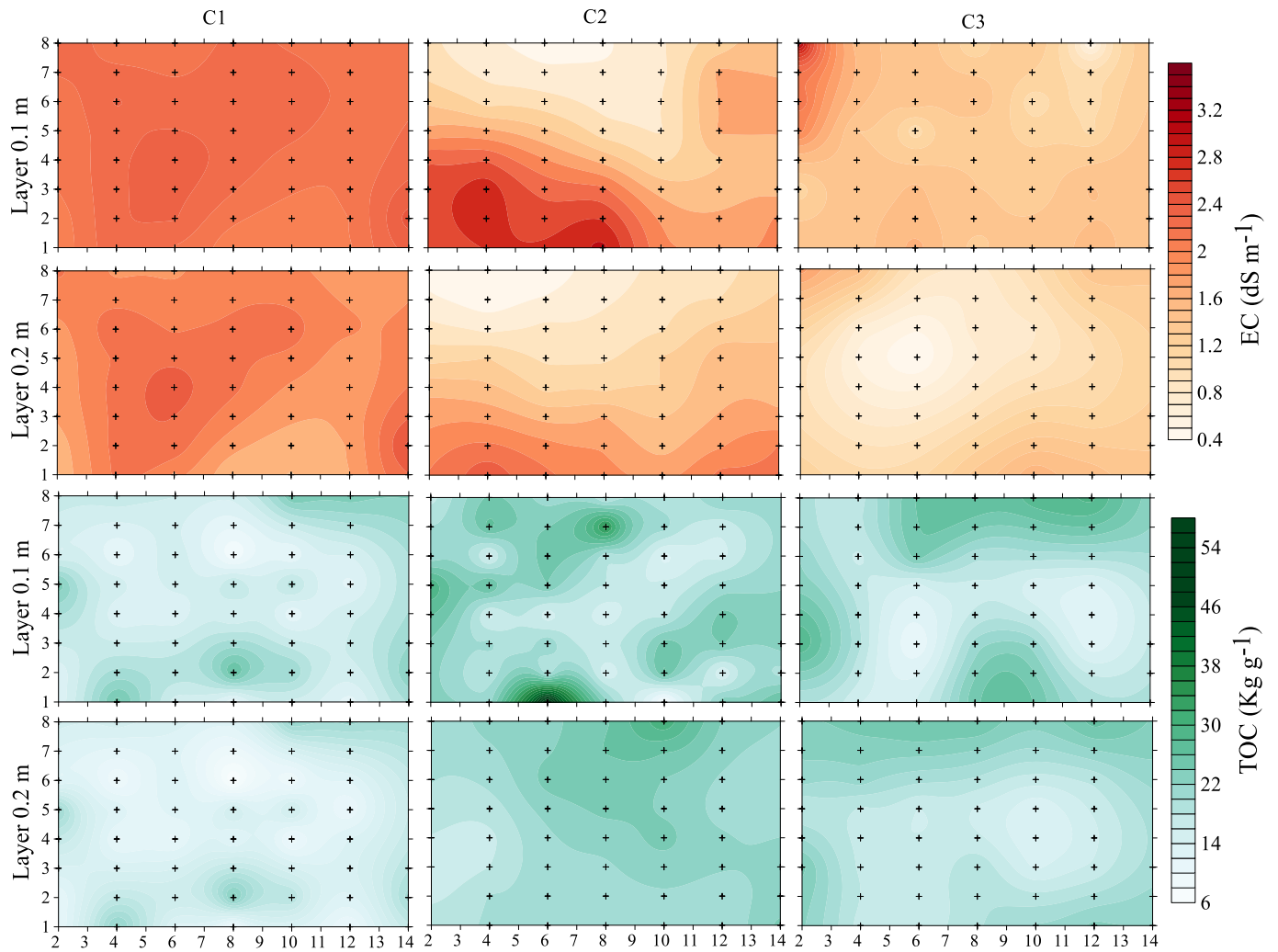


Figure 8. Kriging maps for the evaluated periods (C1, C2, and C3) for total organic carbon (TOC) and soil electrical conductivity (EC) in the 0-0.10 m (Layer 0.1 m) and 0.10-0.20 m (Layer 0.2 m) layers.

Although average salinity values increased by 21% (as shown in Table 4) between evaluations in C1 and C2, this increase was concentrated in the lower part of the plot. This behavior is observed in both the 0-0.10 m and 0.10-0.20 m layers. These higher levels are justified by the effect of slope on the leaching of effluent and salts down the slope (Hashem and Qi, 2021), but they accumulate in the lower part due to the grading and cutting of land at the end of the plot for the allocation of a road. Some other points of salt accumulation are observed corresponding to exposed soil areas. In C3, a decrease in EC was observed, as supported by Carvalho et al. (2021), where the authors highlight that irrigation with treated wastewater showed no negative agronomic impacts on the soil, as natural rainfall events typical of the Brazilian semiarid region facilitated effective salt leaching from shallow sandy soils.

Regarding the spatial variability of carbon, concentration zones highlight the presence of biochar on the soil surface. According to Li and Tasnady (2023), biochar, a sustainable solid material derived from the pyrolysis of carbon-enriched biomass, has emerged as a promising solution for soil carbon sequestration. Among the mechanisms by which biochar enhances soil carbon sequestration, the authors emphasized its role as a physical barrier against carbon loss, its capacity to promote stable soil aggregates, and its influence on soil microorganisms.

Regarding the evaluation of spectral indices, Figure 9 presents the maps of the Normalized Difference Vegetation Index (NDVI), the Normalized Difference Salinity Index (NDSI), and the Disease–Water Stress Index (DWSI-4).

The NDVI ranged from 0.14 to 0.95, being sensitive to the implementation of treatments and increased water input, with higher values observed in the upper and left lateral portions of the area. In C3, after the rainfall events, there was not only greater vegetative vigor in the forage cactus but also an increase in spontaneous vegetation consisting of native species with low water requirements.

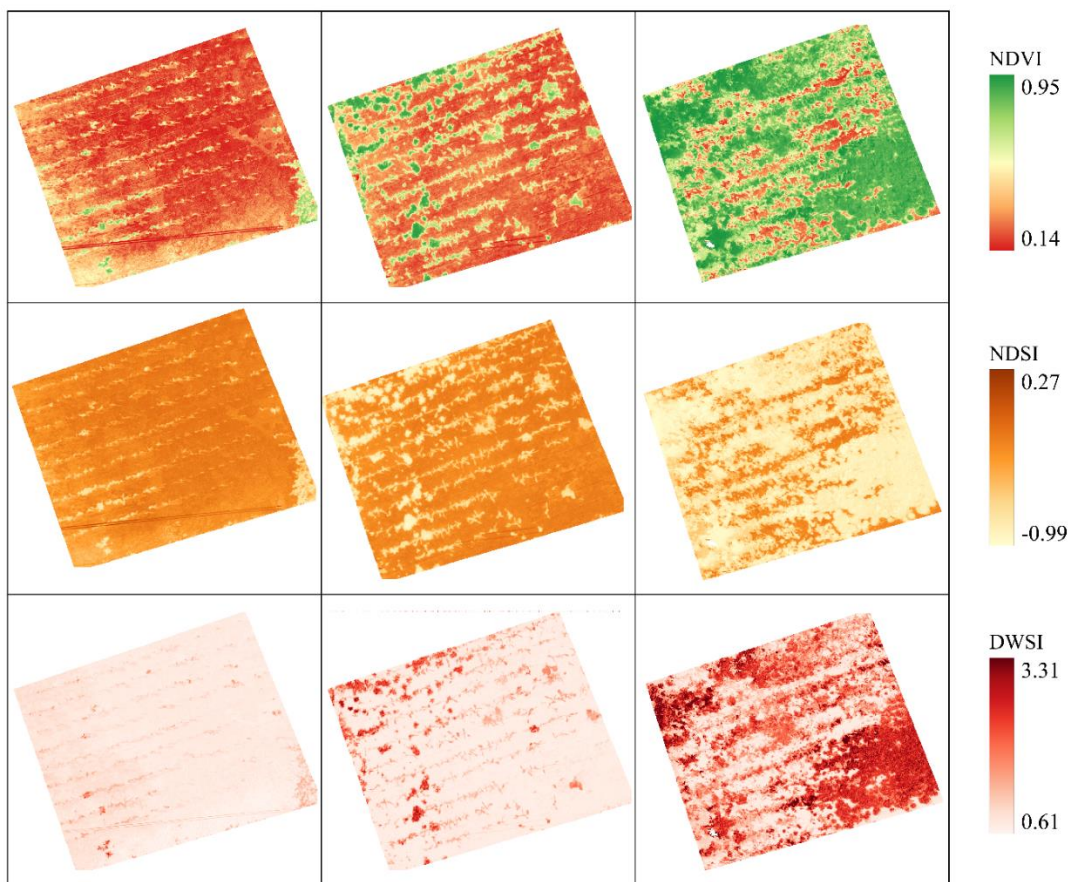


Figure 9. Spatial distribution of NVI, NDSI and DWSI in the selected field plots in three different moments of experiment.

Soil salinity is considered one of the primary factors affecting the interaction between plants and soil, due to its significant negative impact on soil nutrient availability and crop productivity. Recent advancements in remote sensing technology for mapping and monitoring degraded lands, particularly those affected by salinity, have proven beneficial in enhancing the speed, accuracy, and cost-effectiveness of these tasks (Gerardo and de Lima, 2022). Maps of surface soil salinity indices (NDSI) were generated through drone image analysis for the three evaluated periods, effectively depicting the spatial distribution of soil conditions in the study areas and the dynamics of soil salinity. It was observed that during C2, the index enabled the identification of plant species, showing a differentiation pattern similar to NDVI. By C3, following treatment disturbance by rainfall, soil salinity had decreased, and the area had been colonized by vegetation.

The DSWI was not effective in detecting stress vegetation, showing low values for the soil and high values for plant species, even during campaign C3. During this period, despite the Forage Cactus displaying high vegetative vigor (as indicated by NDVI maps), the area also featured dense spontaneous vegetation. Conceptually, this index should ideally register values close to zero for adequately hydrated vegetation, as proposed by Apan et al. (2010). Regarding the performance of the index, Agapiou (2020) highlighted that the effectiveness of visible indices is influenced by the size of the area and its heterogeneity. Indeed, the imaged area in this study exhibited heterogeneity, as observed in the kriging maps, which may have affected the efficiency of the DWSI.

IV.4. Conclusion

Implementation of soil and water conservation systems, including mulching and biochar application, has proven effective in controlling soil salinity, reducing levels from wastewater effluent. The study highlights that mulching acts as a physical barrier limiting upward movement of salts due to soil water evaporation, while biochar enhances soil properties and acts as a retention filter. Biochar increases soil organic carbon levels, and mulching enhances organic material incorporation into the soil. Research underscores promoting organic carbon retention and improving soil fertility.

Geostatistical models of soil electrical conductivity and organic carbon effectively capture their spatial distribution, revealing salt leaching through the soil profile and the impact of conservation-treated blocks on soil carbon dynamics. Studies indicate these models are

valuable for assessing how mulching and biochar influence salt and carbon distribution and retention, supporting sustainable management practices. Multispectral indices NDVI and NDSI enabled precise identification of areas with high heterogeneity, facilitating accurate delineation of exposed soil and vegetation zones.

Finally, it's necessary that long-term research be carried out with the objective of verifying if the reuse of domestic sewage in agriculture can provide water security needed in semiarid regions without impact the environment.

References

- Abrantes, J. R. C. B., Prats, S. A., Keizer, J. J., & de Lima, J. L. M. P. (2018). Effectiveness of the application of rice straw mulching strips in reducing runoff and soil loss: Laboratory soil flume experiments under simulated rainfall. *Soil and Tillage Research*, 180(February), 238–249. <https://doi.org/10.1016/j.still.2018.03.015>
- Allen, R.G., Pereira, L.S., Raes, D., Smith, M., 1998. Crop evapotranspiration – guidelines for computing crop water requirements. In: first ed.; FAO Irrigation and Drainage Paper 56: Rome, Italy, pp. 1–297.
- Almeida, T. A. B., Montenegro, A. A. de A., Mackay, R., Montenegro, S. M. G. L., Coelho, V. H. R., de Carvalho, A. A., & da Silva, T. G. F. (2024). Hydrogeological trends in an alluvial valley in the Brazilian semiarid: Impacts of observed climate variables change and exploitation on groundwater availability and salinity. *Journal of Hydrology: Regional Studies*, 53. <https://doi.org/10.1016/j.ejrh.2024.101784>
- Apan, A., Held, A., Phinn, S., & Markley, J. (2004). Detecting sugarcane “orange rust” disease using EO-1 Hyperion hyperspectral imagery. *International Journal of Remote Sensing*, 25(2), 489–498. <https://doi.org/10.1080/01431160310001618031>
- Araújo, J. C.; Pereira, D. D.; Lira, E. C.; Félix, E. S.; Souza, J. T. A.; Lima, W. B. Palma forrageira: plantio e manejo. Campina Grande: INSA, 2019. 60p.
- Asirifi, I., Kaetzl, K., Werner, S., Heinze, S., Abagale, F. K., Wichern, M., Lübken, M., & Marschner, B. (2023). Biochar for Wastewater Treatment and Soil Improvement in Irrigated Urban Agriculture: Single and Combined Effects on Crop Yields and Soil Fertility. *Journal of Soil Science and Plant Nutrition*, 23(1), 1408–1420. <https://doi.org/10.1007/s42729-023-01132-7>

- Baumann K, Shaheen SM, Hu Y, Gros P, Heilmann E, Morshedizad M, Wang J, Wang SL, Rinklebe J, Leinweber P (2020) Speciation and sorption of phosphorus in agricultural soil profiles of redoximorphic character. *Environ Geochem Hlth.* <https://doi.org/10.1007/s10653-020-00561-y>
- Cambardella, C.A., Moorman, T.B., Novak, J.M., Parkin, T.B., Karlen, D.L., Turco, R.F., Konopka, A.E., 1994. Field-Scale Variability of Soil Properties in Central Iowa Soils.
- Carvalho, A. A., Montenegro, A. A. de A., de Lima, J. L. M. P., da Silva, T. G. F., Pedrosa, E. M. R., & Almeida, T. A. B. (2021). Coupling water resources and agricultural practices for Sorghum in a semiarid environment. *Water (Switzerland)*, 13(16), 1–25. <https://doi.org/10.3390/w13162288>
- Carvalho, A.A., Abelardo, A.A., da Silva, H.P., Lopes, I., de Moraes, J.E.F., da Silva, T.G.F., 2020. Trends of rainfall and temperature in Northeast Brazil. *Rev. Bras. Eng. Agric. e Ambient.* 24, 15–23. <https://doi.org/10.1590/1807-1929/agriambi.v24n1p15-23>
- Chen, L., Ren, C., Li, L., Wang, Y., Zhang, B., Wang, Z., & Li, L. (2019). A comparative assessment of geostatistical, machine learning, and hybrid approaches for mapping topsoil organic carbon content. *ISPRS International Journal of Geo-Information*, 8(4). <https://doi.org/10.3390/ijgi8040174>
- Corrêa, M. M.; Cavalcanti, M. C.; Primo, D. C.; Neto, F. C. R.; Martins, J. M.; Menezes, R. S. C.; Antonino, A. C. D.; Mendes, I. S.; Medeiros, L. R. S. (2021) Wastewater reuse in irrigation: short-term effect on soil carbon and nitrogen stocks in Brazilian semiarid region. *Ambiente & Água*, p.1-15. <https://doi.org/10.4136/1980-993X>
- Crovella, T., Paiano, A., Falciglia, P. P., Lagioia, G., & Ingraio, C. (2024). Wastewater recovery for sustainable agricultural systems in the circular economy – A systematic literature review of Life Cycle Assessments. In *Science of the Total Environment* (Vol. 912). Elsevier B.V. <https://doi.org/10.1016/j.scitotenv.2023.169310>
- Du, Z., Zhao, S., She, Y., Zhang, Y., Yuan, J., Rahman, S. U., Qi, X., Xu, Y., & Li, P. (2022). Effects of Different Wastewater Irrigation on Soil Properties and Vegetable Productivity in the North China Plain. *Agriculture (Switzerland)*, 12(8). <https://doi.org/10.3390/agriculture12081106>
- EMBRAPA. Centro Nacional de Pesquisa de Solos. Sistema Brasileiro de Classificação de Solos. Rio de Janeiro, 2013. 412 p.
- GOLDEN SOFTWARE. Surfer for windows version 9.0. Colorado: Golden, 2010. 66p.

- Harris, F., Moss, C., Joy, E.J.M., Quinn, R., Scheelbeek, P.F.D., Dangour, A.D., Green, R., 2020. The water footprint of diets: a global systematic review and meta-analysis. *Adv. Nutr.* 11 (2), 375–386.
- Hashem, M. S., & Qi, X. bin. (2021). Treated wastewater irrigation-a review. *Water (Switzerland)*, 13(11). <https://doi.org/10.3390/w13111527>
- Hoaglin, D.C., Mosteller, F. and Tukey, J.W., *Análise exploratória de dados: técnicas robustas*. Edições Salamandra, Lisboa, Portugal, 1992, 446 P.
- Ingrao, C., Strippoli, R., Lagioia, G., Huisingh, D., 2023. Water scarcity in agriculture: an overview of causes, impacts and approaches for reducing the risks. *Heliyon* 9, e18507.
- Journel, A.G.; Huijbregts, C.J. *Mining Geostatistics*; Oxford University Press: London, UK, 1978; ISBN 0123910501.
- Kalboussi, N., Biard, Y., Pradeleix, L., Rapaport, A., Sinfort, C., Ait-Mouheb, N., 2022. Life cycle assessment as decision support tool for water reuse in agriculture irrigation. *Sci. Total Environ.* 836, 155486 <https://doi.org/10.1016/j.scitotenv.2022.155486>.
- Khan, N.M.; Guevara, V.V.; Vato, V.; Vhiozawa, S. Assessment of hydrosaline land degradation by using a simple approach of 776 remote sensing indicators. *Agric. Water Manag.* 2005, 77(1-3), 96–109.
- Kun, Á., Simon, B., Zalai, M., Kolozsvári, I., Bozán, C., Jancsó, M., Körösparti, J. T., Kovács, G. P., Gyuricza, C., & Bakti, B. (2023). Effect of Mulching on Soil Quality in an Agroforestry System Irrigated with Reused Water. *Agronomy*, 13(6). <https://doi.org/10.3390/agronomy13061622>
- Landim, P.M.B. *Análise Estatística de Dados Geológicos*, 2nd ed.; Edunesp: Rio Claro, Brazil, 2003; ISBN 9788571395046.
- Lebu, S., Lee, A., Salzberg, A., & Bauza, V. (2024). Adaptive strategies to enhance water security and resilience in low- and middle-income countries: A critical review. In *Science of the Total Environment* (Vol. 925). Elsevier B.V. <https://doi.org/10.1016/j.scitotenv.2024.171520>
- Li, S., & Tasnady, D. (2023). Biochar for Soil Carbon Sequestration: Current Knowledge, Mechanisms, and Future Perspectives. In *C-Journal of Carbon Research* (Vol. 9, Issue 3). Multidisciplinary Digital Publishing Institute (MDPI). <https://doi.org/10.3390/c9030067>
- Lima, C.A., Montenegro, A.A. de A., de Lima, J.L.M.P., Almeida, T.A.B., Dos Santos, J.C.N., 2020. Use of alternative soil covers for the control of soil loss in semiarid regions. *Eng. Sanit. e Ambient.* 25, 531–542. <https://doi.org/10.1590/s1413-41522020193900>

- Lourenço, V.R.; Montenegro, A.A.A.; Carvalho, A.A.D.; Sousa, L.D.B.D.; Almeida, T.A.B.; Almeida, T.F.S.D.; Vilar, B.P. Spatial Variability of Biophysical Multispectral Indexes under Heterogeneity and Anisotropy for Precision Monitoring. *Rev. Bras. Eng. Agríc. Ambient.* 2023, 27, 848–857.
- Mabrouk, O., Hamdi, H., Sayadi, S., Al-Ghouti, M. A., Abu-Dieyeh, M. H., & Zouari, N. (2023). Reuse of Sludge as Organic Soil Amendment: Insights into the Current Situation and Potential Challenges. In *Sustainability (Switzerland)* (Vol. 15, Issue 8). MDPI. <https://doi.org/10.3390/su15086773>
- Mayer, M.C., Medeiros, S., Batista, M., Barbosa, R., Rodrigues Lambais, G., Santos, S., & van Haandel, A. (2021). Tratamento de esgoto na zona rural visando ao reúso agrícola no semiárido brasileiro. *Revista DAE*, 69(229), 104–114. <https://doi.org/10.36659/dae.2021.023>
- Mishra, S., Kumar, R., & Kumar, M. (2023). Use of treated sewage or wastewater as an irrigation water for agricultural purposes- Environmental, health, and economic impacts. *Total Environment Research Themes*, 6. <https://doi.org/10.1016/j.totert.2023.100051>
- Montenegro, A. A. A. 1997. Stochastic hydrogeological modelling of aquifer salinization from small scale agriculture in Northeast Brazil. PhD thesis, Department of Civil Engineering, University of Newcastle Upon Tyne.
- Montenegro, A. A. A., Almeida, T. A. B., de Lima, C. A., Abrantes, J. R. C. B., & de Lima, J. L. M. P. (2020). Evaluating mulch cover with coir dust and cover crop with Palma cactus as soil and water conservation techniques for semiarid environments: Laboratory soil flume study under simulated rainfall. *Hydrology*, 7(3). <https://doi.org/10.3390/HYDROLOGY7030061>
- Montenegro, A. A. A., Lopes, I., de Carvalho, A. A., de Lima, J. L. M. P., de Souza, T. E. M. S., Araújo, H. L., Lins, F. A. C., Almeida, T. A. B., & Montenegro, H. G. L. A. (2019). Spatio Temporal Soil Moisture Dynamics and Runoff under Different Soil Cover Conditions in a Semiarid Representative Basin in Brazil. *Advances in Geosciences*, 48(June), 19–30. <https://doi.org/10.5194/adgeo-48-19-2019>
- Mott MacDonald. 2004. Sustainable use of groundwater in the semi-arid ribbon valleys of northeast Brazil. Inception report for Project R8333.
- Odone, G., Perulli, G. D., Mancuso, G., Lavrić, S., & Toscano, A. (2024). A novel smart fertigation system for irrigation with treated wastewater: Effects on nutrient recovery, crop

- and soil. *Agricultural Water Management*, 297. <https://doi.org/10.1016/j.agwat.2024.108832>
- Qiu L., Research progress on the effects of soil acidity and alkalinity on plant growth, *Open Journal of Applied Sciences*. (2022) 12, no. 6, 1045–1053, <https://doi.org/10.4236/ojapps.2022.126071>.
- Rouse, J.W.; Haas, R.H.; Schell, J.A.; Deering, D.W.; Harlan, J.C. *Monitoring the Vernal Advancement of Retrogradation of Natural Vegetation*; NASA:Washington, DC, USA, 1973.
- Saha, S. K., Tiwari, S. K., & Kumar, S. (2022). Integrated Use of Hyperspectral Remote Sensing and Geostatistics in Spatial Prediction of Soil Organic Carbon Content. *Journal of the Indian Society of Remote Sensing*, 50(1), 129–141. <https://doi.org/10.1007/s12524-021-01459-7>
- Teixeira, P.C., Donagemma, G.K., Fontana, A., Teixeira, W.G. *Manual de métodos de análise do solo*. 3.ed. rev. Brasília: Embrapa Solos, 2017. 573p.
- UN, 2020. *Global Issues Population Our growing population*, United Nation. <https://www.un.org/en/global-issues/population> (Last accessed date 18 December 2023).
- Warrick, A.W. and Nielsen, D.R., 1980. Spatial variability of soil physical properties in the field. In: Hillel, D., (ed.). *Applications of Soil Physics*. Cap. 2, Academic Press, New York, USA, pp. 319-344.
- Webster R, Oliver M (2007) *Geostatistics for environmental scientists*, 2nd edn. Wiley, Chichester.
- Yeomans, J.C. and Bremner, J.M., A rapid and precise method for routine determination of organic carbon in soil. *Communications In Soil Science and Plant Analysis*, 19, pp. 1467-1476, 1988. DOI: 10.1080/00103628809368027
- Zhou, S., Li, W., Lu, Z., Yue, R., 2023. An analysis of multiple ecosystem services in a large-scale urbanized area of northern China based on the food-energy-water integrative framework. *Environ. Impact Assess. Rev.* 98, 106913 <https://doi.org/10.1016/j.eiar.2022.106913>.

Chapter V: Evaluating Daily Water Stress Index (DWSI) using thermal imaging of Neem tree canopies under bare soil and mulching conditions

Abstract: Water stress on crops can severely disrupt crop growth and reduce yields, requiring accurate and prompt diagnosis of crop water stress, especially in semiarid regions. Evaluating neem (Nim) in such environments is crucial due to its adaptation to low water availability and effectiveness in pest control. Infrared thermal imaging cameras are effective tools to monitor the spatial distribution of canopy temperature (T_c), which is the basis of the Daily Water Stress Index (DWSI) calculation. This research aimed to evaluate the variability of plant water stress under different soil cover conditions through geostatistical techniques, using detailed thermographic images of neem canopies in the Brazilian Northeastern semiarid region. Two experimental plots were established with neem cropped under mulch and bare soil conditions. Thermal images of the leaves were taken with a portable thermographic camera and processed using Python language and the OpenCV database. The application of the geostatistical technique enabled the stress indicator mapping at a leaf scale, with the spherical and exponential models providing the best fit for both soil cover conditions. Results showed that the highest levels of water stress were observed during the months with the highest air temperatures and no rainfall, especially at the apex of the leaf and close to the central veins, due to a negative water balance. Even under extreme drought conditions, mulching reduced neem physiological water stress, leading to lower plant water stress, associated with higher soil moisture content and a positive skewness of temperature distribution. Regarding the mapping of the stress index, the sequential Gaussian simulation method reduced the temperature uncertainty and variation at the leaf surface. Our findings highlight that mapping the Water Stress Index offers a robust framework for precise stress detection for agricultural management, as well as soil cover management in semiarid regions. These findings underscore the impact of meteorological and planting conditions on leaf temperature and baseline water stress, which can be valuable for regional water resource managers in diagnosing crop water status more accurately.

Keywords: thermography; computer vision; plant status; semiarid; precision agriculture.

V.1 Introduction

Neem tree (*Azadirachta indica*) has a wide range of economic applications and environmental benefits. Neem belongs to the *Meliceae* family, native of India, which has been used for centuries for the most varied purposes. This culture provides a large number of secondary metabolites with biological activity that draw attention for their efficiency as a natural insecticide (Silva et al., 2021; Brito et al., 2021). This potential use as a crop insecticide has been gaining prominence in family farming, reducing the use of pesticides and the cost of pest management (Albiero et al., 2019). In addition, its planting has become increasingly common in the Brazilian semiarid region, due to the adaptation of the species to the climatic conditions of the region, soil characteristics and for presenting a high resilience, being efficient in the degraded areas reclamation (Lima et al. al., 2020).

The climatic conditions in semiarid areas are often characterized by droughts, which are an inherent part of the environment's natural cycle and can significantly affect the availability of water for various uses (Inocêncio et al., 2021; Nogueira et al., 2023). Carvalho et al. (2020) cautioned that the number of rainy days is expected to decrease in the coming decades, leading to a decrease in the availability of water resources and increased environmental vulnerability and desertification risks in the region. The challenging climate situation in semiarid regions can be observed by high rates of evaporation combined with low and infrequent precipitation events, which creates a negative water balance (Almeida et al., 2024). This is further exacerbated by soil degradation due to improper agricultural use and deforestation.

Drought has a severe impact on developing countries, where local communities, highly dependent on agriculture for their livelihoods, are particularly vulnerable. Frequent drought episodes lead to significant economic disruptions, which in turn cause political and social turmoil with far-reaching implications (Oroud et al., 2021). Bo et al. (2023) highlight that improve the efficiency of water use is critical for ensuring the sustainable development of agriculture and the economy. Recent studies have explored efficient water use technologies for semiarid areas and have shown that the mulch use as soil cover has been an efficient approach to raise rainfed agricultural production. According to Li et al. (2021), mulching with plant residues is a simple, easy-to-manage, ecological and low-cost technique that plays a positive role in soil moisture conservation and can reduce plant water stress. Montenegro et al. (2020)

highlighted in their studies involving the use of low-cost conservation practices, the potential of mulch in reducing runoff and soil loss, and in increasing soil moisture content, thus promoting a higher water availability.

To prevent significant yield reductions and the high costs associated with irrigation equipment, it is essential to gain a scientific understanding of the physiological and biochemical processes involved before implementing deficit irrigation (Bazrgar et al., 2023). Therefore, it is important to apply effective methods for monitoring crop water stress status to better understand and to save water (Pineda et al., 2021; Luan et al., 2021; Bo et al., 2023). Methods for monitoring crop water stress involve measuring soil moisture, photosynthetic rate, and crop characteristics such as height and leaf area index (Ihuoma and Madramootoo, 2017). Most of these methods are time consuming, laborious and, in some cases, destructive to plants. Because these measurements are often limited to a small portion of the field, the results might not be representative of the actual crop water needs or the overall field moisture conditions (Debangshi and Sadhukhan, 2023). Remote sensing, incorporated in precision agriculture, refers to obtaining data without physical contact with the object of study (Shanmugapriya et al., 2019). This technological a, coupled with improvements in computational capacity, enables the collection of data and extraction of vital information for crop management (Sishodia et al., 2020). The utilization of images in this realm has yielded promising outcomes in monitoring various factors, including nitrogen status, water stress, and incidences of pests and diseases (Singh et al., 2020; Menegassi et al., 2022). The canopy temperature (T_c) has long been recognized as an indicator of plant water status. With the advancement of remote sensing technology, measuring canopy temperature remotely to diagnose crop water deficits offers more promising applications than many other methods (Liu et al., 2022; Feiziasl et al., 2022).

In order to assess the impact of different management and water conditions on plants, Brunini and Turco (2016) suggested that the temperature of the vegetation canopy can act as an indicator of biotic and abiotic symptoms of the plants, having a direct influence on their metabolisms and indicating water stress. Huo et al. (2019) noted that canopy temperature reflects the thermal status of the crop, being closely related to stomatal conductance, and affecting the crop's water use and utilization. Valím et al. (2019) calculated grapevine water stress indices from thermal images of the crowns, emphasizing the importance of non-destructive monitoring with thermal proximity sensors to monitor vegetative parameters. Pineda et al. (2021) highlighted that thermography is a crucial tool for the implementation of a more automated, precise, and sustainable agriculture. According to the authors, thermography

is an efficient tool to investigate the interaction among plant, climate conditions, and management, as long as environmental and measuring conditions are correlated with thermography information, allowing for a proper interpretation.

Thermography is a non-destructive and effective technique for studying canopy characteristics related to water stress. It can cover areas of various sizes, such as fields, orchards, or individual canopies, and provides spatial information on the variability of water stress (Liu et al., 2020; Silva et al., 2023). Thermal imaging cameras measure the infrared radiation emitted by plant canopies, which is directly related to their temperature (Menegassi et al., 2022). When plants experience water stress, they close their stomata to reduce water loss, leading to an increase in canopy temperature (Savvides et al., 2022). By analyzing thermal images, indices like the Daily Water Stress Index (DWSI) and Crop Water Stress Index (CWSI) can be calculated, with higher values indicating more severe water stress (Brunini and Turco et al, 2016; Bo et al., 2023).

In addition to the mentioned advances, Liu et al. (2020) emphasized the relevance in extracting the thermal infrared canopy at critical regions of crops and their leaves, as it significantly impacts the study of canopy temperature changes. To address this challenge, expert and intelligent systems based on computer vision algorithms are increasingly integrated into agricultural production management (Tian et al., 2020). Computer vision, leveraging cameras and computers instead of human eyes, identifies, tracks, and measures targets for subsequent image processing. Singh et al. (2020) further underscores the agricultural significance of computer vision, particularly when linked with thermal images, and present various approach techniques, highlighting the diverse applications and potential benefits of this technology in agricultural practices.

Hence, the use of thermal cameras to spatially map temperatures has become increasingly feasible with the aid of geostatistical tools. Using geostatistical techniques allows for the interpretation of these results based on their spatial structure and variability. By modeling the spatial dependence of variables through a semivariogram model, these tools allow highly precise interpolation (Silva et al., 2023). Recent research has demonstrated the applicability of geostatistical techniques to assess the thermal comfort of dairy cows in a compost barn in the Brazilian semiarid region (Silva et al., 2023), as well as to investigate the environmental thermal comfort of a roof slab before and after the installation of a green roof (Santana et al., 2023) and to investigate the environmental water stress in a Basin, using a novel environmental water stress index (EWSI) derived based on stochastic modelling (Kinwatu et al., 2021).

Geostatistics recognizes that the values of a given variable are correlated to their spatial arrangement, meaning that observations taken in closer proximity are more similar than those taken further apart (Landim, 2003). As well, the Gaussian simulation can be employed to generate realistic spatial distributions of canopy temperature and water stress index from thermal imagery. This allows for the characterization of spatial variability in crop water requirements, which is crucial for precision irrigation scheduling (Araújo-Paredes et al., 2022; Andrade et al., 2021).

This study explores how mapping the spatial variability of DWSI (Daily Water Stress Indicator) contributes to the non-destructive evaluation of plant water status in a semiarid environment. The research objectives were threefold: (i) to process thermographic images of the plant canopy using a Computer Vision algorithm, identifying leaves with well-defined edges that accurately represent the canopy. (ii) to determine the spatial variability of DWSI within the designated leaves, considering two soil cover conditions: bare soil and mulch cover. (iii) to mitigate crop temperature mapping uncertainty through Sequential Gaussian Simulation techniques. By achieving these objectives, the study aims to provide insights into the temperature spatial distribution for plants under water stress, offering valuable information for optimizing water management strategies in semiarid regions.

V.2 Material and Methods

V.2.1 Characterization of the study area

The research was conducted at the hillslope of the Mimoso Catchment, which is part of the Alto Ipanema Catchment in the Brazilian semiarid region of Pernambuco State, as seen in Figure 1. Two erosion plots, each measuring 20 m² (2 × 10 m) with the longest side running along the slope, were installed in an area of 0.7 hectares.

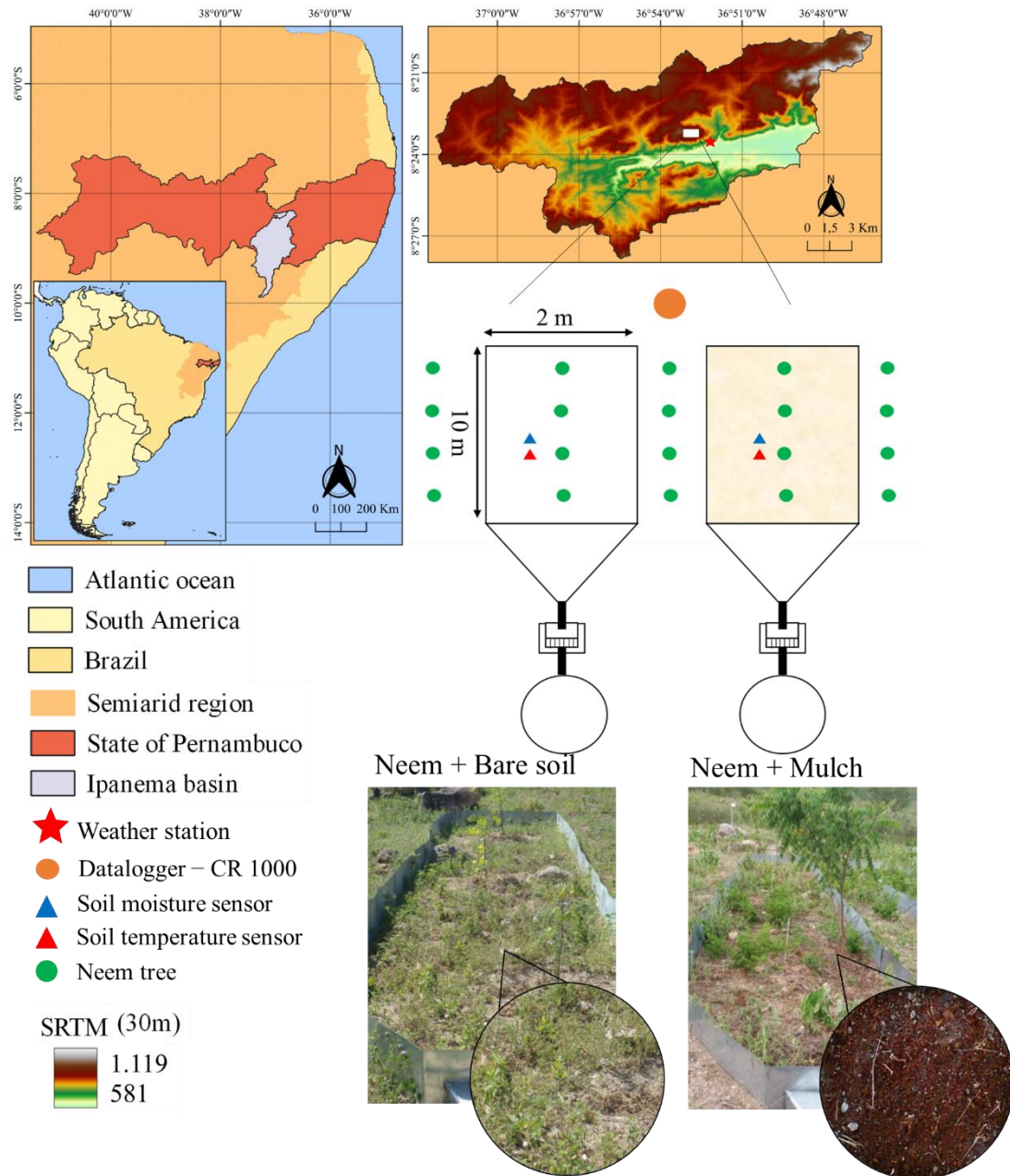


Figure 1. Location of the experimental area in the Alto Ipanema basin in the state of Pernambuco, Brazil and sketches and photographs of two erosion plots and treatments in the studied area: Neem + mulch and Neem + bare soil.

The plots were placed on a longitudinal slope of 10%, and the following treatments were applied to each of them: BS- non-conventional perennial oilseeds Neem (*Azadirachta indica* A. Juss) cultivated under bare soil condition; M- Neem cultivated with coconut powder (*Cocos nucifera* L.) with cover density of 8 t ha⁻¹ (Fig.1). The transplantation of Neem species took place in May 2015, with plants planted spaced 6 m from each other. One and a half year after

transplanting, the morphological characteristics of the species were monitored monthly, as follows: plant height (PH in m), obtained by measuring between the base of the stem and its apex, using a measuring tape, and the diameter of the stem (DC in mm), determined at the base of the plant at a height of 0.15 m, using a digital caliper. At the downstream end of each plot, 500 l reservoirs were installed to collect runoff and sediment transport (data not included in the scope of this study).

The soil in the study area, as described in detail in Lima et al. (2020), was classified as a Regolith Neosol, with a relatively shallow depth of ~0.85 m and a sandy loam texture. According to the Köppen classification, the climate of the region is BSh (hot semiarid), with an average annual precipitation of ~686 mm, a reference potential evapotranspiration of approximately 2,000 mm and a mean temperature of ~23°C (Lima et al., 2020). Natural vegetation (Caatinga Biome) has been suppressed along time, and erosion processes have occurred at the hillslopes, thus requiring conservation techniques adoption to control overland flow and sedimentation down the alluvial valley. More information about the downslope valley can be found in Almeida et al. (2024).

The experiment was conducted from January 1st to December 31st, 2017. The meteorological data for the duration of the experiment was obtained from an automated weather station (Campbell Scientific) located nearby, providing records of air temperature, relative humidity, global solar radiation, atmospheric pressure, wind speed and direction, and rainfall. The minimum and maximum temperatures and relative humidity were used to calculate the reference evapotranspiration (ET_0) (Allen, 1998). The Climatological Water Balance was calculated using the methodology proposed by Thornthwaite and Mather (1955). Campbell CS-616 soil moisture probes were installed in the vertical position at 0.10–0.20 m and temperature probes were inserted at 0.20 m soil depth and connected to the CR 1000 datalogger for detailed wetting and drying processes monitoring in the soil profile, for each treatment.

V.2.2 Image Acquisition and analysis

Forty-eight thermal images of Neem leaves were obtained using a portable hand-held infrared camera (Model E6 from Flir Systems) with an Infra-Red pixel resolution of 19200 (160×120), a field of view of 45°×34° and a thermal sensitivity of < 0.06°C. The images were always recorded at 10:00 am, with the camera positioned at 1.0 m height from soil surface, and 1.0 from the plant. Images were taken for twelve months of 2017 for each treatment condition. To develop the thermal image processing algorithm, the Python language and the OpenCV

database was used, adopting the PyCharm software interface. Opencv's bilateral filter function was used to apply filtering to the input image and reduce noise and thresholding of the images was performed by the *cv.threshold* function from Opencv, where for each pixel the same threshold value is applied. If the pixel value is less than the threshold, it is set to 0, otherwise it is set to a maximum value. Different limits were defined for each image but, for all cases, the objective was to ensure that the canopy was more visible. The simple thresholding type chosen was *cv.thresh_tozero*. Aiming at extracting the leaf contours (e.g., line joining all selected points along the edge of the identified leaves) the *cv2.findContours()* functions of OpenCV were implemented to draw the contours of the respective areas of interest and to extract the X and Y of the same areas approxPolyDP was used which returns a set of (x, y) points.

For the detection of the leaf thermal behavior, a script in Python language was elaborated for the detection and extraction of points and contour of leaves representative of the canopy (e.g., less influence of the wind, absence of shading and ease of liming by the algorithm), for each treatment.

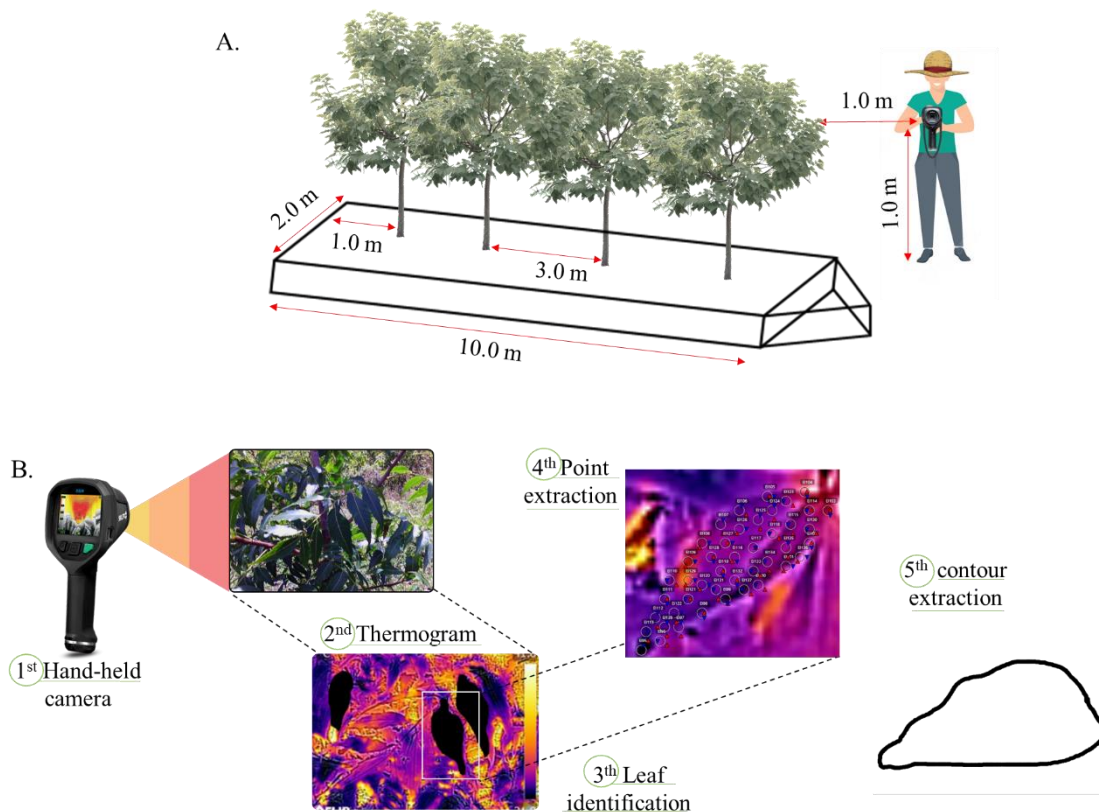


Figure 2. Sketch of the procedure of capturing thermograms (A); processing images and extracting representative grids and contour from sampled leaves (B).

V.2.3 Water stress indicator

The canopy surface temperature data at pixel scale obtained from thermal images were used together with the air temperature to calculate the Daily Water Stress Index, according to the equation proposed by Jackson et al. (1997) (Eq. 1):

$$DWSI = T_L - T_A \quad (1)$$

where: DWSI – daily water stress index, °C; T_L – leaf surface temperature, °C; T_A – air temperature, °C.

V.2.4 Statistical and geostatistical analysis

A statistical analysis was conducted to assess the significance of the variation in water status under different soil cover conditions. Spearman's correlation coefficients among air temperature, DWSI, leaf temperature, rainfall, and soil moisture were calculated over the studied period. Principal Component Multivariate Analysis (PCA) was applied to identify the most important variables related to water stress, soil moisture, air temperature, and soil temperature variability.

The data was submitted to descriptive statistical analysis. The Coefficient of Variation (CV) was categorized according to Warrick and Nielsen's (1980) criteria, with values below 12% classified as low, values between 12% and 24% classified as medium, and values above 24% classified as high. The Kolmogorov-Smirnov (KS) normality test ($p \leq 0.01$) was also applied to verify whether the data had a Normal distribution. Trend analysis was performed by estimating the trend surface using a quadratic polynomial function and examining the coefficients of determination obtained. Trends were considered to exist for R^2 values greater than or equal to 0.7. In such cases, residual values from the detrended data were adopted for the spatial analysis.

For the geostatistical analysis, the GEOEAS software (Deutsch and Journel, 1998) was utilized to detect patterns of spatiotemporal variability and spatial correlation of DWSI for separate leaves for each plant evaluated, under two different soil cover conditions, for the months of March, May, and September, considering the significant variations in climatic conditions. The geostatistical analysis was conducted by calculating the classical semivariances (Eq. 2), which estimates the structure and spatial association between pairs of observations, at pixel scale.

$$\gamma(h) = \frac{1}{2N(h)} \sum_{i=1}^{N(h)} [Z(X_i) - Z(X_i + h)]^2 \quad (2)$$

where $\gamma(h)$ is the estimated value of the experimental semi-variance of the data; $Z(X_i + h)$ and $Z(X_i)$ are the observed values of the regionalized variable; and $N(h)$ is the number of pairs of measured values, separated by a distance h .

Semivariance theoretical fits were tested for the Gaussian, Spherical, and Exponential models, and the parameters C_0 (nugget effect), $C_0 + C_1$ (sill) and a (range of spatial dependence) estimated. The three theoretical models considered are presented below (Equations 3 to 5).

Exponential Model:

$$\gamma(h) = C_0 + C_1 \left\{ 1 - \exp \left[- \left(\frac{h}{a} \right) \right] \right\}, \quad h \neq 0 \quad (3)$$

Spherical Model:

$$\gamma(h) = C_0 + C_1, \quad h \geq a, \quad (4)$$

$$\gamma(h) = C_0 + C_1 \times \left[1.5 \left(\frac{h}{a} \right) - 0.5 \left(\frac{h}{a} \right)^3 \right], \quad 0 < h < a \quad (5)$$

Gaussian Model:

$$\gamma(h) = C_0 + C_1 \times \left\{ 1 - \exp \left[- \left(\frac{h}{a} \right)^2 \right] \right\}, \quad h \neq 0 \quad (6)$$

where: C_0 is the nugget effect; $C = C_0 + C_1$ is the sill; a is the range; h is the distance between points.

The degree of spatial dependence (DSD) was assessed based on the methodology proposed by Cambardela et al. (1994), which uses the relationship between the nugget effect and the sill of the adjusted semivariogram, classifying the spatial dependence as strong, moderate or weak, as observed in Equation 5. Values below 25% are characterized by strong spatial dependence, values between 25% and 75% are considered moderate, while values above 75% indicate weak spatial dependence.

$$\text{DSD}(\%) = \frac{C_0}{C_0 + C_1} \quad (7)$$

The best models were selected by analyzing the coefficient of determination (R^2) and performing cross-validation using the Leave-one-out cross-validation (Webster and Oliver, 2007), assuming a mean error close to zero and a standard deviation close to one.

After modeling the semivariograms, the values were interpolated at non-sampled sites using Kriging (K). This technique uses both correlation with auxiliary maps and spatial correlation, where the drift (or trend) is modeled as a function of coordinates. The Sequential Gaussian Simulation (SGS) algorithm randomly selects a simulated value at each location from an estimated conditional cumulative distribution function. The distribution function is determined by the mean and variance of the kriging calculated from neighborhood information. Running the SGS requires transforming the original data into a Gaussian distribution, which is accomplished by transforming the normal score. The cumulative density function is characterized by the mean and covariance, assuming a random Gaussian field. Repeating these sequential steps with different random paths can provide various runs of the spatial distribution. In this study, to obtain an accurate probability calculation, the SGS algorithm was conducted once hundred runs using the GS+ software, following Sousa et al. (2023) recommendation.

After modeling the semivariograms, the values were interpolated using ordinary kriging, to characterize the leaf superficie of the plants studied, in three different months. The SURFER version 9 software was used to make the kriging maps (Goldens Software, 2010).

V.3. Results and discussion

V.3.1 Changes in soil moisture and climatic conditions

Soil surface temperature and moisture, for the bare soil and mulch treatments, including air temperature and rainfall variations in time are plotted in Figure 3. In general, the year 2017 could be classified as water-scarce, with a total of 50 rainfall events throughout the year. The highest precipitation depth was recorded in May with 266 mm, which constituted 35% of the total annual rainfall. The single highest rainfall event of that month was 60 mm. The months of April, June and July presented rainfall amounts higher than 90 mm, while February, March, September, October and December all had less than 30 mm. No rainfall was recorded in November.

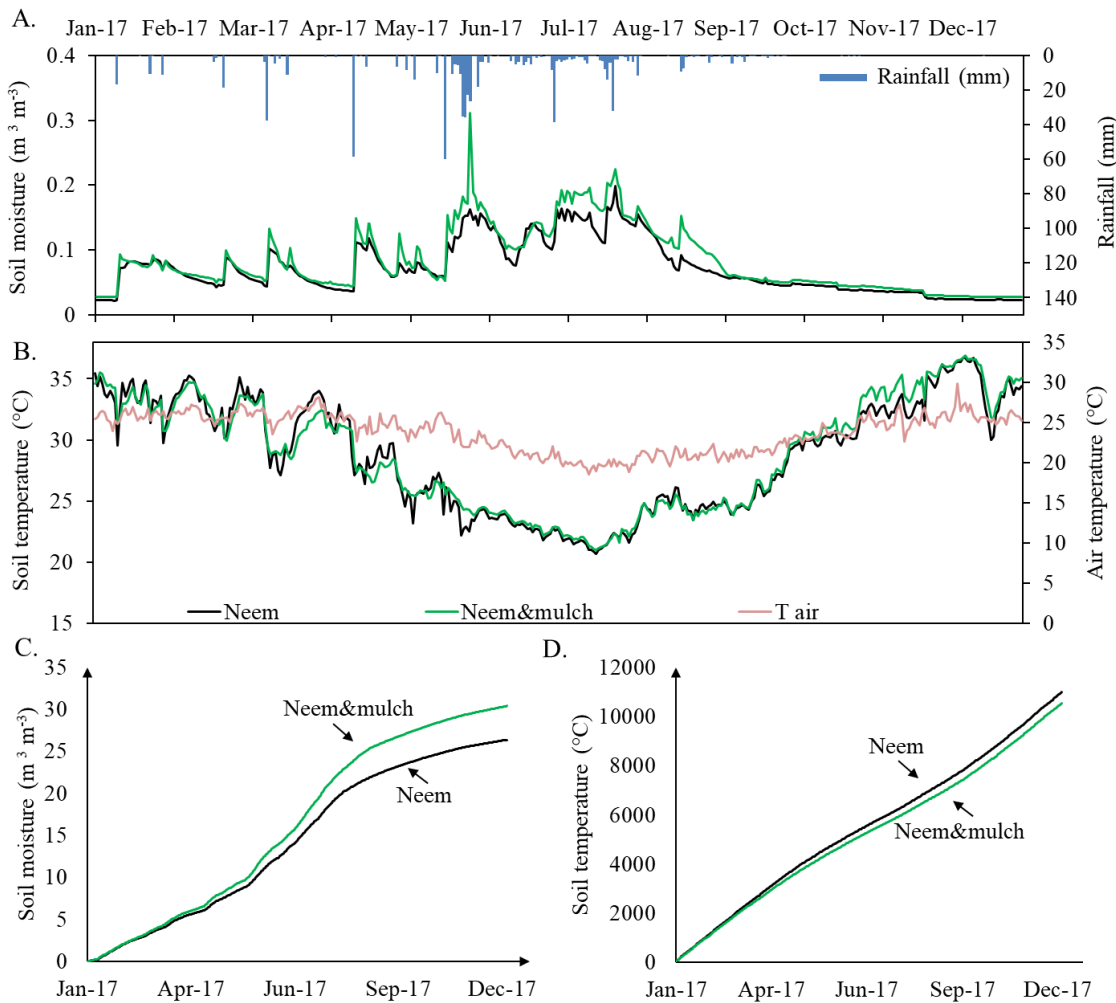


Figure 3. Daily time series of soil moisture and rainfall (A), air and soil temperature (B), accumulated soil moisture (C) and accumulated soil temperature (D) at the two plots in 2017: Neem (bare soil in black) and Neem with mulch cover (in green).

During the period evaluated, the average air temperature was 23.7°C, with a maximum of 29.84 °C Day⁻¹ and a minimum of 18.54°C Day⁻¹. It can be observed that air temperature followed the climatic seasonality of the semiarid region (Fig.3), with higher values in the dry season and lower values in the rainy season, consistent with the temperature dynamics observed by Almeida et al. (2024) while assessing climatic trends in the same alluvial valley as the present study. In general, leaf temperatures were lower during periods with lower air temperatures, consequently showing lower levels of water stress, in line with the findings of King and Shellie (2023). The authors highlight that canopy temperature increases when solar radiation is absorbed and decreases when water evaporates (transpiration) within the leaf

structure. A plant canopy experiencing water stress will reduce transpiration and exhibit a higher temperature compared to a canopy without stress.

Regarding to soil temperature, it is observed a temporal variation among the seasons, with greater values in December (dry period) and lower in May, with the maximum greater than 36 °C and the minimum of 20.1°C for the treatment with mulch, and 37.8°C and 21.5°C for the treatment without mulch cover, respectively. Additionally, when analyzing the seasonal changes in soil moisture levels between the two soil cover treatments, higher soil moisture was observed during the rainy season for the treatment with mulch which contributed to retain water, reducing evaporation, and thus increasing soil moisture. In general, the cumulative evolution of soil moisture (Fig.3C) and temperature (Fig.3D) shows significant differences when comparing both treatments. For bare soil condition it was observed a decrease of 5% for the cumulative soil moisture and an increase of ~5% in comparison to mulch application plot, along of 2017.

The Figure 4 compares the monthly variation of soil moisture along full year for both soil cover conditions. Higher soil moisture contents along hillslopes contributes not only for crop development, but also to control overland flow and enhance subsurface flow, which is of utmost relevance for semiarid areas (Hewlett, 1982).

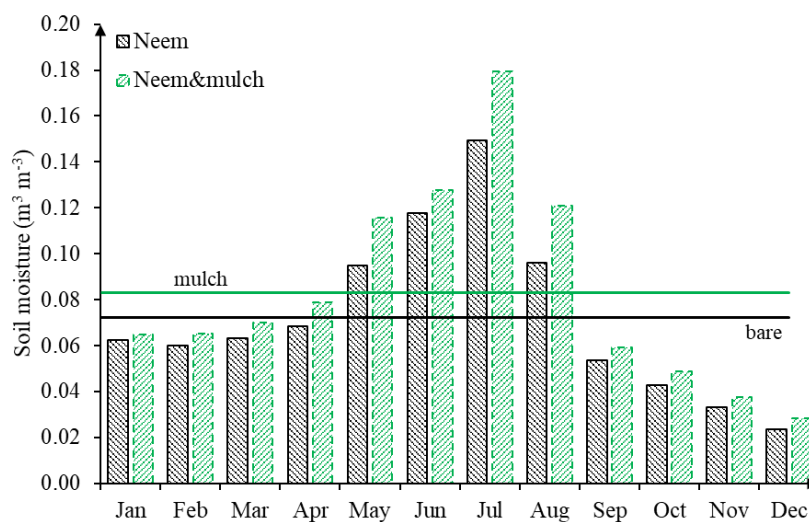


Figure 4. Monthly soil moisture variation for both soil cover condition (bare in black and mulch in green), along 2017.

Studies have suggested that the mulch cover was efficient for soil water retention in relation to uncovered soils, especially for wet period when moisture levels ranging from 0.13 and 0.15 $\text{m}^3 \text{m}^{-3}$ were observed, with remaining humidity in the dry months 17% higher than the humidity for the bare soil treatment. For the period between April and August, the average of soil moisture exceeds the annual mean of 0.083 $\text{m}^3 \text{m}^{-3}$ to mulch soil cover condition and 0.07 $\text{m}^3 \text{m}^{-3}$ to bare soil, as a result of rainfall events. In the absence of precipitation, the mulch cover works as an alternative soil protection technique.

Wind velocity is another critical factor influencing plant water stress. Figure 5 illustrates the temporal dynamics of wind from January to December 2017. The wind speed values exhibited an average of 3.13 m s^{-1} , with a standard deviation of 0.8 m s^{-1} .

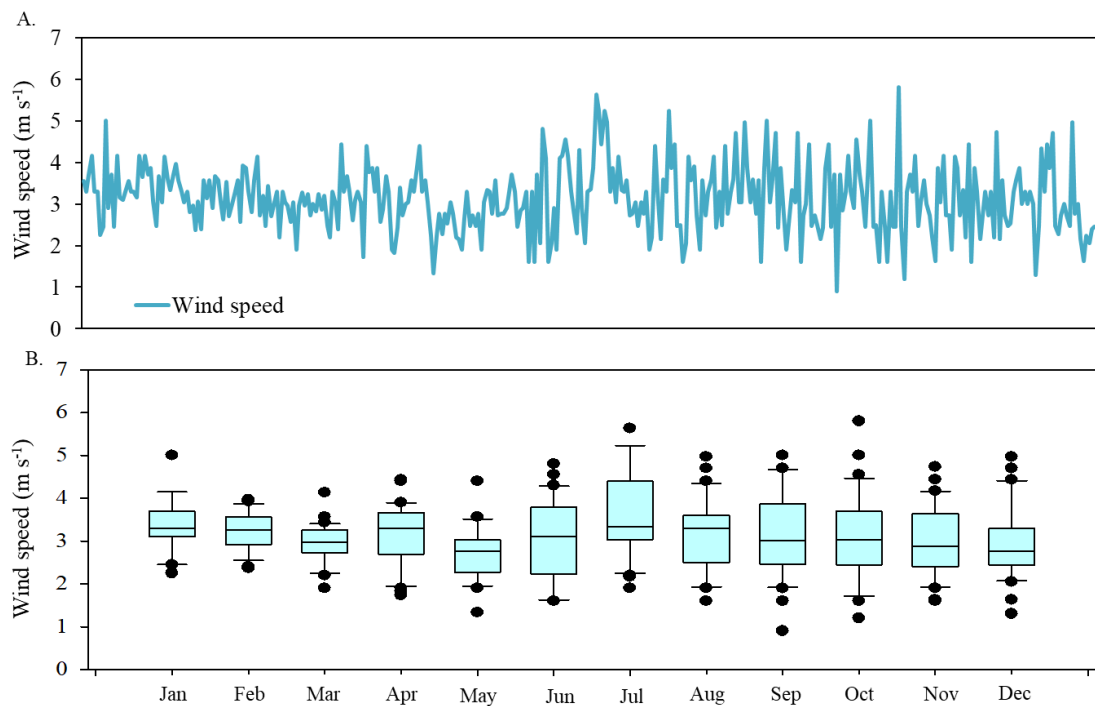


Figure 5. Temporal distribution of wind speed, in meter per seconds, to 2017 and box plot of monthly values.

The average wind speeds ranged from 2.94 m s^{-1} in December to 3.6 m s^{-1} in July. The period from June to November experiences the highest variability. Lower temperature periods, typically during or immediately after rainy months, also correspond to higher wind speeds. As highlighted by Miri and Webb (2022), wind speed is a significant factor contributing to plant

water stress by increasing transpiration and water loss from leaves. Higher wind speeds lead to greater wind stress and water loss from plants.

V.3.2 Daily Water Stress Index

Table 1 presents the daily recorded data for rainfall, evapotranspiration, and air temperature. It also includes a mean leaf temperature measured by a thermal camera and the mean Daily Water Stress Index, measured at 35 pixels. The capture of thermal images and data in January, April, May, and July occurred on rainy days with accumulated rainfall of 11.2, 2.6, 8.6, and 0.4 mm, respectively.

Table 1. Daily values of rainfall, evapotranspiration, air and leaf temperature and stress indicator for 2017, where BS – Bare Soil conditions and M- Mulch soil cover conditions.

Date	Cover	DR (mm)	R (mm)	ET ₀ (mm)	WS (m s ⁻¹)	T _A (C°)	T _L (C°)	DWSI (C° C° ⁻¹)
January (27/01/2017)	BS	11.2	11.4	4.74	2.46	25.93	47.35	21.42a
	M						44.79	18.86a
February (27/02/2017)	BS	0	23.8	5.56	3.93	27.33	39.08	11.75a
	M						38.04	10.71b
March (23/03/2017)	BS	0	60.2	4.61	2.73	26.24	40.6	14.36a
	M						39.2	12.96a
April (24/04/2017)	BS	2.6	72.6	4.56	3.4	25.62	33.97	8.35a
	M						33.62	8.00a
May (26/05/2017)	BS	8.6	138.8	3.7	3.1	23.91	26	2.09a
	M						24.64	0.73b
June (22/06/2017)	BS	0	30.0	3.47	4.55	23.42	25.94	2.48a
	M						23.9	0.52b
July (26/07/2017)	BS	0.4	79.2	2.19	2.16	20.1	25.36	5.26a
	M						23.45	3.35b
August (25/08/2017)	BS	0	20	2.36	4.9	20.7	29.41	8.71a
	M						27.58	6.88b
September (27/09/2017)	BS	0	9.1	2.6	3.3	21.3	32.3	11.01a
	M						27.4	6.11b
October (26/10/2017)	BS	0	0	3.32	3	23.1	37.48	14.38a
	M						34.51	11.41b
November (30/11/2017)	BS	0	0	4.99	2.46	26.4	41.51	15.11a
	M						37.32	10.93b
December (22/12/2017)	BS	0	0	4.66	2.56	27.12	45.55	18.43a
	M						41.86	14.74b

DR: daily rainfall; R: accumulated rainfall of 15 days before the monitoring date, ET₀: Reference evapo-transpiration, T_A: air temperature, T_L: leaf temperature, average DWSI: daily water stress

indicator. DWSI values followed by different letters on the same column do not differ at 5% level of significance, by Tukey test.

Air temperature ranged from 20.1°C to 26.4°C for the monitored days, with lower values observed from May to September. The daily leaf temperature ranged from 25.36°C in July to 47.35°C in January for bare soil conditions, and from 23.45°C in July to 44.79°C in January for mulch soil cover conditions. The sensitivity of plant water stress to meteorological factors was also observed by Andrade et al., (2021), where the authors highlighted the monthly variation in air temperature and canopy temperature patterns between the rainy and dry periods, mainly in the period nocturnal, corroborating the DWSI variations found.

A significant difference in crop status between bare soil and mulch cover was observed, particularly in months without precipitation. Such result highlights the effectiveness of mulch in maintaining soil moisture from previous rainfall events, as also shown in Fig. 3. Generally, the highest levels of water stress were recorded in January and December 2017 due to high evapotranspiration rates and low antecedent rainfall.

The influence of daily evapotranspiration is observed, as a response to air temperature, together with the absence or presence of rain in the daily water status dynamics. Plant height, stalk diameter, leaf temperature, daily water stress and water balance measured during the experimental time can be observed in Figure 6.

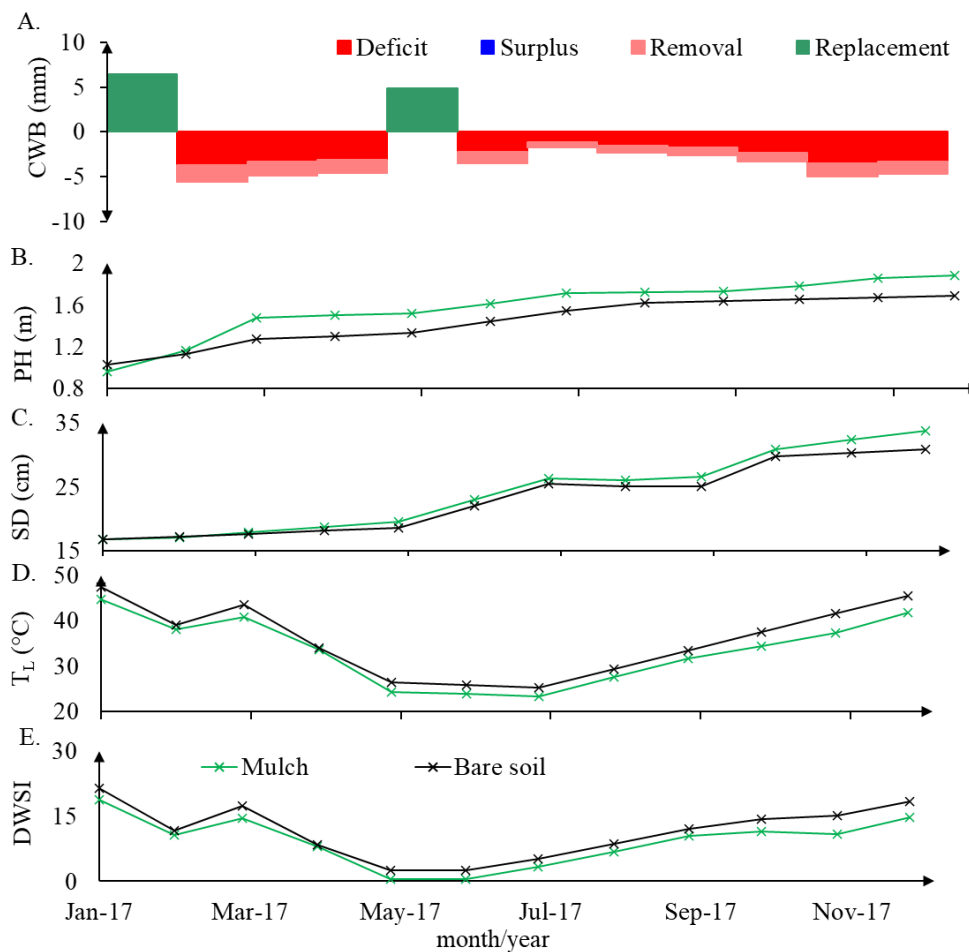


Figure 6. Monthly Water Balance (CWB), monthly average plant height (PH), stem diameter (SD), leaf temperature (T_L) and DWSI under bare soil and mulch soil cover conditions.

It is observed a long water deficit period from February to April and from June to December, when reference evapotranspiration is higher than rainfall. For January and May, when there is no water surplus, rainfall is higher than reference evapotranspiration, however there is still available soil water content because of rainfall antecedent conditions. There is a statistically significant difference in the height of plants and stem diameter between January and December 2017, demonstrating the growth that resulted from the water replenishment events in January and May.

The value of DWSI reflects the physiological characteristics of the plants in relation to the environment (Brunini and Turco, 2016). Hence plant water status controls many physiological processes and crop productivity, associating the higher the water stress and the greater the daily evapotranspiration of the crop, thus reflecting the biometric crop development (Galindo et al., 2013). Brunini and Turco (2016) observed a decrease in productivity for sugarcane species as

values exceeded 1.5. It is observed that the greater water availability from intense rainfall events as a mitigating factor of stress along the leaf surfaces.

Although canopy temperature and DWSI are closely related to meteorological conditions and cumulative water balance (Fig.6), Bo et al. (2023) emphasized that soil cover condition also influences canopy temperature and consequently water stress. The authors evaluated, in a two-year field experiment, the cultivation of corn under different mulching conditions in northwest China and found positive effects of plastic mulching on canopy temperature and crop water stress index (CWSI), consistent with the results found in the present study.

V.3.3 Relationships between thermal indices and meteorological parameters

Figures 7A, B and C exhibits the relationship among the soil moisture, soil temperature and daily water status, for bare and mulch cover conditions. The lowest data dispersions and strong correlations between soil treatments occurred for values smaller than $0.1 \text{ m}^3 \text{ m}^{-3}$, since the higher the soil moisture, the lower the daily thermal amplitude, given the high specific heat of water, according to Lima et al. (2020). Besides that, some differences in soil moisture have occurred at the beginning of the raining rainfall season, or after periods of intermittency as explained by Montenegro and Monteengro (2006). It has shown, according to Figure 7, a strong relation between both conditions of soil temperature, with slopes close to 1.

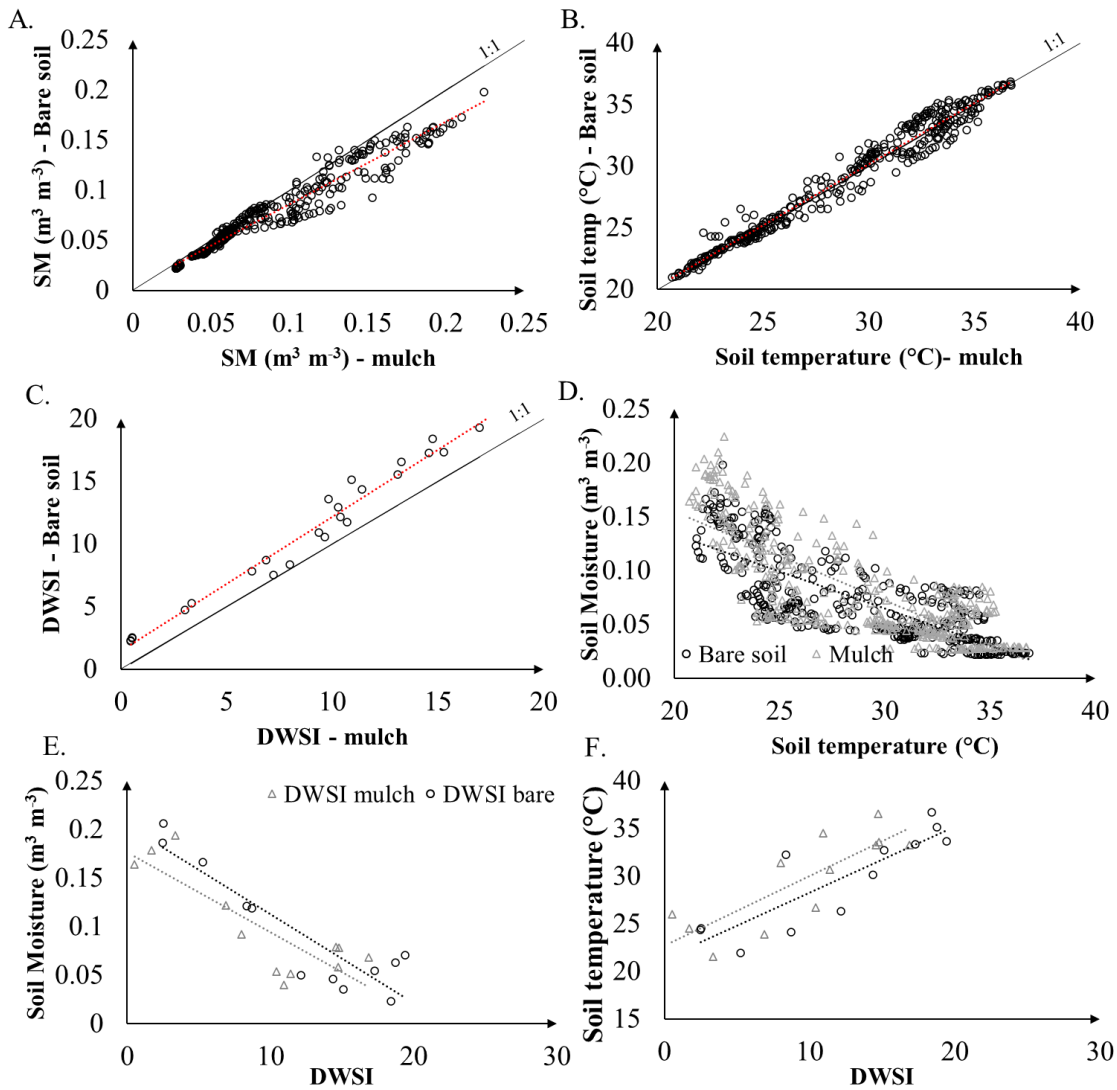


Figure 7. Plots of soil moisture (A), soil temperature (B) and DWSI (C), soil moisture and soil temperature (D), soil moisture and DWSI and soil temperature and DWSI (F), for mulch and bare soil cover condition. Dashed lines represent regression lines. Full line represents the 1:1 line.

Moreover, correlations between soil moisture and temperature, the daily water status, for mulch and bare soil conditions (Figures 7A, B and C) demonstrate that the higher the soil moisture, the lower the thermal amplitude. This reduction in thermal amplitudes was also explained by de Lima et al. (2020) in their study on the effects of mulching on soil temperature and moisture also in the Brazilian semiarid region, where mulching reduces soil surface temperature, acting as a buffer zone and dampening soil surface temperature fluctuations.

Akhtar et al. (2019) also reported significantly increased moisture retention and decreased soil temperature during warm periods with the application of wheat straw mulch in Northwest

China, creating favorable conditions for soybean growth compared to non-mulch treatments. Additionally, Lopes et al. (2019) monitored soil and water dynamics in twelve experimental plots across the same hydrological area with varying coverage treatments. They found that runoff behavior differed; natural cover produced the smallest runoff depth, while bare soil conditions resulted in the highest runoff.

The correlation analysis of DWSI under bare and mulch soil condition with soil moisture and soil temperature show that the plots managed under a conservation way presented a reduction in the water stress index as they showed a higher moisture content, and additionally, a lower soil temperature. The plants that were grown with mulch cover showed better development than those without soil cover. To validate the previous results and to evaluate the effects of temperature and soil moisture on the plant development, Principal Component Analysis (PCA) was applied to the original matrix of temperature and soil moisture, with plant height and DWSI as supplementary variables. The biplot of the PCA for the soil parameters and plant conditions is shown in Figure 8.

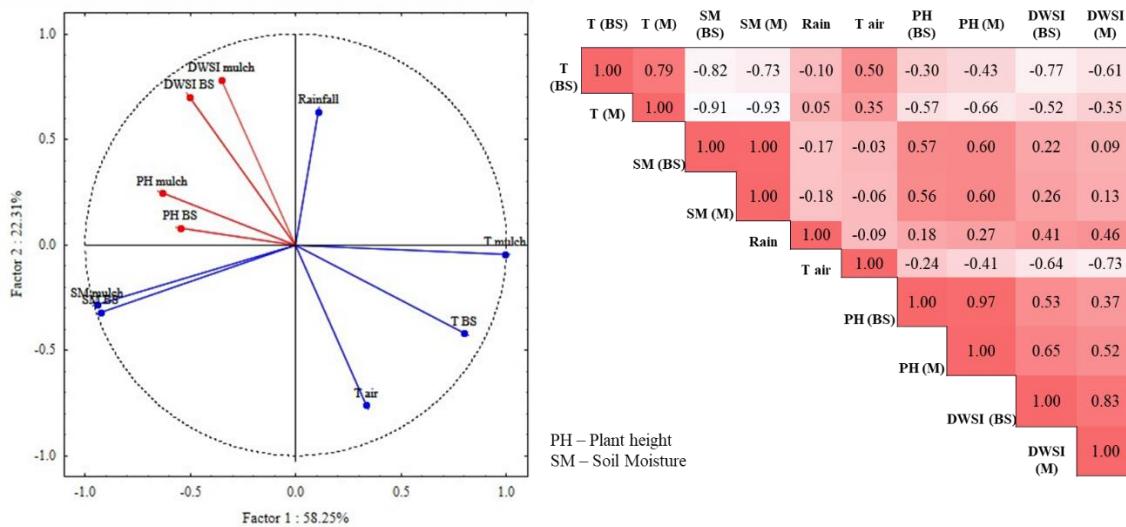


Figure 8. Principal component analysis, plotting of scores of the first two principal components, and Spearman's correlation matrix.

Main components Factor1 and Factor2 explained 74.56% of the total variance, with emphasis on Factor1, which by itself explained 58.25% of the total data variance. For this component, the variables related to temperature of soil under mulch and bare soil, and air temperature were grouped and presented loads of 0.79, 0.99 and 0.33, respectively, denoting a strong negative correlation inversely influenced by soil moisture and rainfall. The stress indicator and the plant height have shown a negative correlation with temperature for both soil

cover conditions. In the correlation matrix, plant higher (PH) and DWSI showed strong correlations ($p < 0.001$) for mulch treatment (0.85) and bare soil.

In Figure 8, it is possible to observe that plants with lower stress indices, promoted by the mulch condition, exhibited better growing in terms of both plant height and stem diameter. The changes in stem diameter have been closely linked to variations in the overall water content of the plant (Galindo et al., 2013). For this reason, several researchers have observed that Leaf Turgidity (LT) values can be a useful indicator of stress when soil water content is not severely depleted, and increases in LT have been observed to correlate with decreases in water potential. As plant growth is controlled by cell division, insufficient amount of water reduces the division coefficient cell and the expansion of all cells, thereby preventing the proper vegetative growth of plants (Liu et al., 2022; Rico-Fernandez et al., 2019; Camoglu et al., 2023).

V.3.4 Plant canopy status mapping

After obtaining the reference temperatures necessary for calculating the DWSI, a spatial representation of the index was created across 6 representative leaves. The months of March, May and September were chosen according to the quality of images, weather conditions on the day of monitoring, significance of results for leaf comparison between treatments. The choice of leaves was made considering the best-defined contours within the canopy. Figure 9 shows the box plot of stress indicator recorded for both conditions of soil cover, for March, May and September. The water stress for March ranged between 11 and 15, for bare soil, and between 11.3 and 11.9, for mulch cover condition. In May, the lowest stress values were identified, with minimum of -0.4 and -0.3 and maximum of 1.2 and 1.6, for bare soil and mulch, respectively. Although low DWSI values were detected for the bare soil condition, a more asymmetric distribution with less presence of extreme values was detected in the mulch soil cover condition. In September the contrast between treatments is evident, with minimum values of 10 and -1.6 and maximum values of 14 and 2, respectively, for the bare soil and mulch treatments. An asymmetry in the data distribution is also observed for the bare soil condition.

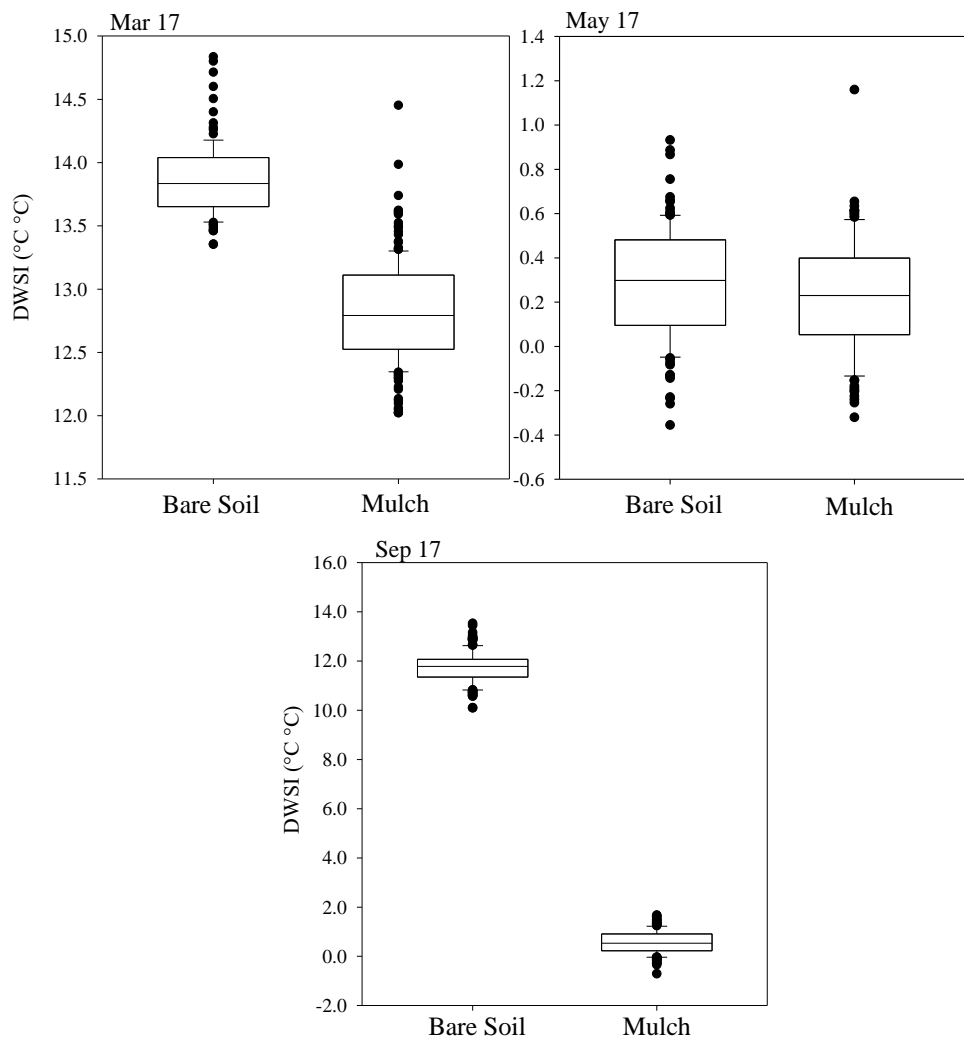


Figure 9. Box plot of daily water stress indicator for March, May and September, of mulching treatment and bare soil, for three different leaves.

The DWSI for May presented smaller variation, with coefficient of variation ($CV < 15\%$) indicating low variability, according to [40], and lower standard deviation values, followed by September and March. All plant samples presented normality at 5% probability, allowing to obtain parameters of theoretical semivariograms from the experimental data (Table 2). The minimum number of pairs for the experimental semi-variograms was 40, based on pixel meshes comprising at least 32 elements.

DWSI showed spatial dependence which was better described by a Gaussian model for both treatments in all months evaluated. The stress indicator presented different ranges of spatial dependence for both treatments, with a minimum value of 43 mm and a maximum of

92 mm, referring to March, for both soil conditions, 43 and 185 mm to March, and 46 and 133 to September, respectively.

Table 2. Parameters of the theoretical models for the semivariance of the DWSI in each leaf sampled for March, May and September.

Month	CC	L	Mod	C ₀	C ₀ +C	DSD	a	R ²	CC	L	Mod	C ₀	C ₀ +C	DSD	a	R ²
MAR	BS	L1	Gaus	0.012	0.293	4.1	45	0.9	BS	L4	Gaus	0.025	0.274	9.1	75	0.8
		L2	Gaus	0.083	0.311	26.7	43	0.9		L5	Gaus	0.042	0.183	23.0	92	0.8
		L3	Gaus	0.075	0.328	22.9	75	1		L6	Gaus	0.067	0.246	27.2	86	0.9
	M	L1	Gaus	0.038	0.182	20.9	62	0.9	M	L4	Gaus	0.081	0.381	21.3	69	0.9
		L2	Gaus	0.022	0.298	7.4	49	0.9		L5	Gaus	0.039	0.141	27.7	78	0.8
		L3	Gaus	0.016	0.238	6.7	61	0.8		L6	Gaus	0.032	0.298	10.7	63	0.8
MAY	BS	L1	Gaus	0.070	0.297	23.6	55	0.9	BS	L4	Gaus	0.022	0.282	7.8	74	0.9
		L2	Gaus	0.082	0.246	33.3	106	0.8		L5	Gaus	0.018	0.131	13.7	133	0.9
		L3	Gaus	0.098	0.297	33.0	78	0.9		L6	Gaus	0.011	0.139	7.9	62	0.9
	M	L1	Gaus	0.018	0.256	7.0	95	0.9	M	L4	Gaus	0.012	0.528	2.3	96	0.8
		L2	Gaus	0.065	0.286	22.7	77	0.8		L5	Gaus	0.001	0.101	1.0	185	0.9
		L3	Gaus	0.028	0.188	14.9	43	0.8		L6	Gaus	0.001	0.147	0.7	82	1.0
SEP	BS	L1	Gaus	0.062	0.265	23.5	46	0.9	BS	L4	Gaus	0.051	0.276	18.5	102	0.8
		L2	Gaus	0.061	0.208	29.3	89	1		L5	Gaus	0.089	0.412	21.6	75	0.9
		L3	Gaus	0.066	0.263	25.1	52	1		L6	Gaus	0.079	0.282	28.0	133	0.9
	M	L1	Gaus	0.046	0.361	12.7	79	0.8	M	L4	Gaus	0.025	0.299	8.4	94	0.8
		L2	Gaus	0.036	0.226	15.9	58	0.9		L5	Gaus	0.01	0.231	4.3	115	0.9
		L3	Gaus	0.035	0.336	10.4	70	0.8		L6	Gaus	0.013	0.151	8.6	91	1.0

where: Mod- Model (tested model: gaussian – Gaus); C₀ - nugget effect; C₀+C – sill; a – range in mm; CC- cover condition; BS – bare soil; M – mulch; MAR – March; MAY- may; SEP- September; L- Leaf; DSD-degree of spatial dependence, in %.

The relationship between the nugget effect and the sill ranged from 0.7% (May - Mulch) to 33% (May – Bare soil), indicating a strong and medium spatial dependence for the analyzed years, according to the classification of Cambardella et al. (1994). In general, the plants

cultivated under mulch soil cover condition present a strong spatial dependence. The coefficients of determination (R^2) for the fitted models were moderate to high, with a minimum of 0.8 and a maximum of 1, all the semivariograms were cross validated based on the Leave-one-out cross-validation [43], yielding residues with averages between -0.001 and 0.013, and standard deviations between 1.004 and 1.006.

The adjusted model was used to produce leaf water status maps from plants grown for the months March, May and September cultivated under bare soil and mulch condition of soil cover (Figure 10). By employing the Sequential Gaussian Simulation (SGS) technique, the fitted models were also used to produce maps of the DWSI with 300 realizations, as shown in Figure 10. The scale of DWSI for March, May, and September varied between 12 to 16, -1 to 2, and -1 to 15, respectively.

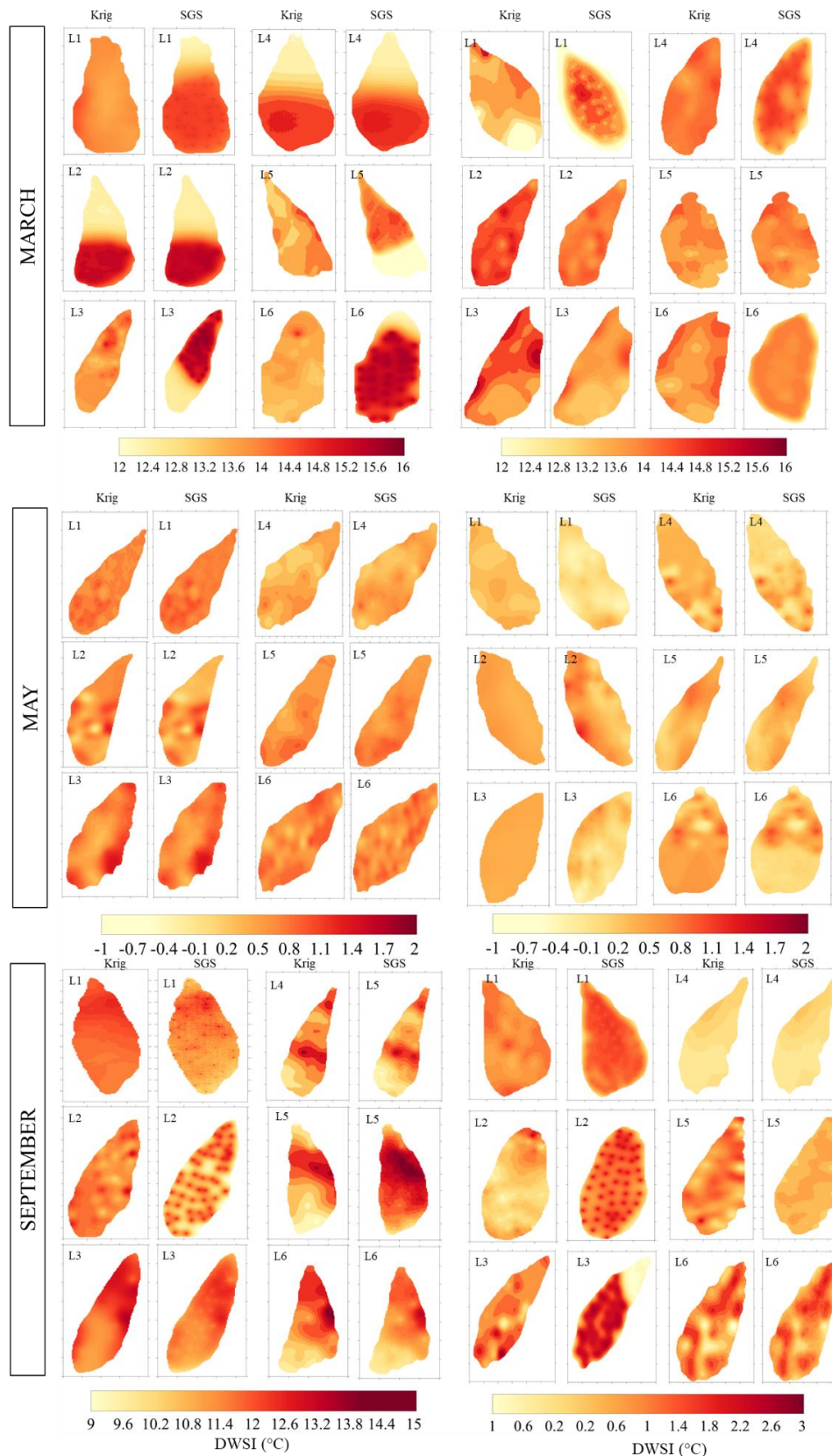


Figure 10. Kriging maps for surface temperature referring to representative leaves for March, May and September, considering bare soil and mulch cover conditions.

It can be seen a distinction between maps, with higher occurrences of red areas representing higher stress due to temperature and climatic effects, indicating lower water status. Some negative values were also found, indicating that the plants were not under any water stress at any part of their leaves, especially in May due to the rainfall and in September to the mulch condition, showing that Mulch facilitates a more even distribution of water and mitigates external effects on the leaf surface, such as wind speed.

In order to effectively measure plant temperature and identify water stress conditions, Paulo et al. (2022) emphasized that Leaf Temperature Maps, validated by thermal images as an effective and practical alternative. Moreover, Luan et al. (2021) emphasized that information of leaf temperature distribution can reflect the water status of the crop. In the DWSI distribution maps (Figure 10), higher values are observed at the leaf apex and outer areas, primarily affected by wind as discussed earlier. These results demonstrate that using average leaf temperature data or considering only the highest marginal values or including very low marginal values, may result in biased unrealistic DWSI values and may not accurately reflect the plant's water status. Therefore, the choice of TL statistics for DWSI calculation is relevant (Luan et al., 2021; Silva et al., 2023, Liu et al., 2022).

We generated cumulative frequency curves based on temperatures extracted from thermal images and air temperature using the kriging and SGS methods (Figure 11). Overall, the curves exhibited similar trends across treatments. However, the DWSI ranges varied according to soil moisture levels and rainfall availability. In March, the DWSI ranged from 12.5 to 16, while in May, it ranged from -1 to 1.5. The most significant variation occurred in September, ranging from -2 to 15. This wide range in September can be attributed to the effective use of mulch cover, which mitigates climatic effects on plants and reduces stress. Specifically, the mulch condition produced a DWSI distribution between -2 to 4, whereas the bare soil condition ranged between 10 to 13.

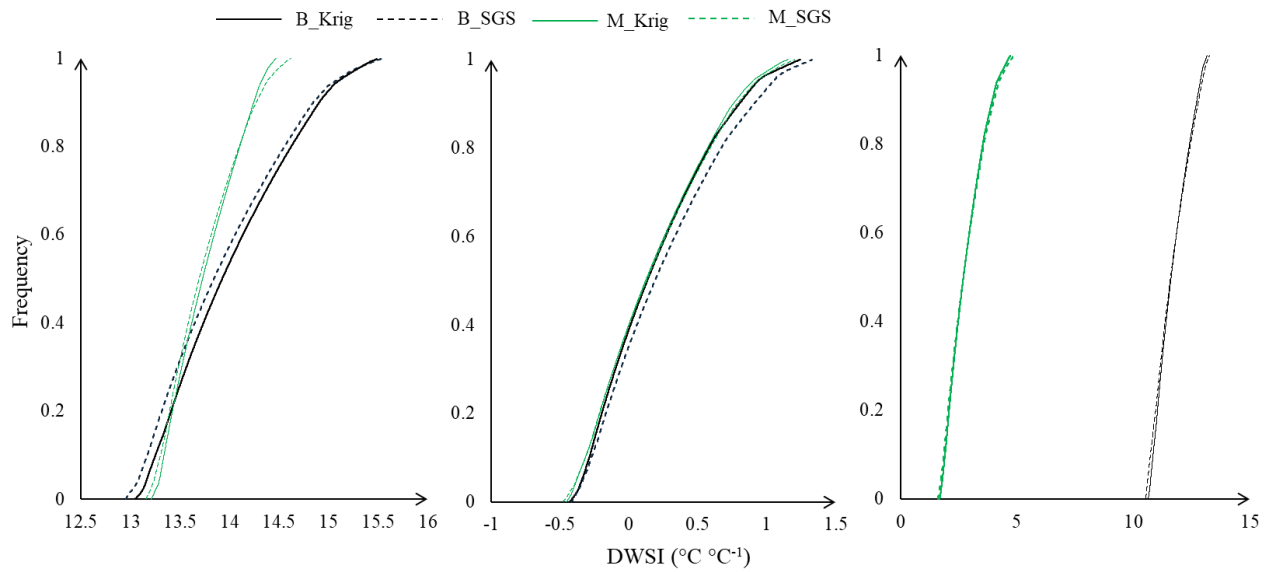


Figure 11 The canopy DWSI cumulative frequency curves for plants evaluated in the respective months (March, May and September) under bare soil and mulch conditions.

When evaluating the average DWSI across months and soil cover conditions (Table 3), a notable difference emerges compared to the previously presented values (Table 1). It is important to note that the earlier values were calculated based on a single plant sample point, whereas the extraction of leaf temperatures represents the plant's actual temperature more critically and rigorously. Additionally, it is observed that both mulch application effectively contributed to reduce water stress and intrafoliar temperature variation, indicating a more uniform stomatal behavior. Furthermore, the SGS technique also led to a reduction in the uncertainty of geostatistical mapping, with lower standard deviations and variation.

Table 3. Parameters of the theoretical models for the semivariance of the DWSI in each leaf sampled for March, May and September.

	Plant / Method	Mean	SD	CV	
March	BS	P1F Krig	13.790	0.617	0.044
		P1F SGS	13.783	0.626	0.043
		P2F Krig	13.699	0.619	0.044
		P2F SGS	13.762	0.646	0.046
	M	P1F Krig	13.984	0.403	0.031
		P1F SGS	13.925	0.431	0.029
		P2F Krig	14.046	0.321	0.023
		P2F SGS	13.950	0.333	0.021
May	BS	P1F Krig	0.248	0.468	0.551
		P1F SGS	0.262	0.476	0.529
		P2F Krig	0.313	0.415	0.827
		P2F SGS	0.311	0.439	0.746
	M	P1F Krig	0.084	0.400	0.336
		P1F SGS	0.145	0.433	0.209
		P2F Krig	0.310	0.344	0.330
		P2F SGS	0.363	0.353	0.313
September	BS	P1F Krig	11.693	0.752	0.143
		P1F SGS	11.642	0.809	0.125
		P2F Krig	11.745	0.670	1.746
		P2F SGS	11.756	0.513	1.363
	M	P1F Krig	5.261	0.655	0.056
		P1F SGS	5.272	0.400	0.060
		P2F Krig	0.384	0.372	0.061
		P2F SGS	0.376	0.380	0.068

The Figure 12 presents the histogram of the DWSI distribution of Kriging (Krig) and Sequential Gaussian Simulation (SGS) methods. When comparing the histograms of Krig and SGS results, it is notably that SGS realizations histogram is similar to the histogram of the Krig

results. However, SGS provides additional information about the uncertainty in the spatial distribution, which is not captured by a smoothed Krig estimate.

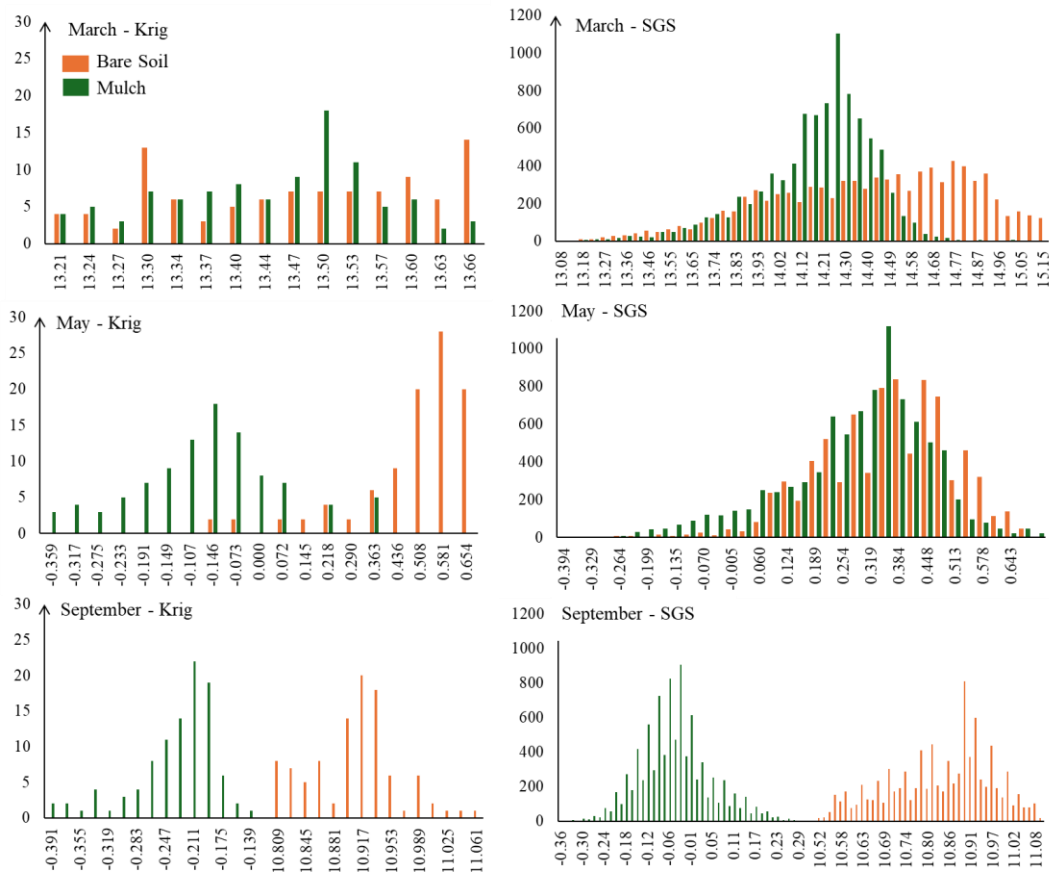


Figure 12. Histograms of distribution of DWSI for the months of March, May, and September, under Mulch and Bare soil conditions, following mapping via Kriging and SGS techniques.

Analyzing the histograms, it is possible to detect greater symmetry in the distribution of DWSI in plants with lower stress levels, being an indicator of plant water comfort. The plants that received conservation management exhibited more symmetrical distributions, indicating better adaptation and a more balanced state of health. Additionally, SGS exhibited a class distribution five times larger than that of kriging mapping. This finding confirms the results of Bai and Tahmasebi (2022), who suggest that kriging can lead to a smoothing effect, resulting in an overestimation of small values and an underestimation of large values, thereby restricting its applicability to assess uncertainties in certain situations and lower scales.

Our results demonstrate the high potential of thermographic data to produce distributed crop water stress indices, which allowed for estimating and interpreting the plant's water status, reducing associated errors through leaf geostatistical mapping. Identifying patterns of variation

that reflect higher or lower stress indices, this method provides a non-destructive and quicker means of detection and monitoring crop temperature variability.

V.4 Conclusions

This chapter investigated the water stress on crops, which can severely disrupt crop growth and reduce yields, especially in semiarid regions. Accurate and prompt diagnosis of crop water stress is crucial. Infrared thermal imaging cameras were utilized to monitor the spatial distribution of canopy temperature (T_c), forming the basis of the Daily Water Stress Index (DWSI) calculation. The application of geostatistical techniques enabled the stress indicator mapping at a leaf scale, with the spherical and exponential models providing the best fit for both soil cover conditions.

In conclusion, DWSI reflects changes in biometric indices, demonstrating high potential as an indicator of the relationship between plant and climatic variables measured on a daily basis. Results indicated that the highest levels of water stress were observed during months with the highest air temperatures and no rainfall, especially at the apex of the leaf and close to the central veins, due to a negative water balance. Even under extreme drought conditions, mulching reduced Neem physiological water stress, leading to lower plant water stress, higher soil moisture content, and a negative skewness of temperature distribution.

Furthermore, the DWSI differs according to soil cover condition, evapotranspiration, and the sequence of rainfall events. The mulching effect during long dry periods, typical of semiarid regions, was essential for preserving soil moisture and promoting plant growth. Even in extreme cases of water scarcity, mulching reduced the physiological water stress of Neem, leading to decreased water stress and reduced recession of soil moisture content, resulting in better biometric parameters.

Regarding the mapping of the stress index, the sequential Gaussian simulation method reduced temperature uncertainty and variation at the leaf surface. Our findings highlight that mapping the Water Stress Index offers a robust framework for precise stress detection in agricultural and soil cover management in semiarid regions. Coupling thermography with geostatistical tools enabled a precise assessment of water stress index mean and variability for a resilient crop in semiarid Brazil. These findings underscore the impact of meteorological and planting conditions on leaf temperature and baseline water stress, which can be valuable for regional water resource managers in diagnosing crop water status more accurately.

References

- Akhtar, K., Wang, W., Khan, A., Ren, G., Afridi, M.Z., Feng, Y., Yang, G., 2019. Wheat straw mulching offset soil moisture deficient for improving physiological and growth performance of summer sown soybean. *Agric. Water Manag.* 211, 16–25. <https://doi.org/10.1016/j.agwat.2018.09.031>
- Albiero, B., Freiberger, G., Moraes, R.P., Vanin, A.B., 2019. Potencial inseticida dos óleos essenciais de endro (*anethum graveolens*) e de nim (*azadirachta indica*) no controle de *sitophilus zeamais*. *Brazilian J. Dev.* 5, 21443–21448. <https://doi.org/10.34117/bjdv5n10-298>
- Allen, R.G., Pereira, L.S., Raes, D., Smith, M., 1998. Crop evapotranspiration – guidelines for computing crop water requirements. In: first ed.; FAO Irrigation and Drainage Paper 56: Rome, Italy, pp. 1–297.
- Almeida, T. A. B., Montenegro, A. A. de A., Mackay, R., Montenegro, S. M. G. L., Coelho, V. H. R., de Carvalho, A. A., & da Silva, T. G. F. 2024. Hydrogeological trends in an alluvial valley in the Brazilian semiarid: Impacts of observed climate variables change and exploitation on groundwater availability and salinity. *Journal of Hydrology: Regional Studies*, 53. <https://doi.org/10.1016/j.ejrh.2024.101784>
- Araújo-Paredes, C., Portela, F., Mendes, S., & Valín, M. I. 2022. Using Aerial Thermal Imagery to Evaluate Water Status in *Vitis vinifera* cv. Loureiro. *Sensors*, 22(20). <https://doi.org/10.3390/s22208056>
- Bai, T.; Tahmasebi, P. 2022. Sequential Gaussian Simulation for Geosystems Modeling: A Machine Learning Approach. *Geosci. Front.*, 13, pp.1–14.
- Bazrgar, G., Nabavi Kalat, S. M., Khorasani, S. K., Ghasemi, M., & Kelidari, A. (2023). Effect of deficit irrigation on physiological, biochemical, and yield characteristics in three baby corn cultivars (*Zea mays* L.). *Heliyon*, 9(4). <https://doi.org/10.1016/j.heliyon.2023.e15477>
- Bo, L., Guan, H., & Mao, X. 2023. Diagnosing crop water status based on canopy temperature as a function of film mulching and deficit irrigation. *Field Crops Research*, 304. <https://doi.org/10.1016/j.fcr.2023.109154>
- Brunini, R.G. & Turco, J.E.P., 2016. Water stress indices for the sugarcane crop on different irrigated surfaces | Índices de estresse hídrico para a cultura de cana-de-açúcar em diferentes superfícies irrigadas. *Rev. Bras. Eng. Agric. e Ambient.* 20, 925–929.
- Cambardella, C.A., Moorman, T.B., Novak, J.M., Parkin, T.B., Karlen, D.L., Turco, R.F., Konopka, A.E., 1994. Field-Scale Variability of Soil Properties in Central Iowa Soils. *Soil*

- Camoglu, G., Demirel, K., Kahriman, F., Akcal, A., & Nar, H. 2024. Plant-based monitoring techniques to detect yield and physiological responses in water-stressed pepper. *Agricultural Water Management*, 291. <https://doi.org/10.1016/j.agwat.2023.108628>
- Carvalho, A.A., Abelardo, A.A., da Silva, H.P., Lopes, I., de Moraes, J.E.F., da Silva, T.G.F., 2020. Trends of rainfall and temperature in Northeast Brazil. *Rev. Bras. Eng. Agric. e Ambient.* 24, 15–23. <https://doi.org/10.1590/1807-1929/agriambi.v24n1p15-23>
- de Andrade, M. D., Delgado, R. C., da Costa de Menezes, S. J. M., de Ávila Rodrigues, R., Teodoro, P. E., da Silva Junior, C. A., & Pereira, M. G. 2021. Evaluation of the MOD11A2 product for canopy temperature monitoring in the Brazilian Atlantic Forest. *Environmental Monitoring and Assessment*, 193(1). <https://doi.org/10.1007/s10661-020-08788-z>
- de Brito, W.A., Siquieroli, A.C.S., Andaló, V., Duarte, J.G., de Sousa, R.M.F., Felisbino, J.K.R.P., da Silva, G.C., 2021. Botanical insecticide formulation with neem oil and D-limonene for coffee borer control. *Pesqui. Agropecu. Bras.* 56, 1–9. <https://doi.org/10.1590/S1678-3921.pab2021.v56.02000>
- de Lima, C.A., Montenegro, A.A. de A., de Lima, J.L.M.P., Almeida, T.A.B., Dos Santos, J.C.N., 2020. Use of alternative soil covers for the control of soil loss in semiarid regions. *Eng. Sanit. e Ambient.* 25, 531–542. <https://doi.org/10.1590/s1413-41522020193900>
- de Lima, J. L. M. P., da Silva, J. R. L., Montenegro, A. A. A., Silva, V. P., & Abrantes, J. R. C. B. (2020). The effect of vegetal mulching on soil surface temperature in semiarid Brazil. *Bodenkultur*, 71(4), 185–195. <https://doi.org/10.2478/boku-2020-0016>
- Debangshi, U., & Sadhukhan, A. (2023). Crop water stress monitoring through precision technologies: A review. *The Pharma Innovation*, 12(11S), 803–808. <https://doi.org/10.22271/tpi.2023.v12.i11sk.24052>
- Deutsch, C.V., A.G. Journel, G.S.L.I.B., 1998. *Geostatistical Software Library and User's Guide*. Second ed, Oxford University Press, New York, 369p.
- Feiziasl, V., Jafarzadeh, J., Sadeghzadeh, B., & Mousavi Shalmani, M. A. 2022. Water deficit index to evaluate water stress status and drought tolerance of rainfed barley genotypes in cold semiarid area of Iran. *Agricultural Water Management*, 262. <https://doi.org/10.1016/j.agwat.2021.107395>
- Galindo, A., Rodríguez, P., Mellisho, C.D., Torrecillas, E., Moriana, A., Cruz, Z.N., Conejero, W., Moreno, F., Torrecillas, A., 2013. Assessment of discretely measured indicators and

- maximum daily trunk shrinkage for detecting water stress in pomegranate trees. *Agric. For. Meteorol.* 180, 58–65. <https://doi.org/10.1016/j.agrformet.2013.05.006>
- GOLDEN SOFTWARE. Surfer for windows version 9.0. Colorado: Golden, 2010. 66p.
- Hewlett, J.D. (1982). *Principles of Forest Hydrology*. The University of Georgia Press.
- Huo, Z.L. Li, Z. Xing. 2019. Temperature/emissivity separation using hyperspectral thermal infrared imagery and its potential for detecting the water content of plants. *Int. J. Remote Sens.*, 40, 1672-1692.
- Ihuoma, S. O., & Madramootoo, C. A. 2017. Recent advances in crop water stress detection. In *Computers and Electronics in Agriculture* (Vol. 141, pp. 267–275). Elsevier B.V. <https://doi.org/10.1016/j.compag.2017.07.026>
- Inocêncio, T. de M., Ribeiro Neto, A., Oertel, M., Meza, F.J., Scott, C.A., 2021. Linking drought propagation with episodes of climate-Induced water insecurity in Pernambuco state - Northeast Brazil. *J. Arid Environ.* 193. <https://doi.org/10.1016/j.jaridenv.2021.104593>
- Jackson, R. D.; Reginato, R. J.; Idso, S. B. Wheat canopy temperature: A practical tool for evaluating water requirements. *Water Resources Research*, v.13, p.651-656, 1977. <http://dx.doi.org/10.1029/WR013i003p00651>
- Kimwatu, D. M., Mundia, C. N., & Makokha, G. O. 2021. Monitoring environmental water stress in the Upper Ewaso Ngiro river basin, Kenya. *Journal of Arid Environments*, 191. <https://doi.org/10.1016/j.jaridenv.2021.104533>
- King, B. A., and Shellie, K. C. (2023). A crop water stress index based internet of things decision support system for precision irrigation of wine grape. *Smart Agricultural Technology*, 4. <https://doi.org/10.1016/j.atech.2023.100202>
- Landim, P.M.B. *Análise Estatística de Dados Geológicos*, 2nd ed.; Edunesp: Rio Claro, Brazil, 2003; ISBN 9788571395046.
- Li, R., Chai, S., Chai, Y., Li, Y., Lan, X., Ma, J., Cheng, H., Chang, L., 2021. Mulching optimizes water consumption characteristics and improves crop water productivity on the semiarid Loess Plateau of China. *Agric. Water Manag.* 254, 106965. <https://doi.org/10.1016/j.agwat.2021.106965>
- Liu, L., Gao, X., Ren, C., Cheng, X., Zhou, Y., Huang, H., Zhang, J., & Ba, Y. 2022. Applicability of the crop water stress index based on canopy–air temperature differences for monitoring water status in a cork oak plantation, northern China. *Agricultural and Forest Meteorology*, 327. <https://doi.org/10.1016/j.agrformet.2022.109226>

- Liu, M., Guan, H., Ma, X., Yu, S., Liu, G., 2020. Recognition method of thermal infrared images of plant canopies based on the characteristic registration of heterogeneous images. *Comput. Electron. Agric.* 177, 105678. <https://doi.org/10.1016/j.compag.2020.105678>
- Lopes, I., Montenegro, A.A.A., de Lima, J.L.M.P., 2019. Performance of conservation techniques for semiarid environments: Field observations with caatinga, Mulch, and Cactus Forage Palma. *Water (Switzerland)* 11. <https://doi.org/10.3390/w11040792>
- Luan, Y., Xu, J., Lv, Y., Liu, X., Wang, H., & Liu, S. 2021. Improving the performance in crop water deficit diagnosis with canopy temperature spatial distribution information measured by thermal imaging. *Agricultural Water Management*, 246. <https://doi.org/10.1016/j.agwat.2020.106699>
- Menegassi, L. C., Benassi, V. C., Trevisan, L. R., Rossi, F., & Gomes, T. M. 2022. Thermal imaging for stress assessment in rice cultivation drip-irrigated with saline water. *Engenharia Agrícola*, 42(5). <https://doi.org/10.1590/1809-4430-ENG.AGRIC.V42N5E20220043/2022>
- Miri, A., and Webb, N. 2022. Characterizing the spatial variations of wind velocity and turbulence intensity around a single Tamarix tree. *Geomorphology*, v.414. <https://doi.org/10.1016/j.geomorph.2022.108382>
- Montenegro, A. A. A., Almeida, T. A. B., de Lima, C. A., Abrantes, J. R. C. B., & de Lima, J. L. M. P. 2020. Evaluating mulch cover with coir dust and cover crop with Palma cactus as soil and water conservation techniques for semiarid environments: Laboratory soil flume study under simulated rainfall. *Hydrology*, 7(3). <https://doi.org/10.3390/HYDROLOGY7030061>
- Montenegro, A.A.A., Montenegro, S.M.G.L., 2006. Variabilidade espacial de classes de textura, salinidade e condutividade hidráulica de solos em planície aluvial. *Rev. Bras. Eng. Agrícola e Ambient.* 10, 30–37. <https://doi.org/10.1590/s1415-43662006000100005>
- Nogueira, D.B., da Silva, A.O., Giroldo, A.B., da Silva, A.P.N., Costa, B.R.S., 2023. Dry spells in a semiarid region of Brazil and their influence on maize productivity. *J. Arid Environ.* 209, 104892. <https://doi.org/10.1016/j.jaridenv.2022.104892>
- Oroud, I. M., & Balling, R. C. 2021. The utility of combining optical and thermal images in monitoring agricultural drought in semiarid mediterranean environments. *Journal of Arid Environments*, 189. <https://doi.org/10.1016/j.jaridenv.2021.104499>

- Paulo, R. L. de, Garcia, A. P., Umezu, C. K., Camargo, A. P. de, Soares, F. T., & Albiero, D. 2023. Water Stress Index Detection Using a Low-Cost Infrared Sensor and Excess Green Image Processing. *Sensors*, 23(3). <https://doi.org/10.3390/s23031318>
- Pineda, M., Barón, M., Pérez-Bueno, M.L., 2021. Thermal imaging for plant stress detection and phenotyping. *Remote Sens.* 13, 1–21. <https://doi.org/10.3390/rs13010068>
- Rico-Fernández, M.P., Rios-Cabrera, R., Castelán, M., Guerrero-Reyes, H.I., Juárez-Maldonado, A., 2019. A contextualized approach for segmentation of foliage in different crop species. *Comput. Electron. Agric.* 156, 378–386. <https://doi.org/10.1016/j.compag.2018.11.033>
- Santana, T.C., Guiselini, C., Montenegro, A.A. de A., Pandorfi, H., da Silva, R.A.B., da Silva e Silva, R., Batista, P.H.D., Cavalcanti, S.D.L., Gomes, N.F., da Silva, M.V., Jardim, A.M. da R.F., 2023. Green roofs are effective in cooling and mitigating urban heat islands to improve human thermal comfort. *Model. Earth Syst. Environ.* <https://doi.org/10.1007/s40808-023-01743-0>
- Savvides, A. M., Velez-Ramirez, A. I., & Fotopoulos, V. 2022. Challenging the water stress index concept: Thermographic assessment of Arabidopsis transpiration. *Physiologia Plantarum*, 174(5). <https://doi.org/10.1111/ppl.13762>
- Shanmugapriya, P., Rathika, S., Ramesh, T., & Janaki, P. (2019). Applications of Remote Sensing in Agriculture - A Review. *International Journal of Current Microbiology and Applied Sciences*, 8(01), 2270–2283. <https://doi.org/10.20546/ijcmas.2019.801.238>
- Silva, A. do N., Ramos, M. L. G., Ribeiro Junior, W. Q., da Silva, P. C., Soares, G. F., Casari, R. A. das C. N., de Sousa, C. A. F., de Lima, C. A., Santana, C. C., Silva, A. M. M., & Vinson, C. C. 2023. Use of Thermography to Evaluate Alternative Crops for Off-Season in the Cerrado Region. *Plants*, 12(11). <https://doi.org/10.3390/plants12112081>
- Silva, É.S. da, Cruz, J.D., Resende, J.J., Campos, N.N., Pinheiro, T.A., 2021. Alternative Control of Insects of Agricultural Importance Using Plant Extracts of *Azadirachta Indica* (Nim), in Feira De Santana, Bahia, Brazil. *Brazilian J. Dev.* 7, 6579–6586. <https://doi.org/10.34117/bjdv7n1-446>
- Silva, M.V. da, Pandorfi, H., Almeida, G.L.P. de, Silva, R.A.B. da, Morales, K.R.M., Guiselini, C., Santana, T.C., Cangela, G.L.C. de, Filho, J.A.D.B., Moraes, A.S., Montenegro, A.A. de A., Oliveira Júnior, J.F. de, 2023. Spatial modeling via geostatistics and infrared thermography of the skin temperature of dairy cows in a compost barn system in the

- Brazilian semiarid region. *Smart Agric. Technol.* 3, 100078. <https://doi.org/10.1016/j.atech.2022.100078>
- Singh, V., Sharma, N., Singh, S., 2020. A review of imaging techniques for plant disease detection. *Artif. Intell. Agric.* 4, 229–242. <https://doi.org/10.1016/j.aiaa.2020.10.002>
- Sishodia, R. P., Ray, R. L., & Singh, S. K. (2020). Applications of remote sensing in precision agriculture: A review. *Remote Sensing*, 12(19), 1–31. <https://doi.org/10.3390/rs12193136>
- Sousa, L. B., Montenegro, A. A., da Silva, M. V., Almeida, T. A. B., de Carvalho, A. A., da Silva, T. G. F., & de Lima, J. L. M. P. (2023). Spatiotemporal Analysis of Rainfall and Droughts in a Semiarid Basin of Brazil: Land Use and Land Cover Dynamics. *Remote Sensing*, 15(10). <https://doi.org/10.3390/rs15102550>
- Thornthwaite, C.W. and Mather, J.R., 1955. *The Water Balance*. Drexel Institute of Technology—Laboratory of Climatology, Publications in Climatology, Centerton, 104 p.
- Tian, H., Wang, T., Liu, Y., Qiao, X., Li, Y., 2020. Computer vision technology in agricultural automation —A review. *Inf. Process. Agric.* 7, 1–19. <https://doi.org/10.1016/j.inpa.2019.09.006>
- Valín, M.I., Araújo-Paredes, C.A., Rodrigues, A.S., Alonso, J., Mendes, S., 2019. Utilização de técnicas de termografia para a avaliação do estado hídrico da vitis vinífera cv Loureiro 899–905. https://doi.org/10.26754/c_agroing.2019.com.3442
- Warrick, A.W. and Nielsen, D.R., 1980. Spatial variability of soil physical properties in the field. In: Hillel, D., (ed.). *Applications of Soil Physics*. Cap. 2, Academic Press, New York, USA, pp. 319-344.
- Webster R, Oliver M (2007) *Geostatistics for environmental scientists*, 2nd edn. Wiley, Chichester.

General conclusions and final considerations

Understanding the principles, practices, and recent advances in indirect field monitoring aimed at enhancing resilience and adaptive capacity in semiarid agriculture amidst on going climate change is crucial. Implementing sustainable land management and proactive adaptation measures is essential to mitigate these impacts. Integrated approaches, such as climate-smart agriculture and nature-based solutions, are highlighted as effective strategies to enhance productivity and resilience in dry areas. In this study, significant results were obtained for water resources management in the semiarid region and for developing actions aimed at promoting productive coexistence with water scarcity:

The occurrence of temporal stability in the potentiometric level in the Mimoso alluvial valley enabled the identification of piezometers that adequately represent the average over time, optimizing continuous area monitoring. Additionally, the identification of increasing trends in temperature and evapotranspiration, along with reductions in annual precipitation and an increase in the extraction flow from wells, and the decreasing trend in piezometric levels, raise concerns about the growing risk of aquifer scarcity in the coming years. Groundwater pumping emerges as a management alternative to control salinity, crucial for mitigating long-term water shortages in this severely water-scarce region.

Wildfires typically transform vegetation and litter into a heterogeneous layer of ash covering the soil surface, substantially modifying the post-fire hydrological and erosive response of the soil. Laboratory and field experiments addressed knowledge gaps by investigating ash mobilization and the impacts of various burning layouts under simulated rainfall. Burning in smaller areas reduced soil disaggregation rates and caused less alteration in soil physical characteristics. Laboratory experiments focused on ash transport observed that smaller ash concentration areas led to less ash mass transported by surface runoff, highlighting rainfall intensity as a significantly more important factor for ash transport compared to the slope factor.

Domestic wastewater reuse in irrigation can have positive effects on water conservation and nutrient recycling, but it also poses risks to soil carbon and salinity if not managed properly. Conservation practices that balance these factors are essential for sustainable agriculture in the

Brazilian semiarid region. The application of treated effluents in agriculture can mitigate water scarcity in the semiarid region and, when combined with soil cover management, can control salinity while significantly increasing the incorporation of organic matter and biochar. This, in turn, boosts the organic carbon content in the soil. Additionally, using salinity and vegetation indices in image processing provides valuable tools for monitoring and identifying management areas.

Daily Water Stress Index (DWSI), using infrared thermal imaging cameras monitored canopy temperature (T_c), accurately reflects biometric index changes, demonstrating potential as a daily indicator of plant-climatic relationships. Highest water stress levels occurred during hot, rainless months, concentrated at leaf apices and central veins. Mulching mitigated Neem's physiological water stress, enhancing soil moisture and promoting growth even amid extreme droughts. Mapping DWSI with sequential Gaussian simulation enhanced precision in stress detection, vital for managing semiarid agricultural resilience.

Along this Thesis, a detailed geostatistical framework was applied to investigate spatio-temporal patterns not only for water resources in an alluvial valley, but also for the Daily Water Stress Index in crops at the hillsides of the domain. Statistical patterns have been successfully identified, contributing to enhance understanding of ecohydrological dynamics and also the temperature distribution in crop leaves under stress.

Groundwater availability in Mimoso Valley has been impacted by (recorded) climate change and irrigation. To achieve sustainable development, water resources plans must be implemented, including environmental protection of the aquifer boundaries and hillslopes. Treated wastewater reuse and mulching can increase water availability and improve soil protection. Wildfires must be controlled, where ashes layout can alleviate environmental degradation and fertility decrease. Moreover, biochar composts might enhance soil quality and also reduce potential impacts and migration of nutrients towards the saturated zone, which could lead to water quality degradation in future.

In general, this thesis presents significant results concerning water resource management in semiarid regions. The seasonal effects of changes in rainfall patterns, temperature, evapotranspiration, and exploitation on the average aquifer level and water quality underscore

the need for policies and actions to control the use of this resource. The assessment of water quality and the mapping of indicator variables aid in decision-making about when and where to irrigate. Additionally, the use of treated wastewater for agricultural crops represents an important alternative for enhancing and maintaining irrigated agriculture in semiarid areas, especially when combined with proper bioretention systems and conservation practices. All these results highlight the importance of constant hydroclimatological monitoring and the determination of soil and crop quality parameters in the region, aiming to optimize natural resources and improve water management. Additionally, they highlight the significance of conducting experiments in a participatory manner, encouraging the involvement of small-scale farmers to strengthen the communal farm.

Knowledge Sharing

The activities proposed in the Thesis aimed at coping with water scarcity were carried out in an applied manner, with a focus on agricultural and livestock production within family-based activities, aiming to ensure the quality of life for the population. Consequently, the activities aimed to disseminate measurements and research results among the target audience. They also involved collaboration with local stakeholders such as students, farmers, and communities, as well as local managers (Figure 1).



Figure 1. Field monitoring with the collaboration of undergraduate students and local school students.

The research conducted had a strong regional focus, encompassing the Agreste region of the state of Pernambuco and contributing to expanding resource management tools in semiarid areas. The emphasis was on efficient water use and the sustainable development of the region. Various techniques, management practices, alternative water sources, and available technologies were essential in establishing goals and protocols that promote agricultural expansion and sustainability in Pernambuco's semiarid areas.

The Thesis encompassed the university triad, involving education through the participation of undergraduate students from the Federal Rural University of Pernambuco, both at its main campus and at the Belo Jardim Academic Unit, as well as high school students from the local community. In research, significant efforts were made in maintaining a climate data bank, data analysis, and gathering information relevant to society. The results of these studies were published in high-impact conferences and journals (Figure 2).



Figure 2. Presentation of scientific works in Symposium and Congresses.

University extension activities were carried out through field days, training sessions, and workshops focusing on the thesis' areas of expertise. These activities included interaction with and support for local stakeholders who regularly participate in monitoring efforts.



Figure 3. Field actions in hydro-agricultural reuse demonstration units and experimental areas.

This project was also aligned with the FACEPE APQ-0414-5.03/20 project and the Academic Master's and Doctorate for Innovation Program (MAI/DAI) (CNPq Call No. 12/2020), enabling positive synergies among the objectives of each project. It is also important to highlight the partnership between UFRPE and INSA in the field of hydro-agricultural reuse. Additionally, the project received support from CEDAPP (Diocesan Center for Support to Small Producers) and TPF Engenharia. Furthermore, it integrated with the National Institute of Science and Technology for Sustainable Agriculture in the Tropical Semiarid (INCTAgriS) in the following areas: Sustainable Irrigated Agriculture, Climate Change and Natural Resource Management, and Knowledge and Technology Transfer.

Publications and other relevant activities conducted on the doctoral research

Papers published in peer-review international journals

Almeida, T. A. B., Montenegro, A. A. de A., Mackay, R., Montenegro, S. M. G. L., Coelho, V. H. R., de Carvalho, A. A., & da Silva, T. G. F. Hydrogeological trends in an alluvial valley in the Brazilian semiarid: Impacts of observed climate variables change and exploitation on groundwater availability and salinity. *Journal of Hydrology: Regional Studies*, 53, 2024.

Almeida, T. A. B., Montenegro, A. A. de A., da Silva, R.A.B., de Lima, J.L.M.P., Carvalho, A.A., da Silva, J.R.L. Evaluating Water Deficit Stress Index (DWSI) using thermal imaging of Neem tree canopies under bare soil and mulching conditions. *Remote Sensing*.

Papers or abstracts published and/or presented in conference proceedings

Almeida, T. A. B.; Montenegro, A. A. A.; Andrade, C. W. L.; Carvalho, A. A.; Ramos, A. H. S. Variabilidade espaço-temporal de padrões de qualidade da água subterrânea para irrigação em vale aluvial do semiárido de Pernambuco In: SIMPÓSIO DE PÓS-GRADUAÇÃO - SIMPOS 2021.

Almeida, T. A. B.; Lima, J. L. M. P.; Montenegro, A. A. A.; Zehsaz, S.; Pinto, J.M.A. avaliação da mobilização de cinzas pós-incêndio em laboratório sob condições de chuva simulada In: XXV Simpósio Brasileiro de Recursos Hídricos. Aracaju, 2023.

Almeida, T. A. B.; Montenegro, A. A. A.; Carvalho, A. A. Experiências científicas de 25 anos de monitoramento hidrológico no Vale Aluvial do Mimoso In: XVI SRHNe - Simpósio de Recursos Hídricos do Nordeste e 15º SILUSBA - Simpósio de Hidráulica e Recursos Hídricos dos Países de Língua Portuguesa, 2022, Caruaru.

Almeida, T.A.B.; Montenegro, A.A.A.; de Lima, J.L.M.P.; Carvalho, A. A.; da Silva, R.A.B; Pandorfi, H. Water stress index analysis using infrared thermography and computer vision to perennial crops in a small basin in the Brazilian semiarid In: 18th Biennial Conference ERB,

2022, Portoferraio. Anais da 18th Biennial Conference ERB. Florença: Editora Universidade de Florença, 2022.

Almeida, T. A. B.; Montenegro, A. A. A.; Ramos, A. H. S.; Araujo, B. G.. Estabilidade temporal dos níveis potenciométricos e da salinidade em aquífero aluvial no semiárido pernambucano In: XV Simpósio de Recursos Hídricos do Nordeste, 2020.

Almeida, T. A. B.; Montenegro, A. A. A.; Andrade, C. W. L.; Ramos, A. H. S.. Tendências Hidrológicas No Vale Aluvial Do Mimoso, Semiárido De Pernambuco In: Xv Simpósio De Recursos Hídricos Do Nordeste, 2020, Caruaru. XV Simpósio De Recursos Hídricos Do Nordeste. Porto Alegre: Abrh, 2020,

Participation in conferences

XXV Simpósio Brasileiro de Recursos Hídricos, Aracajú/SE. 2023

2nd rainfall simulator workshop. Coimbra: Faculdade de Ciências e Tecnologia da Universidade de Coimbra, 2023.

XVI SRHNe - Simpósio de Recursos Hídricos do Nordeste e 15º SILUSBA - Simpósio de Hidráulica e Recursos Hídricos dos Países de Língua Portuguesa, Caruaru, 2022.

XV Simpósio de Recursos Hídricos do Nordeste. Online. 2020

Sandwich Doctorate at Coimbra University

The Sandwich Doctorate was developed from 05/01/2023 until 07/07/2024 at Coimbra University, located in the city of Coimbra, Portugal, under the supervision of PhD João Pedroso de Lima. The subsidy for the development of the research project was contemplated by the NOTICE 04/2022 – CAPES-Print-UFRPE PROGRAM (PDSE Proc. 88887.717355/2022-00) “Assessment of the hydrological and erosive response after fire in laboratory conditions through innovative monitoring techniques” funded by CAPES.

Part of the doctoral research was developed during the Sandwich Doctorate. All sources of information and input data required for the experimental simulation were described previously in Chapter II. The activities performed included laboratory rainfall simulation, the first draft of Chapter II, planning of field experiments, preparation of conference papers, and image analysis. Additionally, there was significant contribution to Chapter V, with substantial collaboration from Professor João Pedroso de Lima in the image analyses.

The period of study carried out in the Sandwich Doctorate was extremely important for this Doctoral research, since important decisions related to layouts definition, such as definition of the setup. For this reason, the sincere thanks are reaffirmed here, to Professor João Pedroso de Lima, as well as to all researchers at Coimbra University, for their generous technical support, in specially for the PhD Ricardo Martins, the PhD student Soheil Zehsaz, the Master student João Pinto.